Patterns and Drivers of Recent Peatland Carbon Accumulation in Northeastern Canada

Submitted by Nicole Katherine Sanderson

to the University of Exeter

as a thesis for the degree of Doctor of Philosophy in Geography

January 2016.

This thesis is available for Library use on the understanding that it is copyright material and that no quotation from the thesis may be published without proper acknowledgement.

I certify that all material in this thesis which is not my own work has been identified and that no material has previously been submitted and approved for the award of a degree by this or any other University.

Signature: ……

Abstract

Northern peatlands are an important component of the global carbon (C) cycle and have been a net sink of atmospheric C during the Holocene. Under current climate warming conditions, the future sink-source balance of these peatlands is uncertain. In particular, peatlands near the southern limit of permafrost are likely to be sensitive to changes in topography as well as climate. In order to predict how the sink-source balance may change, this thesis focuses on determining the generality of observed patterns of C accumulation in Northeastern Canada.

The methodological approach in this thesis is unique. A total of 30 cores were taken from 9 peatlands located in 3 ecoclimatic regions along the North Shore of the Gulf of St Lawrence. This replication of records allows for climate-scale (allogenic) signals to be separated from the internal or local factors (autogenic), and for statistical testing of differences between regions and within sites over time. Trends in carbon accumulation rates (CAR) were analysed on three levels: (1) within individual sites along a hydrological or microtopography gradient, (2) between overall regions located along a climatic or permafrost gradient, and (3) over time on a multi-centennial scale.

Lead-210 (^{210}Pb) dating was used throughout the analysis to increase temporal resolution for the last 150-200 years of C accumulation. The method was thoroughly tested from preparation to analysis and found to produce reliable results, comparable with other dating methods. These dates were then used to develop combined age-depth models for longer-term context. Replicated records of ^{210}Pb inventories and fallout rates were also used to address questions of deposition patterns and post-depositional mobility in peat profiles. Total inventories decreased with water table depth, with lichen hummocks having significantly higher inventories. One site also received significantly higher ^{210}Pb deposition than the other two, as it is more sheltered from the Gulf influence.

Recent carbon accumulation rates for the 150-year period for all microforms across all regions was 62.1 ± 4.4 g C m^{-2} a^{-1}, and were highest for *Sphagnum* hummocks (79.9 ± 8.9 g C m^{-2} a^{-1}) and lowest for dry lichen hummocks (42.7 ± 6.2 g C m^{-2} a^{-1}). Patterns and trends at this scale were mainly driven by autogenic processes, including incomplete decomposition in the acrotelm peat. Models of peat accumulation related to acrotelm thickness were found to be overly simplistic, as carbon accumulation for intermediate microforms showed large natural variability driven by changing

ecohydrological feedbacks, in part due to permafrost degradation at one of the sites. Over a multi-centennial scale, carbon accumulation rates were driven by a combination of climatic changes and ecohydrological feedbacks due to shifts in the microform configuration in response to permafrost degradation. Changes in carbon accumulation rates were detected and coincided with Little Ice Age temperature/solar minima (including the Spörer, Maunder and Dalton Minima), permafrost degradation since the 1950s, and recent climatic changes in the mid-1990s. Snow cover and exposure of sites and microforms were found to play an important role, rather than solely climatic variables. Rapid *Sphagnum* re-establishment in post-permafrost degraded features and increasing temperatures meant that carbon accumulation was highest for the northernmost site in the transect. Age-depth models using a combination of lead-210 and radiocarbon dates allowed for the calculation of carbon accumulation rates at a decadal resolution. While peat carbon sequestration is projected to increase in northern regions, the fate of peatland C near the southern limit of permafrost is complex. Future studies seeking to interpret recent changes should include multiple cores and consider both regional climatic and local ecohydrological drivers.

Acknowledgements

First and foremost, I would like to thank my supervisors, Dan Charman and Iain Hartley in Exeter and Michelle Garneau in Montreal, for giving me this opportunity and always making time. I am so fortunate to have such an excellent advisory team, whose support, enthusiasm, patience and perspective were crucial to preparing this thesis. Huge thanks also to Michelle for welcoming me into her lab (and sometimes home) and for covering my field expenses. Merci aussi aux Tourbeux pour l'hospitalité, et aux assistants d'été, surtout Jean-Pierre Castonguay-Bélanger pour le terrain, la perte au feu sans fin et LA machine.

I would like to thank my parents for their unending belief and support. Particular thanks go to my sister Danielle for making time to help label bags, weigh samples and to transport suspicious suitcases of peat across borders. Thanks especially also to my adoptive Montreal family, Tanya Bradley and Plamen Nikholov (and Sophie) for taking me in summer after summer.

I would like to recognise the invaluable support from Kath Buckell, ex-administration guru, from Caroline Haughian for always getting me in to see Dan, and from past and present Geography lab technicians. Thanks to Dr Stephen Haley for advice and brainstorming sessions; I look forward to continuing to work together. To Ang, Natascha, and other techs, your company and lovely smiles make all the difference in a long day. Thanks especially to Joana for support this past year; it made a huge difference.

Thanks to peaty-palaeo friends (Jamie Johnson, Helen Mackay, Tom Roland, Emma Rice and Rob Barnett) not only for enjoyable and productive discussions but also for keeping me sane at work, and to the Radford Road crew (Anka, Julia, Catriona and Abi) for keeping me sane at home. To unnamed friends near and far, you know who you are. Thanks always for chats over coffee, or at the Globe, or in the office; living far from family in another country, while exciting, can be difficult and lonely at times but who can remember that sort of thing with you all around.

Project Funding

This research was primarily funded by the College of Life and Environmental Sciences at the University of Exeter, with fieldwork and research support from the Université du Québec à Montréal.

I would like to gratefully acknowledge additional contributions from the Geography fund for fieldwork, training and conferences. Thanks also to the lovely folks at the Canadian Centennial Scholarship Fund (CCSF) in London for generously funding me (twice!) and for their genuine interest in my research during discussions and interviews.

Dating peat has been important throughout this project. To that end, thanks to Steve Moreton at the NERC Radiocarbon Facility for providing dates and for hosting me in East Kilbride. Thanks also to Dr Will Blake at CORiF in Plymouth and to Dr Lauren Parry for donating samples, data and time in order to help me figure out ^{210}Pb dating.

Table of Contents

List of Figures

List of Tables

Abbreviations

α	'alpha' or alpha spectrometry
β	beta spectrometry
γ	'gamma' or gamma spectrometry
σ	Standard deviation
λ	Radioactive decay constant
a	year
AD	'Anno Domini', or years on a calendar scale (BC/AD)
^{241}Am	Americium-241 isotope
AMS	Accelerator Mass Spectrometry
ANOVA	Analysis of variance
a.s.l.	above sea level
BC	Baie Comeau region
Bq	Bequerel (s^{-1}), unit of radioactive decay; 1 Bq = 1 decay per second
BS	Blanc Sablon region
C	^{12}C, ^{13}C, ^{14}C; carbon and its stable isotopes and radiocarbon
cal. BP	calibrated years before present; 0 cal. BP = 1950 AD
CAR	carbon accumulation rate
CH_4	methane
CO_2	carbon dioxide
CRS	Constant Rate of Supply model
^{137}Cs	Caesium-137
GDD0	growing degree days above 0^{o}C
GSL	Gulf of St Lawrence
HP	Havre-Saint-Pierre region
IntCal13	2013 radiocarbon age calibration curve for age-depth modelling
IPCC	Intergovernmental Panel on Climate Change
LIA	Little Ice Age
Lich.	Lichen; Lich. hum. Is lichen hummock
LORCA	Long-term apparent rate of carbon accumulation, from age-depth models
LSD	Least significant difference post-hoc test
MAP/MSP	mean annual precipitation; mean summer precipitation

MAT/MST	mean annual temperature; mean summer temperature
MCA	Mediaeval climate anomaly
NCB/NCEB	net carbon balance; net ecosystem carbon balance
NERC	Natural Environment Research Council
NPP	net primary productivity
PAR	photosynthetically active radiation
Pb	^{206}Pb, ^{207}Pb, ^{210}Pb, ^{214}Pb: lead and lead isotopes (^{206}Pb is stable lead)
Pb_{sup}/Pb_{ex}	supported and unsupported lead fractions
Po	^{208}Po, ^{209}Po, ^{210}Po: polonium and polonium isotopes
R^2	correlation coefficient
^{226}Ra	Radium-226
RERCA	recent apparent rates of carbon accumulation, derived from ^{210}Pb dates
^{222}Rn	Radon-222
SCP	spheroidal carbonaceous particles
SD	standard deviation
SEM	standard error of the mean
Sph.	*Sphagnum*; *Sph*. hum. is *Sphagnum* hummock
$t_{1/2}$	half-life
^{238}U	Uranium-238
UQAM	Université du Québec à Montréal
WTD	water table depth

1 Introduction

1.1 Project background

Peatlands are an important component of the global carbon (C) cycle. Cool and moist conditions characteristic of boreal and subarctic environments have facilitated the net accumulation of organic matter and carbon in peatlands by restricting decomposition processes in waterlogged environments (Charman, 2002). Ombrotrophic, i.e. precipitation-fed, peatlands preserve past local climatic and hydrological changes, reflected in the vegetation and state of decomposition over time.

Northern peatlands, usually defined as those peatlands located North of 45^{o}N (MacDonald *et al.,,* 2006), contain up to a third of the global soil C in less than 3% of the land's surface (Gorham, 1991; Turunen *et al.,* 2002), or 547 Pg C in 4 million km^{2} (Yu *et al.,* 2010). While the annual rate of Holocene C accumulation in northern peatlands (0.07-0.10 Pg C a^{-1}; Gorham, 1991) is relatively low compared to the total annual atmosphere-biosphere C exchange (120 Pg CO_2 a^{-1}; Denman *et al,.* 2007), it has been sustained for thousands of years (Yu *et al.,* 2009). C sequestration in peat has been an important net sink for atmospheric carbon dioxide (CO_2) during the Holocene *(Ciais et al.,* 2013; Yu, 2011). However, peatlands are also an important contributor to the global methane (CH_4) flux (50 Tg C a^{-1}; Ciais *et al.,* 2013). Global C model predictions do not typically include peatlands despite their geographical extent and potential large contribution to climate-C feedbacks (e.g. IPCC AR5: Ciais *et al.,* 2013; Global Carbon Budget 2014: Le Quéré *et al.,* 2015).

Under current warming conditions, the future sink-source C balance for peatlands is uncertain (Friedlingstein *et al.,* 2006). While carbon emissions to the atmosphere are projected to rise from respiration from increased microbial activity (Dorrepaal *et al.,*

2009) and CH_4 production from permafrost melt (Turetsky *et al.,* 2002a) (positive feedback), longer growing seasons and higher rates of productivity (NPP) and carbon uptake are also expected (Charman *et al.,* 2013) (negative feedback). As northern latitudes warm faster than the global rate (Jansen *et al.,* 2007), C cycling in peatlands located in these regions is likely to be affected more intensely. In particular, peatlands near the southern limit of permafrost are likely to be sensitive to alterations in microtopography and hydrology as well as climate changes as the limit shifts northward (Schuur *et al.,* 2008; Tarnocai *et al.,* 2009).

During the Little Ice Age (LIA: ca. 1400-1700 AD; Jansen *et al.,* 2007; Mann *et al.,* 2008), permafrost in Canada reached its southernmost extent for the Holocene. Permafrost degradation has been accelerating during the last 50-100 years and this has been linked to warming since the end of the LIA (Payette, 2004). While carbon stocks have been shown to increase as a result in Western Canada (Vitt *et al.,* 2000; Turetsky *et al.,* 2002b) as well as in Arctic and Subarctic Canada (Vardy *et al.,* 2000; Lamarre *et al.,* 2012; Magnan and Garneau, 2014a), the decadal- and centennial-scale changes are poorly understood. Recent work by Garneau *et al. (*2014) indicates that long-term peatland C dynamics in Northeastern Canada are primarily linked with climate with the lowest accumulation rates during LIA. Changes in the peatland carbon accumulation and the C sink-source balance in response to disturbance (fire and permafrost) and associated altered microtopography and ecohydrological feedbacks has been well-documented in Western Canada (e.g. Vitt *et al.,* 2000; Turetsky *et al.,* 2002a,b, 2007; Benscoter *et al.,* 2015); limited work exists for Eastern Canada.

As carbon cycling is complex with considerable spatial and temporal variations not only between but also within individual peatlands (e.g. Roulet *et al.,* 2007), determining the generality of the patterns observed is therefore a priority. Carbon accumulation responses to climate changes in the late Holocene have been variable; however, it has

been suggested that the detection of Little Ice Age climate change-driven signals have been limited by poor dating resolution in recent peat samples. In order to predict how the C balance may change in the future, this thesis focuses on the recent trends in carbon accumulation since the LIA in this region by increasing the dating resolution as well as considering within-site variability with replicate cores from a range of microforms. This novel approach allows for the separation of allogenic and autogenic drivers of changes in carbon accumulation rates. In addition, as dynamic peat accumulation models (e.g. Belyea and Baird, 2006; Frolking *et al.,* 2010; Morris *et al.,* 2011) seek to incorporate greater levels of spatial variability, replication across a microtopography gradient will improve understanding of ecohydrological feedbacks. As Canadian permafrost peatlands contain approximately 44 Gt C (Tarnocai, 2006), climate-driven peat accumulation changes could represent an important future global source or sink for carbon.

1.2 Overall aim and objectives

This thesis aims to answer the following key question: to what extent does climate, permafrost and microtopography influence carbon accumulation rates (CAR) in northeastern Canadian peatlands on decadal and centennial scales? This question will be addressed using the following four objectives:

(1) Construct reliable high-resolution **chronologies** to evaluate high resolution changes in recent CAR (Chapters 5 and 6)
(2) Calculate local, **within**-site spatial variability in carbon accumulated along a **microtopography** gradient for the last 150 years (Chapter 6)
(3) Reconstruct centennial-scale regional and temporal changes in carbon accumulation **between** sites located along a **climatic** and permafrost gradient (Chapter 7)
(4) Evaluate potential **drivers** of changes in CAR over time (Chapters 7 and 8).

1.3 Methodology rationale

In order to address these objectives, three ecoclimatic regions with different permafrost histories were selected along the North coast of the Gulf of St. Lawrence. These regions are part of a larger GEOTOP project considering Holocene carbon accumulation rates for Québec and Labrador (synthesis in Garneau *et al.,* 2014). Two of the three regions were studied in parallel, evaluating Holocene C trends (Magnan and Garneau, 2014a,b) and contemporary C fluxes (Pelletier, 2014; Pelletier *et al.,* 2014). In this thesis, multiple replicated records of high-resolution carbon accumulation rates from a range of microforms from different ecoregions are considered, based on a combination of radiocarbon (^{14}C) and lead-210 (^{210}Pb) dates. The ^{210}Pb dating method was optimised and thoroughly evaluated in order to minimise methodological uncertainty.

The unique replication of records both within regions (3 peatlands per region) and within sites (3-4 microforms per peatland) allows for climate-scale (allogenic) signals to be separated from variability reflecting peatland development or other local (autogenic) factors and testing differences in peat and carbon accumulation rates statistically. Specific hypotheses are listed in Section 2.5.

1.4 Thesis outline

Chapter 1 has outlined the project rationale and overall thesis objectives. **Chapter 2** presents a review of the published literature and provides context to peatland carbon accumulation, in particular allogenic and autogenic drivers, and outlines uncertainties related to constructing chronologies. Based on this review, hypotheses are generated from the research gaps (Section 2.5) in order to address the overall aim.

Chapters 3 and 4 provide an overall perspective of the project design and basic coring results; as this thesis is based on replicate methodology, these chapters are meant to

assemble key data to be referred back to. **Chapter 3** outlines the project design and sampling strategy as well as the methodological rationale used including site descriptions, core types and field/laboratory methods. **Chapter 4** presents basic core information (bulk density, organic matter %, stratigraphy and dates) that will be used as the basis for all carbon calculations and age-depth models.

To address the objectives listed in the previous section, the main results are presented and discussed in Chapters 5, 6 and 7. **Chapter 5** is a stand-alone method chapter, reviewing and evaluating a new method for lead-210 (^{210}Pb) dating peat and discusses sources of uncertainty for subsequent analysis; the sample set for this chapter are different from the rest of this thesis. Different treatments and peat types are tested in order to optimise the method to prepare samples for alpha-spectrometry, the results of which are then compared to gamma-spectrometry results. **Chapter 6** presents recent carbon accumulation results from the ^{210}Pb-dated profiles for the last *ca.* 150 years across all microforms. This chapter evaluates spatial variability within peatlands and regions using replicates as well as changes over time. **Chapter 7** examines centennial-scale changes in carbon accumulation rates for the three regions, using replicates to look at between-site variability.

Finally, **Chapter 8** discusses the main results of this thesis and its limitations and avenues for future research and lists some concluding remarks.

2 Carbon Accumulation in Northern Peatlands

This chapter summarises findings from the literature, including a patterns and drivers of peat accumulation and climate-carbon cycle feedbacks, as well as the importance of chronologies, and regional and temporal context of this project. Key questions to be addressed in the thesis are identified in Section 2.5.

2.1 Peat and peatlands

Peatlands are waterlogged, acidic soils made up of at least 30-40 cm of slowly decomposing organic matter (National Wetland Working Group, 1997; Charman, 2002; Rydin and Jeglum, 2006) leading to a net accumulation of peat in these systems. The phrase 'northern peatlands' is used to differentiate between tropical or southern hemisphere peatlands from those peatlands located North of 45^{o} (Figure 2.1). This section will outline the processes of peat formation and expansion, vertical structure and surface patterning.

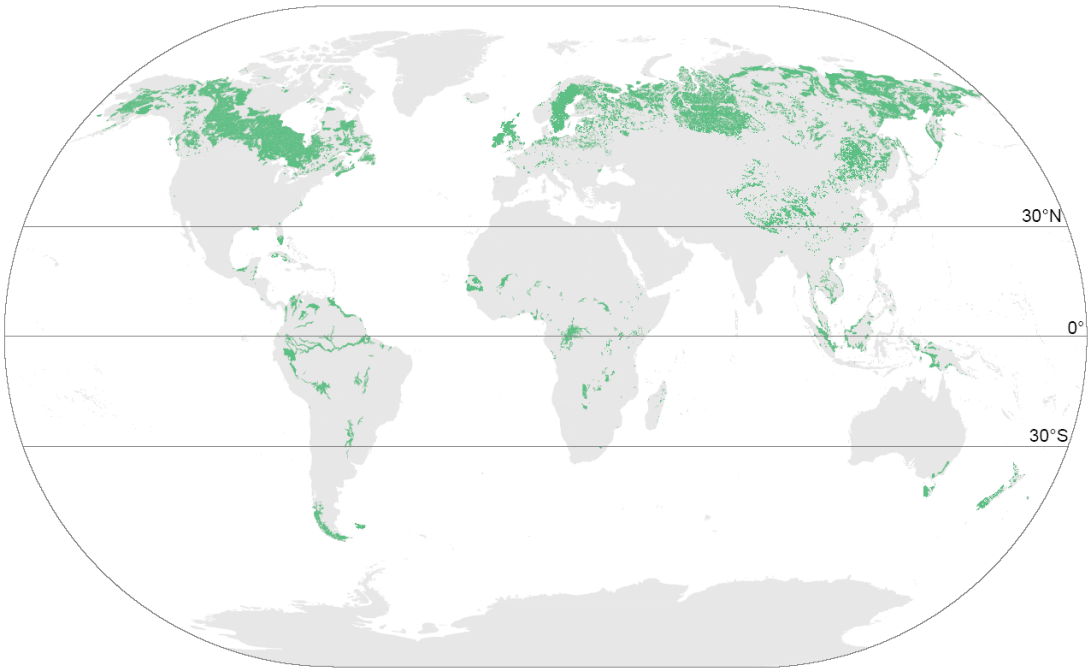

Figure 2.1 Map of global peatland distribution; green represents peatland area (from Yu *et al.,* 2010; Supplementary Material)

2.1.1 Formation and expansion of northern peatlands

Peatland formation and subsequent expansion are driven by a combination of geomorphological, climatic and anthropogenic conditions. Northern peatlands, located in boreal and subarctic regions, provide ideal conditions for peat growth and accumulation (Yu *et al.,* 2009). While initiation times and basal dates differ regionally due to different regional deglaciation timings (Dyke *et al.,* 2004), the majority of peatlands initiated and expanded rapidly after the Last Glacial Maximum (LGM) after the retreat of ice sheets, during the early to mid-Holocene (11-8 ka BP; 1 ka BP = 1000 years before 'present', or 1950AD) (MacDonald *et al.,* 2006; Gorham *et al.,* 2007). Peatlands expand via two main mechanisms: paludification (expansion into terrestrial ecosystem) or terrestrialisation (lake or pond-infilling). Locally, climate, topography and parent material play a role in explaining differing accumulation histories (Yu *et al.,* 2009). In Alaska and Western Canada, maximum peat expansion took place around the Holocene Thermal Maximum (HTM); in Eastern Canada and Labrador, this timing was later during warm/humid periods of the mid-Holocene (5-3 ka BP; Kaufman *et al.,* 2004) as the Laurentide Ice Sheet persisted longer. Net peat accumulation has been taking place since this time (Yu *et al.,* 2011). Trends in peat and carbon accumulation in Eastern Canada will be reviewed in more detail in Section 2.4.2.

Peatland surface vegetation is variable and depends on the hydrology. Along with vascular plants, bryophytes (*Sphagnum* and feather mosses) are the main building blocks of northern ombrotrophic peatlands, with *Sphagnum* mosses forming almost 50% of the biomass (Rydin and Jeglum, 2006). *Sphagnum* is more resistant to acidic conditions and to decay (recalcitrant) and creates feedbacks to acidify and maintains its own environment (van Breemen, 1995). Due to their high cation exchange capacity, i.e. their ability to preferentially bind with cations, these mosses are able to extract nutrients from nutrient-poor systems and to further modify their own environment

(Clymo *et al.,* 1990). This acidifying feedback also favours the lateral expansion of *Sphagnum* over other plants into peatland margins and adjacent areas.

Peatlands form in areas with a positive water balance, i.e. with poor drainage. The source of water (suffix –genous) and nutrient inputs for plant growth (suffix –trophic) characterise the type of peatland. Minerotrophic peatlands (fens) are fed by surface runoff and/or groundwater infiltration and are relatively wet and nutrient-rich; they range from rich fens dominated by sedges (oligotrophic, pH 6.0-8.5 or higher) to *Sphagnum*-dominated poor fens (mesotrophic, pH 4.5-4.4). Ombrotrophic peatlands (bogs) are primarily rain-fed and isolated from groundwater supplies, creating an acidic (pH 4-4.8), nutrient-poor environment dominated by *Sphagnum* mosses and ericaceous shrubs (Vitt *et al.,* 2009). Dry bog surfaces can also be covered in lichens (*Cladonia* sp.). The surface of an ombrotrophic bogs is often raised above the surrounding landscape, but the height and shape depends on the topography, climate, and isolation from the water table (e.g. basin bog, domed bog, blanked bog, plateau bog common in Atlantic regions) (National Wetlands Working Group, 1997). The type of peatland can change over time based on local climate and topography; for instance, as a topographically constrained peatland continues to grow and the surface becomes more distant from the water table, drier conditions and *Sphagnum* feedbacks may lead to a fen-bog transition.

Ombrotrophic bogs are useful as ‘environmental archives’ as their only source of inputs is from the atmosphere (wind-blown dust, precipitation). Peat records are useful for reconstructing local and regional geochemical (e.g. heavy metal deposition, pollution) and palaeoecological (e.g. pollen, testate amoeba) records of past environmental conditions (*cf.* review of proxies in Charman, 2002).

2.1.2 Vertical structure and peat accumulation

2.1.2.1 *Layered structure of peatlands*

Organic matter deposited as litter on the peatland surface collapses and accumulates vertically into two functional layers: the acrotelm and the catotelm. Ivanov (1981) first defined this two-layer structure, and the limits, transition and fluxes between the zones have been much discussed since (e.g. Clymo, 1992: structural and functional layers; Figure 2.2).

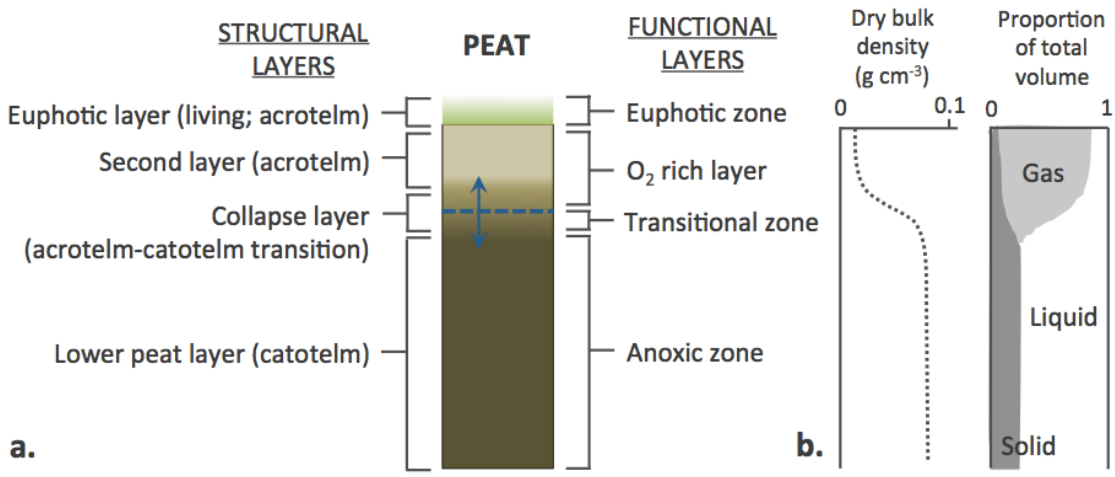

Figure 2.2. a) Schematic representation of structural and functional peat layers, from acrotelm to catotelm (adapted from Clymo, 1992). Blue dotted line is the water table and arrow is seasonal range; b) dry bulk density changes with depth and changes in relative proportions of gas/air/solid – catotelm there is anaerobic.

The acrotelm is composed of the living layer ('euphotic') and recently decaying matter and roots; as it is porous and well aerated, it has higher hydraulic conductivity and allows for the lateral transfer of water beneath the peatland surface. There is the most microbial activity and most decomposition occurring in peatland systems (80-90% dry peat mass) is aerobic, taking place in the acrotelm (Clymo, 1984; Belyea and Clymo, 2001). As decaying plants accumulate in the acrotelm, they eventually get compressed in the catotelm (*ca.* 10-20% of initial surface material; Clymo, 1984). The increasing bulk density with depth reduces pore space and causes the water level to rise and

leading to lower hydraulic conductivity. The catotelm (Figure 2.2), or anoxic zone, is permanently saturated; anaerobic decomposition is orders of magnitude (x1000) slower than aerobic decay but recalcitrant material continues to accumulate (Clymo *et al.,* 1998). The acrotelm-catotelm transition is typically defined as the average depth of the minimum summer water table (Ingram, 1978; Clymo, 1984; Belyea and Clymo, 2001); however, this is not always straightforward to identify in the field as the water table changes seasonally.

Peat accumulation occurs when organic matter inputs are greater than decomposition (Turunen *et al.,* 2002) and peat is added to the catotelm. The amount and rate of peat entering the catotelm depends on the amount and recalcitrance of litter in the acrotelm (organic matter quality and quantity) and its residence time in the acrotelm. This means that peat accumulation varies spatially and temporally based on plant productivity and water table depth. For instance, a higher water table means a shorter period of aerobic decay in the acrotelm, leading to higher net peat accumulation (Yu *et al.,* 2003). Despite short-term fluctuations in inputs, long-term peat accumulation rates have been found to remain steady in the catotelm (Belyea and Clymo, 2001).

2.1.2.2 *Vertical accumulation models*

Two main ‘classical’ peatland growth models are the basis of peatland studies: the Groundwater Mound Hypothesis (GMH: Ingram, 1978) and the Bog Growth Model (BGM: Clymo, 1984). More recently, alternative models are being proposed to attempt to represent dynamic peat accumulation (Belyea and Baird, 2006; the Holocene Peat Model: Frolking *et al.,* 2010; Quillet *et al.,* 2010; Morris *et al.,* 2011).

The Groundwater Mound Hypothesis (GMH: Ingram, 1978) considers hydrology and the water flow in the catotelm. The GMH proposes that bogs reach a hemi-elliptical cross section, the shape of which feeds back with the size and shape of the bog. This model assumes that hydraulic conductivity in the catotelm is constant and that all net

precipitation flows straight through the acrotelm. However, this model is limited as the precipitation-evapotranspiration balance varies seasonally (e.g. winter snow melt) and it only considers catotelm hydrology (Belyea and Baird, 2006).

Clymo's 1984 Bog Growth Model (BGM), also called 'limits to growth' model, describes accumulation patterns typical of maritime raised bogs in the UK. As peatland age increases, long-term catotelm decomposition becomes the dominant process, therefore decreasing apparent accumulation. Conversely, younger peats will have undergone less decomposition and so apparent accumulation rates are higher. This trend produces concave age-depth profiles of peat accumulation. Yu *et al. (*2003) built on this by describing peat accumulation patterns more typical of continental fens, where height-driven long-term drying trends were found to produce convex age-depth peat profiles; accumulation is the dominant trend in these peatlands. The BGM assumes that, in the centre of the peatland, constant proportions are lost by aerobic and anaerobic decay in the acrotelm and catotelm respectively, and that the acrotelm-catotelm transfer rate is constant. At the start of peatland development, litter production is greater than decay loss resulting in peat accumulation; the water table rises at the same rate as the bog growth. At steady state, litter production is equal to decay loss so peatland height and water table depth are maintained (see also Belyea and Baird, 2006 for schematic representation).

Recent models have included a hierarchical approach considering horizontal expansion (van Bellen *et al.,* 2011a) and heterogeneity at different time and spatial scales; these treat peatlands as complex adaptive systems to better represent peatland development and to predict responses to various feedbacks (Belyea and Clymo, 2001; Belyea and Baird, 2006; Frolking *et al.,* 2010). The BGM and GMH approaches assume that the catotelm is homogenous and that the acrotelm depends on catotelm conditions (water table depth). However, they do not include hydrology (GMH) and peat accumulation

processes (BGM) together, nor do they consider impacts of ecohydrological feedbacks, lateral expansion, rapid changes and spatial heterogeneity on acrotelm peat. In reality, microforms differ in their hydrological characteristics, formation and decay rates; for instance, hummock plant species are more recalcitrant than those growing in hollows (Turetsky *et al.,* 2008). Extensive spatial variability may lead to variations in peat accumulation rates across peatlands, such as the expansion of pool complexes in Newfoundland, Canada (Foster and Wright, 1990). When considering recent changes in peat accumulation in response to climate or other changes, hierarchical models of peat accumulation are attempting to include acrotelm dynamics, including the distribution patterns of microforms as well as their persistence over time in order to better represent peatland accumulation responses to ecohydrological changes (Belyea and Baird, 2006; Morris *et al.,* 2011).

2.1.3 Self-organisation and surface patterning

The thickness of the acrotelm can vary considerably within a peatland depending on the microtopography and distance of the surface from the water table. Surface patterning results from internal processes, variations in vegetation type, nutrient availability, and hydrological feedbacks (Eppinga *et al.,* 2007, 2009). The differential rates of peat formation and accumulation between hummocks, hollow and lawns amplify over time and lead to defined microforms (Belyea and Clymo, 2001). Surface patterns can also be amplified, or modified considerably by climate or disturbance (e.g. drought, permafrost, fire). Permafrost aggradation and degradation, in particular, can drastically change the peatland surface by creating new microforms such as palsas (raised peat ice mounds) or thermokarst ponds and collapse scars (Payette, 2004). Feedbacks between climate, permafrost, fire and peat accumulation will be reviewed in Section 2.2.3 on allogenic drivers of change.

Water availability regulates nutrient availability, plant growth and species distribution (Eppinga *et al.,* 2007; 2009). A recent review by Rezanezhad *et al. (*2016) provides a thorough and useful review from a chemistry perspective of peat structure, porosity, and role in regulating biogeochemical processes. There is a positive feedback between water table depth and peat production, but also with the plants themselves. When *Sphagnum* growth and peat accumulation in lawns occurs faster than water storage, plants grow laterally and colonise hollows; conversely, when water storage is faster, a thinner acrotelm wet-adapted species (Belyea and Malmer, 2004; Loisel and Yu, 2013). The resistance of plant litter to decay (recalcitrance) increases with microform height (hollow < lawn < hummock) (Johnson and Damman, 1991) with the highest rates of decay occurring in the zone of water table fluctuation (Belyea, 1996; Belyea and Clymo, 2001). Plants can also be involved in such feedbacks; for instance, *Sphagnum cuspidatum* carpets in hollows turn white from hyaline cell loss as water table depth increases in hollows, thus increasing the albedo and lowering local evapotranspiration, The different water content of the microforms result in varying relative thermal conductivity, daily and seasonal insulation (van der Molen and Wijmstra, 1994).

In topographically constrained peatlands, the rate of peat formation shows a humpbacked pattern in relation to water table depth. For small acrotelm-microforms (high water table), the system is too wet; for larger acrotelm-microforms (low water table), hummocks evolve to a steady state wherein taller hummocks (thick acrotelm) compensate for variations in bog surface wetness. A three-year transplant study found that hummock plant and moss species are more recalcitrant than those that grow in hollows as the latter are composed of more vascular plants (Turetsky *et al.,* 2008), and that vascular plant litter and roots decay faster than moss species (Turetsky, 2004; Turetsky *et al.,* 2008). As this material remains, peat under hummocks has lower hydraulic conductivity and hummocks act as barriers to water flow controlling water and nutrient availability, thus allowing them to persist (Foster, 1984; Couwenberg and

Joosten, 2005). Higher peat accumulation rates for hummocks are offset by higher rates of decay in the acrotelm, as *Sphagnum* accumulating in an aerated hummock will undergo greater aerobic decay as opposed to in a waterlogged hollow (Belyea and Baird, 2006). So while hummock-forming species decay slowly, the rate of peat decay is highest in hummocks. Indeed, intermediate microforms (lawns, small hummocks and hollows) have greater rates of peat formation in comparison to high hummocks and pools (Belyea and Clymo, 2001).

The drivers of surface patterning and microform self-organisation have been discussed as a combination of autogenic (internally-driven) and allogenic (externally, often climatically-driven) processes. Osvald's (1923) regeneration cycle theory suggests that hummocks and hollows accumulate peat at different rates leading to self-regulated alternating stratigraphic changes; that is, stratigraphically, dark horizons result degraded old hummocks preceding each lighter hollow stage. More recently, it has been suggested that hummocks and hollows grow upwards together, not cyclically (van der Molen and Hoekstra, 1988). Alternatively, Barber (1981) suggested that the changes from dark and light stratigraphic bands were controlled climatically by wet and dry phases with different decomposition-accumulation balances; wet hollows expand or contract at the expense of dry hummocks and vice versa. However, Swindles *et al. (*2012) and Loisel and Yu (2013; Patagonia) found that the shifts in water table from hummock-lawn and lawn-hollow margins in their respective studies were not always related to climate and that ecohydrological feedbacks should be taken into consideration when interpreting proxy results related to water table depth, especially when results come from a single core representing local or regional changes.

2.2 Carbon accumulation and climate-carbon feedbacks

Plants take up atmospheric carbon dioxide (CO_2) by photosynthesis, accumulate C in peat by accumulating organic matter, and emit CO_2 and methane (CH_4) via aerobic and

anaerobic decomposition (Charman, 2002; Rydin and Jeglum, 2006). The context and importance of studying the sensitivity of peatland carbon (C) storage has been raised in Chapter 1 (e.g. Gorham, 1991; Frolking and Roulet, 2007). The current impact of northern peatlands on atmospheric greenhouse gas concentrations, radiative forcing and climate is primarily determined by the magnitude of methane emissions and the C accumulation rate (Yu *et al.,* 2011). This section will look at peatland carbon cycling, storage, and potential feedbacks, including a range of autogenic and allogenic drivers, such as the roles of climate change, permafrost, fire, and associated ecohydrological feedbacks.

2.2.1 Carbon cycling in peatlands

2.2.1.1 *Uptake and storage*

Peat is primarily composed of water, organic matter and a small component of mineral material, so peat deposits are composed of approximately 50% carbon, found in plant litter and fossil plant matter (Turunen *et al.,* 2002; Beilman *et al.,* 2009). Therefore, an abundance of peat indicates a significant long-term net transfer of C from the atmosphere to the soil (Turunen *et al.,* 2004). The time-weighted average for Holocene C uptake by northern peatlands is 18.6 g C m^{-2} a^{-1}, with the highest accumulation rates occurring during the early Holocene (11,000-8,000 yr. BP) when peatlands were developing and expanding (Indermühle *et al.,* 1999). Yu *et al. (*2009) calculated that, by 8,000 a BP, 73-98 Pg C was stored in *ca.* half of the current Northern peatland extent (1 Pg = 1 Gt). While the annual rate of Holocene C accumulation in northern peatlands (0.07-0.10 Pg C/year; Gorham, 1991) is relatively low compared to the total annual atmosphere-biosphere C exchange (120 Pg CO_2/year; Denman *et al.,* 2007), it has been sustained for thousands of years (Yu *et al.,* 2009). Indeed, in the IPCC AR5, peat accumulation was modelled as being the main mechanism contributing to CO_2 uptake from the atmosphere for the last 7 ka (Figure 2.3; Ciais *et al.,* 2013). Recent estimates

of C storage in northern peatlands range from 270-370 Pg C (Turunen *et al.,* 2002), 455 Pg C (Gorham, 1991) to 547 Pg C (Yu *et al.,* 2010), and most recently 436 Pg C northern peatland carbon pool (Loisel *et al.,* 2014). While the variation in storage estimates reflects uncertainties in basal age, depth, bulk density and extent estimates globally, the order of magnitude and long-term nature of this storage compared to other terrestrial sinks or to the atmosphere is important as changes could change the uptake to emissions balance and the contribution of carbon to the atmosphere.

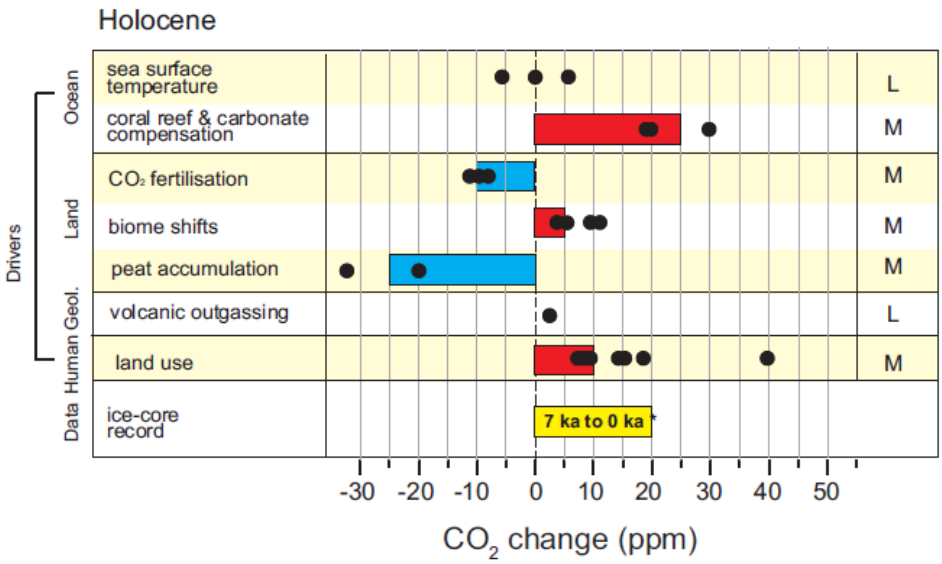

Figure 2.3. Role of peatlands in carbon uptake: mechanisms contributing to CO_2 concentration changes from the early/mid Holocene (7 ka) to the late Holocene. Filled black circles represent individual model-based estimates. Solid colour bars represent expert judgement (to the nearest 5 ppm) rather than a formal statistical average. Confidence levels are indicated in the right column (M: medium; L: low confidence). Figure from the IPCC AR5 (Ciais *et al.,* 2013).

2.2.1.2 *Carbon emissions in undisturbed peatlands*

As well as representing an important C sink, northern peatlands are also an active component of the terrestrial carbon cycle. CO_2 and CH_4 are emitted through aerobic (acrotelm) and anaerobic (catotelm) decomposition. C is also lost through fluvial dissolved organic carbon (DOC) losses (Dawson *et al.,* 2004).

Wetlands overall are the largest single source of atmospheric CH_4 (Solomon *et al.,* 2007), and northern peatlands are a significant global source because of the

importance of anaerobic decomposition releasing 20-50 Tg C a^{-1} from terrestrially-sourced CH_4 emissions to the atmosphere (Mikaloff Fletcher *et al.,* 2004; Ciais *et al.,* 2013). Indeed, a rise in atmospheric CH_4 during the early Holocene has been linked to the large-scale peatland initiation and expansion (MacDonald *et al.,* 2006; Korhola *et al.,* 2010; Yu, 2011). CH_4 emissions are controlled by water table depth and temperature, which directly impact microbial activity (Christensen *et al.,* 2004), so microtopography and surface vegetation can predict emission rates (Bubier *et al.,* 1995; Belyea and Baird, 2006). While methane has a higher global warming potential (GWP) than CO_2 (25 times stronger forcing on a 100-year timescale), it is relatively short-lived in the atmosphere (12 years) (Denman *et al.,* 2007). Changes in methane emissions could have important short-term impacts on atmospheric C (Section 2.2.3)

2.2.2 Measuring carbon in peatlands

There are two main measures for carbon cycling in peatlands: accumulation to measure net uptake and fluxes to estimate emissions and the amount of C uptake.

2.2.2.1 *Carbon accumulation*

Measuring C accumulation rates is of interest when considering peatland sensitivity to climate change. This involves knowing the amount of C stored in peatlands over a period of time. Dating techniques will be considered and reviewed in the next section (2.3). This section will look at the different terminology used in the literature and the different types of rates that are considered.

Most studies looking at C accumulation in peatlands consider the complete peat core, including the entire history of acrotelm and catotelm decay (Turunen *et al.,* 2002). They use basal dates to calculate the 'long-term apparent rate of carbon accumulation' (LORCA or LARCA). The longer a peatland has been accumulating, the greater the catotelm contribution relative to the acrotelm; care should be taken when considering

LORCA for different peat profiles in terms of age and developmental stage (Clymo *et al.,* 1998). Accumulated C mass is also represented in order to account for the influence of peat age on C sequestration (e.g. Beilman *et al.,* 2009; Magnan and Garneau, 2014a). Considering recent rates of changes are of growing importance with permafrost melt and climatic changes; 'recent apparent rates of C accumulation' (RERCA) can be used. This measure is defined typically as the rate of accumulation covered by the ^{210}Pb dating range (last 150-200 years; e.g. Bao *et al.,* 2010; Loisel and Garneau, 2010; Section 2.3); however, any recent age estimates can be used. Many studies do not consider the acrotelm at all (e.g. van Bellen *et al.,* 2011a; Magnan and Garneau, 2014a) as decay and transfer of carbon to the catotelm have not yet finished (Belyea and Clymo, 2001). However, including RERCA can be useful when considering the nature of accumulation and decomposition, or relative rapid processes between microforms or regions, even if the long-term fate of the peatland C is uncertain. Additional dates throughout the peat profile are used to calculate carbon accumulation rates (CAR) changes over time, calculated as the mass accumulated over each time interval (e.g. Loisel and Garneau, 2010; Magnan and Garneau, 2014a).

Rates are qualified as 'apparent' as the methods consider the C remaining in a core and do not take into account decomposition. Over a longer period of time, more material decomposes in the catotelm. LORCA < RERCA is explained by the larger catotelm contribution of the former, as RERCA usually covers only acrotelm accumulation with little decomposition. Upscaling using these methods can be challenging, as studies typically use one value for LORCA from a central peatland without considering spatial variability or lateral expansion.

2.2.2.2 *Carbon balance*

Eddy covariance flux towers and chamber methods are among the methods used to measure C balance, by recording net ecosystem exchange (NEE), CO_2 and CH_4

fluxes, temperature, etc. Carbon sequestration has been calculated at 20 g C m^{-2} a^{-1} (Roulet *et al.,* 2007). In comparing net ecosystem productivity (NEP, not including CH_4 and DOC) and RERCA from the top 50 cm of a Serbian mire, (Schulze *et al.,* 2002) found that these methods tend to overestimate the amount accumulated, as they do not account for long- or short-term decomposition (Roulet *et al.,* 2007). A range of microforms can be measured; however, long-term measurements are necessary as the C flux varies annually and spatially. For instance, a peatland region in Finland was recorded as a net sink of 32 g C m^{-2} a^{-1} in 1997, and a source of 157 g C m^{-2} a^{-1} two years later after a dry summer at a nearby site (Alm *et al.,* 1997, 1999).

Upscaling these rates to larger spatial scales can be challenging, as fluxes vary annually and spatially. In addition, few carbon balance studies take place over several years and also include dissolved organic carbon (DOC) export and methane (CH_4) into the carbon balance, which can be on the same order of magnitude as carbon dioxide (CO_2) uptake and emissions (Nilsson *et al.,* 2008; Koehler *et al.,* 2011; Cliche-Trudeau *et al.,* 2013, 2014).

2.2.3 Climate-C cycle feedbacks: allogenic controls on C accumulation

Carbon accumulation rates have been correlated with latitude in Siberian peatlands (Beilman *et al.,* 2009) and continentality in Finland (Tolonen and Turunen, 1996) as these both constrain vegetation and climate. Climate, i.e. temperature and moisture availability, affects both water table depth and vegetation. This section considers allogenic drivers of change on CAR, including climate, permafrost and fire.

2.2.3.1 *Temperature and precipitation*

The main driver of the positive accumulation balance in peatlands was thought to be the result of autogenic processes slowing anaerobic decay, as recalcitrant material is stored in the catotelm (Clymo, 1984; Belyea and Baird, 2006). Therefore, changes in

processes affecting in the decomposition balance likely would have more of an impact on peat accumulation. At higher latitudes, warmer conditions under projected climate scenarios (IPCC) would lead to higher decomposition rates and CO_2 emissions because of increased microbial activity (Ise *et al.,* 2008; Dorrepaal *et al.,* 2009), and increased radiative forcing from CH_4 emissions from ponding and permafrost melt (Turetsky *et al.,* 2002a). However, Charman *et al. (*2013) recently showed that that during the last millennium, higher accumulation is the more likely driver of peatland growth, as primary productivity (NPP) increases due to improved conditions for plant growth with C accumulation linearly related to the number of growing degree days above 0^{o}C (GDD0) and available photosynthetically active radiation (PAR) in the long term.

Peatland and C accumulation response to climate warming has been shown to be variable, but it is clear that climate affects decomposition and accumulation processes. Seasonal temperature and precipitation changes have direct impacts on vegetation/photosynthesis and water balance. Results from a metadata study show that temperature is the single most important factor controlling *Sphagnum* production (Gunnarsson *et al.,* 2005). North-South transects in Europe (Sweden to Germany) show an increase in CAR linked with temperature change the northern sites but a decrease in the Southern sites with warming, possibly linked to decomposition changes (van der Linden *et al.,* 2014). Indeed, microbial activity and biogeochemical cycles are sensitive to climate extremes; transplant experiments showed that a simulated increase in temperature of 5^{o}C and decrease in precipitation of 60% meant that peat productivity was almost 2/3 lower after 3 years due to increased respiration (Bragazza *et al.,* 2016).

The highest carbon accumulation rates for northern peatlands were previously recorded in Western Canada (Yu *et al.,* 2003) and Siberia (Beilman *et al.,* 2009). The ranges for optimal conditions of peatland growth therefore suggested to be 0-2.5^{o}C and

450-500mm annual precipitation (Yu *et al.,* 2009; Yu, 2011). CAR was found to be lowest in the Arctic and extreme conditions, such regions of high temperature or high precipitation such as Eastern Canada (Yu *et al.,* 2009). However, recent work by Magnan and Garneau (2014a) and Garneau *et al. (*2014) show that rates of carbon accumulation were found to be 2-3 times higher than the global average for northern peatlands along the North Shore of the Gulf of St Lawrence, where annual precipitation is greater than 1000 mm a^{-1}. These high accumulation rates in this region are likely the result of a combination of hydrological and internal factors.

One such feedback is driven by *Sphagnum.* Mosses insulate the peat subsurface in summer (low thermal conductivity maintains cool temperatures), which leads to drying (and cooling) in the summer. In winter, thermal conductivity increases (heat loss) because of the higher moisture content (Halsey *et al.,* 1995), and frost can penetrate deeper. This can lead to permafrost formation or persistence (Treat *et al.,* 2016), and highlights the importance of considering wind, snowfall insulation and exposure as climatic factors driving peat and carbon accumulation (Magnan and Garneau, 2014a).

Whether a peatland becomes a sink or a source of C is a key question. One study indicated that Western Canadian peatlands will likely switch from sinks to sources of C within 20-62 years (Wieder, 2001); however, Turetsky *et al. (*2007, 2015) found that peatlands in that region overall will remain as small net sinks when accounting for surface complexity and disturbance, such as permafrost and fire.

2.2.3.2 *Permafrost*

Permafrost occurs when soils remain frozen (< 0^{o}C) for more than 2 consecutive years (e.g. Smith *et al.,* 2007; Vitt *et al.,* 2000). The advance and degradation of permafrost is correlated to mean air temperature (Halsey *et al.,* 1995) can significantly affect peatland carbon cycling. Recent estimates place permafrost peat storage at 277 Pg C (Treat *et al.,* 2016). As discussed previously, the insulation properties of *Sphagnum*

mosses and the persistence of frost and wind exposure in open peatlands can mean that permafrost can be found in peatlands where there is none in the surrounding areas. It can persist as localised ice lenses in hummocks, palsas and is limited to ombrotrophic peatlands in the discontinuous and sporadic permafrost zones (Turetsky *et al.,* 2000). Permafrost advance and degradation affect microtopography (e.g. hummock-hollow configurations) and the distance of the surface from the water table, which in turn determines plant community structure and productivity (Christensen *et al.,* 2004; Sillasoo *et al.,* 2007).

The aggradation of permafrost where forming ice in peatlands creates a positive feedback – it raises the ground surface, increasing distance from the water table (Zoltai and Tarnocai, 1972), which also increases exposure. Ice lenses form in dry hummocks (Figure 2.4), and positive feedbacks take hold such as increasing albedo in dry lichen-topped hummocks and different thermal conductivity and insulation of microforms (van der Molen and Wijmstra, 1994). Palsas, or 'perennial cryogenic mounds' (Gurney, 2001), and peat plateaus eventually form (Vitt *et al.,* 1994, 2000; Zoltai, 1972). Drifting snow collecting on ground around the palsa edges, inhibiting further ice spread (Seppälä, 1994). As the peat surface dries it becomes highly decomposed and forms a dark ligneous layer. Surface permafrost inhibits accumulation, and decomposition does not occur below the frozen layer; the dry surface can also lead to increased fire feedbacks (Turetsky *et al.,* 2007; Schuur *et al.,* 2008).

Carbon accumulation has been found to be uniform from the permafrost table downwards, likely because of the lack of decay in the catotelm (e.g. Northwest Territories: Vardy *et al.,* 2000). Permafrost degradation is more complex (Vitt *et al.,* 2000; Halsey *et al.,* 1995). Melting creates a mosaic of permafrost features including thermokarst formations, internal lawns (i.e. open, wet lawn dominated by *Carex and Sphagnum* spp., as in Foster, 1984; Vitt *et al.,* 1994), collapse scars and thaw pools

(Turetsky, 2004; Turetsky *et al.,* 2007). As the ice melts, the surface is no longer supported. As it collapses, the water table rises, affecting local hydrology and vegetation and increasing the C pool available for decomposition.

Incubation experiments with shallow and deep Alaskan permafrost peats showed that, while temperature change had a strong positive effect on C emissions, the effect of permafrost on C also depended on hydrology, permafrost history, vegetation dynamics and organic matter quality (Treat *et al.,* 2016). In combination, temperature, hydrological and permafrost changes will influence CH_4 emissions to the atmosphere, with a mire in Sweden showing 22-66% in emissions increases between 1970-2000 (Christensen *et al.,* 2004). In Western Canada, fluxes of CO_2 and CH_4 were projected to respectively increase 1.6- and 30-fold after permafrost melt, which is important in the short term as CH_4 has a larger global warming potential than CO_2 (Turetsky *et al.,* 2002a). Depending on the stage of degradation, methane emissions or subsequent re-accumulation (e.g. 'internal lawns') could be dominant; however, analytical constraints limit the investigation into the timing of the switch from sink to source (Swindles *et al.,* 2015), highlighting the importance of considering within-site variability. Alaskan peatland sites in close proximity to each other (within 2 km) with different permafrost regimes (stable permafrost, collapse features, no permafrost) were found to have variable carbon fluxes from year to year, with the permafrost sites responding to warmer temperatures and increasing emissions (Euskirchen *et al.,* 2014). Indeed, considering spatial heterogeneity within sites as C emissions and accumulation changes with hydrology, snow cover, etc.

2.2.3.3 *Fire and ecohydrology*

Sources of peatland fires may be natural, e.g. from lightning strikes or by spreading from nearby forested areas, or anthropogenic, such as from slash and burn agricultural practices. Fire histories, reconstructed using charcoal, tree ring and pollen analyses,

can provide records of past climate changes and changes in vegetation composition (e.g. Grant *et al.,* 2014); these may be confounded (Campbell and Campbell, 2000; Ohlson *et al.,* 2011), and the relative importance shifts over time (Gavin *et al.,* 2006).

In North American boreal forests, infrequent high-density crown fires dominate, while low- to moderate-intensity surface fires of moderate frequency are recurrent in northern Asian forests (de Groot *et al.,* 2013). Indonesian peat fires, linked with climatic changes driven by the onset of the El Niño Southern Oscillation (ENSO), were responsible for *ca.* 13-14% of the global fossil fuel emissions for that year (Page *et al.,* 2002; Wang *et al.,* 2004). Other studies suggest that, by the end of the 21st century, the annual area burned in Western Canada and Alaska will increase 2- to 5.5-fold (Flannigan *et al.,* 2005; Balshi *et al.,* 2009) and the fire intensity and duration will be longer for those areas (Flannigan *et al.,* 2013). Modelled impacts of altered fire frequency predict more frequent and intense fires, therefore higher fuel consumption and an associated increase in C emission rates; total C emissions are also predicted to increase due to a larger burn area (de Groot *et al.,* 2013).

Surface fires remove the top layer of vegetation do not tend to affect local ecohydrological feedbacks and plant succession in the long term (Kurhy, 1994). While, changes are limited to a few decades, increasing fire frequency can significantly affect peat and carbon accumulation rates (e.g. in Western Canadian bogs: Turetsky *et al.,* 2002a). In dry years, fire can remove the top layer of vegetation down to the reduced water table (Sillasoo *et al.,* 2007). Smouldering fires in deeper peat layers have the potential to release substantial amounts of old carbon to the atmosphere (Turetsky *et al.,* 2015). Experiments have shown that peat moisture levels control ignition conditions (Rein *et al.,* 2008). In undisturbed, pristine peatlands, most of the C stock in the catotelm is protected from smouldering fires; therefore warmer, drier climates will likely

increase the frequency, extent and intensity of peat fires and increase C emissions (Wieder *et al.,* 2009; Turetsky *et al.,* 2015).

For Western Canadian peatlands, typically closed and forested (Glaser and Janssen, 1986), Turetsky *et al. (*2002a) estimated that disturbances, primarily fire-related), release 6460 ± 930 Gg C/a to the atmosphere and that an increase of 17% of the area burned would alter the sink-source relationship of this area. In contrast, in Eastern Canadian peatlands, no clear correlation was found between fire and changes in carbon accumulation (Magnan *et al.,* 2012; van Bellen *et al.,* 2012). In these typically open peatlands dominated by pools (Glaser and Janssen, 1986), wet and treeless bogs act as firebreaks (Hellberg *et al.,* 2004).

Spatial heterogeneity feeds back with fire regime, as fire alters peatland hummock-hollow configuration and plant distribution (Benscoter *et al.,* 2005, 2015). Following disturbance by fire, *Sphagnum* carpets overgrow feathermosses, and *Sphagnum fuscum* covers *Cladonia* lichens on hummocks (Foster, 1984). Dry-adapted species including *Polytrichum strictum, Sphagnum fuscum* and *Pleurozium schreberi* are indicators of early post-fire succession (Benscoter and Vitt, 2008; Camill *et al.,* 2009). The relative abundance of hollows and low-elevation microforms increased in response to wildfire in a large-scale natural experiment in Western Canada, and the microtopography gradient range doubled (Benscoter *et al.,* 2015). Hummocks expand into hollows through rapid succession, increasing peat and carbon accumulation rates (Sillasoo *et al.,* 2007; Turetsky *et al.,* 2008). Fire can also impact permafrost development as cold can penetrate deeper below the peat surface, or conversely, drying during permafrost aggradation or wetting during permafrost thaw can change peatland fire risk (Robinson and Moore, 2000). In addition, as the afforestation of peat soils may increase the risk of peat fires (Davies *et al.,* 2013), large-scale anthropogenic

tree planting C sequestration projects and the expansion of boreal forests under climate change conditions will change existing fire regimes.

2.2.4 Ecohydrological feedbacks: autogenic controls on C accumulation

On a large scale, the net rate of C accumulation decreased throughout the late Holocene, likely due to physical constraints on lateral expansion and vertical limits to growth imposed by peatland age and depth, i.e. distance of the surface from the water table and the persistent slow decay of recalcitrant material (Clymo, 1984; Clymo *et al.,* 1998). For instance, the high variability in long-term C accumulation patterns in the climatically uniform Eastmain region in northern Quebec may be due to differential timing in site development (van Bellen *et al.,* 2011a,b). Along the North Shore of the Gulf of St. Lawrence, peatlands with different basal ages accumulating over different substrates (marine vs. deltaic) within the same region were shown to have different Holocene LORCA values (Magnan and Garneau, 2014a,b). Model results based on the groundwater mound calculations suggest that autogenic processes exert major controls over the expansion and lateral development of peatlands (Foster and Wright, 1990), and therefore on carbon accumulation rates. The smallest fluctuations in water table depth have been recorded in the dome centre for ombrotrophic bogs, while base cations, acidity and DOC concentrations vary over time (Howie and van Meerveld, 2012); the dome centre is therefore ideal for considering autogenic vs. allogenic drivers of changes in carbon accumulation as inter-annual variability in hydrology is less important.

On a small scale, autogenic processes dominate and are driven by complex interactions between shade and water table depth, i.e. acrotelm thickness along physical and chemical gradients (Graham *et al.,* 2015). Surface structure is an important factor controlling carbon accumulation rates (Belyea and Malmer, 2004; Eppinga *et al.,* 2009). While the pre-existing peatland surface structure influences the

magnitude and direction of peatland carbon responses to climate change (Belyea and Malmer, 2004), changes in carbon accumulation and ecohydrology, e.g. alternating dark/light bands (Barber, 1981), are not necessarily driven by climate but can result from rapid vegetation assemblage changes (Swindles *et al.,* 2012; Loisel and Yu, 2013).

Across 23 sites and over 150 years in eastern Canada, rates of carbon accumulation were significantly larger in hummocks (78 g C m^{-2} a^{-1}) than in hollows (65 g C m^{-2} a^{-1}). RERCA and cumulative C mass were less variable for hummocks than for hollows (Turunen *et al.,* 2004). Hummocks emit CO_2 but are C sinks, while hollows tend to be C sources, e.g. CH_4 emissions or oxidation from wet hollows and mud bottoms (Karofeld, 2004; Laine *et al.,* 2007). In northeastern fens, where the water table rises over time under warmer and wetter conditions, pools contribute to CO_2 (Pelletier *et al.,* 2014) and CH_4 fluxes (Cliche-Trudeau *et al.,* 2013). Rapid changes in water table, e.g. post-permafrost degradation, lead to *Sphagnum* encroaching as a broad carpet over recently exposed mud bottoms in hollows (Foster, 1984; Belyea and Clymo, 2001). These ‘internal lawns’ have higher carbon accumulation rates (e.g. Turetsky *et al.,* 2000).

When small-scale patterns (1-10 m) in peatland surfaces are ignored in carbon cycle simulations, models tend to produce errors (Moore *et al.,* 1998). As discussed previously, individual microforms expand or contract vertically in response to water table fluctuations and ice content (e.g. van der Molen and Hoekstra, 1988). Belyea and Clymo (2001) suggest that limitations in carbon sequestration estimates can be overcome by including carbon-hydrology-microform feedbacks, whereby hummocks reach a steady state and their acrotelm progressively thickens, thus decreasing carbon accumulation. Due to sampling constraints and the large variability leading to upscaling issues within peatlands, these models investigating surface patterning (e.g. Eppinga *et*

al., 2007; Loisel and Yu, 2013) have not been tested with field observations. Using multiple cores could in part account for natural variability in carbon accumulation. While Gao and Couwenberg (2015) found no difference between centennial-scale carbon accumulation rates for a selection of microforms from a Siberian permafrost peatland, a multi-core study of one site in Northern Ireland found a range of accumulation rates over 450 years (Watson *et al.,* 2015).

A number of anthropogenic practices also affect carbon accumulation in peatlands, primarily through practices affecting peat surface (e.g. forestry practices) structure or water table depth (e.g. drainage or harvesting). These, in combination with climate changes, can increase C emissions and further alter the hydrological feedbacks. Peatland extent is being affected in northern Alberta by open-pit mining for oil sands extraction, where peatlands are replaced by reclamation/tailings storage lakes. Rooney *et al. (*2012) estimated that post-mining landscapes support > 65% less peatland area, and that such landscape changes will emit an additional 11.4-47.3 Mt C and reduce sequestration by 5-7 kt C/year. Pollution in northern UK moorland regions in the Peak District (Holden *et al.,* 2006) and degradation (Yeloff *et al.,* 2006a) also reduce peat and carbon accumulation. Drainage and deforestation for agriculture is important in Southeast Asia, where CO_2 emissions from decomposition and fire from drained peatlands ranged between 355-855 Mt CO_2 a^{-1} in 2006, adding the equivalent of 1.3-3.1% of current fossil fuel combustion emissions to the atmosphere (Hoojier *et al.,* 2010). Peatland restoration practices using drainage ditches in the UK have found that reducing DOC and runoff means that peatlands can act as water filters (e.g. Grand-Clement *et al.,* 2013; Gatis *et al.,* 2015). Peat is also removed for horticulture or for fuel; C previously stored in the catotelm is exposed and subjected to oxidation, decomposition processes, and combustion in the case of fuel. A 1990-2000 life cycle analysis for gardening peat in Canada found that peat decomposition was the largest source of greenhouse gases, responsible for 71% of emissions during this period

(Cleary *et al.,* 2005). Scandinavian studies had higher rates of end emissions due to the combustion of 'turf' or peat fuel (Nilsson and Nilsson, 2004), with Finland, Ireland, Russia, Sweden and Belarus responsible for 90% of the global energy peat consumption (Crill *et al.,* 2000).

2.2.5 Carbon accumulation summary

Figure 2.4 effectively illustrates the complex relationships between controls on carbon accumulation. Allogenic (e.g. climate, biota) and autogenic (e.g. topography and parent material) 'state' factors influence initial peat formation and expansion over time. Carbon accumulation is directly controlled by the balance between plant productivity and decomposition rates (Yu *et al.,* 2009). When considering recent carbon accumulation rates, within-site variability due to microtopography and relative acrotelm thickness adds an additional layer of complexity. Using replicate cores would be a way to separate autogenic from allogenic drivers at all scales.

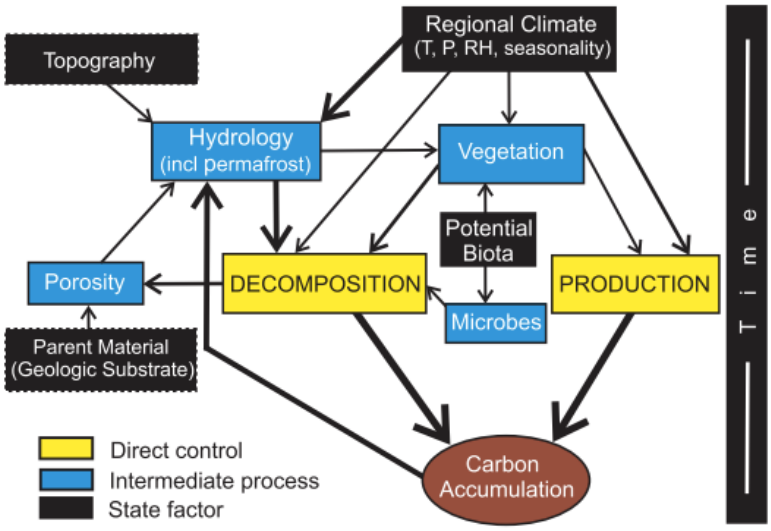

Figure 2.4. Conceptual model of northern peatland growth and carbon accumulation controls (copied from Yu *et al.,* 2009) showing the complex interactions between autogenic and allogenic factors over time. State factors (dashed boxes) are relevant to initial expansion; arrow line thickness indicates the relative importance of controls; T: temperature, P: precipitation; RH: relative humidity.

2.3 Dating recent peat accumulation

As ombrotrophic peatlands are archives of environmental change due to primarily atmospheric inputs (Charman, 2002), they not only store carbon and preserve vegetation histories, but also provide a record of geochemistry over time, either in the plants themselves (C isotopes) or from atmospheric chemical deposition (Turetsky *et al.,* 2004). While relative changes in stratigraphy and accumulation can be observed and tested between similar cores, absolute dates are preferred for setting changes in a chronological context and for calculating rates of carbon accumulation. A wide range of tools is available depending on the time frame of interest, the site location and history, and the peat type. The use of multiple techniques is recommended, if possible, to minimise dating error (Turetsky *et al.,* 2004; Le Roux and Marshall, 2011). Radiometric dating methods including radiocarbon (^{14}C) and lead-210 (^{210}Pb) will be discussed in this section, as well as some additional stratigraphic markers.

2.3.1 Radiocarbon dating

The most common method for dating peat is measuring carbon-14, or radiocarbon (^{14}C). The principles were developed in the 1940s and can theoretically be used for dating samples up to *ca*. 50,000 years of age (Reimer *et al.,* 2013). Here, the method is considered for dating recent peat.

2.3.1.1 *C isotopes*

Plants take up CO_2 during photosynthesis. In C_3 plants such as *Sphagnum* mosses and peatland vascular plants, the carbon-fixing enzyme RuBisCO discriminates against $^{13}CO_2$. The fractionation of C isotopes is the foundation of the radiocarbon dating method, as ^{14}C is heavier than the natural stable ^{13}C and ^{12}C isotopes (Table 2.1), and plants preferentially take up the lighter $^{12}CO_2$ (Farquhar *et al.,* 1989).

Table 2.1 Natural isotopes of C

Isotope	Protons	Neutrons		Abundance
^{12}C	6	6	Stable	98.93%
^{13}C	6	7	Stable	1.07%
^{14}C	6	8	Unstable	10^{-10}%

Factors such as temperature directly affect the stable C fractionation in C_3 peatland plants, as metabolism increases in mosses, the discrimination against $^{13}CO_2$ is reduced and the $\delta^{13}C$ values, or ratio between stable isotopes, increase; altitudinal gradient (CO_2 partial pressure) and humidity (stomatal conductance) also affect fractionation (Ménot and Burns, 2001).

As well as being key to the radiocarbon calibration process, $\delta^{13}C$ also has been used to help to determine bog surface wetness and serve as a potential indicator for methane flux in Canadian *Sphagnum* peatlands (Loisel *et al.,* 2009, 2010), however correlations between *Sphagnum* α-cellulose $\delta^{13}C$ with surface moisture gradients and other proxies, including temperature, were not consistent. In New Zealand vascular peatland plants, $\delta^{13}C$ was found to be significantly negatively correlated with temperature, photosynthetically active radiation (PAR) and growing degree days > 0^{o}C (GDD0); in contrast, there was no significant relationship with precipitation, relative humidity, soil moisture or water table depth (Amesbury *et al.,* 2015).

2.3.1.2 *^{14}C dating principles*

Unstable ^{14}C, a cosmogenic nuclide, is produced in the upper atmosphere by the collision between nitrogen (N) atoms and cosmic rays (Libby *et al.,* 1949). Living peatland plants absorb $^{14}CO_2$, and upon their death, the level of ^{14}C is equivalent to that in the atmosphere. ^{14}C decays into stable ^{14}N with a half-life of 5730 ± 40 years (Libby's half-life, used by convention). Using standard decay equations, a radiocarbon age for the organism's death can be calculated based on the half-life, then calibrated.

C isotopes (^{12}C, ^{13}C and ^{14}C) are separated and corrected using a known standard (Oxalic Acid 1 for organic material: $\delta^{13}C$ -25‰ for wood). Historically, bulk material was used for dating as large sample sizes (5-10g) were required in order to use radiometric methods to measure decay emissions for a given period. This meant a potential for error due to sample contamination and reduced dating resolution. More recently, advances in Accelerator Mass Spectrometry (AMS) technology, where the number of ^{14}C atoms is measured, meant that smaller samples (1-10 mg C) and individual plant remains can be dated, allowing for higher dating resolution and reduced age uncertainty (Blaauw *et al.,* 2003). The principle of radiocarbon dating relies on the assumption that the material dated is representative of annual growth, thus ensuring that the ^{14}C is from atmospheric $^{14}CO_2$ at the time of deposition. This means that sample selection is important; for instance, roots should be avoided, while ericaceous leaves and seeds are preferable. *Sphagnum* remains were found to be the most reliable material for dating peat, as measurements from a range of *Sphagnum* species did not differ in absolute C, and did not differ from the atmospheric level; they also did not assimilate 'old' CO_2 in large enough quantities to affect dates (Nilsson *et al.,* 2001).

2.3.1.3 *Calibrating ages and modelling age-depth relationships*

Atmospheric ^{14}C has not been constant over time, and radiocarbon ages need to be calibrated in order to obtain 'real' ages. Calibration curves were developed using known dates such as tree rings or other annually resolved varves in lake cores; the most commonly used are the IntCal curves (Reimer *et al.,* 2009, 2013). These curves can be used to calibrate single dates, or to generate age-depth models. Programmes, such as CALIB 7.1 (http://calib.qub.ac.uk/calib/) or OxCal 4.2 (Bronk Ramsey, 2009), and R packages (R Development Team, 2014) including clam 2.2 (CLassical Age-depth Modelling: Blaauw, 2010) and BACON 2.2 (Bayesian ACcumulatiON: Blaauw and Christen, 2011) can be used to calibrate and model dates using the latest IntCal13 curve.

'Classical' age-depth models (e.g. clam) use linear interpolation or spline modelling, not considering error or assuming an even error distribution around the calibrated age (Telford *et al.,* 2004; Parnell *et al.,* 2011). Wiggle-matching AMS dates can be used to obtain high-resolution chronologies by matching uncalibrated dates with 'wiggles' in the calibration curve using a linear regression model (Blaauw and Heegaard, 2012). Wiggle matching can require a large number of individual dates, or dates spanning more than one 'wiggle', and therefore may not be suitable for some project designs and time periods. Wiggle-matching is most reliable in sections of the calibration curve with the most pronounced 'wiggles', such as the Little Ice Age (Mauquoy *et al.,* 2002a,b). The use of Bayesian statistics in age-depth modelling (e.g. BACON or OxCal) combines measured data with prior knowledge about the site, including surface age and accumulation rates, and runs millions of iterations in order to obtain the most likely age estimate (Yeloff *et al.,* 2006b; Parnell *et al.,* 2011). Calibration problems can arise when an age or around one of the calibration curve 'plateaus', which can result in ages with large errors (examples in Figure 2.4). The post-1950AD (0 BP, before present) can be difficult to date as atmospheric C isotope ratios were altered by nuclear testing and anthropogenic factors such as increased fossil fuel consumption (Garnett *et al.,* 2000). Recent carbon accumulation rates calculated using only a few ^{14}C dates, especially dates with large errors within the last few centuries, may need to be evaluated with care.

2.3.1.4 *Key assumptions*

Major sources of error include: (1) dating error due to sample composition, (2) hiatuses causing sudden changes in peat accumulation, (3) changing accumulation rates, and (4) sampling error from contamination (Kilian *et al.,* 2000). The main assumption of ^{14}C dating is that age increases with depth. While hiatuses, if known, can be included into age-depth relationships, models cannot be constructed in the event of age reversals due to sediment mixing, e.g. cryoturbation in permafrost soils (Blaauw *et al.,* 2004a).

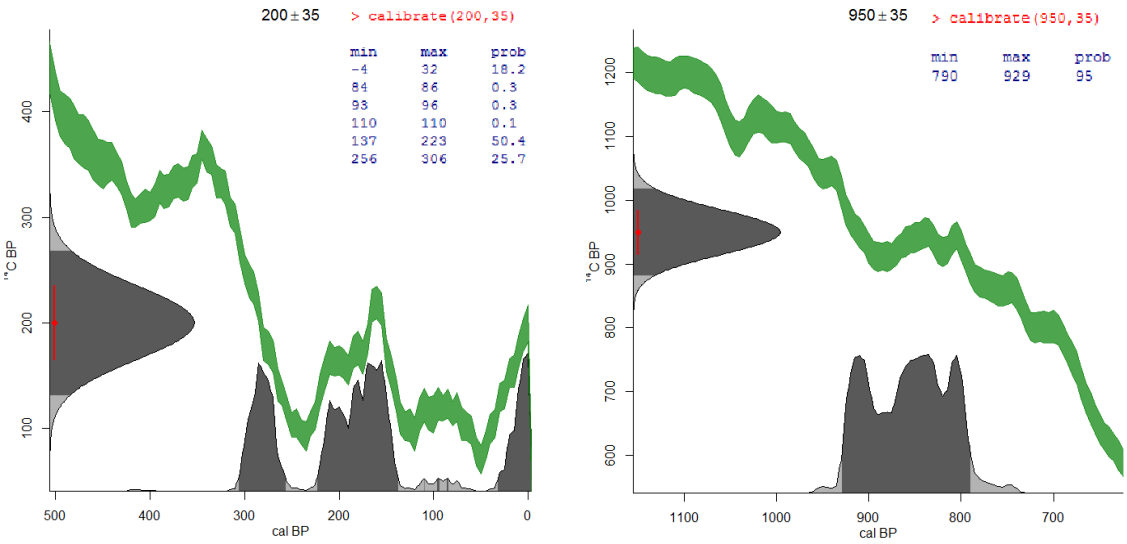

Figure 2.5. Examples of single radiocarbon date calibrations using clam v2.2 (Blaauw 2010; R Development Team, 2014). Green: calibration curve (IntCal13); grey: probability distributions; left: along a 'plateau', right: higher probability, smaller error range.

Dating small plant remains was only made possible by technological AMS advances, allowing for greater precision with much less material. However, as AMS analysis relies on the ^{14}C concentration in the sample rather than the activity and decay, contamination can become a large source of uncertainty. The preparation techniques can also affect the radiocarbon age, where results were different for non-treated (deionsed water-washed) and alkali treated samples, as well as the for the different size fractions for each sample (Nilsson *et al.,* 2001). Indeed, age differences between humic acids and corresponding humin fractions were reported without correlation with humification, pollen or δ13C (Shore *et al.,* 1995).

A 'reservoir' effect from fungus contamination was proposed by Kilian *et al. (*1995) for hummock and hollow cores, wherein 'old' carbon, in particular methane from deeper peat fixed by mycorrhizal fungi, is recycled. It was also suggested that CO_2 rising through the peat profile from catotelm decomposition may have become incorporated. For instance, pure *Sphagnum* samples containing 2-4% ericaceous rootlets were 100-150 years too old; this was in contrast to expected results, as the presence of roots should increase the relative proportion of modern carbon (Kilian *et al.,* 1995, 2000).

Blaauw *et al. (*2004b) found no evidence of this effect in a relatively dry hummock core; however, dating samples containing rootlets and bulk samples should generally be avoided.

2.3.2 Lead-210 dating

Lead-210 (^{210}Pb) dating is an alternative to ^{14}C dating for the last *ca.* 150-200 years, providing a continuous record of absolute dates for this period. It was first introduced by (Goldberg, 1963) as a dating technique and has since been adapted for peatlands.

2.3.2.1 *Basic principle*

^{210}Pb and other radionuclides are atoms with unstable nuclei that undergo alpha (α) or beta (β^-) radioactive decay by emitting or receiving subatomic particles. It is a product of the decay series of uranium-238 (^{238}U), a primordial nuclide found in all soil, sediment and rocks (Appleby and Oldfield, 1978; Turetsky *et al.,* 2004; Le Roux and Marshall, 2011). ^{210}Pb decays to stable lead (^{206}Pb) via 2 daughter isotopes: bismuth-210 (^{210}Bi, β^- decay, $T_{1/2}$ = 5.01 days) and polonium-210 (^{210}Po, α-decay, $T_{1/2}$ = 138.4 days); because of their relatively short half-lives, they rapidly reach equilibrium with ^{210}Pb (Table 2.1; Figure 2.6).

Table 2.2 ^{210}Pb decay information (adapted from Ebaid and Khater, 2006 and Matthews *et al.,* 2007).

Parent isotope	Daughter product	Half-life ($T_{1/2}$)	Decay type	Activity
^{210}Pb	^{210}Bi	22.4 y	β^-	16 and 63 keV
			γ	46.5 keV
^{210}Bi	^{210}Po	5 d	β^-	1.2 MeV
^{210}Po	^{206}Pb	138 d	α	5.3 MeV

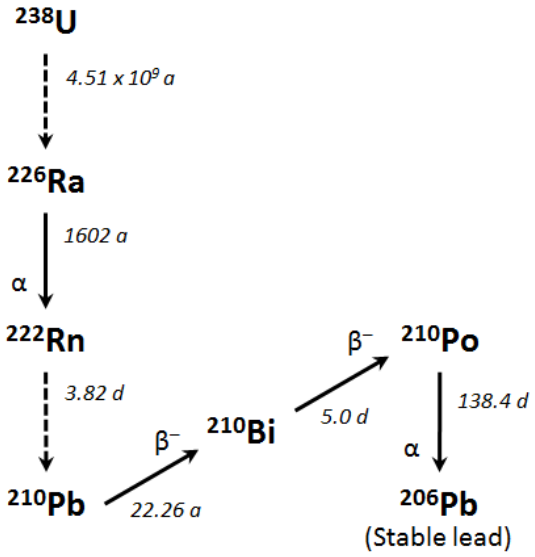

Figure 2.6 Partial decay chain of the uranium or radium series. This terminates with stable lead (^{206}Pb). Also indicated are decay mode (α or β^- particle emitted) and half-lives ($T_{1/2}$) in italics (a = years, d = days) of selected decay products. Dotted lines indicate where some elements have been omitted. Adapted from Eakins and Morrison (1978).

In the soil, ^{238}U decays to radium-226 (^{226}Ra, $T_{1/2}$ = 1602 years), then to inert radon-222 (^{222}Rn, $T_{1/2}$ = 3.82 days) gas, which then decays in the soil or in the atmosphere through short-lived isotopes to ^{210}Pb ($T_{1/2}$ = 22.26 years). The total ^{210}Pb pool in the soil, sediment or peat includes: 1) the **supported fraction ($^{210}Pb_{sup}$)** produced by *in situ* radioactive decay of ^{222}Rn, and 2) the **unsupported or excess fraction ($^{210}Pb_{ex}$)** from ^{222}Rn gas diffused into the atmosphere, decayed into ^{210}Pb and removed from atmosphere through wet deposition and dry fallout (Figure 2.7) (Turetsky *et al.,* 2004; Le Roux and Marshall, 2011). The residence time of ^{210}Pb in the atmosphere is *ca.* 15 days; the deposition rate varies depending on local geology (uranium concentrations in the rocks and soils) and precipitation patterns (Matthews *et al.,* 2007). The main component of the total ^{210}Pb pool for ombrotrophic bogs is the unsupported fraction ($^{210}Pb_{ex}$) as the main inputs are from precipitation (Figure 2.7); the supported fraction ($^{210}Pb_{sup}$) can be measured in deeper peat samples.

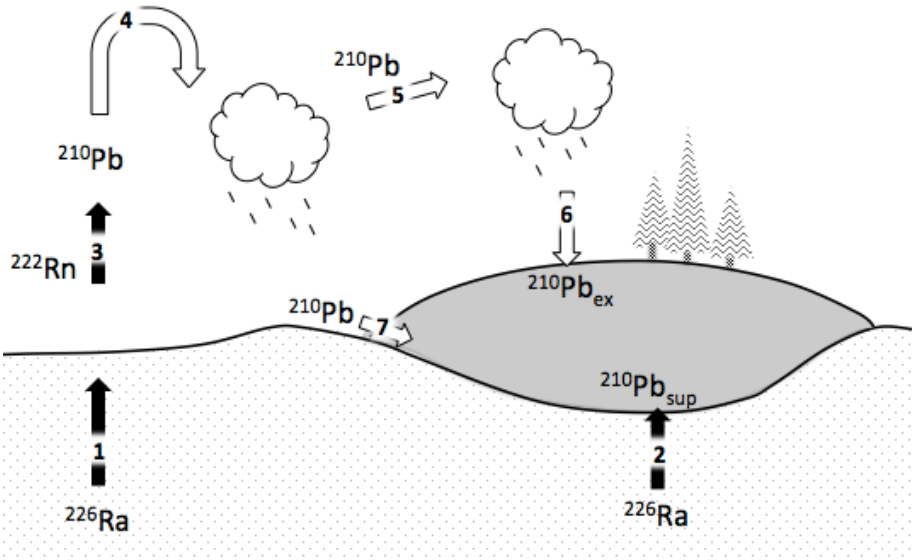

Figure 2.7 Pathway of ^{210}Pb formation, transport, deposition and accumulation in peat. Naturally occurring ^{238}U decays in the surrounding soil/rock into ^{222}Rn which either: decays in situ (1) and is leached to the mineral surface (2) into $^{210}Pb_{sup}$ (the supported fraction); or is emitted into the atmosphere (3) where its daughter product ^{210}Pb is bound to atmospheric particles (4), transported (5) and is subsequently deposited by dry fallout or precipitation (6) (unsupported or excess fraction, $^{210}Pb_{ex}$). ^{210}Pb can also be transported via runoff (7), contributing to $^{210}Pb_{sup}$. Adapted from descriptions in Turetsky *et al. (*2004).

The basic principle of radiometric dating is to compare the number of half-lives since decay began by comparing the number of parent isotopes remaining to daughter products present. Quantifying particle emissions resulting from the decay of ^{210}Pb or one of its daughters in a sample by measuring the specific energy released allows for the calculation of sample-specific activity (in Bq kg^{-1} where 1 Bq is equivalent to 1 disintegration per second); in a core, each sample activity can then be compared to the total $^{210}Pb_{ex}$ inventory in order to provide absolute and continuous dates for *ca*. last 150 years, or 7 half-lives relative to the 'present', i.e. the date of sample collection.

2.3.2.2 *Review of methods*

There two main methods used for measuring ^{210}Pb activity in peat, either directly or indirectly by measuring decay emission spectra (Table 2.2).

Alpha spectrometry (henceforth 'alpha') indirectly measures ^{210}Pb activity by ^{210}Po decay. Gamma-ray spectrometry ('gamma') directly measures ^{210}Pb (Appleby, 2001). These are evaluated in the following section. A third method, beta spectrometry ('beta') indirectly measures ^{210}Pb activity by measuring ^{210}Bi decay. However, this method has not been used for peat, and rarely used for other sediments and soils (Turetsky *et al.,* 2004). As both ^{210}Pb and ^{210}Bi decay via β^- (emit electron), it is necessary to separate them chemically before measurement, or based on the respective measured energy spectra (Le Roux and Marshall, 2011). Beta will not be considered beyond this point.

Alpha spectrometry (α) indirectly measures ^{210}Pb activity by counting the number of alpha particles emitted during decay over time of its daughter product, polonium-210 (^{210}Po). Alpha particles have 2 protons and 2 electrons ($^4_2$He). ^{210}Po must first be chemically extracted from the sample, usually by acid digestion, and along with a chemical yield tracer, or spike, deposited onto a silver disc for counting in an alpha-spectrometer. Analysing ^{210}Po was found to accurately represent ^{210}Pb activity (Eakins and Morrison, 1978; Church *et al.,* 2012). There is no standard published method for ^{210}Pb detection via ^{210}Po using α-spectrometry as resources, laboratory facilities and sample composition varies greatly, even within the same peat core. The original Po extraction method, i.e. electroplating onto a silver disc, was developed to monitor polonium in effluent without much organic matter (Flynn, 1968). It was adapted for lake and marine sediments (Eakins and Morrison, 1978) and for aquatic deposits with higher organic contents (El-Daoushy *et al.,* 1991).

Gamma spectrometry (γ) directly measures weak γ-rays emitted during ^{210}Pb decay. During this process, the daughter nucleus that results from ^{210}Pb decay is usually left in an excited state; it can then decay to a lower energy state by emitting a gamma ray photon (Tanner *et al.,* 2000). However, only a small fraction of ^{210}Pb decays emit gamma rays (4%) and these are often below the lower detection limits for many

gamma counters in deeper samples. It requires larger sample sizes (5-10 g) that may not be available in the case of peat samples with low bulk densities. Large sample sizes may also cause problems with self-absorption of the gamma ray, which needs to be corrected (e.g. Miller, 1987). However, self-absorption is less of an issue and this method is used increasingly as detector technology improves (Tanner *et al.,* 2000). This technique requires minimal processing; samples are dried, ground, weighed and stored for a minimum of *ca.* 21 days for secular equilibrium between ^{222}Rn and ^{210}Pb before being placed in a gamma counter. In addition, independent chronostratigraphic markers can be measured in parallel including the artificial radionuclides caesium-137 (^{137}Cs) and americium-241 (^{241}Am) (Turetsky *et al.,* 2004; Le Roux and Marshall, 2011).

Measurement techniques vary in sample requirements, cost, preparation method and analysis time (Table 2.3). Indeed, there is no standard method for sample preparation for alpha-spectrometry; well-established methods (Flynn, 1968; Eakins and Morrison, 1978) are less than effective for peat samples with a high organic content (~90% organic matter) and currently there is variety in preparation between labs based on resources available (De Vleeschouwer *et al.,* 2010). Inter-method comparisons of alpha and gamma measurement techniques have been done on lacustrine (Sikorski and Bluszcz, 2008), estuarine (Tanner *et al.,* 2000) and marine sediments (Zaborska *et al.,* 2007) as well as soil and geological sediment (Ebaid and Khater, 2006); however, none have yet been published for peatlands.

2.3.2.3 *Modelling dates*

While sample-specific ^{210}Pb activity measured using either alpha or gamma detection methods is debated, the same models are applied to these data typically used to calculate ages, sedimentation rates, ^{210}Pb inventories and fallout rates.

Table 2.3 Parameters of analytical techniques for the determination of ^{210}Pb in environmental samples; adapted for peat from (Ebaid and Khater, 2006) unless otherwise indicated.

	Alpha	**Beta**	**Gamma**
Sample size (g)	0.1[a]-3[b]	5	5-10[c]
Sensitivity (s^{-1} Bq^{-1})	5	2.5	2.9 x 10^{-4}
Background (counts min^{-1})	0.005	0.5	0.5
Counting efficiency	20	40	7
MDA (mBq per 1000 min)	1	7.1	440
Duration of prep. (no. days)	1-3[d]	> 10	1 (+21)[e]

1 Bq = 1 Becquerel = equivalent to 1 radioactive disintegration per second; MDA = minimum detectable activity;

[a] minimum sample size (Pratte, Mucci, & Garneau, 2013);

[b] max sample size (Vile *et al.,* 2000);

[c] (Parry *et al.,* 2013);

[d] Olid *et al. (*2008) suggest that surface samples should equilibrate ^{210}Pb/^{210}Po for 3-6 months, or up to 2 years;

[e] samples should be sealed for 21 days for ^{222}Rn/^{210}Pb to reach secular equilibrium (Tanner *et al.,* 2000).

There are three basic models (reviewed in detain in Appleby, 2001, 2008; Turetsky *et al.,* 2004): (1) the constant flux-constant sedimentation (CF-CS) model assumes a constant rate of ^{210}Pb input as well as a constant sediment accumulation rate (e.g. some lake cores); (2) the constant rate of supply (CRS) model assumes a constant rate of fallout ^{210}Pb to the surface irrespective of accumulation rates (Appleby and Oldfield, 1978) which is more appropriate for peatlands where peat accumulation varies but ^{210}Pb deposition is assumed to be constant in the long-term; and (3) the Constant Initial Concentration (CIC) model assumes that ^{210}Pb supply and accumulation rate vary directly and is more suited to systems with additional sources of ^{210}Pb influx, such as from groundwater or runoff.

Applying the CRS model requires estimating the supported lead, $^{210}Pb_{sup}$. In ombrotrophic peatlands, it can be estimated by measuring ^{210}Pb activity in deeper peat. However, the unsupported $^{210}Pb_{ex}$ activity becomes statistically undetectable against the instrumental background or $^{210}Pb_{sup}$ after 7-10 half-lives, or close to 150-200 years

(Evans *et al.,* 1986; Turetsky *et al.,* 2004; Le Roux and Marshall, 2011). In addition, as counting error is high when the number of counts is low, the error in sample age increases with depth (Turetsky *et al.,* 2004) and ages may be overestimated (MacKenzie *et al.,* 2011). This highlights the importance of using a combination of dating methods to validate deeper ages.

2.3.2.4 *Key assumptions*

The $^{210}Pb_{ex}$ fraction is mainly influenced by atmospheric flux and residence time; however, post-depositional processes such as bioturbation, cryoturbation, surface runoff and potential down-core mobility are also important. Main assumptions of this dating technique are: (1) a constant and even supply of ^{210}Pb to the surface, and (2) post-depositional immobility in the peat column.

^{210}Pb supply to an ombrotrophic peatlands depends on surrounding stratigraphy and precipitation and wind patterns. While there are estimates for regional deposition (e.g. Appleby, 2001; Le Roux and Marshall, 2011), within-site deposition and the effect of microtopography have not been widely studied. In addition, recent studies have been investigating the validity and applicability of the CRS method due to local factors such as mine effluent and volcanism (Matthews *et al.,* 2007) and increased external fossil fuel contamination which may cause a 20% difference in $^{210}Pb_{ex}$ estimates (Olid *et al.,* 2013) which has important implications for resulting calculations of carbon accumulation and sedimentation rates. Accurately accounting for these factors is important in peatland areas where recent ^{210}Pb dating is being considered because of recent environmental changes.

Down-core mobility has been reported with lower total inventories in hollows and fluvial losses of up to 75% of total ^{210}Pb (Urban *et al.,* 1990) as well as with ^{210}Pb accumulation around the zone of water table fluctuation (Damman, 1978). However, other studies disagree with this, showing that ^{210}Pb dating is reliable technique for

peatlands by core replication and agreement of dates and inventories between profiles (e.g. Parry *et al.,* 2013). ^{210}Pb-derived dates were also found to agree with independent chronostratigraphic markers including artificial radionuclides from nuclear testing (^{137}Cs and ^{241}Am), ^{14}C bomb-spike and pollen horizons (Oldfield *et al.,* 1995). This is mainly due to the ombrotrophic nature of peat and the high cation exchange capacity (CEC) of *Sphagnum* moss; heavy metal cations (Pb^{2+} and Zn^{2+}) have been shown to bind preferentially to humic acids over base metal cations (Ca^{2+}, Mg^{2+}, K^{+} and Na^{+}) (Bunzl *et al.,* 1976; Clymo *et al.,* 1990; Wieder, 1990; Vile *et al.,* 1999). In order to gauge whether any irregularities in the ^{210}Pb profile may be due to disturbance or mobility, the method for estimating activity must be reliable.

2.3.3 Chronostratigraphic markers

Using a combination of dating techniques is recommended to reduce the uncertainties associated with a single method. This thesis considers only ^{14}C and ^{210}Pb dating; however, some alternative and complementary methods, which can be used as independent markers to date single events, are briefly reviewed here.

2.3.3.1 *Fallout radionuclides*

Caesium-137 (^{137}Cs, $t_{1/2}$ = 30.2 years) and americium-241 (^{241}Am, $t_{1/2}$ = 432.2 years) were released into the atmosphere as a result of nuclear weapons testing throughout the 1950s and early 1960s. If detected, activity peaks can be used to date a core at 1963AD when the Limited Test Ban Treaty was signed against aboveground nuclear testing, and at 1986AD, the date of the Chernobyl accident in Ukraine (Turetsky *et al.,* 2004; Le Roux and Marshall, 2011). The global distribution of these radionuclides varies based on precipitation and wind patterns; detecting the Chernobyl peak is variable in Europe and difficult to detect in the Southern Hemisphere (Cambray *et al.,* 1989).

^{210}Pb, ^{137}Cs and ^{241}Am can be measured together using gamma spectrometry. While ^{137}Cs has often been found to be highly mobile with fluctuating water table depth and biological uptake in acidic peat (Schell *et al.,* 1989; Urban *et al.,* 1990; MacKenzie *et al.,* 1997), ^{241}Am is relatively static in the peat column than ^{137}Cs (Clymo *et al.,* 1990; Oldfield *et al.,* 1995; Parry *et al.,* 2013) and may be more useful in the long-term as it has a longer half-life. If peaks are detected, these markers can provide valuable constraints for very recent decadal peat accumulation.

2.3.3.2 *Tephrochronology*

Tephra are shards of ash deposited by volcanic eruptions. If detected, tephra layers can be geochemically correlated to known and dated eruption events, which each have a unique chemical signal. Shards are deposited as isochrons in peat layers and can be correlated between archives and to linked to eruptions with fixed ages (Lowe, 2011; Swindles *et al.,* 2011). They have been found to be geochemically stable and maintain their integrity both in the peat profile and during the extraction and preparation method (Dugmore *et al.,* 1992). Microscopic shards, or cryptotephra (< 125 μm; Swindles *et al.,* 2011) can be transported thousands of km downwind from a volcano. Alaskan and North Pacific eruptions have been detected on the East Coast of North America (transport > 7000 km) (Mackay *et al.,* 2016). The White River Ash eastern lobe (*ca.* 841AD, Alaska) has been detected from Newfoundland to Maine (Pyne-O'Donnell *et al.,* 2012), while the Mount St Helens Set W (1479-1482AD) and potential sources from the tropics (Mexico), from Japan (Hokkaido) and from Russia (Kamchatka) have also been detected at some sites for the last 2000 years (Mackay *et al.,* 2016).

Tephra deposition depends on wind and precipitation conditions, and shard counts can vary within the same peatland by an order of magnitude, as their distribution is patchy (Watson *et al.,* 2015). Shards can also be mobile in the peat profile, e.g. down-core mobility through a porous acrotelm or along root channels, and detection methods can

be time-consuming, especially at the distal end (Gehrels *et al.,* 2008). Chronologies have also been found to be affected by reworked tephra released to the atmosphere by the burning of peatlands and associated erosion (Swindles *et al.,* 2013).

2.3.3.3 *Pollen stratigraphy*

Changes in pollen abundance or species composition may provide another dating marker and can record changes in vegetation cover due to disease, range expansion, or changes in land use such as agricultural practices (Turetsky *et al.,* 2004). Records of disease or migration and settlement are necessary to establish absolute dates and relative timing. Some examples of often-used pollen records include changes in the abundance of ragweed (*Ambrosia*) in North America, associated with the settlement by Europeans (e.g. Truman, 1937; Brugham, 1978). As the westward migration of people across North America has been well-documented, this can be a reliable marker. In North America, the decline of arboreal pollen and the arrival of non-endemic pollen types to an area are also associated with the spread of agriculture (Brugham, 1978). The spread of tree-borne diseases in North America and Europe has also been well-documented; for instance, declining abundance in chestnut (*Castanea dentata* (Marsh.) Borkh.) pollen began in New England in 1912AD due to the spread of chestnut blight (Wieder *et al.,* 1994), and Dutch Elm disease has been linked to declining *Ullnus* pollen on both sides of the Atlantic (e.g. Cole *et al.,* 1990).

This technique does not yield continuous chronologies, and as with other dating techniques, it assumes post-depositional immobility. As the preparation and counting pollen grains for abundance measurements are time-consuming , this method is best used in conjunction with other dating techniques (Turetsky *et al.,* 2004). Bonk *et al. (*2015) compared varved lake sediments from Poland, and validated dates with a combination of methods, including ^{137}Cs peaks, tephra (1875AD), major known land

use changes recorded from pollen analysis, and 32 AMS 14C dates. They found good agreement between records for the last millennium.

2.3.3.4 *Charcoal*

Charcoal particles are deposited during wildfilres and are the result of incomplete combustion. Unlike pollen, charcoal is produced irregularly but in large quantities. Particle quantity and form depend on fire intensity, the nature of the source material, and dispersal modes including wind and precipitation. Charcoal horizons can be correlated between cores or dated if the fire event date is known; fire histories and recurrence patterns can also be established (Patterson *et al.,* 1987). Anthropogenic events and large-scale climatic changes can also be detected, such as the rise of agriculture and deforestation, or Spruce establishment, respectively (Pitkänen et al 2003). Climatic signals from fire histories can be hidden by local vegetation changes and stand-level differences fire regimes (Gavin *et al.,* 2006).

Charcoal distribution has found to be heterogeneous in some peatlands, with particles only detected at the edges or on hummock tops (van Bellen *et al.,* 2012). Spatial variability can be considerable in concentration and in botanical assemblages, even for neighbouring peatlands, e.g. 350x difference within a few m (Touflan and Talon, 2009; Kasin *et al.,* 2013). Results from experimental forest burns using traps showed that macroscopic charcoal was unevenly distributed within the burn area for a single event with 14% of traps showing no charcoal deposition (Ohlson and Tryterud, 2000). Therefore, while the presence of large charcoal particles indicate fire, the absence of charcoal does not mean that there was no fire. Charcoal particles may also be re-circulated, e.g. laterally by wind, or vertically by water (Patterson *et al.,* 1987). While a 10% background rate of microscopic charcoal particles was measured in the North Yorkshire Moors, most were deposited near the source (Innes and Simmons, 2000).

2.3.3.5 *Anthropogenic markers*

These include lead isotopes and other heavy metal contaminants, as well as Spheroidal Carbonaceous particles (SCPs), the concentrations or ratios of which have been altered from the natural background fluxes by anthropogenic and industrial activities (Bollhöfer and Rosman, 2001; Turetsky *et al.,* 2004).

Ratios of stable lead isotopes, mainly $^{206}Pb/^{207}Pb$ but also $^{206}Pb/^{204}Pb$, $^{207}Pb/^{204}Pb$ and $^{208}Pb/^{204}Pb$, can be used to distinguish between natural atmospheric Pb deposited from soil dust and precipitation, and anthropogenic sources of Pb such as coal burning, mining, smelting, waste incineration and fossil fuel combustion(Shotyk *et al.,* 1998; Komárek *et al.,* 2008). Sources of Pb were found to be generally local (< 10 km) or regional (< 500 km), and did not reflect hemispheric or continental-scale dispersal (Kylander *et al.,* 2010), and while regional concentrations vary, pre-industrial concentrations in Europe are of a similar level to present-day concentrations in remote areas of North America (Komárek *et al.,* 2008). Other metals can also be measured, including arsenic (As), cadmium (Cd), nickel (Ni), aluminium (Al) and zinc (Zn) documenting metallurgy, industrial and mining processes, and agricultural practices where fertilisers are used (e.g. Bollhöfer and Rosman, 2001; Pratte *et al.,* 2013). Pb is relatively immobile in peat (e.g. Weiss *et al.,* 1999); however, it was shown in the early 2000s, up to 98% of the Pb deposited was from re-suspended city soil contaminated by lead gasoline in a site in Armenia (Kurkjian *et al.,* 2001).

Roman and Medieval periods have been recorded from the increase in mining and ore exposure to the atmosphere (Le Roux *et al.,* 2004). The rise and fall of lead gasoline use can be recorded throughout the 20th century, from the 1920s to late 1970s when it was phased out in North America (Weiss *et al.,* 1999; Pratte *et al.,* 2013). The collapse of the Soviet Union was also detected in Armenia, where the drop in industrial activity was visible in the Pb profiles (Kurkjian *et al.,* 2001). Anthropogenic sources have been

dominant since *ca*. 3000 a BP, and while recent efforts to remove lead from industry processes and gasoline have reduced the overall anthropogenic sources, the present rate of Pb deposition is orders of magnitude higher than the background rate (Shotyk *et al.,* 2000).

SCPs are also emitted from fossil fuel combustion since the Industrial Revolution; their shape and size depends on the source (e.g. wood, coal, or oil combustion) and their density depends on the regional industrial history. This technique has been shown to be more or less in agreement with ^{210}Pb dates in Dartmoor in the UK (Parry *et al.,* 2013).

2.3.4 Dating summary

Projects considering recent peat accumulation should use a combination of multiple dating methods. As peat and carbon accumulation rates can change quickly over time, reliably dating recent samples with limited resources can be an issue due to the large ^{14}C dating uncertainties for the last *ca.* 200 years. Dating methods rely on assumptions of post-depositional immobility, and mobility of ^{210}Pb and other artificial radionuclides (^{137}Cs and ^{241}Am) has been highlighted as an area of concern. Using replicate cores may reduce some of the uncertainty related to natural variability; this is a novel approach and could clarify pre- and post-depositional patterns.

2.4 Regional context

2.4.1 Late Holocene climate change

Climate model prediction capabilities are tested and improved by including data from periods outside their calibration range (Cox and Jones, 2008; Jungclaus *et al.,* 2010). The last 1,000 years of change are particularly relevant as a target for modelling future change for several reasons. First, the magnitude of climate shifts is of a similar scale to

present conditions (Braconnot *et al.,* 2012; Charman *et al.,* 2013). Second, records are less likely to include differences due to large-scale autogenic changes such as limits to growth (Clymo, 1984; Belyea and Clymo, 2001) or lateral and vegetation range expansion (MacDonald *et al.,* 2006). Finally, climate models are able to reliably replicate temperature changes that occurred over this period (Frank *et al.,* 2010). Understanding changes in carbon cycling over this period is useful for predicting climate-C cycle sensitivity.

2.4.1.1 *Global trends*

In the long-term, global climate changes are driven by Milankovitch cycles; during the late Holocene, a cooling trend for the Arctic (North of 60^{o}N) was caused by an orbitally-driven reduction in summer insolation (precession of solstices). The last millennium was characterised by an overall cooling trend until 20th century anthropogenic warming; within this period, the warmest temperatures were recorded between 830-1100AD (MCA). Cool Northern Hemisphere temperatures during the Little Ice Age (LIA: *ca.* 1400-1850AD) coincided with a decrease in radiative forcing (Jansen *et al.,* 2007; Mann *et al.,* 2008, 2009; PAGES 2K Consortium, 2013; Wanner *et al.,* 2014). Within the LIA, fluctuating periods of cooler conditions corresponded to solar activity minima (Bard *et al.,* 2000).

In the UK, several studies have linked increasing bog surface wetness with LIA sunspot minima during the last millennium (e.g. Mauquoy *et al.,* 2002b; Wolf and Maunder minima: Turner *et al.,* 2014); however, Schurer *et al. (*2014) suggest that, during this period, solar forcing has played a minor role compared to volcanism and greenhouse gas influences (Sigl *et al.,* 2015). There is global asynchrony of climate responses within these periods, with the LIA reported as cool and dry in North America, and cool and wet in Europe (Schindell *et al.,* 2001). This Neoglacial cooling trend (0.3-0.5^{o}C/1000 years) was reversed since 1950AD, with five of the warmest decades from

the last 2000 years occurring in the 1950-2000AD period, as recorded by lake and ice cores, tree ring records and instrumental data (Kaufman *et al.,* 2009; Figure 4: PAGES 2k Consortium, 2013).

2.4.1.2 *Eastern Canada*

During the early Holocene, Eastern Canada was relatively cool and dry compared to the rest of the country and Alaska, due to the influence of the remaining Laurentide Ice Sheet, which persisted until *ca.* 8 ka BP. For the last millennium, temperature gradients varied across the country. The warm MCA was most pronounced in the central regions, while the LIA was most pronounced in the Eastern and Western regions. In addition, precipitation anomalies were inverted: Eastern Canada was relatively cool and dry in the early Holocene while Central Canada was warmest at the time while the West was moist in the early to mid-Holocene (Viau and Gajewski, 2009; 2012: pollen records).

Modern temperature increases in Northern Canada far exceed the natural millennial variability (Viau and Gajewski, 2009; PAGES 2k Consortium, 2013). Recent advances in temperature reconstructions fill the gap for the poorly represented Eastern Canadian boreal regions for the last millennium. July/August Summer Temperature Records for Eastern Canada were constructed using: (1) a dendrochronological record from *Picea mariana* tree ring widths (STREC: Gennaretti *et al.,* 2014), and (2) a record of changes in oxygen isotope ratios (i-STREC: Naulier *et al.,* 2015). Both records are similar to widely-used pollen temperature records for the region by Viau and Gajewski (2012). There are differences between the temperature curves between the two reconstructions in both the timings and the magnitude of temperature changes; tree ring width responds directly to photosynthesis changes and is sensitive to temperature and light availability, while $\delta^{18}O$ responds to solar processes (Naulier *et al.,* 2015). Indeed, the onset and persistence of cold periods recorded in the STREC reconstruction are closely linked with a series of volcanic eruptions, such as the 1257

AD Salamas eruption. The coldest 40 year period in the Quebec/Labrador region was recorded from 1815-1857AD, coinciding with the Dalton Minimum and likely triggered by the Tambora eruption (1815AD) and maintained by solar forcing and the Cosignïna eruption (1835AD) (Gennaretti *et al.,* 2014; Sigl *et al.,* 2015). Cold conditions persisted into the mid-1950s, coinciding with the start of permafrost degradation in northeastern Canada for the last 50 years (Payette, 2004).

The additional oceanic influence in the eastern arctic and subarctic regions of Canada means that the decline of sea ice cover during the last 150 years also affects regional climate for coastal regions; however, there is some decadal variability, with large sea ice retreat recorded in the 1920s followed by an increase in cover from *ca.* 1960-1990AD, likely driven in part by a positive North Atlantic Oscillation (NAO) (Halfar *et al.,* 2013).

2.4.2 Carbon accumulation in northeastern Canada

2.4.2.1 *Peatland distribution*

In Canada, peatlands cover 12% of the area (1.136 million km^2) and contain an estimated 56% of the soil carbon (Tarnocai, 2006). 97% of these peatlands are located in boreal and subarctic regions (Tarnocai *et al.,* 2009) and provide a national sink of 0.03 Pg C/year (Roulet, 2000). Figure 2.8 illustrates peatland % area cover for all of Canada.

Peatlands in Québec currently cover 9-12% of the land; the two regions with significant proportions of peatlands are the Eastmain/La Grande Rivière regions around James Bay in northern Québec, and along the North Shore of the St-Lawrence. Permafrost is distributed along latitudinal gradients, as are major vegetation types (Payette and Rochefort, 2001; Figure 2.9).

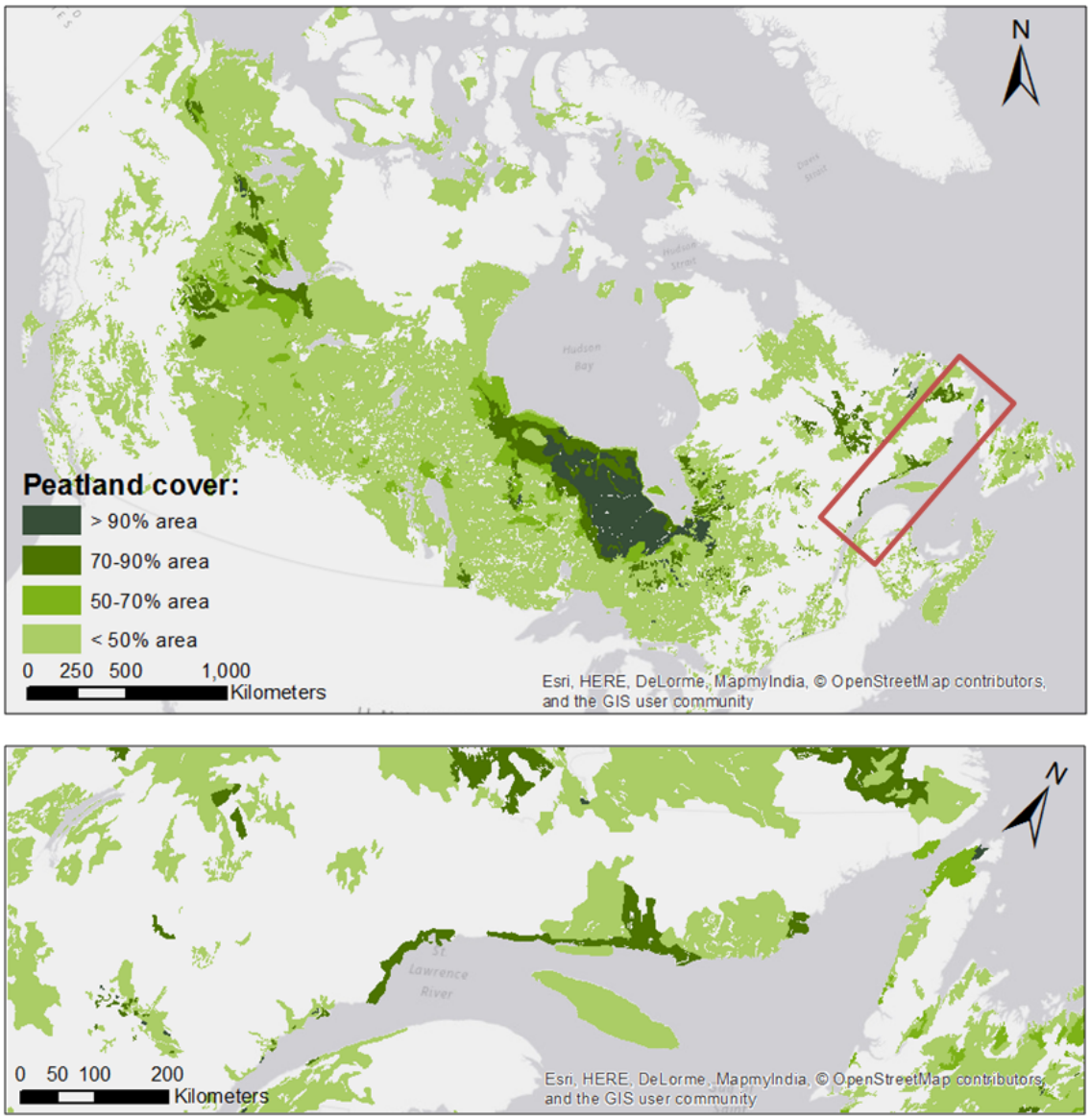

Figure 2.8. Map of peatland cover in Canada (top) and along the North Shore of the St Lawrence in Quebec and Labrador (bottom); map created using shapefiles from Tarnocai *et al.* (2011) in ArcMap 10.2.

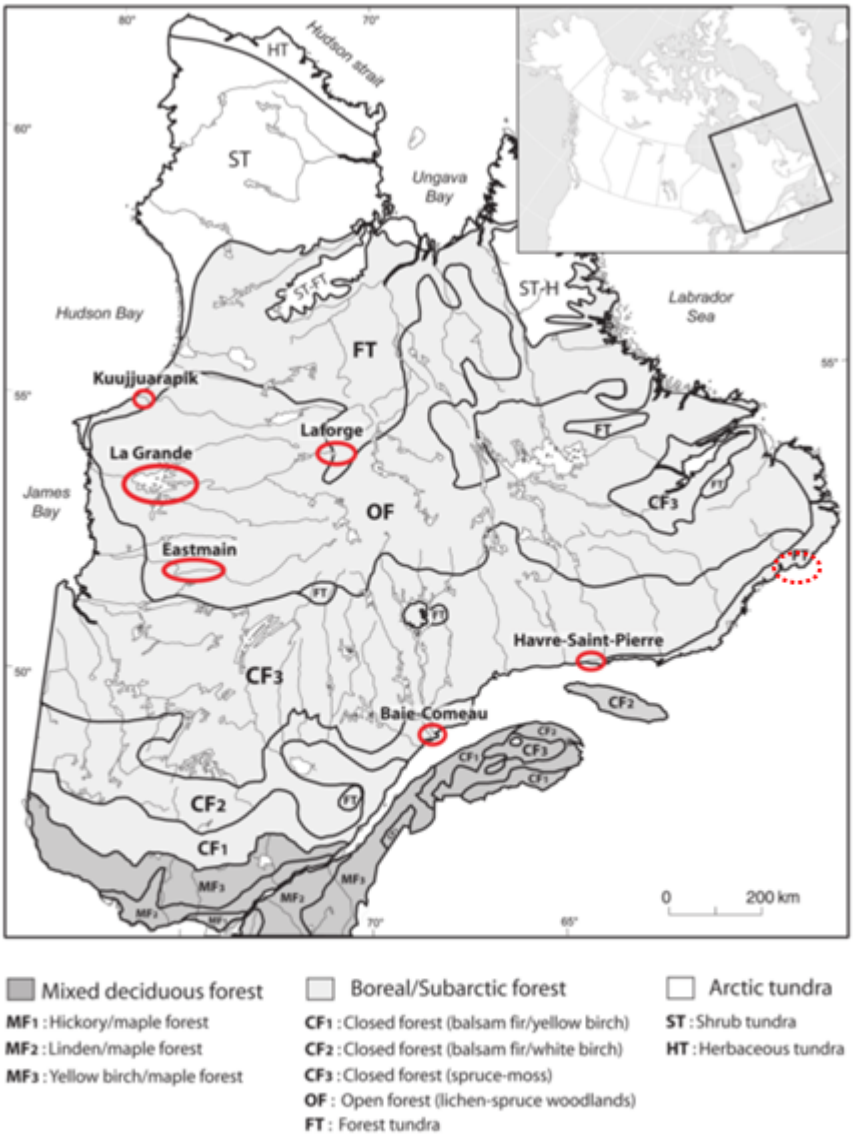

Figure 2.9 Location of the six sites studied in Garneau *et al. (*2014) circled in red, within the bioclimatic regions of Québec, Canada. Work is in progress in the Blanc Sablon region (unpublished, and in this thesis), circled in the red dotted line. The map was originally modified from Payette and Rochefort (2001).

2.4.2.2 *Permafrost and carbon accumulation in Canadian peatlands*

During the transition between the MCA to the LIA, northern peatland C sequestration rates declined globally (slope: -0.0026 g C m^{-2} a^{-1} from 1000-1850AD). The lowest rates of peat and carbon accumulation in northern peatlands during the last millennium were recorded during the LIA, likely due to a combination of decreased spring-summer temperatures, cloudiness, shorter growing seasons and high water tables *Charman et al.,* 2013). Based on climate model scenarios, including a doubling of atmospheric CO_2, ecoclimatic regions are predicted to shift northward with significant changes at the southern limit of the discontinuous permafrost zone (Tarnocai *et al.,* 2009); sensitivity predictions estimate that 53% of the organic carbon stored in Canadian peatlands and 60% of surface peatland areas will be 'severely' to 'extremely severely' affected by permafrost degradation and climate warming (Kettles and Tarnocai, 1999).

Permafrost formed and reached its southernmost extent in Canada during the Little Ice Age (*ca.* 350 cal. BP). Its degradation began around 150-200 years ago in the West (Vitt *et al,.* 2000) and 50 years ago in the East (Payette, 2004), timed with the end of the Little Ice Age for each region. Since the LIA, permafrost has been degrading and this trend is predicted to continue (Payette, 2004). The degradation of palsas and peat plateaus in northern Quebec, established during the LIA, into thermokarst ponds and collapse scars has led to rapid re-establishment of Bryophytes, i.e. terrestrialisation, compensating for emissions (Arlen-Pouliot and Bhiry, 2005; Fillion *et al.,* 2014). In Western Canada, permafrost degradation has been taking place over more than 2500 km^2 of peatlands (Beilman *et al.,* 2001; Vitt *et al.,* 2000) and may have increased regional peatland C stocks by an estimated 100 ± 12 Gg C in total (Turetsky, *et al.,* 2002b). During the LIA, peatland records showed low carbon accumulation rates in individual sites in Quebec (Loisel and Garneau, 2010; van Bellen *et al.,* 2011a; Lamarre *et al.,* 2012; Magnan and Garneau, 2014a). However, the impact of the LIA on

carbon accumulation in Quebec as a whole is likely masked in part by low dating resolution (Garneau *et al.,* 2014).

While methane emissions are projected to rise, the effect of widespread permafrost thaw on the carbon balance in Canada is debated, as system productivity and aerobic decay are both expected to increase (Robinson and Moore, 2000; Turetsky *et al.,* 2000). However, Treat *et al. (*2016) showed that in the short-term (< 1000 years) permafrost degradation leads to higher C accumulation. Turetsky *et al. (*2000) recorded increases in internal lawns of organic matter accumulation by 60%, accelerated during the past 100-200 years with permafrost degradation in Western Canada. CH_4 emissions may therefore be partially offset by this enhanced peatland sink for *ca.* 70 years post-degradation (Turetsky *et al.,* 2007).

2.4.2.3 *Carbon accumulation in North Shore peatlands*

The peatlands along the North Shore of the Gulf of St Lawrence are located in the lower Boreal and Atlantic Subarctic ecozones (NWWG, 1997). They fall within the Eastern North American peatland space as described by Yu *et al. (*2009) (Figure 2.10). While Yu *et al. (*2009) attributed typically low rates of carbon accumulation to the Eastern North American region, local studies in Quebec have yielded variable results (summarised in Garneau *et al.*, 2014; Figure 2.9).

Peatlands along the North Shore of the Gulf of St. Lawrence are of particular interest as they are dense and spread along the coast, and have an average accumulation rate of 42 g C m^{-2} a^{-1}. This rate of accumulation is comparable to other Atlantic peatlands at the same latitude (Sottocornola and Kiely, 2005), and double the global average for the Holocene of 18.6 g C m^{-2} a^{-1} (Yu *et al.,* 2011). At two sites on the North Shore, average long-term rates of carbon accumulation for the Holocene were found to vary depending on initiation substrate (55.2 g C m^{-2} a^{-1} over marine deposits and 30.8 g C m^{-2} a^{-1} over delta peat deposits) and along the Gulf (60.6 g C m^{-2} a^{-1} in the southwestern part and

32 g C m^{-2} a^{-1} further Northeast) (Magnan and Garneau, 2014a) indicating a combination of allogenic and autogenic drivers.

2.4.3 Context summary

Ecohydrological feedbacks from changing permafrost regimes and the influence of the Little Ice Age cool periods on carbon accumulation rates have been well-documented in Western Canada; however, the impact of microtopography changes in Eastern Canada has not yet been studied, and the influence of the LIA has been recorded as variable in continental and some coastal peatlands, in part due to poor dating resolution.

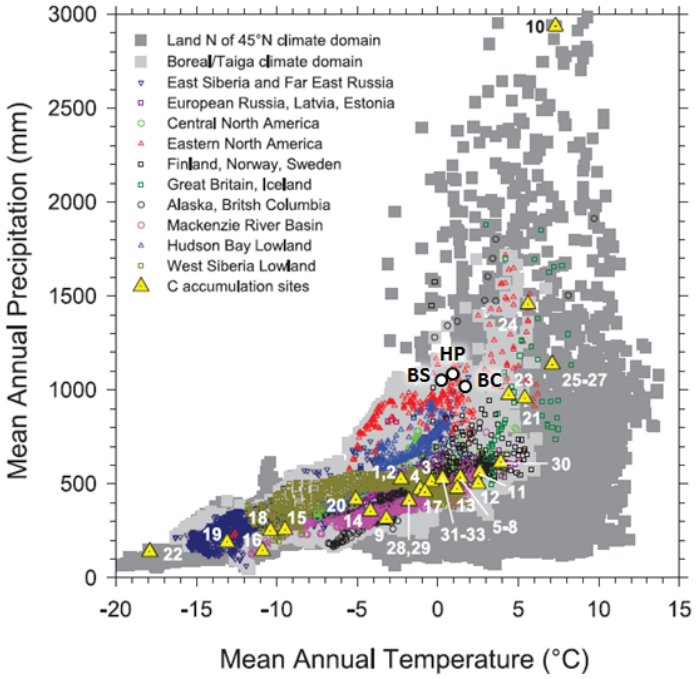

Figure 2.10 The climate space of mean annual temperature and precipitation (T-P space) of total land area north of 45°N (dark grey), the boreal/taiga biome (light grey) and northern peatland regions based on 0.5° x 0.5°-gridded instrumental climate data for the period 1960-1990. The location in climate space of C accumulation sites is shown by yellow triangles for Yu *et al. (*2009); for this thesis, the three sites are shown as black circles.

2.5 Hypotheses

Five main hypotheses have been generated from the literature review and will be addressed throughout the main results chapters.

H1 ^{210}Pb analysis provides reliable dates, i.e. the method is consistent and there is no leaching or mobility. (Ch. 5 and 6)

H2 Within sites, carbon accumulation rates vary along a microtopography gradient; *Sphagnum* hummocks have the highest rates and dry lichen hummocks the lowest. (Ch. 6)

H3 Regional carbon accumulation is influenced along a latitudinal gradient by climate between sites. (Ch. 7)

H4 Age-depth models using a combination of radiocarbon and ^{210}Pb dates allow for the interpretation of decadal patterns in carbon accumulation. (Ch. 7 and 8)

H5 A regional-scale Little Ice Age signal will be detectable and changes over time are due to recent permafrost degradation. (Ch. 7)

3 Research design

This chapter will outlines this unique project design, including:

(1) The coring strategy: selecting replicate cores for statistical analyses;
(2) The rationale for site selection and site characteristics;
(3) Key microform definitions; and
(4) The main methods used throughout the analysis (field sampling, laboratory and data analyses).

3.1 Coring strategy

Palaeoecological reconstructions typically use long cores taken from the central dome within each peatland. However, peat accumulation varies not only between sites (e.g. different stages of development, Belyea and Clymo, 2001) but also within sites with microform type and position along a hydrological gradient (Belyea and Malmer, 2004), due to lateral expansion (van Bellen *et al.,* 2011a) and to annual seasonal variability (Roulet *et al.,* 2007). One of the aims of this thesis is to address within-site as well as between-site changes in carbon accumulation rates (CAR) using replicate cores and statistical analysis. This multi-level replication strategy allows for the distinction between regional (climatic) changes and local variability.

Figure 3.1 is a schematic representation of the coring strategy designed for the fieldwork component of this thesis. Three distinct ecoclimatic regions with different permafrost histories were selected along the North Shore of the Gulf of St. Lawrence (GSL). Within each of the 3 regions (blue ovals), three peatlands (green ovals) were cored (Objectives 3 and 4: n = 9) as near as possible to the central dome. This allows the comparison of CAR between the 3 regions, and to consider variability within each region using one well-dated lawn core per peatland (Figure 3.1: open circles). Within

each peatland, 3-4 microforms were cored depending on the dominant representative microforms of each area (Objective 2: n = 30). Within each peatland (green ovals), rates of carbon accumulation can be compared along wet to dry microtopography gradients for the last 150 years (Figure 3.1: open and closed grey circles).

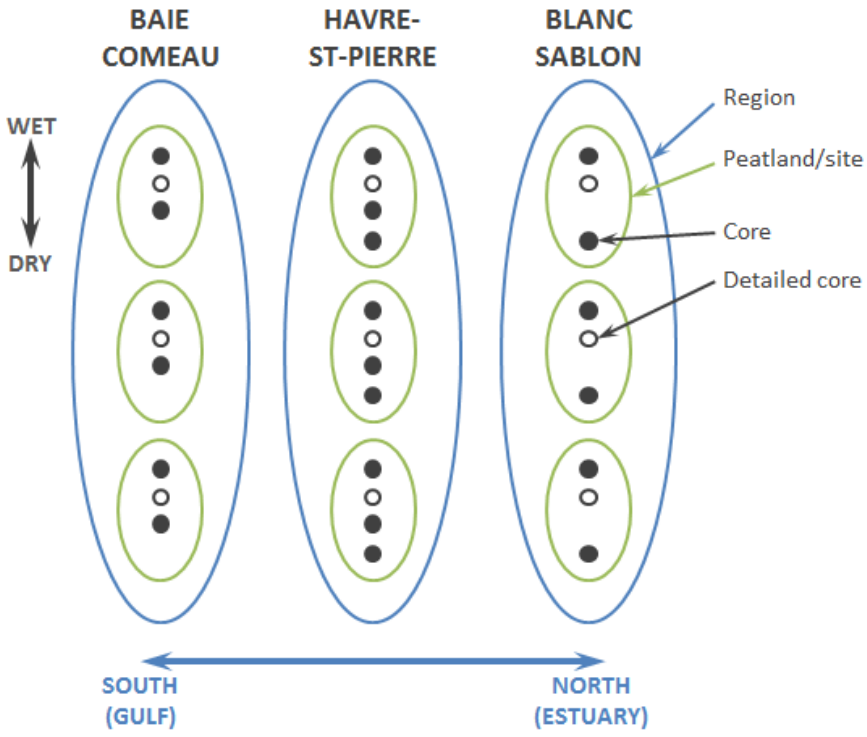

Figure 3.1 Schematic representation of the coring strategy. Blue ovals represent the three ecoclimatic regions; green ovals represent individual peatlands; open circles represent lawn cores selected for radiocarbon (^{14}C) dating; grey closed circles are cores from other microforms. Microform cores from Havre-St-Pierre were also ^{14}C dated.

3.2 Site selection

This section will briefly outline some of the environmental history and climatic conditions of the region and the main characteristics for site selection (Table 3.1).

3.2.1 Site Descriptions

Peatlands in Quebec currently cover 9-12% of the land surface. The two regions with the most peat are the Eastmain/La Grande/James Bay complex in northern Quebec

(continental peatlands) and along the North Shore of the Gulf of the St Lawrence (GSL) (coastal peatlands) (Payette and Rochefort, 2001; Garneau *et al.,* 2014).

Peat inception in this region began during the mid-Holocene following the retreat of the Laurentian ice sheet (Dyke, 2004). The peatlands formed between 7400 and 4200 cal a BP, by paludification on the post-glacial sandy deltaic terraces deposited by tributaries of the Goldthwaite Sea (*ca.* 8 ka) and on marine silt/clay deposits nearer the coast from the Laurentian Transgression (*ca.* 4.2 ka) (Bernatchez and Dubois, 2004; Dionne and Richard, 2006; Garneau *et al.,* 2014; Magnan and Garneau, 2014b)

The North Shore peatlands are located in the lower Boreal and Atlantic Subarctic ecozones (NWWG, 1997). From southwest to northeast, there is an important transition in peatland surface characteristics associated with regional ecoclimatic conditions and permafrost history (Figure 3.2). At the peatland surface, vegetation cover changes from *Sphagnum and* dense shrubs and trees to treeless plateaus or palsas with small shrubs and *Sphagnum*/lichen patches, while pool size and density increase. The easternmost regions are subject to changes in the cold Labrador Current (Magnan and Garneau, 2014a,b). See Figures 3.3 to 3.5 for photos and brief site descriptions. Table 3.1 at the end of this section summarises the main site characteristics and meteorological data.

The peatlands and coring locations along the North Shore of the GSL were selected using two main criteria: ombrotrophic and as near as possible to existing studies (Dionne and Richard, 2006; Magnan and Garneau, 2014a,b) and to the central peatland dome to provide a historical context. They are located (from East to West) near the outflows of the Manicouagan (Baie Comeau), La Romaine (Havre-Saint-Pierre) and Blanc Sablon (Blanc Sablon) Rivers.

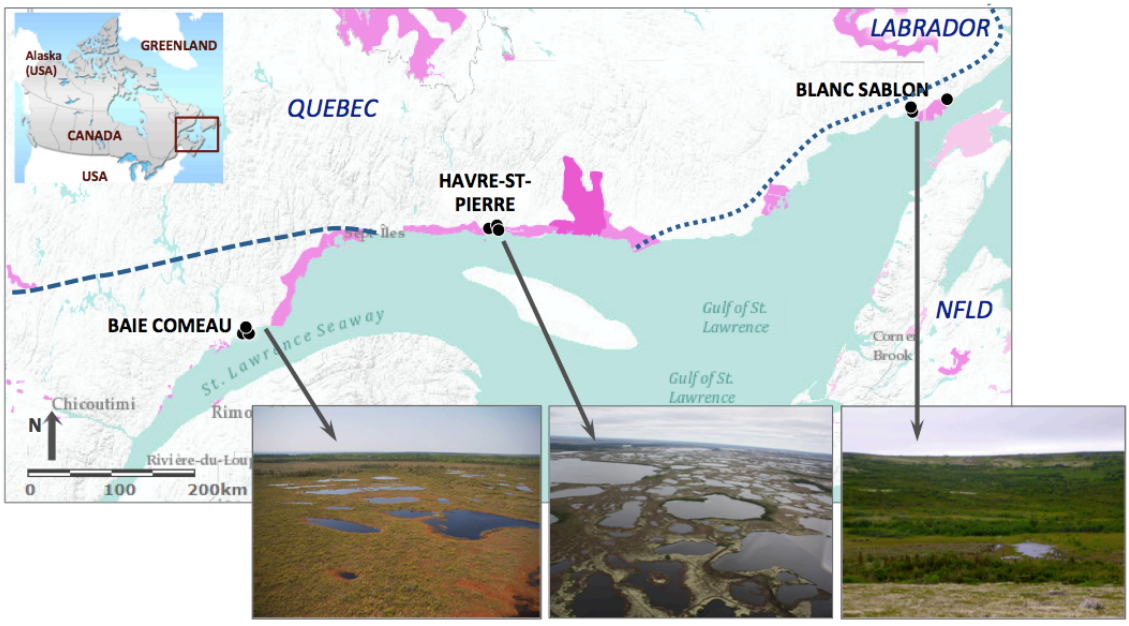

Figure 3.2 Map of study sites. Black dots: coring locations; Dashed line: southern permafrost limit; region between dashed and dotted line: Sporadic permafrost zone (< 2% permafrost cover); to the right of dotted (not including Newfoundland): Discontinuous permafrost zone (< 50% permafrost cover); Pink represents areas with (~ 50%) peatland cover (data adapted from Tarnocai *et al.,* 2011 using ArcMap 10.2.2).

The Baie Comeau (BC, Figure 3.3) peatland region (< 40 m a.s.l), is made up of non-forested, closed peatlands. They have a slightly convex surface with a patterned pools, typical of temperate peatlands of that region (Payette and Rochefort, 2001; Garneau *et al.,* 2014; Table 3.1). To the northeast is a peat-harvesting site (Figure 3.3). The Lebel peatland was formed over deltaic sands (*ca.* 5.8 ka), while Manic and Baie were formed over clay/silt marine sediments (*ca.* 4 ka) (Magnan and Garneau, 2014b). Long-term apparent carbon accumulation rates (LORCA), ranging from 52.8-67.8 g C m^{-2} a^{-1}, are elevated compared to the global and regional averages (Magnan and Garneau, 2014a). Havre-St-Pierre (HP; Figure 3.4) peatlands (< 40 m a.s.l.) are located at the transition between the closed boreal forest and the tundra forest. Treeless plateau bogs with dry lichen- (*Cladonia*-) topped surfaces dominate the region, which is similar to the sub-arctic and oceanic bogs of Northeastern Canada. Large pools occupy up to 50% of surfaces in some areas (Payette and Rochefort, 2001; Garneau *et al.,* 2014). The Morts peatland was formed over clay/silt sediments (*ca.* 3.2 ka) while the Romaine

and Plaine bogs are on deltaic sands (*ca.* 5.4 and 7.5 ka, respectively) (Magnan and Garneau, 2014b). LORCA estimates range from 16.0-45.7 g C m^{-2} a^{-1} (Magnan and Garneau, 2014a). The Blanc Sablon (BS; Figure 3.5) peatlands (*ca.* 60 m a.s.l.) have been less studied. The region was submerged by the Goldthwaite Sea until *ca.* 9 ka; peat accumulated at an average rate of 0.32 mm/year since its inception (9320 cal a BP; Dionne and Richard, 2006). Peatlands are surrounded by Cambrian age rocky hills and peat deposits contain a combination of palsas, permafrost hummocks or collapse scars. The vegetation is similar to that at Havre-St-Pierre; however, there are fewer flat lawn areas.

3.2.2 Meteorological data

Table 3.1 summarises site information as well as mean instrumental meteorological data. Monthly mean annual temperature, snowfall and precipitation are represented for the 1971-2000 period in Figure 3.6 for all three regions. Baie Comeau (southern) is the warmest site and has the highest number of growing degree days above 0^{o}C (GDD0), and Blanc Sablon (northern) is the coldest both for overall temperatures and for temperature extremes and has the fewest GDD0. While mean annual precipitation is similar for all three regions, Blanc Sablon receives the most snowfall.

Temperature records from 1971-2003 show that the mean annual temperature has been increasing at all three sites during this period. The slope is significant for Havre-St-Pierre and Blanc Sablon over time (linear regression: $p < 0.05$ in both cases) and the rate of increase is highest at the Blanc Sablon (northern) site (Figure 3.7; Hutchinson *et al.,* 2009). As this region is influenced by the cold Labrador current, it is likely that temperature has been affected by the decline in sea ice in this region during this same period (Halfar *et al.,* 2013).

BAIE COMEAU:

Figure 3.3 Baie Comeau region: photo of peat surface (top: Manic bog) and satellite view (bottom) with peatland locations (Manic, Lebel and Baie bogs) indicated by blue points.

HAVRE-ST-PIERRE

Figure 3.4 Havre-St-Pierre region: photo of peat surface (top: Romaine bog) and satellite view (bottom) with peatland locations (Plaine, Romaine and Morts bogs) indicated by green points.

BLANC SABLON

Figure 3.5. Blanc Sablon region: photo of peat surface (top: a collapse zone and small palsa at the back at the Lac à la Truite bog) and satellite view (bottom) with peatland locations (Lac à la Truite and Vallée) indicated by red points. The site of previously published work at Blanc Sablon by Dionne and Richard (2006) is shown by a yellow pin. The Red Bay peatland is not shown here due to poor resolution.

Table 3.1 Summary table of site information

	Baie Comeau	**Havre-Saint-Pierre**	**Blanc Sablon**
Lat./Long.	49°06'N / 68°14'W	50°16'N / 63°40'W	51°29'N / 57°11'W
Peatland	Domed bog	Plateau	Palsa edge
Peat depth (m)	4-6	2-3	1.5-2
Region area (km^2)	120	300	
Basal age (cal a. BP)	5820, 4210, 4100[a]	7450, 3240, 5390[a]	9320[b]
Holocene LORCA (g C m^{-2} a^{-1})	52.8-67.8[a]	16.0-45.7[a]	n/a[b]
Dominant surface vegetation type	*Sphagnum* and shrubs	*Sphagnum* and lichen	Lichen
Region	Closed boreal	Closed boreal/ Forest tundra	Tundra forest
Permafrost zone	n/a	Sporadic (< 2% cover)	Discontinuous (< 50% cover)
Mean annual temperature (°C)[d]	1.5 ± 0.9 Min: -14.4 (January) Max: 15.6 (July)	1.1 ± 2.0[c] Min: -14.2 (January) Max: 14.4 (July)	0.2 ± 1.1 Min: -13.3 (January) Max: 12.6 (August)
Mean annual precipitation (mm)[d]	1014	1080[c]	1067
Snowfall (mm eq)[d]	362	251[c]	412
GDD > 0[e]	2057	1949[c]	1609

[a] Magnan and Garneau, 2014a

[b] Dionne and Richard, 2006, nearby (inaccessible) peatland, 0.32 mm/year

[c] Data from station nearest to Havre-St-Pierre: Rivière-au-Tonnerre station, 110km due West

[d] Temperature, precipitation and snowfall data from Climate Normals 1971-2000 (Environment Canada, 2015)

[e] Degree days from Climate Normals for 1981-2010 (Environment Canada, 2015)

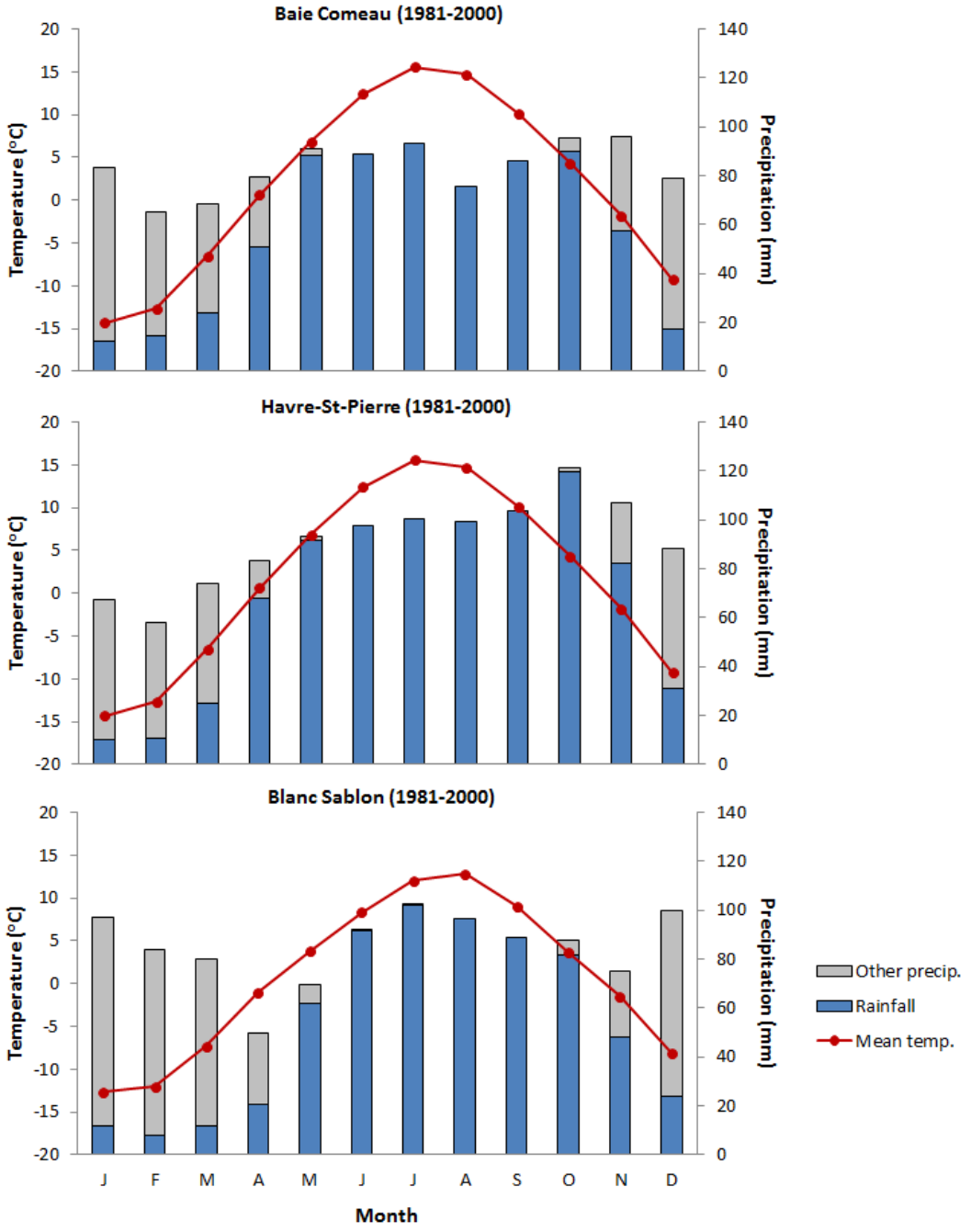

Figure 3.6. Mean annual temperature (MAT), precipitation (MAP) broken down in rain- and snowfall for the three regions (Environment Canada, 2015)

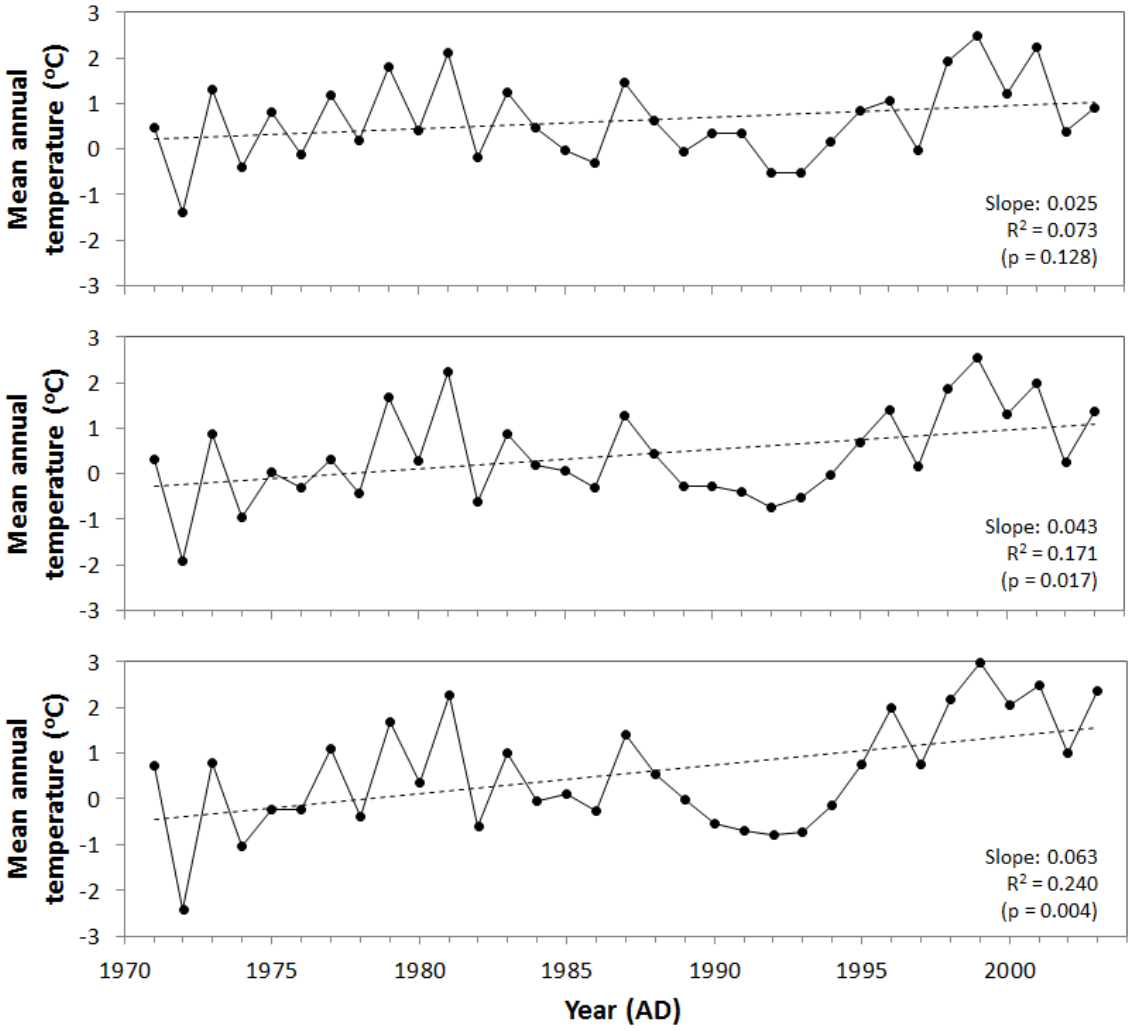

Figure 3.7. Mean annual temperature change (solid black line) for the three regions. Linear regression results (slope, R^2 and statistical significance) and trendline (dotted line) are represented for each site. Data compiled for 1971-2003 from the National Land and Water Information Service (Hutchinson *et al.,* 2009).

3.3 Microform selection

Differentiating between microforms along a gradient was important for this project. There is a range of terminology in the literature, and some overlap between terms. For instance, a 'hollow' may be a wet depression between hummocks at Mer Bleue (e.g. Turunen *et al.,* 2004) or a wet area surrounding a pool (Karofeld, 2004). As the same spatial pattern was not present at all the sites, terms used to differentiate between microforms are defined in this section. Microforms were differentiated in the field by their relative height (if applicable), i.e. distance from the water table, and surface vegetation. The hummock-mud bottom series is used here (Rydin and Jeglum, 2006, p.15). See Figure 3.8 for a list of species used to identify microforms in the field.

- **Hummocks** are raised compared to other microforms (surface is furthest from the water table), often covered in dwarf shrubs or covered in lichen species as well as other mosses and plants indicating dry conditions.

- **Lawns** are typically the intermediate microform; these are usually considered for palaeoclimate studies as less sensitive to small changes. As hummocks and hollows grow in increments depending on water table depth, the lawn-hollow and hummock-lawn borders vary; therefore, lawns are more sensitive to climate variations (Barber, 1981; van der Molen and Hoekstra, 1988) and are less likely to register annual precipitation variability.

- **Hollows** encompass pool edge and carpet/mud bottom (Karofeld, 2004) rather than referring to the depression between hummocks (e.g. Finland; Mer Bleue); they are soft, dominated by bryophytes, sparse cyperaceous and water table is just above or under.

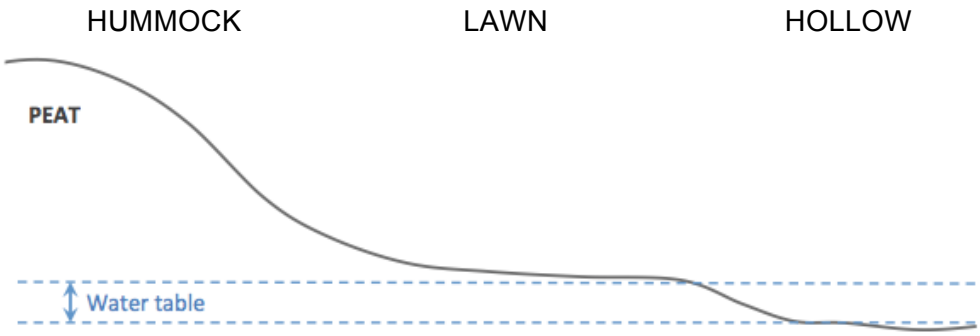

	HUMMOCK	LAWN	HOLLOW
pH	2.7-3.1	Intermediate	3.4-4.0
MOSSES	*Sphagnum fuscum* *Sphagnum capillifolium* *Polytricum strictum* *Pleurozium schreberi* *Dicranum undulatum*	*Sphagnum magellanicum* *Sphagnum capillifolium*	*Sphagnum cuspidatum* *Sphagnum magellanicum* *Sphagnum fallax* *Gymnocolea inflata*
VASCULAR PLANTS	*Rubus chamaemorus* *Kalmia angustifolia* *Ledum groenlandicum* *Empetrum nigrum* *Chamaedaphne calyculata*	*Carex oligosperma* *Eriophorum angustifolium* *Eriophorum vaginatum* *Scirpus cespitosus* *Vaccinium oxycoccos*	*Carex limosa* *Eriophorum vaginatum* *Rhynchospora alba* *Andromeda glaucophylla* *Drosera rotundifolia* *Sarracenia purpurea*
LICHEN	*Cladonia rangiferina* *Cladonia sp.*		

Figure 3.8. Species used to identify microforms in the field. Adapted from Payette and Rochefort (2001; p.132); note that not all species are included, only those noted down at particular sites. See also plant list in front matter.

3.4 Methodology

3.4.1 Field sampling

Coring sites were selected for the 2011 and 2012 field campaigns at Baie Comeau and Havre-St-Pierre as near as to the coring sites of Magnan and Garneau (2014a,b). These were close to the centre of the peatland dome as there are smaller seasonal fluctuations in water table depth compared to outer peatland edges (e.g. Malmer, 1986). The Blanc Sablon peatland studied by Dionne and Richard (2006) was inaccessible during the 2013 field season; therefore, two nearby peat deposits were cored, and the Red Bay palsa peatland was selected as a third site with a known palsa from previous field campaigns (Garneau *et al.,* unpublished).

Figure 3.9 represents the microform transects at each of the sites. At two of the Blanc Sablon peatlands, there were no lawn areas as defined in all other sites. The 'lawn' cores were taken from 'inter-hummocks' in-filled with *Sphagnum*; this is typical of drier continental wooded bogs (Rydin and Jeglum, 2006, p.16). At these sites, 'hollows' refer to the wettest microform: *Sphagnum* regrowth over collapse scar mud-bottoms.

Table 3.2. Microform distribution for all sites

Region	Hollow	Lawn	*Sphagnum* hummock	Lichen hummock
Baie Comeau	3	3	3	--
Havre-St-Pierre	3	3	3	3
Blanc Sablon	3	3	--	3

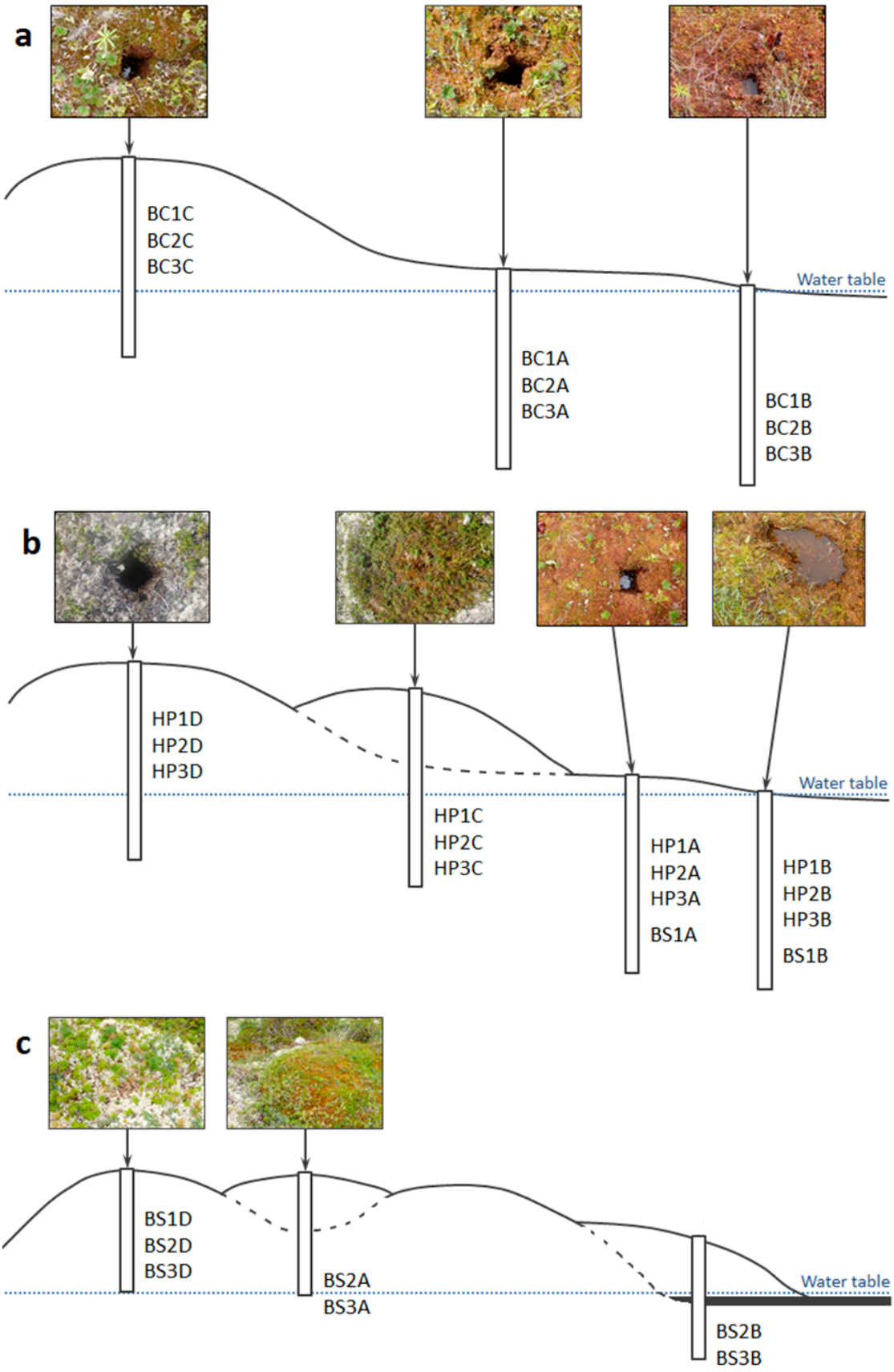

Figure 3.9. Schematic representation of coring transects for a) Baie Comeau, b) Havre-Saint-Pierre and c) Blanc Sablon. Note that the topography at BS1 resembled HP but with a palsa. Photo not available for Blanc Sablon wet microforms (BS2B and BS3B).

Cores were taken with a box corer (8 x 8 x 105 cm; Jeglum *et al.,* 1991) in HP and BC. For one BC core (BC1A: Lebel), an additional 50 cm peat section, cored using a Russian peat corer (diameter: 7.5 cm), was used for this thesis (from Sauvé, 2016). At BS, monoliths were extracted up to 50 cm depth, or until ice was reached. The upper 10 cm were in all cases sampled with minimal compression (< 2 cm), in microform transect, where possible. Cores were wrapped in plastic film and PVC tubes and stored at 4^{o}C. Basic stratigraphy was described on-site using a modified version of the Troëls-Smith classification system (Kershaw, 1997). Water table depths were recorded within an hour after coring.

3.4.2 Laboratory analysis

3.4.2.1 *Subsampling*

Cores were sliced into 0.5 cm contiguous sections using a Plexiglas slicing device with a screw on the end (Figure 3.10). This was done to ensure that all future analyses were done consistently on the same peat sections, thus avoiding problems with core compaction between sampling stages, and to preserve high sampling resolution for future examination into water table depth. They were cut semi-frozen to ensure that roots and branches sliced cleanly (Figure 3.10). Tools were cleaned to avoid cross-sample contamination.

Subsampling for carbon analysis and dating using lead-210 (^{210}Pb) and radiocarbon (^{14}C) dating techniques was as in Table 3.3. The remaining peat was archived (0.5 cm resolution) for potential future multi-proxy analysis (e.g. testate amoebae and plant macrofossils).

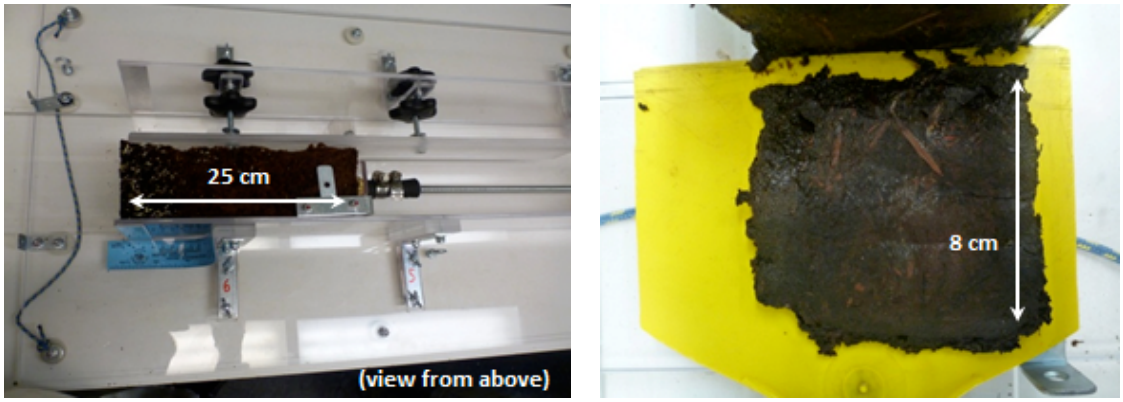

Figure 3.10. Photographs of the core cutting process: a Plexiglas apparatus wedged the semi-frozen monoliths and allowed cutting at 0.5 cm resolution (left). The technique was effective at cutting through woody remains, *Sphagnum* and roots without disturbing the position (right). Each 8 x 8 cm section was then subsampled for analyses.

3.4.2.2 *Carbon analysis*

Each 0.5 cm section was subsampled with a volumetric sampler (3 cm^3) and analysed for bulk density (BD) and loss-on-ignition (LOI) as soon as possible at the GEOTOP and University of Exeter laboratories. To measure BD and sample water content, samples were weighed then dried at 105^oC overnight and weighed again (Equations 3.1 and 3.2). The same samples were then ashed at 550^oC for 3.5 hours and weighed one final time (Equation 3.3; Dean, 1974; Heiri *et al.,* 2001). Carbon content was calculated in relation to organic matter (OM) content as 0.5 g C/g OM (Equation 3.4; *sensu* Tolonen and Turunen, 1996).

Table 3.3. Breakdown of subsampling distribution for the main methods.

Analysis	Sample size	Method	Resolution
Bulk density/C %	3 cm^3	Volumetric sampling	0.5 cm; contiguous
^{210}Pb dating	0.5 g dry weight	Alpha spectrometry	1 cm; generally every 2 cm for top 30 cm, then every 10 cm
^{14}C dating	2 cm^3	Sieve and wash	0.5 cm section; depths allocated by NERC

Bulk density (BD): $$BD = \frac{Dry\ weight}{Volume}$$ Equation 3.1

Water content (WC): $$WC = \frac{Fresh\ Weight - Dry\ weight}{Volume}$$ Equation 3.2

Loss-on-ignition (LOI): $$LOI\ (\%) = \frac{Dry\ weight - Ashed\ weight}{Dry\ weight} \times 100$$ Equation 3.3

Carbon content (C): $$C(\%) = (Organic\ matter\ content) \times 50\%$$ $$= \frac{Dry\ weight - Ashed\ weight}{Volume} \times 0.5$$ Equation 3.4

3.4.2.3 *Dating strategy*

Lead-210: All cores (n = 30) were analysed for ^{210}Pb at Exeter using the alpha counting method discussed in detail in Chapter 5. Samples were 1 cm thick and measured every 1-2 cm for the top 30 cm, then every 5-10 cm for deeper samples. A sample size of 0.5 g freeze-dried and homogenised sample was spiked with a ^{209}Po yield tracer, then acid digested (HNO_3:H_2O_2:HCl, 1:2:1). Po was chemically extracted from the sample and electroplated onto a silver disc before being counted. ^{210}Pb activity was calculated from decays of its daughter product, ^{210}Po.

Radiocarbon dates: 'Lawn' (intermediate) cores (n = 9) were also dated using a total of 35 radiocarbon (^{14}C) dates (NERC Radiocarbon allocation code 1737.1013). All lawn cores were allocated a minimum of 2 dates; one core per region was dated in more detail (4-5 dates) (Objectives 3 and 4; *cf.* Figure 3.1 for a schematic representation of the distribution of dated cores). Havre-St-Pierre microform cores were also each allocated 2 additional radiocarbon dates. Samples were washed through a 125µm sieve with deionised water; *Sphagnum* stems (also some branches and leaves) were separated and sent to the NERC Radiocarbon Facility in East Kilbride. Samples to date

were selected based on available ^{210}Pb dates, and rangefinder dates (allocated to this project as part of the MILLIPEAT Project: NERC Standard Grant NE/I012915/1). Further dates were selected based on stratigraphic horizons, or evenly spaced when no basal dates were available; due to time constraints, the remainder were evenly spaced (Bennet, 1994), or adjacent to stratigraphic horizons.

3.4.3 Data analysis

3.4.3.1 *Age-depth models*

Lead-210 ages were calculated using a Constant Rate of Supply (CRS) model (Appleby and Oldfield, 1978; Appleby, 2001; Chapter 5); total inventories, annual fallout rates, and the 'sedimentation' or peat accumulation rate (r) were also calculated (Appendix A4 and A5). Using replicate cores allowed for the statistical comparisons of the total measured ^{210}Pb inventories and to address the questions of ^{210}Pb preferential deposition and post-depositional mobility in peat often raised in the literature (Chapter 6). Radiocarbon ages were calibrated using the IntCal13 curve (Reimer *et al.,* 2013) and age-depth models were constructed incorporating these ^{14}C ages combined with calendar dates from the ^{210}Pb analysis in BACON v.2.2 (Blaauw and Christen, 2011), a statistical package for R (R Development Team, 2014), which uses Bayesian statistics to produce outputs for accumulation per year/cm. The peat surface was set at -61 to -63 cal a BP depending on the coring year.

3.4.3.2 *Carbon accumulation rates*

C mass and total C accumulated over time were calculated and compared using analyses of variance (see individual chapters for details). The recent apparent rate of carbon accumulation (RERCA) for the last *ca.* 150 years was calculated for all cores (n = 30) by dividing the total mass of C accumulated for that period by the age of the ^{210}Pb-datable peat (Objective 2, Chapter 6). The long-term apparent rates of carbon accumulation (LORCA), here defined as the total apparent accumulation calculated for

a given time period (300, 500 and 1000 years) using combined ^{210}Pb and ^{14}C age depth-models were calculated for n = 9 cores (lawns; Objective 3, Chapter 7). These data were also calculated for additional Havre-St-Pierre microform cores. Temporal variations in carbon accumulation rates (CAR) were calculated by dividing the C mass in each depth increment by the accretion rate (yr/cm) (Magnan and Garneau, 2014a) and statistically compared in 10-, 50- and 100-year bins.

3.4.3.3 *Statistical analyses*

Statistical analysis methods and corrections used are discussed in detail within each of the results chapters.

4 Stratigraphy

The aim of this chapter is to assemble the basic core information that will be used as the basis for all carbon accumulation rate calculations and age-depth model development for Chapters 6 and 7. As there are 30 replicate cores used in this thesis, this chapter will be a point of reference throughout the thesis.

Shown in the next 9 pages for each core (n = 30) are:

- **Basic** stratigraphy for the dominant peat type (Rydin and Jeglum, 2006):
    (1) *Sphagnum* peat;
    (2) Ericaceous-*Sphagnum* mix (e.g. *Sphagnum* peat with some woody bits, large amounts of ericaceous leaves or *Vaccinium* stems);
    (3) Sedge-*Sphagnum* (*Sphagnum* mixed with some *Cyperaceae* sp., e.g. *Eriophorum spissum*)
    (4) 'Humic' peat, i.e. highly decomposed, unidentifiable organic matter with the naked eye.
- The water table depth measured at time of coring in the field;
- The dry bulk density;
- The ash content (calculated as the material remaining after loss on ignition);
- The deepest ^{210}Pb date with error < 10% (See Chapter 5 for method discussion and Chapter 6 for CRS modelling of these dates);
- Calibrated radiocarbon dates (single date calibrations using clam 2.2: Blaauw, 2010; R Development Team, 2014). See Chapter 3 for a discussion of the dating strategy, and Chapter 7 for age-depth modelling.

Each of the following figures (Figures 4.1-4.9) shows all the microforms (from left to right: wet to dry) cored for each peatland, i.e. 3 or 4 cores depending on the region. Note that the x- and y- axis scales are in most cases the same for all cores, except for

BC1A (Lebel, lawn core), where additional deeper material was available; a few sites also have higher bulk density.

Changes in stratigraphy (colour, substrate) and bulk density indicate changes in vegetation, hydrology or in accumulation and decomposition rates, which could reflect large-scale climate changes or changes in local hydrological conditions, such as the relationship between Von Post humification scale and bulk density (Rydin and Jeglum, 2006). For instance, a change in bulk density and stratigraphy at HP3C at 27 cm depth from dark, consolidated peat with ericaceous leaves/wood to light and well-aerated *Sphagnum fuscum* could indicate a microform succession (autogenic peatland dynamics), or a change in accumulation due to climate warming or a higher water table (allogenic). The overall ash content is relatively low (< 5-10%), and changes in ash content with depth could reflect road construction (e.g. BS1), or natural processes.

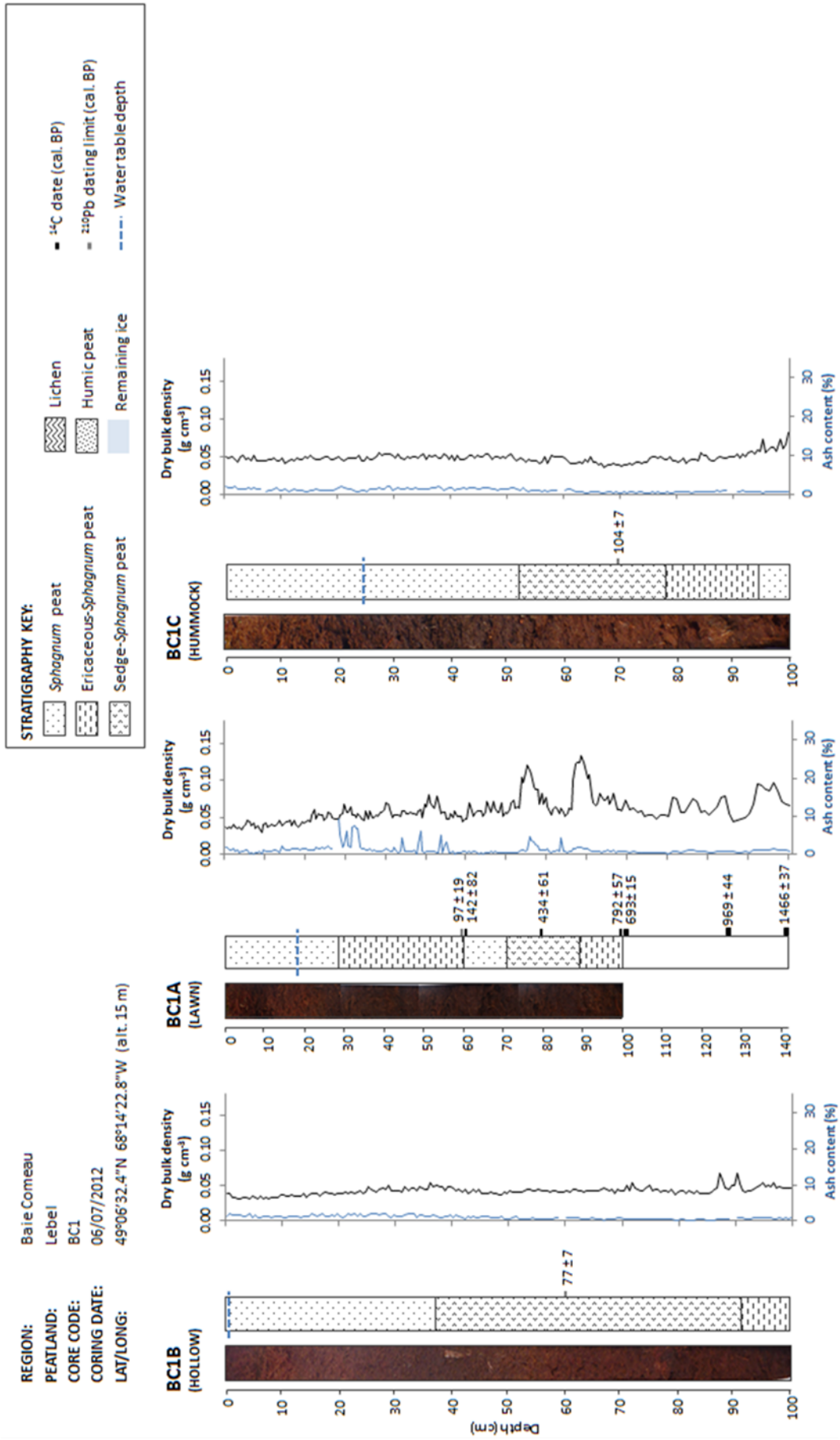

Figure 4.1. Basic stratigraphy, bulk density and ash content results for BC1 (Lebel) cores, presented from wettest (left) to driest (right) microform. Water table depth measured in the field (dotted blue line), calibrated ^{14}C dates (black bar) and the deepest ^{210}Pb date (grey bar) are indicated.

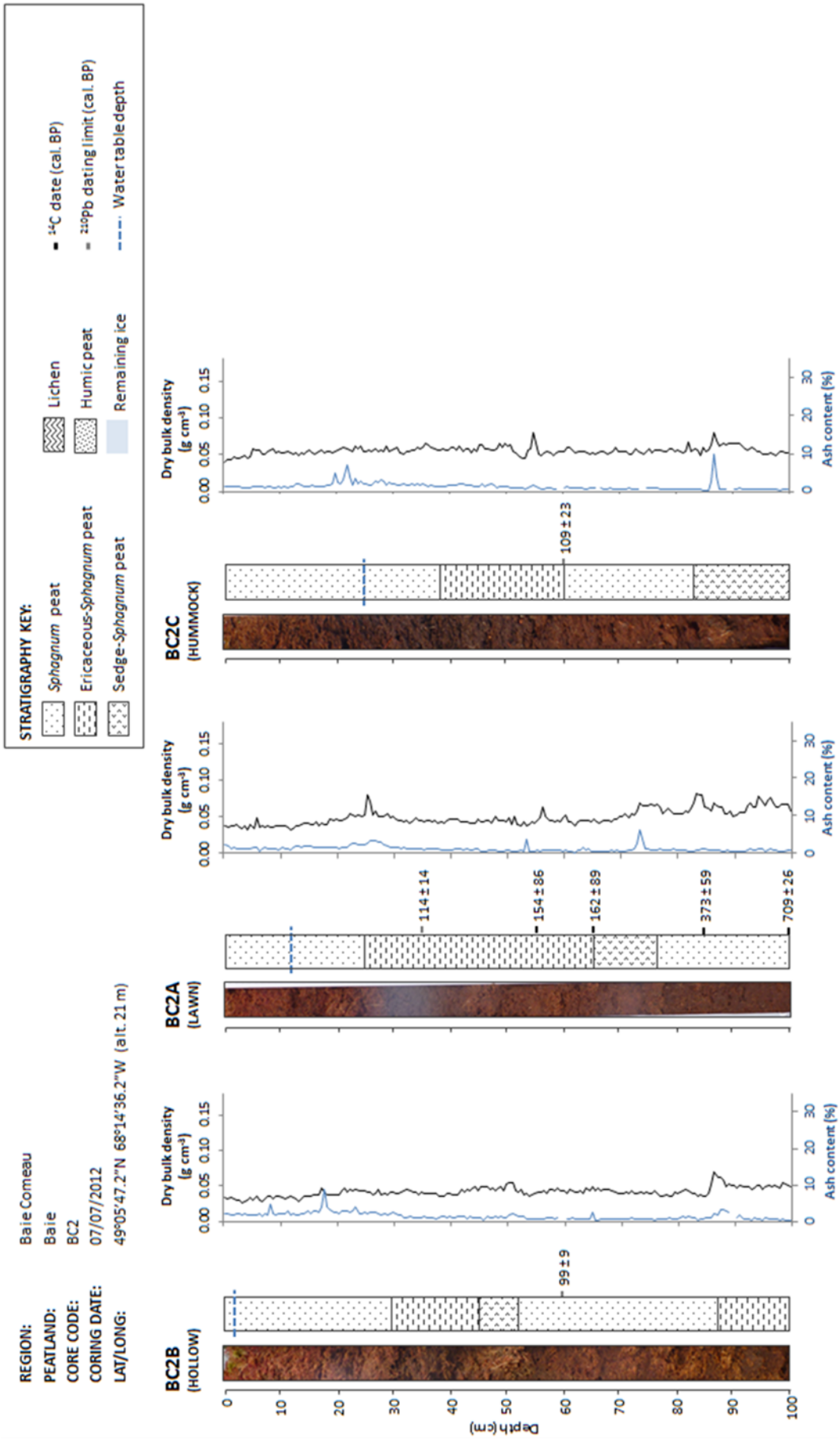

Figure 4.2. Basic stratigraphy, bulk density and ash content results for BC2 (Baie) cores, presented from wettest (left) to driest (right) microform. Water table depth measured in the field (dotted blue line), calibrated ^{14}C dates (black bar) and the deepest ^{210}Pb date (grey bar) are indicated.

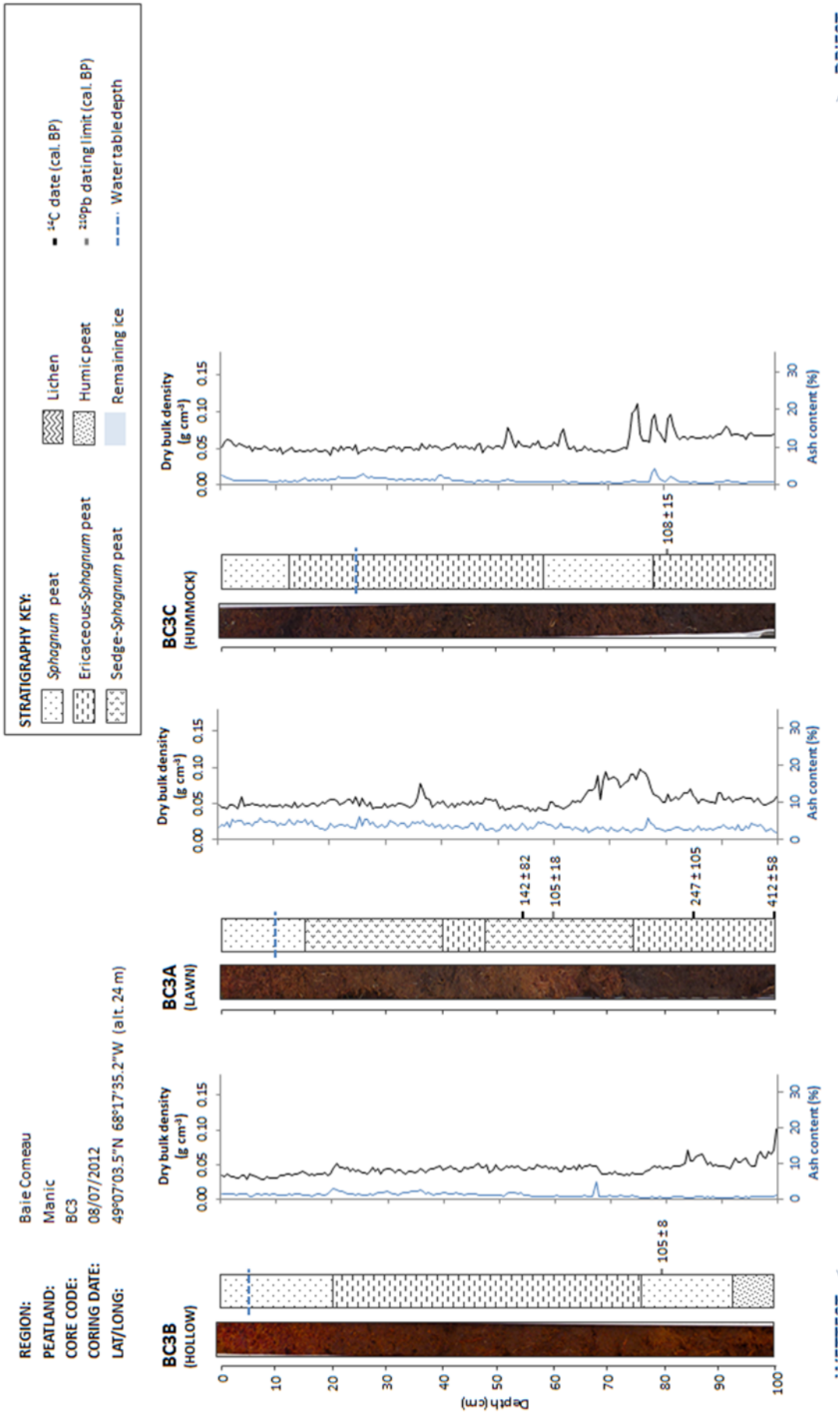

Figure 4.3. Basic stratigraphy, bulk density and ash content results for BC3 (Manic) cores, presented from wettest (left) to driest (right) microform. Water table depth measured in the field (dotted blue line), calibrated ^{14}C dates (black bar) and the deepest ^{210}Pb date (grey bar) are indicated.

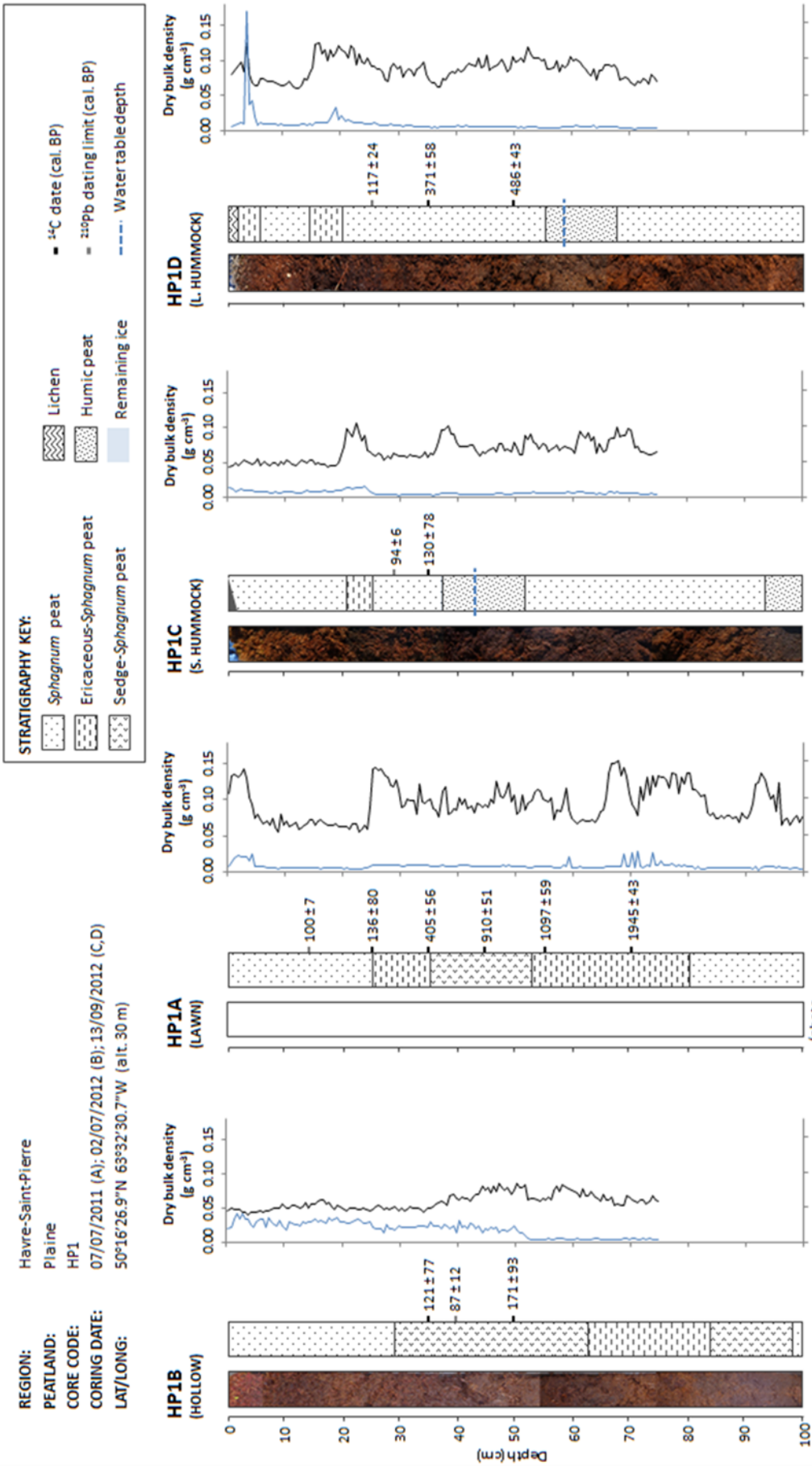

Figure 4.4. Basic stratigraphy, bulk density and ash content results for HP1 (Plaine) cores, presented from wettest (left) to driest (right) microform. Water table depth measured in the field (dotted blue line), calibrated ^{14}C dates (black bar) and the deepest ^{210}Pb date (grey bar) are indicated.

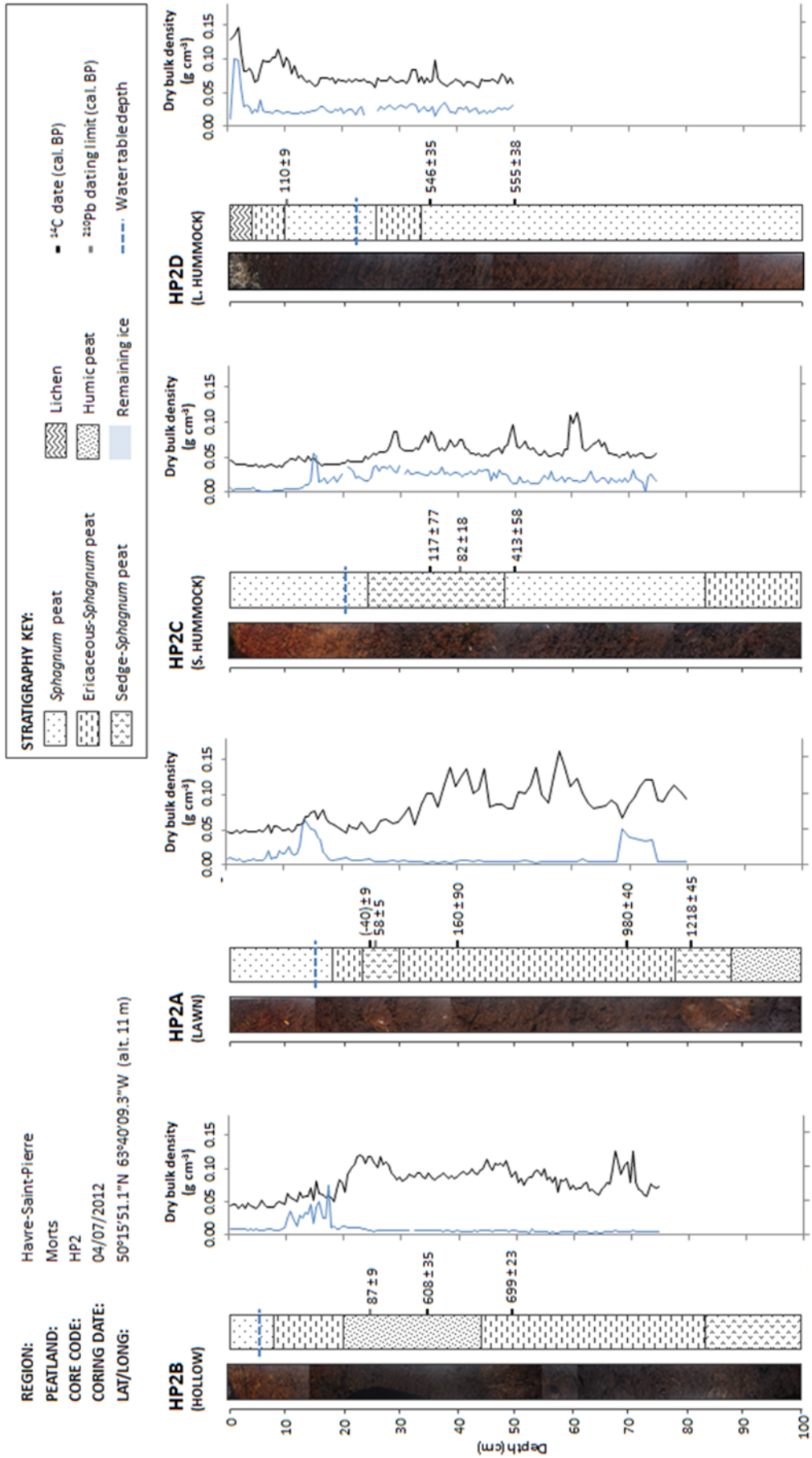

Figure 4.5. Basic stratigraphy, bulk density and ash content results for HP2 (Morts) cores, presented from wettest (left) to driest (right) microform. Water table depth measured in the field (dotted blue line), calibrated ^{14}C dates (black bar) and the deepest ^{210}Pb date (grey bar) are indicated.

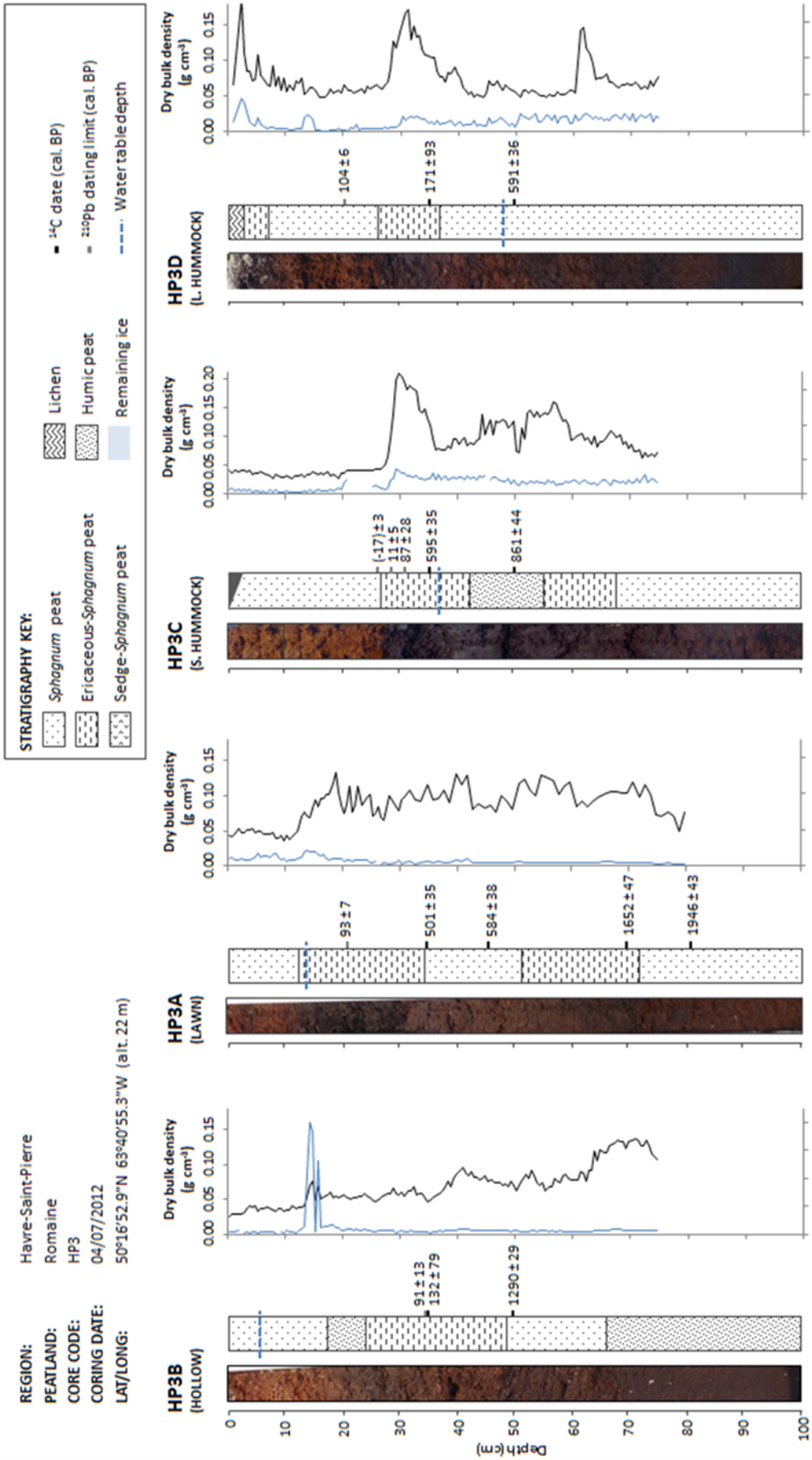

Figure 4.6. Basic stratigraphy, bulk density and ash content results for HP3 (Romaine) cores, presented from wettest (left) to driest (right) microform. Water table depth measured in the field (dotted blue line), calibrated ^{14}C dates (black bar) and the deepest ^{210}Pb date (grey bar) are indicated.

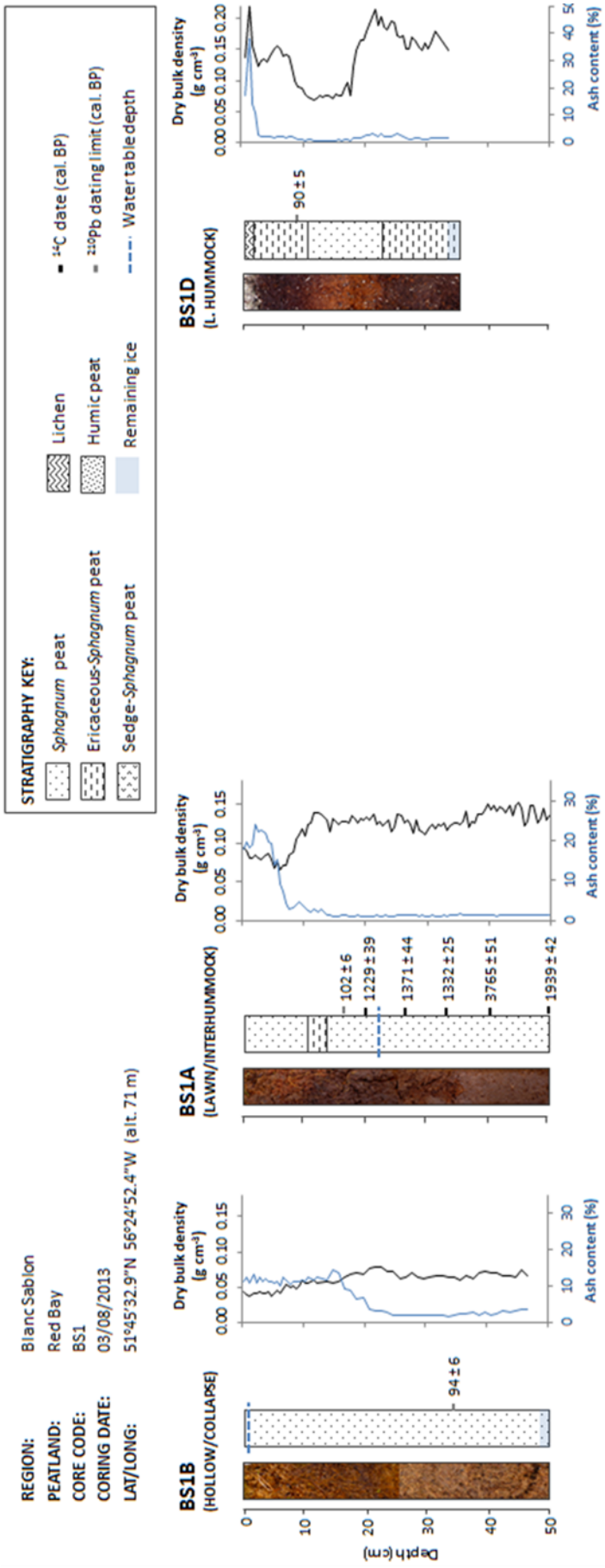

Figure 4.7. Basic stratigraphy, bulk density and ash content results for BS1 (Red Bay) cores, presented from wettest (left) to driest (right) microform. Water table depth measured in the field (dotted blue line), calibrated ^{14}C dates (black bar) and the deepest ^{210}Pb date (grey bar) are indicated.

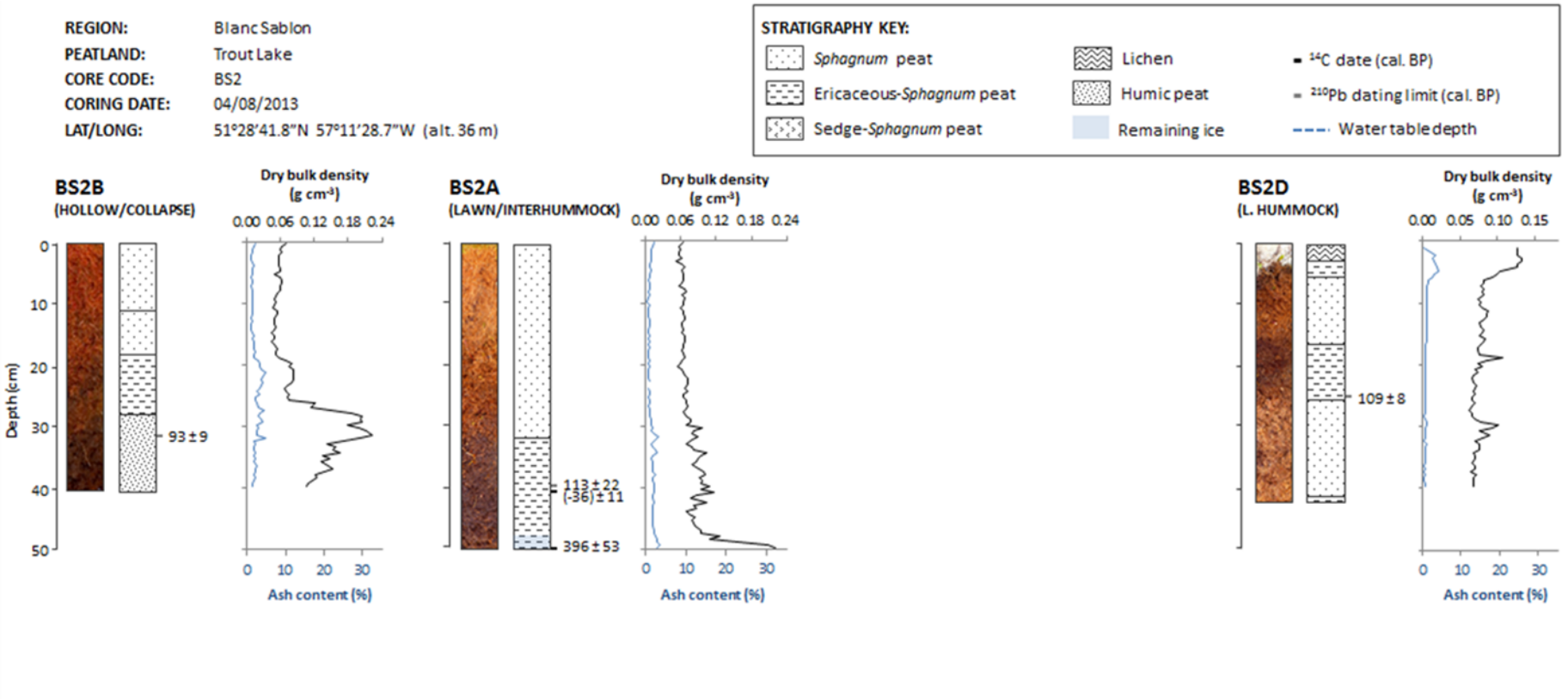

Figure 4.8. Basic stratigraphy, bulk density and ash content results for BS2 (Lac à la Truite) cores, presented from wettest (left) to driest (right) microform. Water table depth measured in the field (dotted blue line), calibrated ^{14}C dates (black bar) and the deepest ^{210}Pb date (grey bar) are indicated.

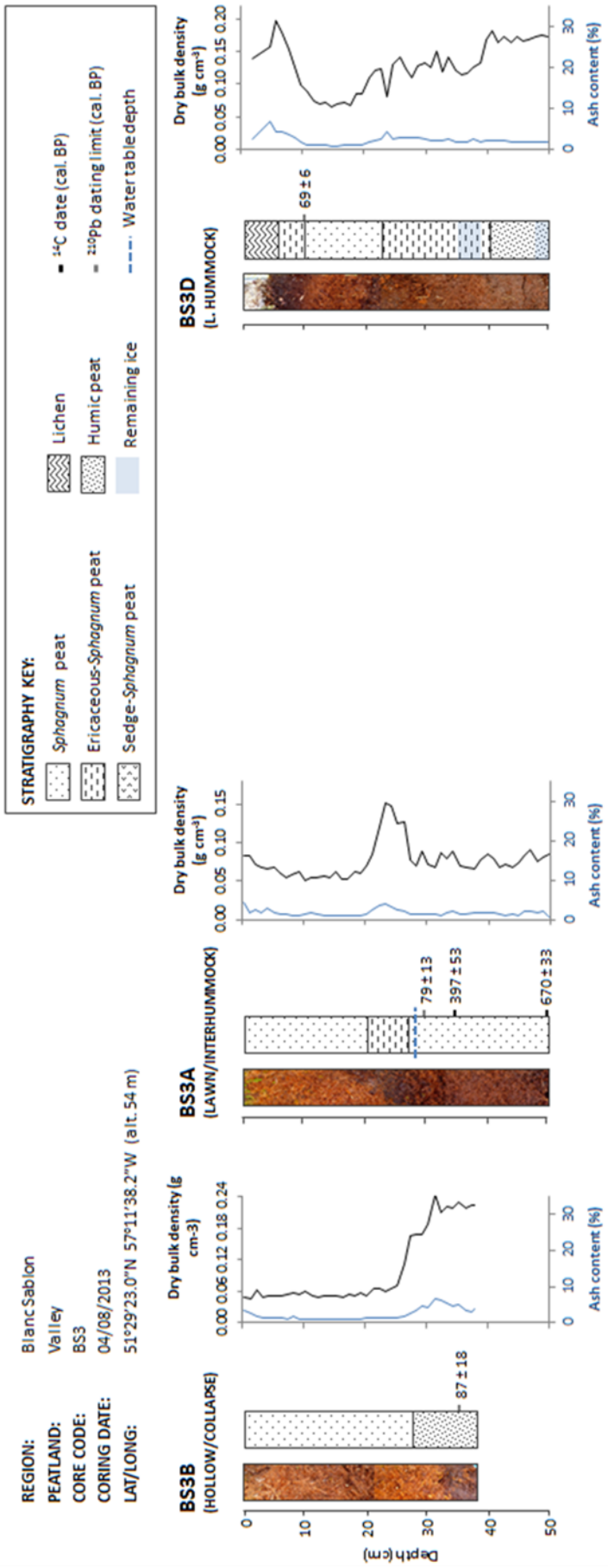

Figure 4.9. Basic stratigraphy, bulk density and ash content results for BS3 (Vallée) cores, presented from wettest (left) to driest (right) microform. Water table depth measured in the field (dotted blue line), calibrated ^{14}C dates (black bar) and the deepest ^{210}Pb date (grey bar) are indicated.

Table 4.1.Mean bulk density (g/cm^3) for all sites and microforms (± standard deviation). Based on n = 3 for each microform. Note that core depths vary.

	Baie Comeau	**Havre-Saint-Pierre**	**Blanc Sablon**	**OVERALL MICROFORM**
Hollow	0.043 ± 0.002	0.070 ± 0.010	0.085 ± 0.023	0.066 ± 0.022
Lawn	0.055 ± 0.006	0.076 ± 0.017	0.092 ± 0.025	0.074 ± 0.022
Sph. hummock	0.053 ± 0.005	0.069 ± 0.014	--	0.061 ± 0.013
Lich. hummock	--	0.079 ± 0.008	0.115 ± 0.030	0.097 ± 0.028
OVERALL SITE	0.050 ± 0.007	0.073 ± 0.012	0.097 ± 0.027	0.074 ± 0.024

Overall, average site bulk density increases significantly with latitude, or region (linear regression: R^2 = 0.37; slope 0.024; $p < 0.001$), even for the same microform (Table 4.1; Figure 4.10). Across all sites, *Sphagnum* hummocks have the lowest average bulk density (highly aerated); lichen hummocks, as the most compact and dry microforms, have the highest overall bulk density. Indeed, the relationship between microform (i.e. acrotelm thickness) and bulk density is not statistically significant (linear regression: R^2 = 0.173; slope = 0.008; p = 0.223).

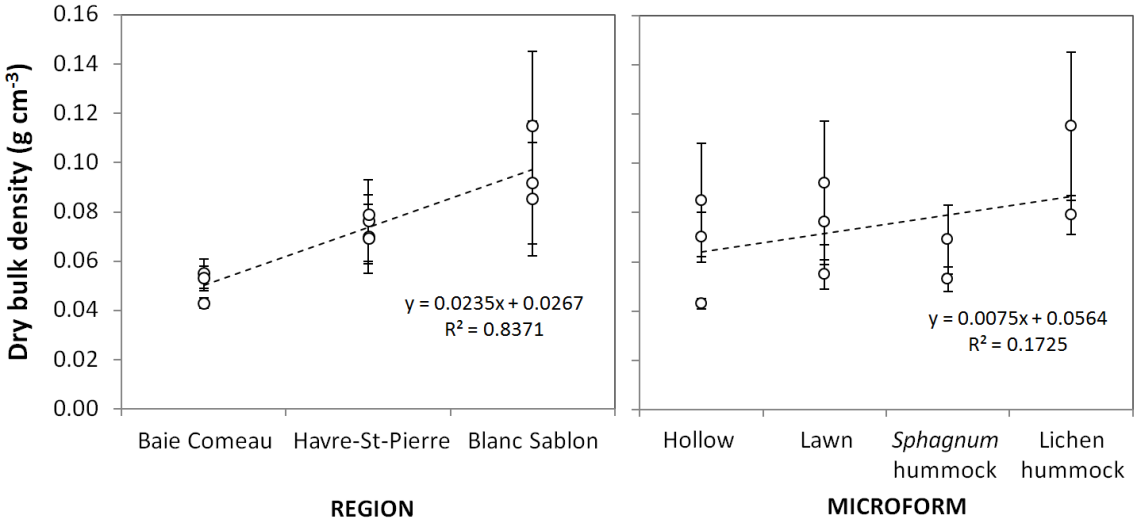

Figure 4.10. Mean dry bulk density for all sites and microforms. Error bars represent the standard deviation from the mean. The equation and R^2 value from linear regressions for each dataset (dotted line) are indicated on the plot.

Given the variability in peat type, water table depth, bulk density and age between cores from the same site and cores from the same microform type, ensuring robust high-resolution chronologies is essential.

5 Establishing a chronology: lead-210 dating peat cores

Cores and bulk densities for this chapter were provided by: the NERC-funded PRECIP project (Petite core) and Dr Lauren Parry (PhD Thesis, 2011: Dartmoor cores). Dr Will Blake from the Consolidated Radio-isotope Facility (CORiF, Plymouth University) measured lead-210 activities using gamma-spectrometry and modelled the dates.

The method described in this chapter has been used in published (Swindles et al., 2015; Kelly et al., submitted) and on-going projects in a range of environments including the Arctic, Patagonia, the Amazon and Antarctica.

5.1 Overview

Given the variability between microform cores from within the same peatland presented in Chapter 4, establishing accurate surface chronologies and increasing the temporal resolution for recent accumulation rates are necessary to better understand sub-decadal changes in response to rapid, recent events such as permafrost degradation. While radiocarbon (^{14}C) wiggle matching has been shown to capture these changes (Mauquoy *et al.,* 2002a, 2004; Blaauw *et al.,* 2004), this technique can be costly and single date markers (e.g. tephra) may not be able to capture rapid changes. Using lead-210 (^{210}Pb) dating provides a continuous, absolute dating alternative to ^{14}C for last *ca.* 150-200 years.

There has been increasing interest in this technique during the last decade in peatlands (see reviews by Turetsky *et al.,* 2004; Matthews *et al.,* 2007; Le Roux and Marshall, 2011). As reviewed in Chapter 2, ombrotrophic peatlands are well suited to this technique and act as a geochemical archive for lead deposition. *Sphagnum* mosses, the main building blocks of ombrotrophic peatlands, have a high cation

exchange capacity which allows for a good Pb-retaining ability (Clymo *et al.,* 1990). The unsupported ^{210}Pb fraction ($^{210}Pb_{ex}$) is supplied by precipitation and dry deposition. The supported fraction ($^{210}Pb_{sup}$), usually supplied via runoff or groundwater infiltration, is negligible in ombrotrophic peatlands, therefore the radioactive decay of $^{210}Pb_{ex}$ is used to calculate ages (Appleby, 2001; Oldfield *et al.,* 1995).

To date a peat core ^{210}Pb activity in a sample is measured and calculated directly or indirectly using alpha or gamma spectrometry (Turetsky *et al.,* 2004). However, ^{210}Pb measurement techniques via alpha and gamma spectrometry have been used interchangeably. See Chapter 2.3.2 for ^{210}Pb dating principles and a review of both methods (also summarised in Table 5.1).

Table 5.1 Summary table comparing alpha and gamma-ray spectrometry techniques for peat.

	Alpha	**Gamma**
+	- High-resolution analysis: small sample size[a] - High sensitivity: good at detecting low activity[b] - Lower cost - High sample turnover	- Direct measurement of ^{210}Pb activity - Simple sample preparation (drying, homogenising and weighing) - Non-destructive process - Can also analyse independent markers (^{137}Cs, ^{241}Am)[d]
–	- Indirect ^{210}Pb measurements, i.e. need to correct for prep - Destructive - Potentially long preparation[c] - Topmost sediments may need to be left for > 3-6 months	- Large samples may be required (5-10 g) - 21 days to reach equilibrium - Higher cost; - High background radiation (error): correct for self-absorption - Difficult detection in low-energy samples (older ages)

[a] generally 0.3-1 g; however, 0.1 g was successful in Pratte *et al.,* 2013.

[b] Applications for sites with estimated low ^{210}Pb flux (e.g. Antarctica, Patagonia).

[c] 2-3 days until the start of counting.

[d] These do not always produce clear peaks in peat; ^{137}Cs is highly mobile.

Alpha spectrometry ('alpha', or α) measures high-energy decay of polonium-210 (^{210}Po), a daughter product of ^{210}Pb decay by extracting Po from a sample using acid digestion and electroplating it onto a silver disc. This method is effective at detecting low activities, even with small sample sizes. While it is relatively inexpensive and the turnover is high, the sample preparation may be time-consuming and inconsistent depending on the sample type. An inter-lab calibration study has been conducted for ^{210}Po and ^{210}Pb measurement in seawater samples in order to standardise alpha counting results (Church *et al.,* 2012); however this consistency in results may be more challenging for peat due to the wide variety of sample composition and digestion stages. Sample preparation methods are varied depending on resources available and sample composition; the method previously in use at the Radiometric Laboratory at the University of Exeter was developed for floodplain sediments (Aalto and Nittrouer, 2012) and a pilot study (Section 5.2.1) showed that it was not adapted for peat samples.

Gamma spectrometry ('gamma', or γ) directly measures ^{210}Pb decay; it is non-destructive and the dating markers caesium-137 (^{137}Cs) and americium-241 (^{241}Am) can also be measured at the same time. However, analysing a core with gamma may be costly and requires larger sample sizes.

The relative merits and effectiveness of these two methods have been compared for lakes (Sikorski and Bluszcz, 2008), marine cores (Zaborska *et al.,* 2007), estuaries (Tanner *et al.,* 2000) and soils (Ebaid and Khater, 2006); they have not yet been compared in peatlands.

Chapter aim and objectives:

The main aim of this chapter is to adapt and to test the effectiveness of a method for determining ^{210}Pb activity in peat samples using alpha spectrometry that will be used to date the recent portion of peat cores in Chapters 6 and 7.

Objective 5.1: To develop a method for the preparation and analysis of ^{210}Pb in organic samples via alpha spectrometry.

In order to test the effectiveness of the Po extraction method, decay count, recovery rate and ^{210}Pb activity for replicate samples will be compared using several treatments.

Objective 5.2: To evaluate the relative strengths and weaknesses of using alpha and gamma spectrometry for dating peat cores.

This will be addressed by comparing measured activities and modelled ages using different techniques; in addition to testing the effectiveness of the method from Objective 5.1 on a wider range of sample types, this allows us to standardise results between two independent laboratories.

This is a methodological chapter, and the cores used were selected from a range of previously analysed cores (bulk density and gamma spectrometry) with remaining sample for comparison purposes. Section 5.2 considers the main steps to prepare samples for alpha counting. Sections 5.3 and 5.4 outline the methods used to address both objectives and the results, respectively. Section 5.5 will discuss these results and the method choice. Finally, Section 5.6 summarises some concluding remarks and applications for the rest of the project.

5.2 Review of alpha method

5.2.1 Pilot study

The default method employed at the University of Exeter Radiometry Laboratory before the start of this project was developed to extract Po from mineral floodplain sediments (Aalto and Nittrouer, 2012). Henceforth, this method will be the ‘mineral’ method, in contrast to the ‘organic’ method adapted in this chapter.

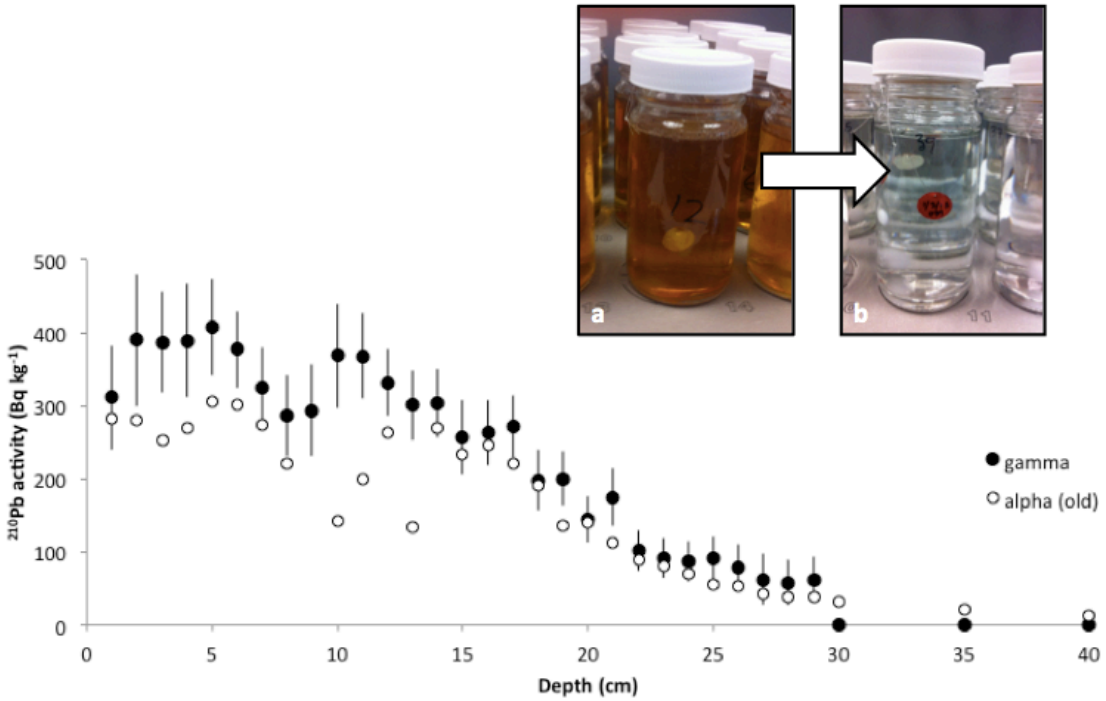

Figure 5.1. Initial trial of ^{210}Pb activities determined using alpha and gamma comparison for a core from Petite bog (PTB.1). Closed (black) circles represent results determined using gamma spectrometry; open (white) circles are from alpha spectrometry following the 'mineral' (or 'old') preparation method. Photos show the plating solution with suspended silver planchet (red side painted): (a) using the 'mineral method' and (b) the final 'organic' method, after adaptation.

At the start of this project, it was tested for its effectiveness at extracting Po from peat on samples from PTB.1 (Petite Bog core; see Section 5.3 for list of cores used in this chapter). This method was found to be poorly adapted to the high organic content of the samples based on initial comparisons with gamma results in the surface samples (top 15 cm) and the colour/consistency of the plating solution (Figure 5.1). The reduced clarity of the solution indicates possible interference with Po-plating due to incomplete acid digestion. This, combined with the multitude of techniques for analysis reviewed in the next section, justified the need for further trials and investigation into the most important steps for analysis.

5.2.2 Po extraction preparation

A review of analytical techniques for peat and other substrates (listed in this section) suggests the following main breakdown (Figure 5.2): (1) sampling; (2) sample

dissolution and organic matter breakdown to extract and recover Po; and (3) source preparation/plating (Matthews *et al.,* 2007).

5.2.2.1 *Sample preparation*

Peat samples are dried and ground, then spiked with a chemical yield tracer (^{208}Po or ^{209}Po), which has the same chemical properties as ^{210}Po but emits α-particles at different energy levels. The spike is added at the start to account for analytical loss. While ^{208}Po has been used historically ^{209}Po has a longer half-life and a more distinct peak on the spectrum (Table 5.2; Martin and Blanchard, 1969; Matthews *et al.,* 2007). Sample sizes range from peat dry weights of 0.1 g (Pratte *et al.,* 2013), 0.3 g (Ali *et al.,* 2008), 0.5 g (De Vleeschouwer *et al.,* 2010; Wieder *et al.,* 1994), 1 g (MacKenzie *et al.,* 1997) to 2-3 g (Turetsky *et al.,* 2000; Vile *et al.,* 2000). The sample size selected determines the quantities and type of acids used in the following steps and the amount of available ^{210}Po to be recovered, i.e. larger samples will likely require more resources (time and materials) and more recalcitrant material may require stronger acids. In addition, peat samples with low bulk density (e.g. *Sphagnum* peat) may require more material than is available to make up large sample sizes. Sample size should be considered in order to optimise available materials and Po recovery. Some studies suggest that surface sediments should be held for 3-6 months (Ebaid and Khater, 2006) or up to 2 years (Tanner *et al.,* 2000; Turetsky *et al.,* 2004) to guarantee secular equilibrium between ^{210}Pb and measured ^{210}Po. There is also some discussion as to whether surface samples should be analysed and included in order to more accurately capture the total inventory (Olid *et al.,* 2008).

Table 5.2 Decay information and activities of Po isotopes (adapted from Matthews *et al.,* 2007).

Parent isotope	**Daughter product**	**Half-life ($T_{1/2}$)**	**Decay type**	**Activity**
^{210}Po	^{206}Pb	138 d	α	5.3 MeV
^{208}Po	^{204}Pb	2.9 y	α	5.1 MeV
^{209}Po	^{205}Pb	125 y	α	4.8 MeV

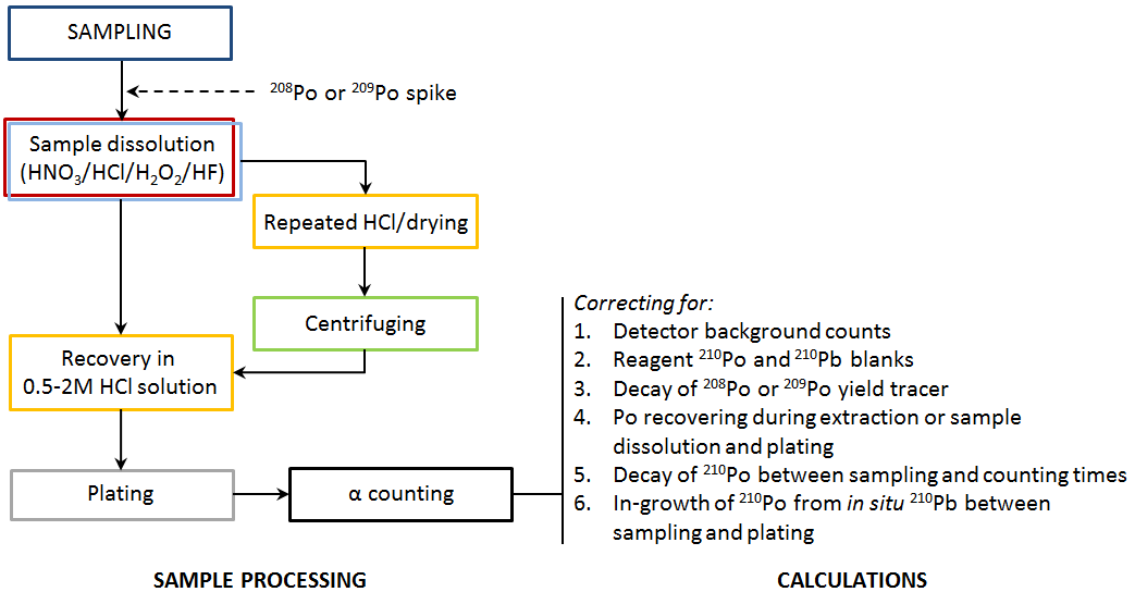

Figure 5.2 Po extraction procedure; diagram adapted from Church *et al. (*2012). Flow chart of main steps of sample preparation for ^{210}Pb analysis by alpha spectrometry, colour-coded: sampling (dark blue), dissolution/leaching via acid attack (light blue), organic matter breakdown (red), HNO_3 removal (yellow), particulate removal (green) and deposition/plating (grey).

5.2.2.2 *Polonium extraction and separation*

This typically involves acid digestion using a combination of acids. The most common technique for peat is wet acid digestion using heated nitric acid (HNO_3) then hydrochloric acid (HCl) or in some cases *aqua regia* (HNO_3:HCl, 1:3) with added hydrogen peroxide (H_2O_2) to facilitate organic matter breakdown (Turetsky *et al.,* 2004; Yafa and Farmer, 2006; Ali *et al.,* 2008). The addition of H_2O_2 is considered important for organic samples (molluscs/algae: Jia *et al.,* 2001; lake cores: Sikorski and Bluszcz, 2008). Depending on sample composition, standard wet digestion methods are not always effective so it may be necessary to add sulphuric acid (H_2SO_4) (El-Daoushy *et al.,* 1991) or hydrofluoric acid (HF) to eliminate silicates (Yafa and Farmer, 2006; Pratte *et al.,* 2013). In some cases, samples are sealed in high-pressure Teflon containers or microwave 'bombs' (Sanchez-Cabeza *et al.,* 1998; Tanner *et al.,* 2000; DeVleeschouwer *et al.,* 2010: 'classic' method) or ashed before analysis (Eakins and Morrison, 1978; Yafa and Farmer, 2006; DeVleeschouwer *et al.,* 2010: 'ashing' method). However, these methods have increased health and safety risks and good

results have been obtained with a standard wet digestion when comparing methods for some peat samples (Yafa and Farmer, 2006). Care should be taken during heating stages as Po is volatile above 100°C with 90% losses incurred above 300°C (Flynn, 1968; Martin and Blanchard, 1969); however, while questions still remain concerning Po volatility losses for different methods and sample types, these losses should be accounted for by the addition of the ^{208}Po or ^{209}Po tracer as no fractionation with ^{210}Po is suspected (Matthews *et al.,* 2007).

After acid digestion, repeated HCl evaporations cause Po oxides to form a chloride salt; the elimination of HNO_3 is essential for the subsequent self-deposition step (Flynn, 1968; Eakins and Morrison, 1978). Centrifuging or filtering removes remaining particulates and Po is recovered in a mildly acidic HCl solution (Lee *et al,.* 2014 suggest an optimal pH 0.5).

5.2.2.3 *Source preparation*

At this stage, a metal disc is suspended in the plating solution and Po is reduced and auto-deposited onto the disc. As with acid digestion methods, plating conditions also vary considerably in the literature in terms of plate size and metal, time, solution volume and temperature (Equation 5.1; Po deposition reviewed in Lee *et al,.* 2014).

$$PoCl_2(aq) + 2Ag(s) \rightarrow Po(s) + 2AgCl\ (aq) \qquad \text{Equation 5.1}$$

Ascorbic acid is added at the start of the plating stage to eliminate interference from iron (Fe^{2+} and Fe^{3+}) and other oxides; ascorbic acid has been shown not to interfere with Po deposition and is more effective than other iron-reducing complexing agents used such as hydroxylamine hydrochloride or sodium citrate. Silver (Ag) plates were found to have a higher yield than nickel or copper plates; enamel paint to cover one side of the plate was better suited to suspension in the acidic plating solution than tape. The disc should not be larger than the detector, as larger plates have lower detection

efficiency despite having greater surface recovery. Plates are suspended in solution on a heated or unheated magnetic stirring plate. The Po recovery rate for sea water samples was found to be optimal at 80-90 ^{o}C for 3 hours (Jia *et al.,* 2001) and 96 ± 1% for a plating time of 15 hours at room temperature (Lee *et al.,* 2014); however these samples require fewer preparation steps for Po separation than organic peat samples. Finally, plates are rinsed with DI water, dried and cooled before being placed in the alpha-counters to avoid detector contamination.

5.3 Materials and methods

This section describes the materials and methods used to address the chapter objectives. First, the samples used are described. Second, some key variants on Po extraction methods are compared in order to test the method used to calculate peat ages for this thesis in Chapters 6 and 7. Finally, ^{210}Pb concentrations using this method for alpha counting are compared with gamma results for the same samples; modelled inventories, fallout rates and dates using data from both techniques are also compared.

5.3.1 Samples

Several peat cores were used to address the previous objectives (Table 5.3). As stated in the chapter outline, the sites selected are variable (and from outside of the regional context of this thesis) due to the availability of gamma-dated material with which to test the method. However, this allows for the method to be tested on a range of peat types, with cores taken from Canadian *Sphagnum*- ombrotrophic peatlands (Plaine and Petite bogs) and UK blanket bog peatlands under varying disturbance status (Dartmoor cores: control, drained and burned).

Table 5.3. Core information, location and reference

Obj	Core name	Code	Lat. (^{o}N)	Long. (^{o}W)	Site description	Reference
1	Plaine Bog (Havre-St-Pierre, QC)	HP1A	50.274	63.541	Plateau bog; Closed boreal forest; *Sphagnum* and lichen dominated	Section 3; Garneau *et al.,* 2014
1-2	Petite Bog (NS)	PTB.1	45.871	63.937	Ombrotrophic bog; *Sphagnum*-dominated with ericaceous and vascular plants present	Amesbury *et al.,* 2013
2	Dartmoor (UK)					
	Control 6	D.C06	50.601	-3.999	Blanket mire vegetation including *Sphagnum* and *Eriophorum*	Parry *et al.,* 2013
	Drained 5	D.D05	50.589	-4.008	Predominantly vascular plants with some *Sphagnum*; Infilled shallow drainage ditches	Parry *et al.,* 2013
	Burned 13	D.B13	50.645	-3.977	Vascular plants; Hagged with small vegetated gullies	Parry *et al.,* 2013

The Plaine Bog core (Havre-St-Pierre, Quebec, Canada), taken as a duplicate 'test' core in addition to the HP1A core used in this thesis, was extracted using a box corer (7 x 7 x 100 cm). Stratigraphy and site details are in Chapter 3 and Garneau *et al. (*2014). To test the Po extraction method with multiple replicates (Objective 5.1), peat samples from 0-20 cm were bulked together, dried, finely ground and homogenised, and subsampled for analysis using 7 treatments (see next section).

Four additional cores were selected in order to test the Po extraction method and alpha counting results; these cores were previously dated using gamma spectrometry and are only included in this project to test the method. The Petite Bog core (Nova Scotia, Canada; Amesbury *et al.,* 2013), from an ombrotrophic bog in Eastern Canada, was used to test the results from the alpha preparation method in Objective 5.1. Results from this core were also used to address the relative advantages and disadvantages of alpha and gamma counting in Objective 5.2.

Three Dartmoor cores (30 cm monoliths) were taken from blanket peatland sites in the North of Dartmoor National Park, UK. Each site was located in hydrologically and topographically similar areas but with differing management histories and peat conditions. A control site represents undisturbed conditions with a high and relatively stable water table. The drained site has a lower and more variable water table and the degraded site is the driest due to on-site erosion and past burning (Parry *et al.,* 2013).

5.3.2 Po extraction

The sample preparation method for alpha spectrometry used in future chapters was adapted for peat based on the basic steps outlined in the method review (Section 5.2). The emphasis compared to the previous method was on organic matter breakdown by adding an H_2O_2 step and on sample size reduction as organic matter is able to bind ^{210}Pb. This was then tested using 7 variations on the method or treatments with 3 replicates per treatment (n = 21; Table 5.4). These treatments were constrained by lab availability (e.g. no Teflon beakers/microwaves) and safety considerations (e.g. avoiding HF). The method is outlined in detail in Appendix A.1.

Table 5.4 List of treatments and references

Treatment	Description	Modified from
Control	- 0.5 g sample - HNO_3:H_2O_2:HCl (1:2:1) digestion - 12h H_2O_2 organic matter breakdown stage added	Ali *et al.,* 2008; DeVleeschouwer *et al.,* 2010; Pratte *et al.,* 2013
No H_2O_2	H_2O_2 step omitted	Aalto and Nittrouer, 2012
1-day	All in 1 day	Aalto and Nittrouer, 2012
1 g	Larger sample size (1 g)	MacKenzie *et al.,* 1997 (1 g); Vile *et al.,* 2000; Turetsky *et al.,* 2000 (2-3 g)
0.25 g	Smaller sample size (0.25 g)	Ali *et al.,* 2008; Pratte *et al.,* 2013
Filter	Filtering stage added	Vile *et al.,* 2000; Yafa and Farmer, 2006
Volume	Smaller plating volume (60 ml)	Flynn, 1968; El-Daoushy *et al.,* 1991; Lee *et al.,* 2014

5.3.2.1 *Chemical analysis*

Sample numbers and treatments were randomly allocated to eliminate bias from cross-contamination or preferential heating based on each sample's position on the hotplate.

Sample preparation: Bulk peat from HP1A was freeze-dried, finely ground and homogenised. For all treatments except '1 g' and '0.25 g', 0.5 g subsamples were taken. In all cases, 1 ml ^{209}Po spike was added before any additional steps were taken as a chemical yield tracer.

Extraction/Separation: For all treatments, 10 ml HNO_3 were added and heated until near-dryness; in all but the 'no H_2O_2' treatment, 10-20 ml H_2O_2 were added and gently heated for 1 hour to monitor for strong reactions with organic material. In samples from the '1-day' treatment, preparation continued; all other samples were then left overnight. Samples were then heated to dryness. Successive additions and drying of 5 ml 6 M HCl eliminated HNO_3 and formed a chloride salt (white residue); this was then dissolved in 6 M 5 ml HCl and washed with 0.5 M HCl into 50 ml centrifuge tubes, then washed into 120 ml plating jars. In the 'filter' treatment, an additional filtering step used (Whatman no. 42 filter paper) to reduce residual organic matter.

Source preparation: Plating jars were topped up to 120 ml with 0.5 M HCl, except in the 'Volume' treatment (60 ml). A small scoop (0.2 g) of ascorbic acid was added to eliminate soluble Fe interference. Silver planchets were washed with acetone and coated with enamel paint on the convex side. A hole was punched in the top and they were labelled and suspended in the middle of the solution for spontaneous deposition for 24 hours.

5.3.2.2 *Counting*

Samples are placed concave side up in counting chambers under the detector and counted using Ortec Octête Plus Integrated Alpha-Spectrometry System with Maestro

software. See Appendix A.2 for the spectrometer use. ^{209}Po and ^{210}Po were recorded at 6 h, 24 h and 48 h from the start of analysis.To calculate the excess ^{210}Pb activity in Bq/kg (1 Bq = 1 Becquerel = 1 disintegration per second) from Po counts, the ^{210}Po/^{209}Po ratio is calculated using the known amount of spike added to account for experimental loss, corrected for sample size, decay rates and time between preparation and measurement (Appendix A.3; Turetsky *et al.,* 2004; EPA, 2011; Sikorski and Bluszcz, 2008). Errors are 1σ calculated from counting statistics and methodological error (Appendix A.2); the instrumental error from blanks and background rate is small (< 0.01%) for this counting method.

5.3.2.3 *Testing method effectiveness:*

In addition to the visible improvement in the clarity of the solution (clear solution in Figure 5.1b), the effectiveness of the method was tested in four main ways:

1) Comparing the number of ^{209}Po and ^{210}Po counts over time to evaluate variability of replicated samples within and between treatments;
2) Calculating and comparing ^{209}Po recovery rate over time for each sample/treatment based on known amount added of spike;
3) Comparing calculated ^{210}Pb activities over time;
4) Comparing results to other dating methods; in this case sample-specific ^{210}Pb activity measured by gamma spectrometry.

Statistical analyses were performed using SPSS v.23 (IBM, 2012). In (1), (2) and (3) above, relationships were examined for each variable overall, then for each treatment and time period. Measurements were assumed to be independent. Normality of the data was tested using the Kolmogorov-Smirnov test. Differences were tested with a one-way ANOVA, with LSD post-hoc tests if significant differences were detected between factors ($p < 0.05$); otherwise, differences were tested using the Kruskal-Wallis

(KW) non-parametric test. In (4), relationships were evaluated with Pearson's correlation coefficients.

5.3.3 Alpha/Gamma comparison

The cores selected for this study were from a range of locations and peat types (Table 5.3): 1 core from Petite Bog (PTB.1), an ombrotrophic *Sphagnum*-dominated peatland from Eastern Canada (Amesbury *et al.,* 2013), and 3 cores (D.C06, D.D05 and D.B13) from blanket peatlands in Dartmoor National Park (UK) differing in plant cover, land use and water table depth (Parry *et al.,* 2013).

For all 4 cores, 1 cm subsections were freeze-dried and homogenised. Subsamples were sealed into 50 mm Petri dishes and stored for a minimum of 21 days prior to analysis. Activity concentrations were measured using a low background EG&G Ortec planar (GEM-FX8530-S N-type) HPGe Gamma spectrometry system at the Plymouth University Consolidated Radioisotope Facility (CORiF). Total excess ^{210}Pb was measured by its gamma emissions at 46.5 keV. Activities of ^{137}Cs and ^{241}Am were determined by their gamma emissions (662 keV and 59.2 keV, respectively). Activity concentrations were reported using ORTEC Gammavison software (Parry *et al.,* 2013). As gamma spectrometry is non-destructive, the same samples were subsampled for alpha spectrometry using the method tested in the previous section (Appendix A.1).

The CRS model was then applied to results from both spectrometry techniques; errors were determined using a propagation of error method (Appendix A.3 for calculations; Appleby and Oldfield, 1978; Appleby, 2001). For alpha spectrometry results, ages were calculated using the CRS model as described. For gamma spectrometry results, ages were calculated in two ways:

(1) The equilibrium depth was selected as the sample with the lowest detectable activity from the gamma results ('tail not inferred'); and

(2) The equilibrium depth was modelled based on exponential decay rates and additional dating markers (^{137}Cs or ^{241}Am) if available ('inferred tail').

As in the previous section, activities and ages for each core were compared using Pearson's correlation coefficient, and differences between total inventories and fallout rates between sites were analysed using ANOVA (for normally distributed data).

5.4 Results

5.4.1 Po extraction

5.4.1.1 *Decay counts*

Mean decay counts for ^{209}Po and ^{210}Po are shown in the Table 5.5. There are significant differences between the overall number of ^{209}Po counts measured over time (KW: $p < 0.001$) and for each treatment (ANOVA, $p < 0.005$). The number of counts increases with time. The lowest ^{209}Po counts and largest errors are for the smaller sample size (0.25 g) and filtering treatments; the highest ^{209}Po counts are for the '1-day' treatment and smallest errors are for the 'no H_2O_2' and larger sample size (1 g) treatments (Figure 5.3). However, no statistically significant difference was detected between treatments. These results are as expected, as 1 ml ^{209}Po spike was added to all samples.

The number of ^{210}Po counts (Figure 5.4) measured overall is significantly different according to treatment (KW: $p = 0.006$) and time (KW: $p < 0.001$). For each treatment, there is a significant difference between time periods (ANOVA: $p < 0.005$). Within each time period, the two sample size treatments are significantly different from the other treatments ($p = 0.05$). This is expected as the treatments have different sample sizes and therefore contain different levels of ^{210}Po.

Table 5.5 Mean ^{209}Po and ^{210}Po count numbers (n = 21) over time for each treatment; statistical standard errors and % error are indicated.

	Treatment	6 hours	24 hours	48 hours
^{209}Po	Control	291 ± 19 (7%)	1192 ± 72 (6%)	2326 ± 151 (7%)
	No H_2O_2	300 ± 6 (2%)	1226 ± 12 (1%)	2369 ± 9 (< 1%)
	1-day	411 ± 23 (6%)	1686 ± 66 (4%)	3224 ± 102 (3%)
	1 g	326 ± 13 (4%)	1220 ± 51 (4%)	2453 ± 11 (< 1%)
	0.25 g	225 ± 34 (15%)	969 ± 158 (16%)	1885 ± 312 (17%)
	Filter	226 ± 27 (12%)	938 ± 119 (13%)	1799 ± 223 (12%)
	Volume	300 ± 11 (4%)	1188 ± 45 (4%)	2603 ± 109 (4%)
	Overall	297 ± 15 (5%)	1203 ± 58 (5%)	2378 ± 114 (4%)
^{210}Po	Control	381 ± 22 (6%)	1537 ± 84 (5%)	2976 ± 154 (5%)
	No H_2O_2	399 ± 22 (6%)	1677 ± 66 (4%)	3219 ± 89 (3%)
	1-day	411 ± 23 (6%)	1686 ± 66 (4%)	3224 ± 102 (3%)
	1 g	847 ± 4 (< 1%)	3484 ± 58 (2%)	6645 ± 81 (1%)
	0.25 g	194 ± 19 (10%)	743 ± 86 (12%)	1458 ± 157 (11%)
	Filter	330 ± 39 (12%)	1323 ± 191 (14%)	2325 ± 368 (16%)
	Volume	397 ± 18 (5%)	1542 ± 58 (4%)	3387 ± 140 (4%)
	Overall	424 ± 42 (10%)	1714 ± 178 (10%)	3358 ± 335 (10%)

Table 5.6 Mean % Po recovery rates (n = 21) over time for each treatment; statistical standard errors and % error are indicated.

Treatment	6 hours	24 hours	48 hours
Control	13.7 ± 0.9 (7%)	14.0 ± 0.9 (9%)	13.6 ± 0.9 (7%)
No H_2O_2	14.1 ± 0.3 (2%)	14.3 ± 0.1 (1%)	13.9 ± 0.1 (1%)
1-day	14.9 ± 0.8 (5%)	15.2 ± 0.6 (4%)	14.6 ± 0.5 (3%)
1 g	15.3 ± 0.6 (4%)	14.3 ± 0.6 (4%)	14.4 ± 0.1 (1%)
0.25 g	10.6 ± 1.6 (15%)	11.3 ± 1.8 (16%)	10.9 ± 1.8 (17%)
Filter	10.7 ± 1.3 (12%)	11.0 ± 1.4 (13%)	10.6 ± 1.3 (12%)
Volume	14.1 ± 0.5 (4%)	14.0 ± 0.5 (4%)	15.4 ± 0.6 (4%)
Overall	13.3 ± 0.5 (4%)	13.4 ± 0.5 (4%)	13.3 ± 0.5 (4%)

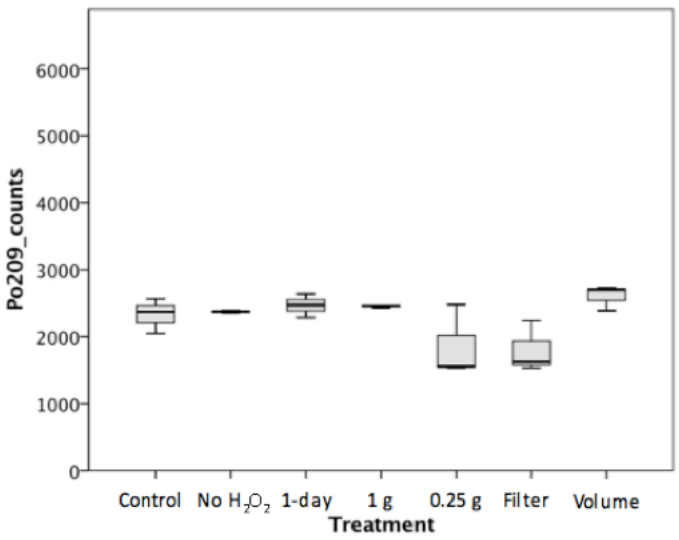

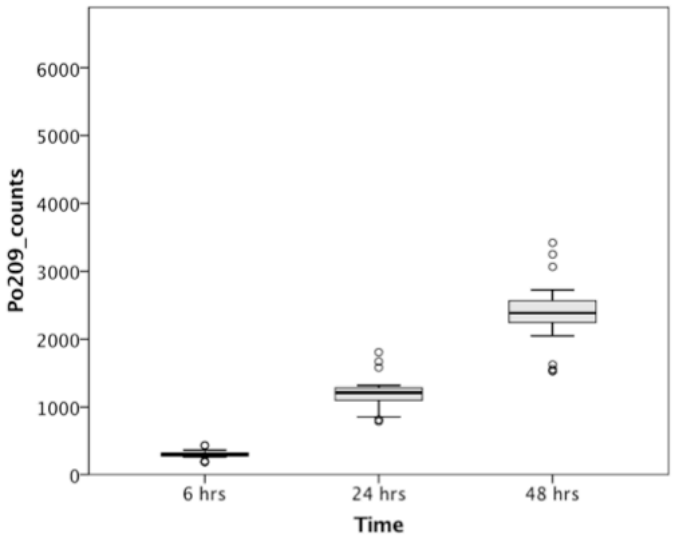

Figure 5.3 Number of counts for ^{209}Po for each treatment (n = 3 per treatment) recorded after 48 hours from the start of counting (left), and (b) over time (n = 7 per time period; right).

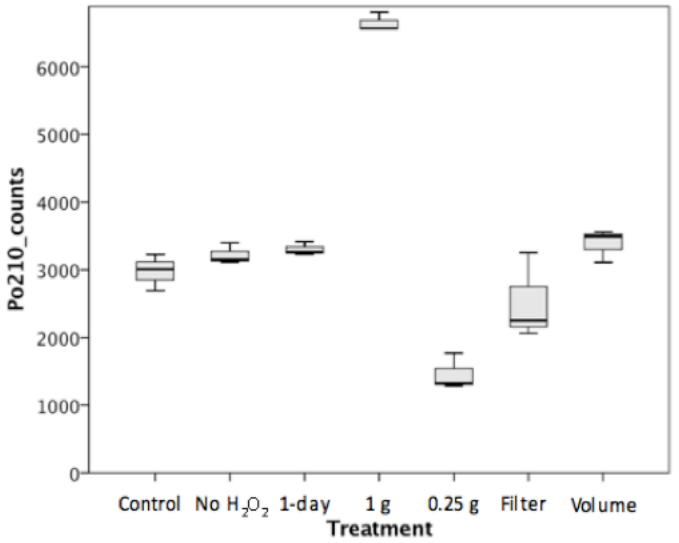

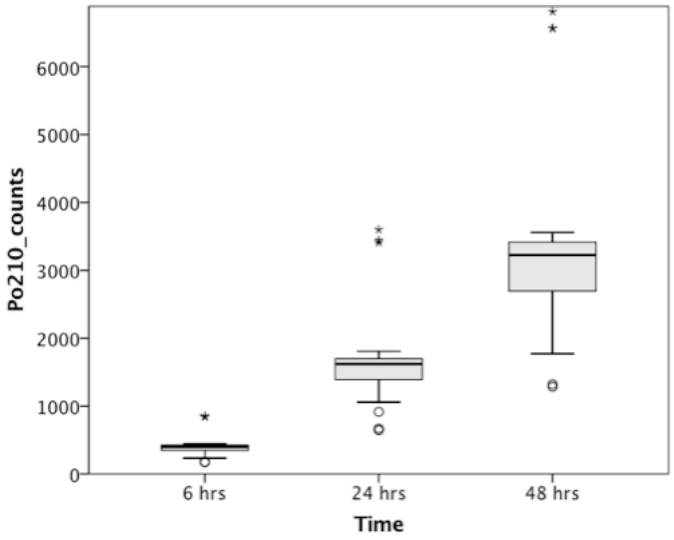

Figure 5.4 Number of counts for ^{210}Po for each treatment (n = 3 per treatment) recorded after 48 hours from the start of counting (left), and (b) over time (n = 7 per time period; right).

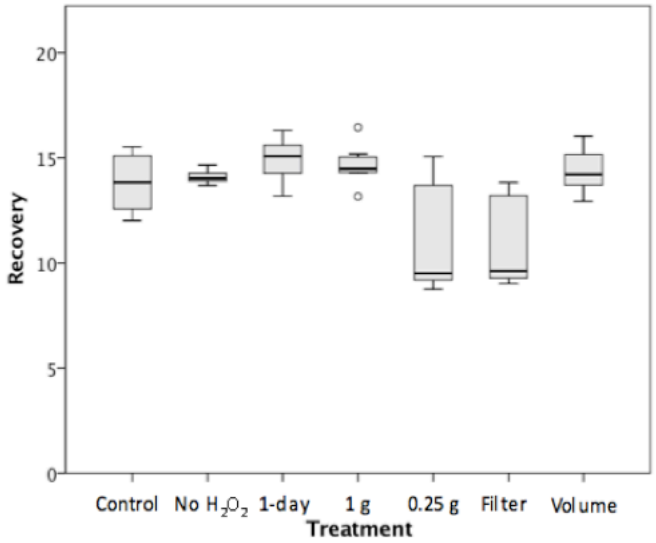

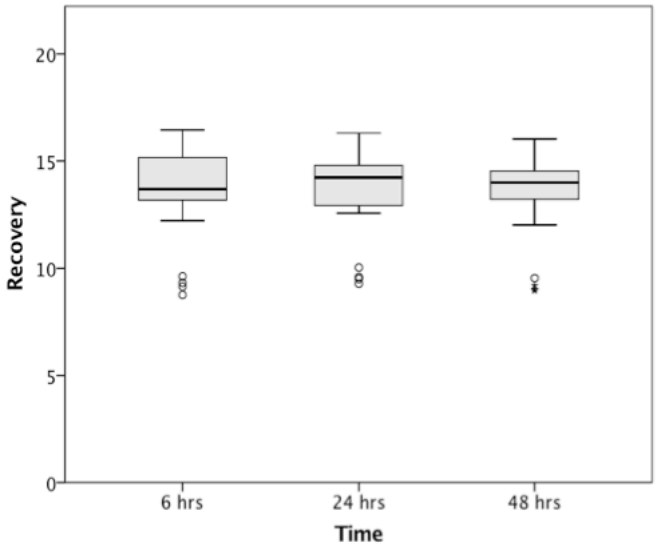

Figure 5.5 Po recovery rates (in %) for each treatment (n = 3 per treatment) recorded after 48 hours from the start of counting (left), and (b) over time (n = 7 per time period; right)

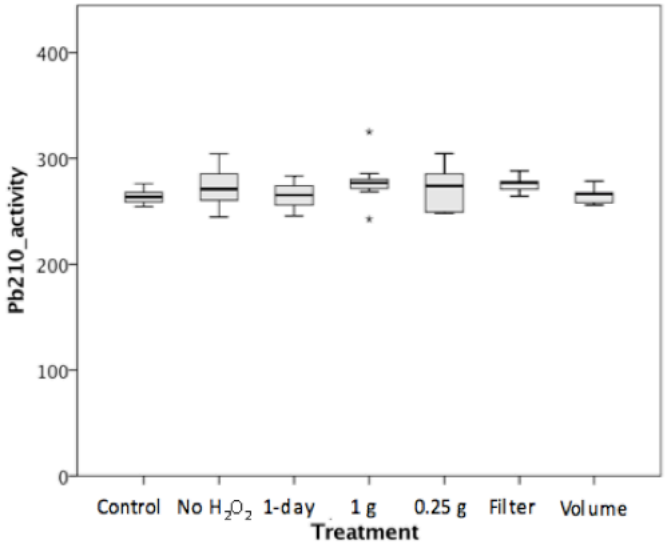

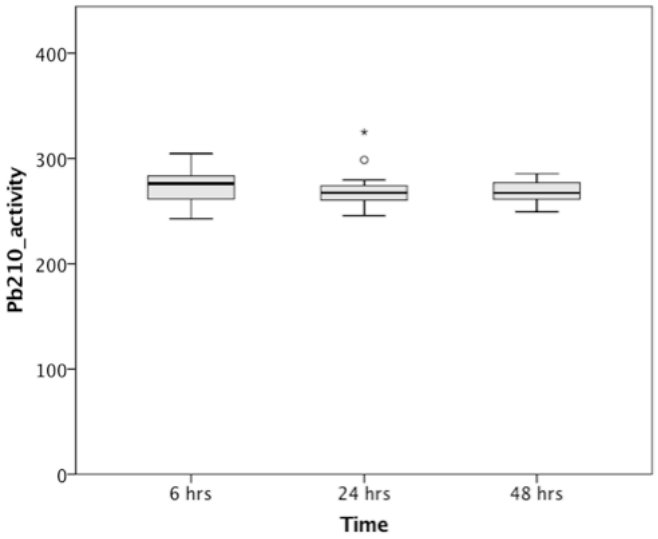

Figure 5.6 Measured ^{210}Pb activities (in Bq kg^{-1}) for each treatment (n = 3 per treatment) recorded after 48 hours from the start of counting (left), and (b) over time (n = 7 per time period; right)

5.4.1.2 *Recovery rates*

Recovery rates are calculated based on time and the ^{209}Po spike counts. Mean % Po recovery for each treatment over time are summarised in Table 5.6 and Figure 5.5. Po recovery rates vary from 10-20% (13.4 ± 0.3 % Po recovered overall). As for ^{209}Po counts, the lowest recovery rates and largest error are for the small sample size and filtering treatments.

The largest recovery is for the '1 day' treatment; the 'no H_2O_2' treatment has the lowest error, along with the larger sample size treatment after 48 hours of counting. However, there is no statistically significant difference between recovery rates over time or between treatments.

5.4.1.3 *^{210}Pb activities*

^{210}Pb activity is calculated as the ratio between ^{210}Po and ^{209}Po, corrected for decay, time since preparation and sample size. Mean activity is 270.3 ± 1.9 Bq kg^{-1} and is summarized for each treatment over time in Table 5.7 and Figure 5.6. Standard errors are less than 5% in most cases even when measured at 6 hours from the start of counting. Overall, there is no significant difference in activity over time, within each time period, between treatments and within treatments.

Table 5.7 Mean ^{210}Pb activity (Bq/kg; n = 21) over time for each treatment; standard errors and % error are indicated.

Treatment	6 hours	24 hours	48 hours
A	267 ± 5 (2%)	263 ± 5 (2%)	262 ± 3 (1%)
B	269 ± 18 (7%)	277 ± 11 (4%)	275 ± 6 (2%)
C	267 ± 9 (3%)	262 ± 9 (3%)	266 ± 7 (2%)
D	266 ± 12 (5%)	292 ± 17 (6%)	277 ± 2 (< 1%)
E	289 ± 8 (3%)	257 ± 8 (3%)	265 ± 11 (4%)
F	283 ± 3 (1%)	273 ± 4 (1%)	272 ± 3 (1%)
G	268 ± 7 (3%)	263 ± 3 (1%)	264 ± 3 (1%)
Overall	273 ± 4 (1%)	269 ± 4 (1%)	269 ± 2 (1%)

5.4.2 Testing the method

There is good agreement between activity calculated from samples prepared with the adapted ^{210}Po extraction method and the gamma spectrometry results (Figure 5.7 and Figure 5.8: linear regression: $R^2 = 0.98$, $p < 0.001$). Alpha measurements are slightly lower than gamma at high activities and lower for low activities.

In the pilot study (Section 5.2.1), the 'mineral' method underestimated the ^{210}Pb activity in the top 15 cm of the core; however, there was good agreement between all three methods ('mineral' and 'organic' alpha, and gamma) for deeper samples. Activities determined by gamma spectrometry tend to have a larger counting error, and dropped below the instrumental minimum detectable activity at 30 cm; this could have implications for future age calculations.

5.4.3 Alpha vs. Gamma comparison

5.4.3.1 *^{210}Pb activity*

There is generally good agreement between alpha- and gamma-determined ^{210}Pb activities (Figure 5.9). In deeper samples, gamma profiles drop below the instrumental minimum detectable activity (MDA) (PTB.1: 30 cm; D.C06: 16 cm; D.D05: 21 cm; D.B13: 13 cm) while alpha profiles gradually tail off, reflecting exponential decay of ^{210}Pb. Where $^{210}Pb_{ex}$ activities are detected using gamma spectrometry (above the MDA), there good statistical agreement between the methods (linear regression: $R^2 = 0.96$; $p < 0.001$; Figure 5.11). Gamma-derived activities are slightly higher than alpha at low activities. In addition, there are some discrepancies at the surface in Dartmoor cores, in particular D.D05 (0-5 cm), while the *Sphagnum* Petite core (PTB.1) shows consistent results for both methods (Figure 5.9). It should be noted that the topmost sample for D.D05 is ± 2 g (smaller than the rest). Gamma errors are also larger than those calculated from alpha as these reflect counting statistics and instrumental error.

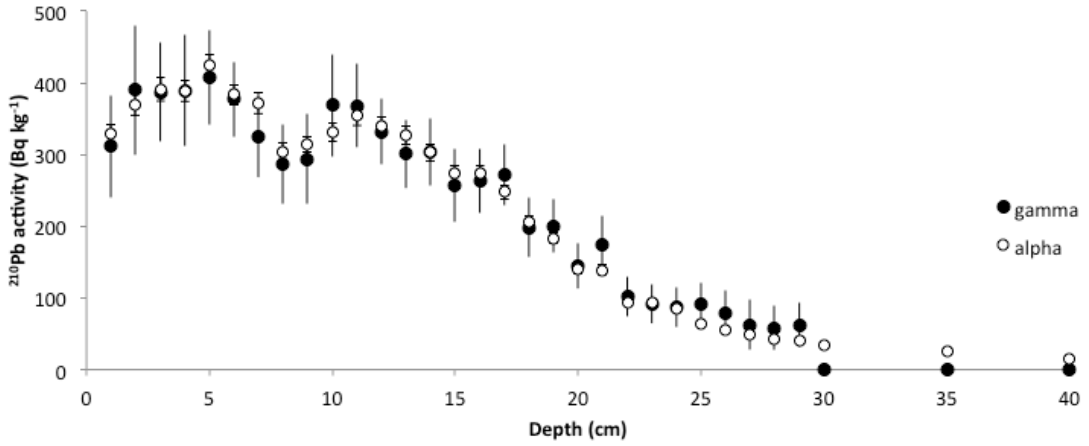

Figure 5.7 Comparison of ^{210}Pb activities determined using alpha and gamma comparison for a core from Petite bog (PTB.1). Closed circles (black, uncapped error bars) represent results determined using gamma spectrometry; open circles are from alpha spectrometry following the new adapted 'organic' analysis method. Agreement between the methods is consistent (vs. Figure 5.1: pilot study).

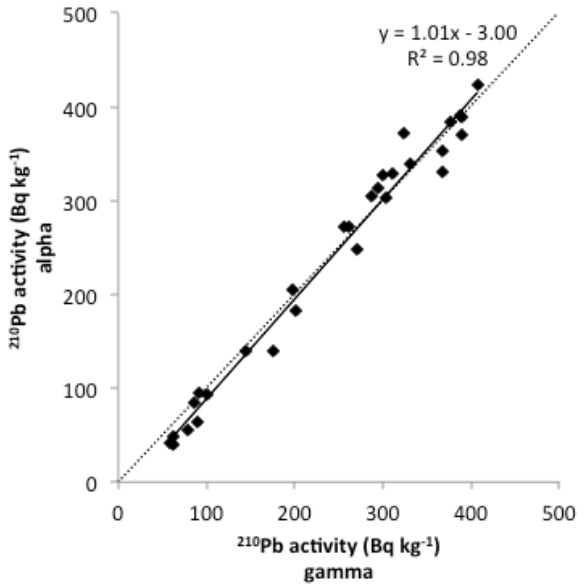

Figure 5.8. Comparisons of ^{210}Pb activities using both alpha ('organic') and gamma spectrometry techniques. The solid line is the trendline and the dotted line is the 1:1 line.

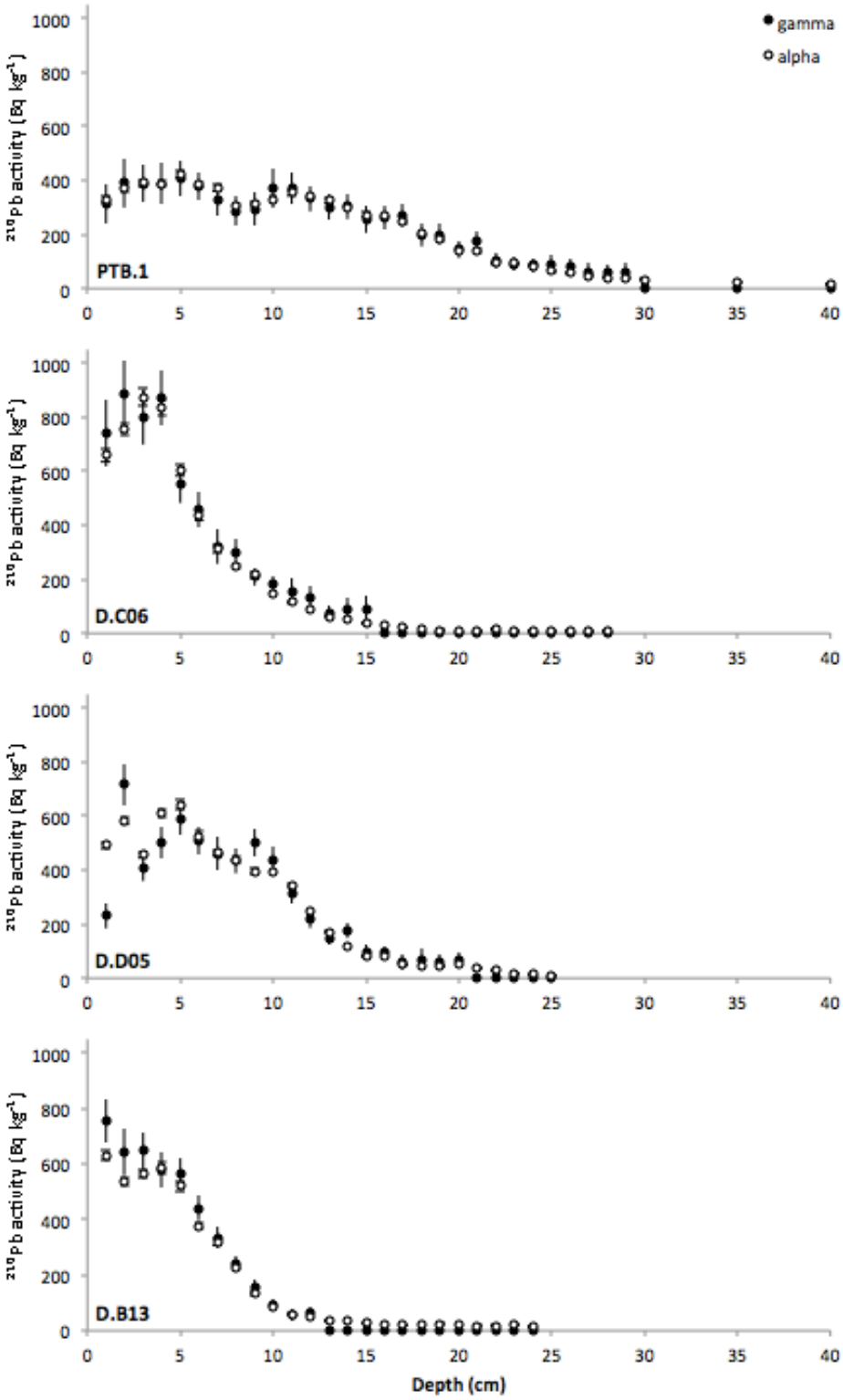

Figure 5.9 ^{210}Pb activity (Bq kg^{-1}) determined using alpha (open circles) and gamma (closed circles) spectrometry for Petite Bog (PTB.1) and three Dartmoor cores (control: D.C06, drained: D.D05 and burned D.B13 from Parry *et al.,* 2013).

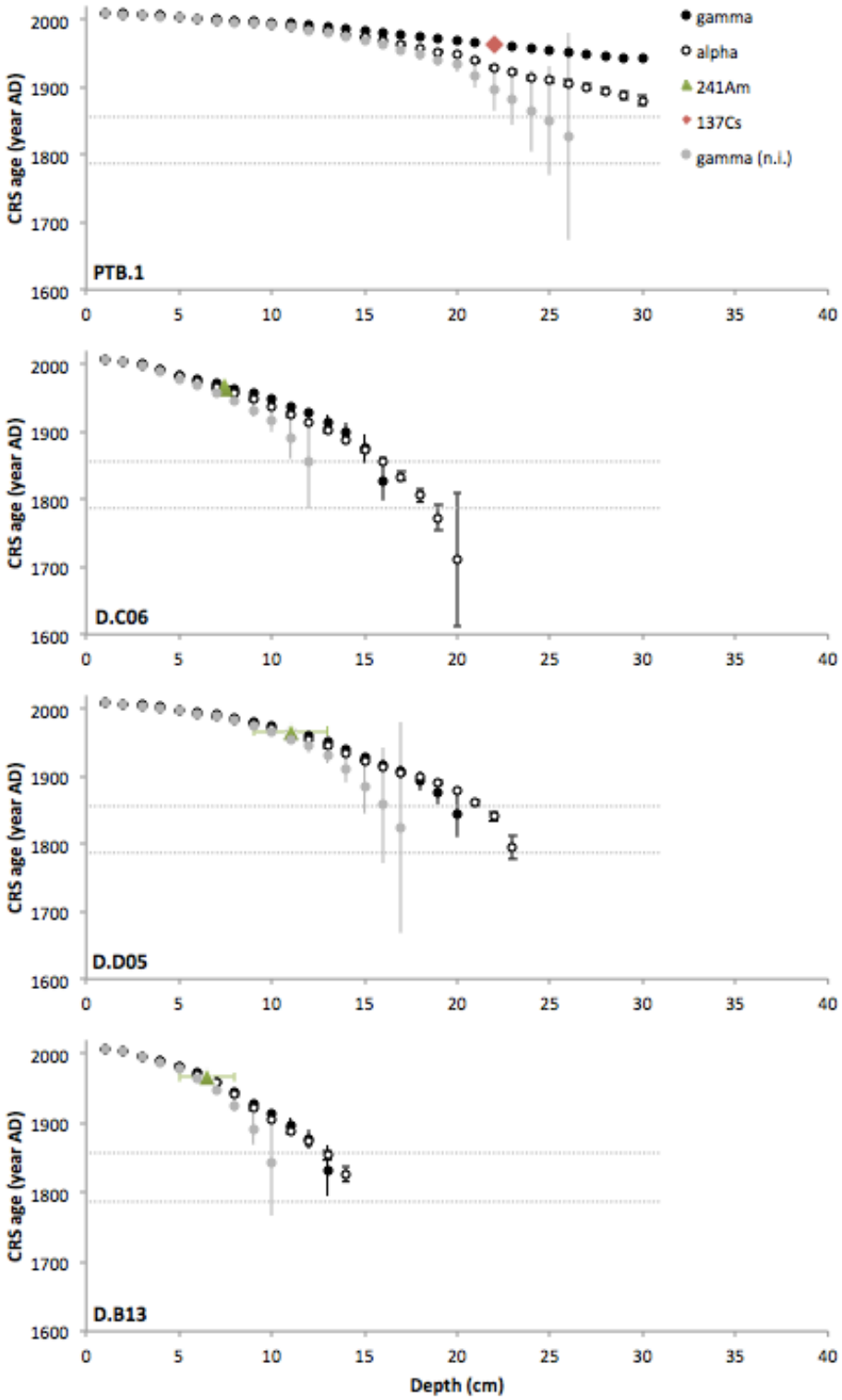

Figure 5.10 ^{210}Pb ages determined using alpha (open circles) and gamma spectrometry (closed black circles: modelled equilibrium depth; closed grey circles: equilibrium depth = sample with lowest detectable activity) for Petite Bog (PTB.1) and three Dartmoor cores (control: D.C06, drained: D.D05 and burned D.B13 from Parry *et al.,* 2013). Dotted lines represent 7 and 10 ^{210}Pb half-lives from the core collection date.

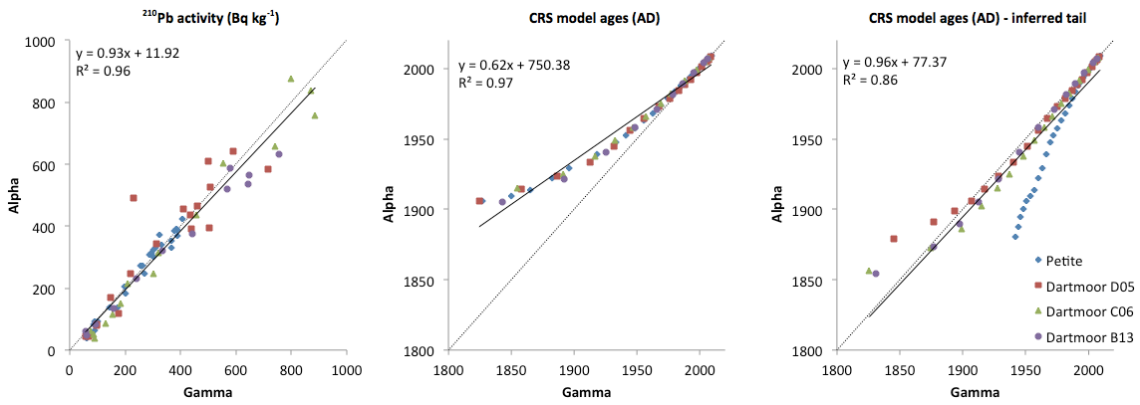

Figure 5.11 Alpha and gamma comparisons for activities (left) and CRS modelled ages (centre and right, unmodelled (n.i.) and with modelled or inferred tail, respectively). Dotted lines are 1:1 lines and solid black lines are trendlines for each relationship.

5.4.3.2 *CRS ages*

CRS-derived ages are shown in Figure 5.10, calculating using activities measured from (1) the 'organic' method and alpha spectrometry, (2) gamma spectrometry and using only the measured data (not-inferred, or n.i.), and (3) gamma spectrometry, fitting the results to the ^{137}Cs and ^{241}Am dates (if available) and including data from modelling the 'tail' based on exponential decay.

Alpha-derived models provide the longest record over time, and generally show good agreement with the modelled gamma dates, except in the case of PTB.1, the only core for which a ^{137}Cs peak was detected (Figure 5.10 and 5.11). 'Not-inferred', or unmodelled gamma results are consistently older and have larger age uncertainties than results obtained using the other two methods. While the measured ^{210}Pb activities for PTB.1 (Petite) were in agreement, the modelled gamma dates are considerably younger than the alpha-derived dates; however, this model takes into account the ^{137}Cs contribution, which has been found to be highly mobile in peat (Oldfield *et al.,* 1995; Parry *et al.,* 2013).

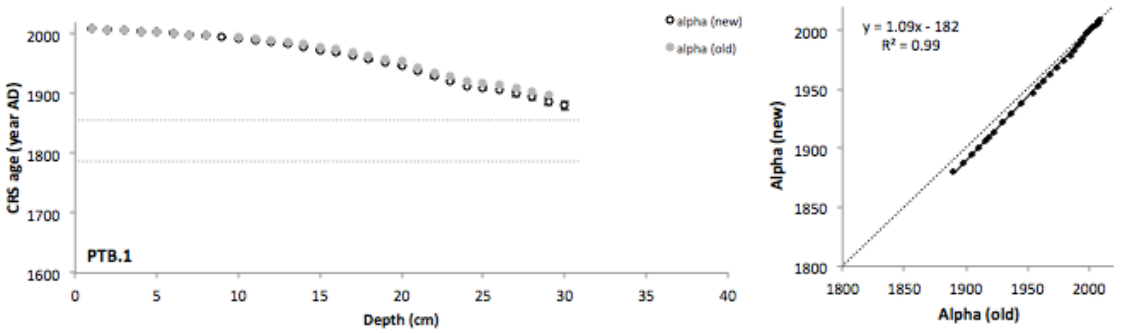

Figure 5.12 CRS ages calculated using the 'mineral' (or 'old') preparation method used in the pilot study (grey circles) and the new adapted 'organic' method for this thesis (closed circles) (right), and correlation between the two alpha methods (left).

Despite the differences in ^{210}Pb activities reported during the initial pilot study (Figure 5.1), there is no significant difference in the CRS ages calculated using activities measured from the 'mineral' and the 'organic' alpha preparation methods (Figure 5.12). The CRS modelled ages were not significantly different between the two methods (ages were *ca.* 10 years older in the 'old' method pre-1900AD, but similar after 1900AD). However, the total inventory was underestimated using the 'mineral' method, i.e. there was an incomplete Po extraction, and therefore deposition rates are underestimated.

5.4.3.3 *Total inventories and fallout*

Table 5.8 summarises total unsupported ^{210}Pb inventory and annual fallout rate estimated using the CRS model for each core. ANOVA showed no significant difference between inventories determined using alpha spectrometry and those from gamma spectrometry. There is a significant difference between the Dartmoor cores and the Petite Bog core (ANOVA: $p < 0.005$). This result is expected as different regions have different ^{210}Pb deposition patterns.

Table 5.8 Core total inventories and annual fallout for alpha and gamma spectrometry (both raw CRS and inferred-tail CRS) results. Errors are calculated based on counting statistics, instrumental/analytical error and propagation of error.

	Total $^{210}Pb_{ex}$ inventory (Bq m^{-2})			**Annual ^{210}Pb fallout (Bq m^{-2} yr^{-1})**		
Core	**α**	**γ (n.i)**	**γ (i)**	**α**	**γ (n.i)**	**γ (i)**
PTB.1	2456 ± 39	1950 ± 122	n/a	76 ± 1	61 ± 4	n/a
D.C06	5520 ± 132	4663 ± 287	6326 ± 1071	171 ± 2	145 ± 9	197 ± 33
D.D05	7118 ± 133	5677 ± 320	5399 ± 561	222 ± 4	177 ± 10	168 ± 21
D.B13	4495 ± 110	4438 ± 227	4387 ± 546	140 ± 3	138 ± 7	137 ± 17

5.5 Discussion

5.5.1 Sample preparation for alpha spectrometry

Treatments were selected based on laboratory resources, material availability, key questions raised from the pilot trial with the 'mineral' method, and a review of published preparation methods for other sample types. Here, each treatment is discussed individually, and then the 'organic' method ('control' treatment) is evaluated relative to other methods.

5.5.1.1 *Acid treatment*

The combination of acids used was the key step for analysing organic vs. mineral samples. Po recovery rates were slightly higher and the error lower when the H_2O_2 step was omitted, possibly due to the lack of additional heating required bringing the sample to dryness and Po volatility; this was not a significant difference. The opposite was found in comparing activities – the mean activity was slightly higher but the range was also larger; perhaps not all ^{210}Po was extracted from the sample. While there was no difference between using and not using H_2O_2 in this trial, it should be noted that the peat used was surface *Sphagnum* peat; different acid digestion results may arise when applied to different peat types (e.g. deeper recalcitrant material). The H_2O_2 step should be applied for consistent down-core sample preparation.

5.5.1.2 *Preparation time*

Po recovery was slightly but not significantly higher with shorter preparation time, likely due to reduced evaporation, as the samples were not left overnight to stand in H_2O_2. A possible solution to this would be to cover the beakers overnight with a watch glass. Preparation time can therefore be determined at the discretion of the user, with more recalcitrant samples requiring larger quantities of acids, and controlled heating.

5.5.1.3 *Sample size*

After 48 hours, large sample sizes (1 g) tended to have the smallest range of activities; however, larger than 1 g may require additional acids (as with the original lab method for mineral soils) and counting time. As there was no significant difference with other treatments, it is possible but not necessary to use 1 g of sample. It is not always available for surface peats and results are comparable when smaller sample sizes were used. It may be recommended to use larger sample sizes if the peat composition is very heterogeneous.

The samples with less material (0.25 g) have the lowest Po recovery rate and highest error (> 10%) over time, although this is not statistically significant. This result is expected, as the Po concentration of the plating solution is lower than for the other treatments. This difference is not reflected in the sample-size corrected ^{210}Pb activity, indicating the effectiveness of the yield tracer. Smaller sample sizes could therefore be used in order to accurately estimate ^{210}Pb activity (Ali *et al.,* 2008; Pratte *et al.,* 2013); this is especially relevant for peat surface samples with low bulk densities, e.g. acid digesting more than 0.1 g dried peat may not be possible with other analyses from a core taken with a Russian corer or a small monolith.

5.5.1.4 *Filtering*

When the samples were filtered, Po recovery was lower and has a larger error (> 10%) over time than other treatments, possibly due to interference from the filter paper; however, this is not significant. Despite this, there is no statistically significant difference in activities calculated between filtering and not filtering the plating solution meaning that ^{209}Po and ^{210}Po were lost more or less evenly. Adding a filtering step to the method could be considered if there are floating particulates present in the plating solution from incomplete digestion of more recalcitrant samples that could affect the deposition stage by sticking to the plate and reducing the area.

5.5.1.5 *Plating volume*

The hypothesis was that smaller plating volumes, i.e. a more concentrated plating solution, might yield higher Po recovery. There was no significant relationship reported here for 60 ml and 120 ml. While smaller plating volumes could be tested, new plating jars would be required as suspending plates in < 60 ml would be difficult so this was not investigated further for this study.

5.5.1.6 *Counting time*

For both ^{209}Po and ^{210}Po, counts increased linearly with time at 6, 24 and 48 hours as expected; no levelling off as half-lives are 125 years and 138 days, respectively. For these samples, there was no significant difference between time periods and all samples had reached > 400 counts by 24 hours and the error was lowest at this point. In low-activity samples this may be more important, especially if the whole core is low-activity: with low ^{210}Po counting rate, it is not necessary to leave ^{210}Po until 400 counts, as the ratio doesn't change with high ^{209}Po and the longer they are left the more the background error increases.

5.5.1.7 *The 'organic' method for peat samples*

The 'control' treatment method was found to have the most consistent results (smallest error) in activity over time; however, as no significant differences were found in activities between treatments, there is flexibility when choosing between steps and the method can be adapted based on sample type and quantity available. For ombrotrophic peat, the sample size (0.5 g) and acids used are optimal but can be more or less depending on depth, i.e. samples from surface *Sphagnum* peat with high activity and low bulk density can be smaller (but care should be taken to homogenise the sample) while deeper peat might require additional H_2O_2 or filtering to eliminate more recalcitrant material. Stronger acids such as HF (as in Pratte *et al.,* 2013) or 'bombs' (as in Yafa and Farmer, 2006) may increase the Po recovery rate, but also increase health and safety risks. Results from this method were compared with gamma results and dates from different cores from Dartmoor in lieu of further trials with different peat types (discussed in the next section). The comparison with activities for the same samples from PTB.1 derived from alpha and gamma spectrometry demonstrates that the results are not biased due to the incomplete extraction of Po. The key step is to carefully account for the ^{209}Po tracer addition.

Po recovery rates were low for all treatments (~13%) possibly due to incomplete extraction or experimental errors such as over-heating; however, they were consistent over time and between treatments. Further optimising the method to increase recovery rates (e.g. 9-99% for ashing method in DeVleeschouwer *et al.,* 2010; heating during the plating process in Jia *et al.,* 2001) may not be necessary as the results are consistent with those from gamma spectrometry. This shows that the spike is acting as a yield tracer and there is no fractionation between ^{209}Po and ^{210}Po. Care should also be taken when heating the samples, as Po is volatile at temperatures above 100 ^{o}C and hotplates may not be well regulated.

5.5.2 Alpha and gamma spectrometry comparison

The ^{210}Pb activities calculated with both alpha and gamma spectrometry methods agree. This indicates that the results for measured activity are comparable (within error) between both methods on a range of peat types. Alpha-counted ^{210}Pb activities were smaller than gamma-counted results overall, but fell within the error range as for alpha/gamma spectrometry comparisons in lake and estuarine samples *(Tanner et al., 2000; Zaborska et al.,* 2007). As the gamma-derived dates in this chapter were calibrated using reference soil material spiked with certified mixed radioactive standards supplied by AEA Technology PLC and compared against other laboratories using materials supplied by the IAEA (International Atomic Energy Agency) (Parry *et al.,* 2013), we can conclude that the Po extraction method used for this thesis is effective for estimating ^{210}Pb activities using alpha spectrometry, and that down-core uncertainties in ^{210}Pb dates will not be due to methodological errors, but more likely environmental factors such as post-depositional mobility, discussed in Chapter 6 (e.g. Urban *et al.,* 1990; Vile *et al.,* 1995).

Main discrepancies between alpha and gamma-derived activities include the differences between high-activity surface samples (e.g. top 5 cm of Dartmoor cores) and deeper samples where gamma activity drops below the minimum detectable activity; these are likely to affect CRS modelled ages and sedimentation rates if the total inventory is not accounted for. The 'dip' in activities for the surface samples is likely due to lack of compression and percolation through the top layers of peat; this may be addressed by using an updated alternative to the CRS method, such as the new 'Initial-Penetration-Constant Rate of Supply' (IP-CRS) model discussed by Olid *et al. (*2015).Results from the pilot study indicated that the measured ^{210}Pb activities in the top 15 cm samples were lower using the 'mineral' alpha method compared to the 'organic' alpha method and gamma spectrometry, meaning that the total ^{210}Pb inventory and annual fallout rate were underestimated (Figure 5.1). The total ^{210}Pb

inventory calculated using the CRS model was lower for the 'mineral' method than for the 'organic' method (1856 (± n.a.) vs. 2456 ± 39 Bq kg^{-1}), as activities for the samples in the top 15 cm were underestimated, thus also underestimating annual fallout. Despite these differences in activity and inventory, this had little impact on the calculated CRS ages which were similar for both alpha methods (Figure 5.12), indicating uncertainties related to the CRS model. As indicated previously, modifications to this model may resolve this issue (Olid *et al.,* 2015).

The inventories and fallout rates were consistent between the two techniques for each core; this is true even if the model used for gamma was with an inferred tail or not. No one method yielded consistently higher or lower inventories/fallout rates. The fallout rates in all cases were consistent with estimates for global average fallout (166 Bq m^{-2} yr^{-1}, range 95-329: Appleby and Oldfield, 1978); Dartmoor fallout was also within the range for the UK (Smith *et al.,* 1997; Parry *et al.,* 2013). Fallout for Petite Bog was lower than nearby areas (e.g. 1.1 dpm cm^{-2} yr^{-1} = 183 Bq m^{-2} yr^{-1} in south central Ontario: Evans *et al.,* 1986), as expected for coastal areas where precipitation patterns are influenced by marine air (Du *et al.,* 2015).

Gamma ages without modelling the 'tail' were overestimated; as the total inventory was not significantly different, this difference was from selecting the equilibrium depth as approximately 5 cm shallower than with alpha or modelled gamma leading to systematically overestimating the ages (e.g. by 60-80 years for older samples). The error is also larger and propagated down-core. Care should be taken with gamma-derived data, as the minimum depth detected may not be the equilibrium level. Indeed, when these data are modelled, ages are not significantly different between gamma and alpha. For the Petite core, gamma dates were modelled to agree with ^{137}Cs and differ from alpha dates (Figure 5.11). However, if in this case the ^{137}Cs was mobilised in the core, ages are then underestimated. Without additional date constraints at deeper

samples, which are the 'real' ages? This will be considered further in following chapters.

5.5.3 Selecting a method for ^{210}Pb dating

Figure 5.13 summarises key considerations and steps when selecting a method for ^{210}Pb dating from the available resources, to sampling, source preparation, spectrometry, and age-depth modelling.

5.6 Conclusion

The choice of a preparation for Po extraction method for ombrotrophic peat can be flexible, as is the counting method for a variety of peat types (*Sphagnum*-dominated, vascular/ericaceous plants, various decomposition stages). Estimating accurate ^{210}Pb ages is mainly related to: (1) selecting an appropriate equilibrium depth, (2) accurately adapting the CRS model (e.g. if sample activity is below the instrumental MDA), and (3) monitoring for disturbance (e.g. mobility).

The alpha preparation/Po extraction method selection is not a critical factor; assuming the preparation/counting has been done with high confidence, i.e. complete digestion and low counting error, any age-depth uncertainties will more likely be related to post-depositional mobility rather than method-based errors. Deposition patterns and mobility will be investigated in Chapter 6. The Po extraction method tested in this chapter can therefore be confidently used to analyse samples using alpha spectrometry, and to accurately measure ^{210}Pb dates when analysing peat cores.

This inter-laboratory comparison between the two spectrometry methods shows good agreement, with internationally calibrated standards, indicating that the choice between alpha and gamma spectrometry methods should be guided by available sample size and type, laboratory resources, cost and time. The source of the samples should also

be considered; e.g. alpha counting would be preferable when analysing cores from predicted low-activity areas such as Antarctica or Patagonia. While the spectrometry methods agree in terms of inventory and activity calculations, additional considerations for dating are suggested. The same questions arise for both methods, namely calibrating the CRS model with additional dating markers (when available) and taking into account instrumental limitations affecting the key equilibrium depth selection. Main differences between age-depth profiles are from the deeper samples where selecting the 'wrong' equilibrium depth can incur considerable errors. Deeper markers would be beneficial, e.g. pollen or ^{14}C post-bomb dates.

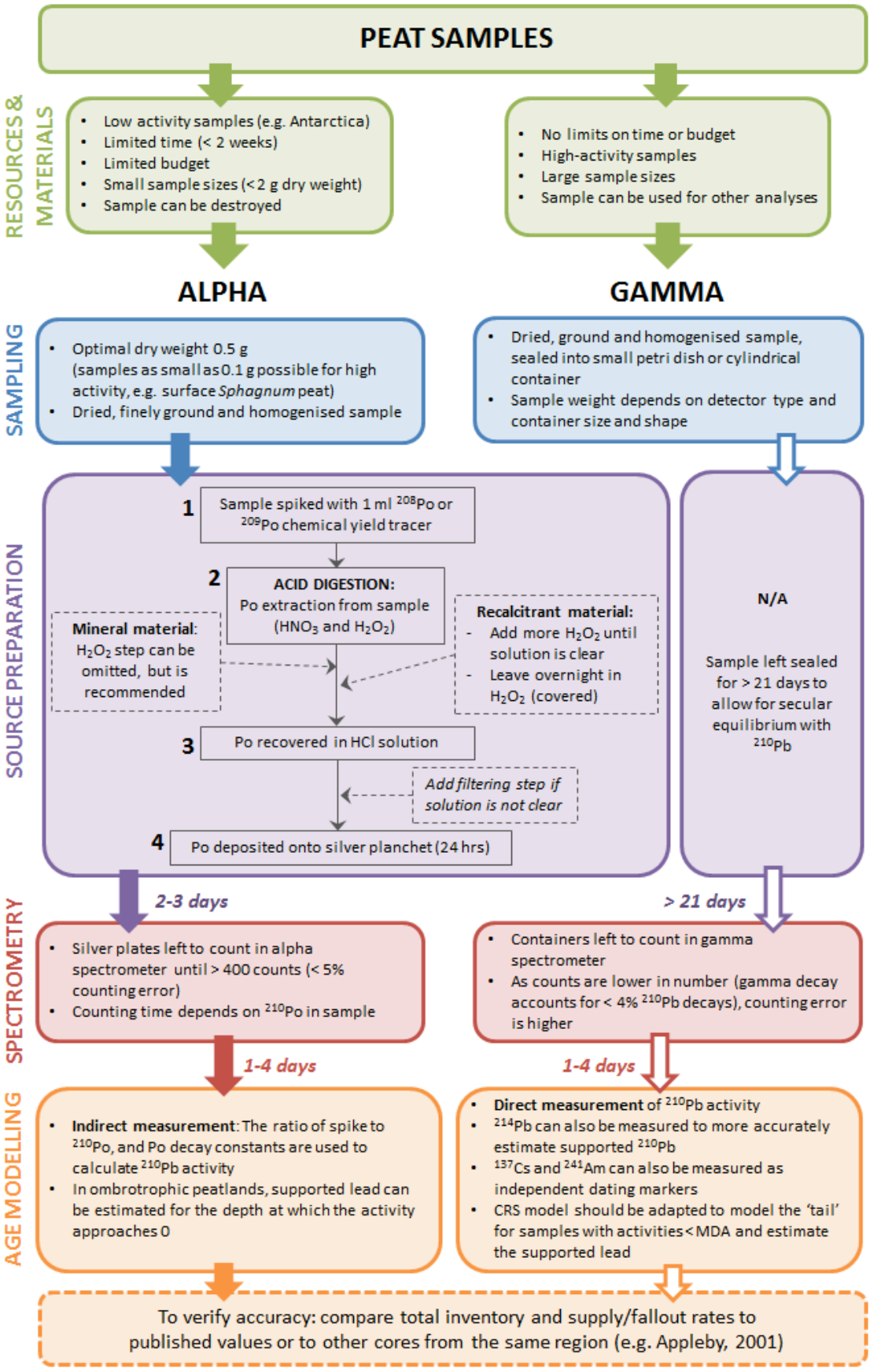

Figure 5.13 Summary flow chart for ^{210}Pb dating method selection, including suitability for alpha or gamma spectrometry, and considerations for Po extraction and age-depth modelling.

6 Recent peat accumulation and within-site variability

6.1 Overview

Permafrost in Northeastern Canada has been degrading since the 1950s, and the degradation is projected to continue in response to recent temperature increases (Payette, 2004). The last few decades have been the warmest on record, and this trend is projected to continue (Kaufman *et al.,* 2009; PAGES 2k Consortium, 2013). In Western Canada, permafrost-driven changes in microtopography have altered the sink-source balance of peatlands during and since the end of the Little Ice Age (LIA) (Turetsky *et al.,* 2002a, 2007).

This recent period of the last 150-200 years is often omitted from studies of millennial-scale carbon accumulation (e.g. Charman *et al.,* 2013; Magnan and Garneau, 2014a; van Bellen *et al.,* 2011b) as it contains the acrotelm and peat that has not fully undergone decomposition. During this time period, within-site variability and microtopography play important roles, as surface structure is a driver of carbon uptake and short-term changes in accumulation (Belyea and Malmer, 2004; Eppinga *et al.,* 2007, 2009). Links between climate, water table and peatland accumulation responses to rapid decadal change are complex and poorly understood. Changes in carbon accumulation may occur independently from climate due to autogenic factors and ecohydrological feedbacks, which may be difficult to interpret for a region based on the analysis of a single palaeoecological record (Swindles *et al.,* 2012; Loisel *et al.,* 2014). As Watson *et al. (*2015) found for the past 450 years based on tephra records in Ireland, carbon accumulation rates vary considerably within the same peatland for the same time period. As reviewed in Chapter 2 (Section 2.2), peatlands are 'complex adaptive systems' and recent dynamic peat growth models (e.g. Belyea and Clymo,

2001; Frolking *et al.,* 2010) do not account for spatial variability in peat accumulation and the potential feedbacks of surface structure and hydrology. While directly comparing rates of carbon accumulation for the acrotelm and older/deeper sections that have been undergoing long-term decomposition in the catotelm is not always valid, comparing recent apparent accumulation between cores within and between sites for the same period may help to look at dominant processes and mechanisms of change to explain some of the complexity of peat accumulation responses to climate or hydrology. In this study, the 'humpbacked' relationship between acrotelm thickness or water table depth and peat accumulation modelled by Belyea and Clymo (2001) can be evaluated with replicate cores in the field (hummocks persist). According to this model, microforms of intermediate wetness have highest peat accumulation rates, up to a threshold.

Considering changes over the last 150-200 years is further complicated by potentially poor dating resolution, as there may be a large error associated with using few recent radiocarbon dates (Turetsky *et al.,* 2004). Therefore, accurately dating recent peat accumulation is important to estimating rapid changes in carbon accumulation rates (e.g. Garneau *et al.,* 2014). The previous chapter has highlighted the benefits of using lead-210 (^{210}Pb) dating; however, it was noted that there is some uncertainty in the literature. Some studies show that ^{210}Pb profiles in peat may be impacted by decomposition, lateral water movements between microforms and pools and dissolved organic carbon (DOC) leaching (Damman, 1978; Oldfield *et al.,* 1979; Urban *et al.,* 1990). There may also be some local effects such as cryoturbation due to permafrost degradation (Turetsky *et al.,* 2004). Conversely, other studies found no issue with mobility (e.g. Parry *et al.,* 2013; Vile *et al.,* 1994). Statistically comparing total inventories along a microtopography gradient may be a way to establish whether movement occurred. This chapter will consider the Constant Rate of Supply (CRS)

dating model assumptions, as using replicate cores provides an opportunity to study deposition patterns and post-depositional mobility.

Chapter aim and objectives:

The overall aim of this chapter is to evaluate the role of microtopography on local spatial variability in recent carbon accumulation (Section 1.2, Objective 2). In order to consider this question, two main objectives will be addressed using replicate cores from different microtopographical units: (1) to evaluate the validity of ^{210}Pb dating the sites by considering spatial variability in deposition and post-depositional mobility; and (2) to calculate and compare within-site carbon accumulation along a microtopography gradient for the past 150 years.

It was hypothesised from the literature review findings (Section 2.5) that CAR would vary along a microtopographical gradient, similarly to Belyea and Clymo's (2001) humpbacked relationship between peat accumulation and acrotelm thickness, with *Sphagnum* hummocks having the highest accumulation rates, and the 'extreme' microforms (e.g. lichen hummocks and hollows) having the lowest CAR. This chapter uses replicate cores to consider these relationships in a range of ecoclimatic conditions.

6.2 Methodology

6.2.1 Core collection

All cores (n = 30) were analysed for this chapter, representing the spatial variability within each region. From each of the three regions, Baie Comeau (BC: 49°06'N, 68°14'W), Havre-Saint-Pierre (HP: 50°16'N, 63°40'W) and Blanc Sablon (BS: 51°29'N, 57°11'W), 3 to 4 cores were collected along a hydrological gradient from three replicate peatlands. Coring locations were selected from the central dome, based on previous

studies of Holocene peat accumulation (Magnan and Garneau, 2014a,b). Microforms were selected a few metres apart when possible along a hydrological transect, from hollows (wettest) near pool edges, lawns (intermediate), to *Sphagnum* and lichen-topped hummocks (driest). They were differentiated in the field by their relative height and surface vegetation (*cf.* Chapter 3 for site descriptions and definitions). Water table depth was measured in the field 1 hour after coring, except at Blanc Sablon sites where there was still ice.

6.2.2 Laboratory methods

For all cores, bulk density and carbon content were measured at 0.5 cm increments (Equations 3.1 to 3.4, Chapter 3). Lead-210 (^{210}Pb) activity was measured for 1 cm depth increments at every 2 cm at the surface, and every 5-10 cm down-core. Samples were prepared using the polonium (Po) extraction and plating method discussed in Chapter 5, followed by alpha spectrometry using and Ortec Octête Plus Integrated Alpha-Spectrometry System with Maestro software. Continuous chronologies, total ^{210}Pb inventory and supply rates, and peat accretion rates were calculated using the CRS model (Appleby and Oldfield, 1978; Appleby, 2001) (*cf.* Chapters 3 and 5). Exponential decay was assumed between sampled points to model the ^{210}Pb-derived ages.

6.2.3 Evaluating the CRS assumptions

The main assumptions of the CRS model are: (1) a constant supply of ^{210}Pb to the peat surface; (2) rapid transfer of ^{210}Pb to peat; and (3) post-depositional immobility (Appleby and Oldfield, 1978; Oldfield *et al.,* 1995). As the peatlands are ombrotrophic, the main component of the ^{210}Pb inventory is the 'excess' or 'unsupported' lead-210 ($^{210}Pb_{ex}$); therefore activity profiles meeting the assumptions should decrease exponentially with depth to near-0 with depth. Indeed, the coefficient of determination (R^2) from a linear regression between log($^{210}Pb_{ex}$) and cumulative mass for an 'ideal'

core approaches 1 (Appleby, 2001; Le Roux and Marshall, 2011), with deviations indicating potential mobility or changes in peat accumulation rate. Assuming constant ^{210}Pb supply to a region, replicate ^{210}Pb inventories are compared here in order to address potential mobility within a site along a hydrological gradient. Within- and between-site differences in total $^{210}Pb_{ex}$ inventories for each region were tested using one-way analysis of variance (ANOVA) (Dytham, 2010; Laerd Statistics, 2015) in SPSS v. 21.0 (IBM, 2012); normality and homogeneity of variances were assessed using Kolmogorov-Smirnov and Levene's tests, respectively. Significant ($p < 0.05$) ANOVA results were considered using Fisher's least significant difference (LSD) post-hoc test.

6.2.4 Comparing carbon accumulation rates

Carbon accumulation rates have been defined in variable ways, using RERCA (recent apparent rate of carbon accumulation) and CAR (carbon accumulation rate) interchangeably (*cf.* Chapter 2; e.g. Turunen *et al.,* 2004; Bao *et al.,* 2010; Turner *et al.,* 2014). In this thesis, RERCA is defined this thesis as the rate of carbon accumulated over the ^{210}Pb-dated period (Ali *et al.,* 2008; Lamarre *et al.,* 2012; Loisel and Garneau, 2010). CAR is the rate of change in carbon accumulation, calculated by multiplying the C mass of each 1 cm peat horizon, or C density (in g C cm^{-2}), by the accretion rate (in yr cm^{-1}) for each depth (*sensu* Garneau *et al.,* 2014) based on the CRS model dates and calculated using clam v.2.2 (Blaauw, 2010).

As ^{210}Pb dating allows for decadal resolution, mean CAR were calculated and compared for 50- and 10-year bins in SPSS v.21.0 (IBM, 2012) between microforms within sites, with a minimum of n = 3 replicates. All datasets were tested for normality and homogeneity of variances using Kolmogorov-Smirnov and Levene's tests, respectively. Trends over time were tested using one-way Repeated Measures ANOVA and the interaction between carbon accumulation, time, and microform was tested using a one-way Mixed ANOVA, using the Greenhouse-Geisser correction for

sphericity if the assumption was violated. In the case of an overall significant ANOVA, pairwise comparisons were considered for each time period using Bonferroni confidence interval adjustments in order to reduce the likelihood of Type I error (Greenhouse and Geisser, 1959; Maxwell and Delaney, 2004; Dytham, 2010; Laerd Statistics, 2015). Results are reported for $p < 0.1$; statistically significant results ($p < 0.05$) are reported in bold where applicable.

6.3 Results

Core properties including bulk density, basic stratigraphy and ash content measured by loss on ignition are presented in Chapter 4.

6.3.1 Lead-210 dating

6.3.1.1 *^{210}Pb activity*

Lead-210 profiles for all 30 cores are shown in Figures 6.1-6.3. Water table depth was also represented, where possible.

For all cores, activity profiles tail off to values approaching 0, which is expected for ombrotrophic peatlands where geochemical inputs are solely from atmospheric deposition. As this unsupported, or excess, lead deposition ($^{210}Pb_{ex}$) is assumed to be constant, deviations of the activity profiles from exponential decay reveal potential post-depositional movement of ^{210}Pb or changes in peat accumulation.

Blanc Sablon peat accumulation was hypothesised to be lower than that at Baie Comeau and Havre-St-Pierre (*cf.* key hypotheses in Section 2.5). The depth of the ^{210}Pb activity profiles was greater than expected at BS2 and BS3 (Lac à la Truite and Vallée peatlands in the Blanc Sablon region), indicating high peat accretion for the last 150 years. Similarly, the equilibrium depth, i.e. the depth at which it is assumed that all $^{210}Pb_{ex}$ has decayed, is near 60 cm at Baie Comeau.

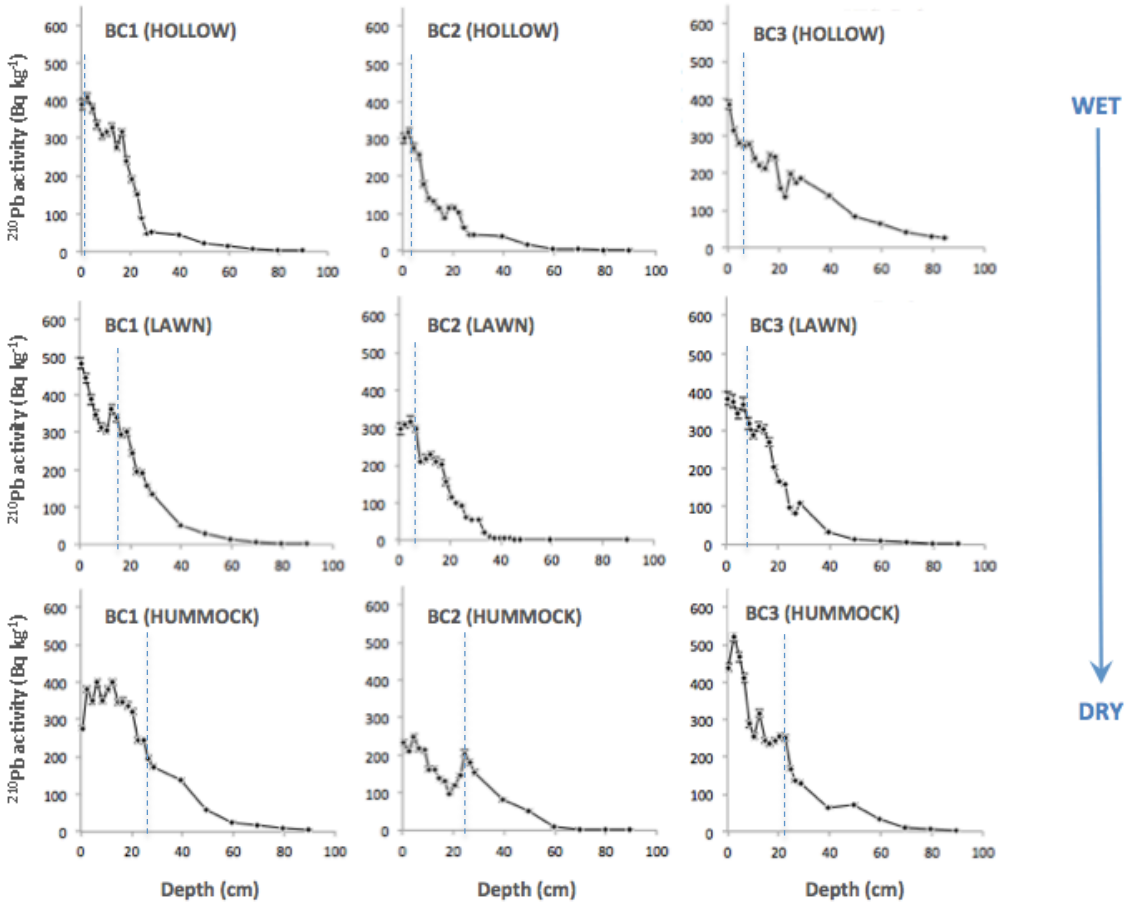

Figure 6.1. ^{210}Pb activity profiles (in Bq kg^{-1}) plotted against depth for all Baie Comeau cores; each column is one peatland (from left to right, 1: Lebel, 2: Baie, 3: Manic) and each row is one replicate microform core, from wet (top) to dry (bottom). Water table depth (dotted blue line) was measured in the field. Note that all axes are the same scale.

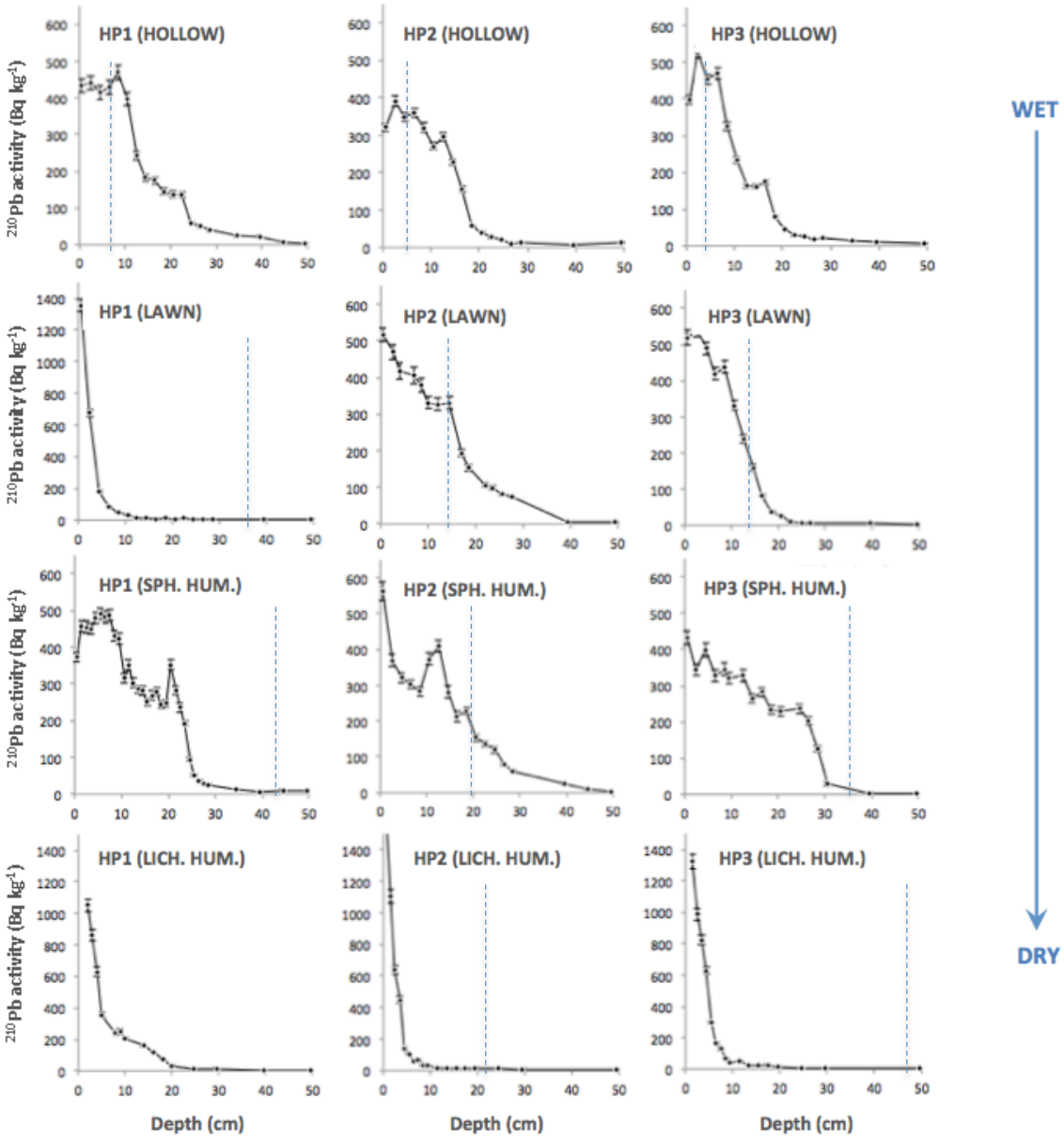

Figure 6.2. ^{210}Pb activity profiles in (Bq kg^{-1}) plotted against depth for all Havre-St-Pierre cores; each column is one peatland (from left to right, 1: Plaine, 2: Morts, 3: Romaine) and each row is one replicate microform core, from wet (top) to dry (bottom). Water table depth (dotted blue line) was measured in the field; the depth for HP1D was 58 cm. Note that the x and y axes are the same except for HP1A and HP1,2,3D

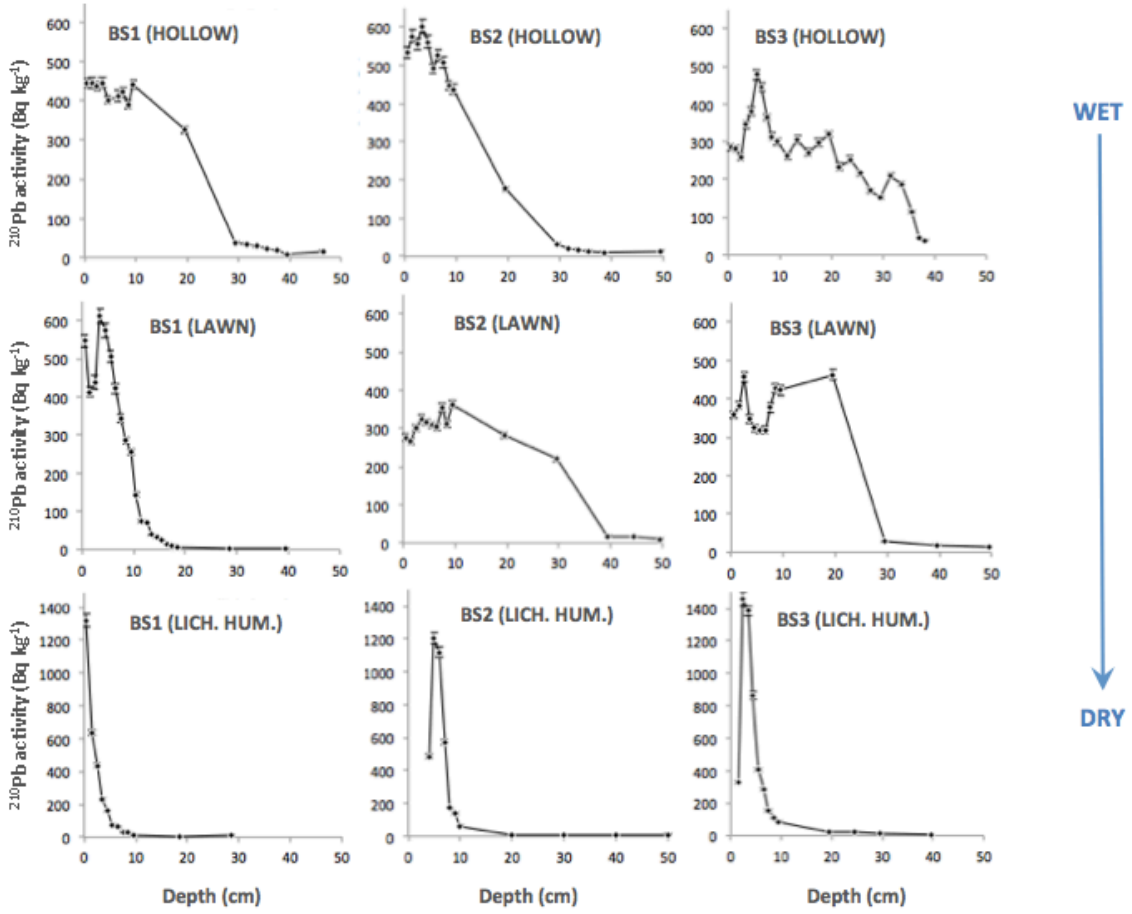

Figure 6.3. ^{210}Pb activity profiles (in Bq kg^{-1}) plotted against depth for all Blanc Sablon cores; each column is one peatland (from left to right, 1: Red Bay, 2: Lac à la Truite, 3: Vallée) and each row is one replicate microform core, from wet (top) to dry (bottom). Water table depth is not represented here, as there was ice at the time of coring (see Stratigraphy; Chapter 4). Note that y-axes for D cores are on a different scale.

The coefficients of determination (R^2) from linear regressions of log-transformed $^{210}Pb_{ex}$ plotted against cumulative mass indicate the proportion of activity profile variations explained by exponential decay (Le Roux and Marshall, 2011); these R^2 values are presented in Table 6.1. Non-monotonic features are evident in some profiles, such as a dip in activity at the peat surface, and small peaks around the zone of mean water table depth (e.g. BC2). Overall, R^2 values are mostly greater than 0.80, and range up to 0.99. Only two cores have $R^2 < 0.80$ (HP3A: $R^2 = 0.76$ and BS3B: $R^2 = 0.61$); both cores have marked changes in stratigraphy. The R^2 values are highest for lichen hummocks overall, and lowest for *Sphagnum* hummocks at Havre-St-Pierre and hollows at Blanc Sablon, which was expected as peat accumulation is higher for the top 20-30 cm of these cores, indicated by changes in bulk density and stratigraphy (Chapter 4).

Table 6.1 Coefficient of determination (R^2) for linear regressions between log-transformed unsupported $^{210}Pb_{ex}$ and cumulative mass for each dating profile (n = 30 cores).

		MICROFORM			
Region	**Peatland**	**(B) Hollow**	**(A) Lawn**	**(C) *Sph.* hummock**	**(D) Lich. hummock**
Baie Comeau	1 (Lebel)	0.96	0.98	0.92	--
	2 (Baie)	0.97	0.90	0.80	--
	3 (Manic)	0.95	0.97	0.95	--
Havre-St-Pierre	1 (Plaine)	0.97	0.87	0.76	0.94
	2 (Morts)	0.93	0.95	0.95	0.96
	3 (Romaine)	0.95	0.88	0.84	0.92
Blanc Sablon	1 (Red Bay)	0.95	0.93	--	0.99
	2 (Lac à la Truite)	0.99	0.80	--	0.88
	3 (Vallée)	0.61	0.86	--	0.99

6.3.1.2 *Ages*

Calendar ages and peat accumulation rates calculated using the CRS model are shown in Figures 6.4-6.6. Radiocarbon (^{14}C) dates are included for illustrative purposes, if they fall within the range; they were not used in the age-depth models in this chapter (*cf.* Chapter 7). Overall, dating was possible until 7-10 half-lives (Le Roux and Marshall, 2011); in some cores, older dates were obtained.

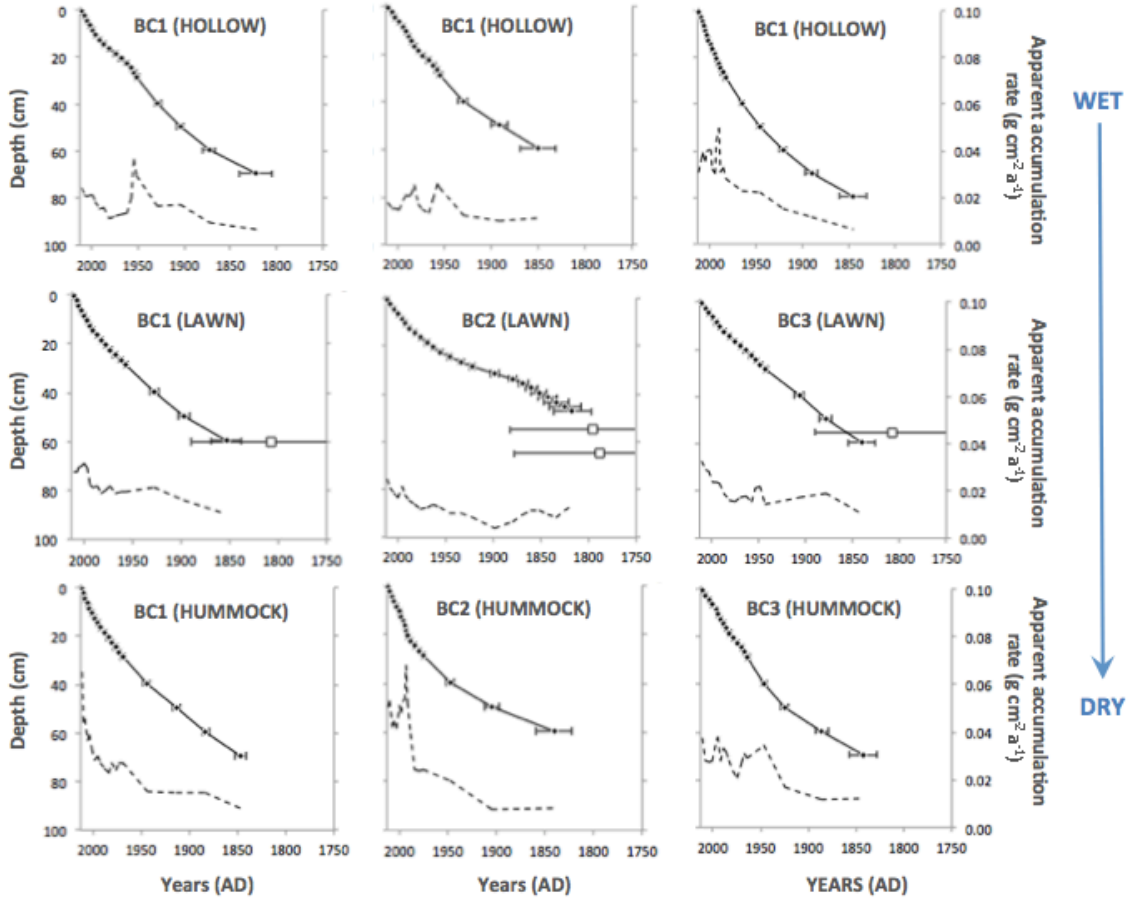

Figure 6.4. ^{210}Pb CRS age models (solid line) plotted against depth for all Baie Comeau cores; each column is one peatland (from left to right, 1: Lebel, 2: Baie, 3: Manic) and each row is one replicate microform core, from wet (top) to dry (bottom). The dotted line is the CRS-derived apparent accumulation rate; open squares are available calibrated ^{14}C dates.

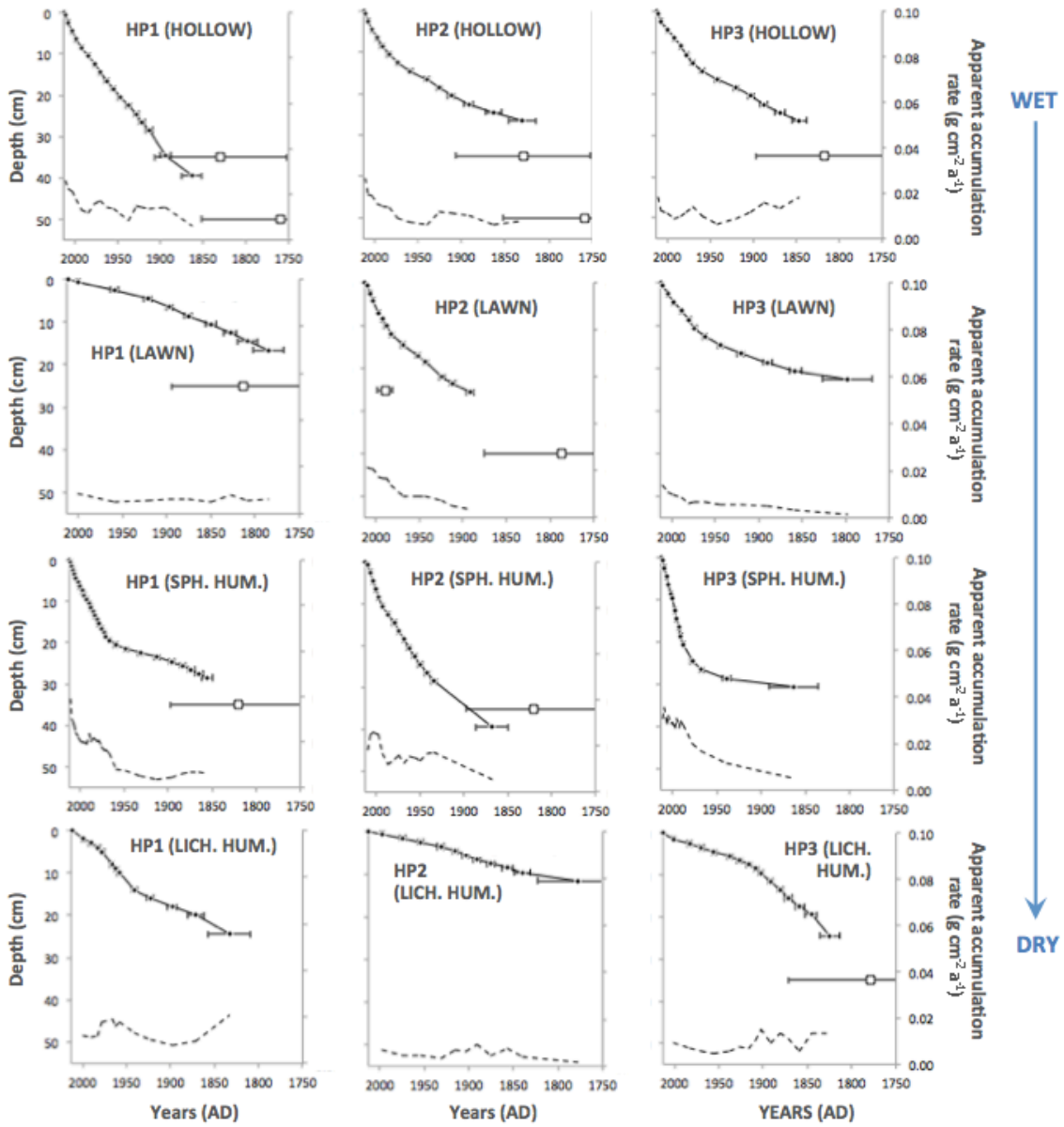

Figure 6.5. ^{210}Pb CRS age models (solid line) plotted against depth for all Havre-St-Pierre cores; each column is one peatland (from left to right, 1: Plaine, 2: Morts, 3: Romaine) and each row is one replicate microform core, from wet (top) to dry (bottom). The dotted line is the CRS-derived apparent accumulation rate; open squares are available calibrated ^{14}C dates.

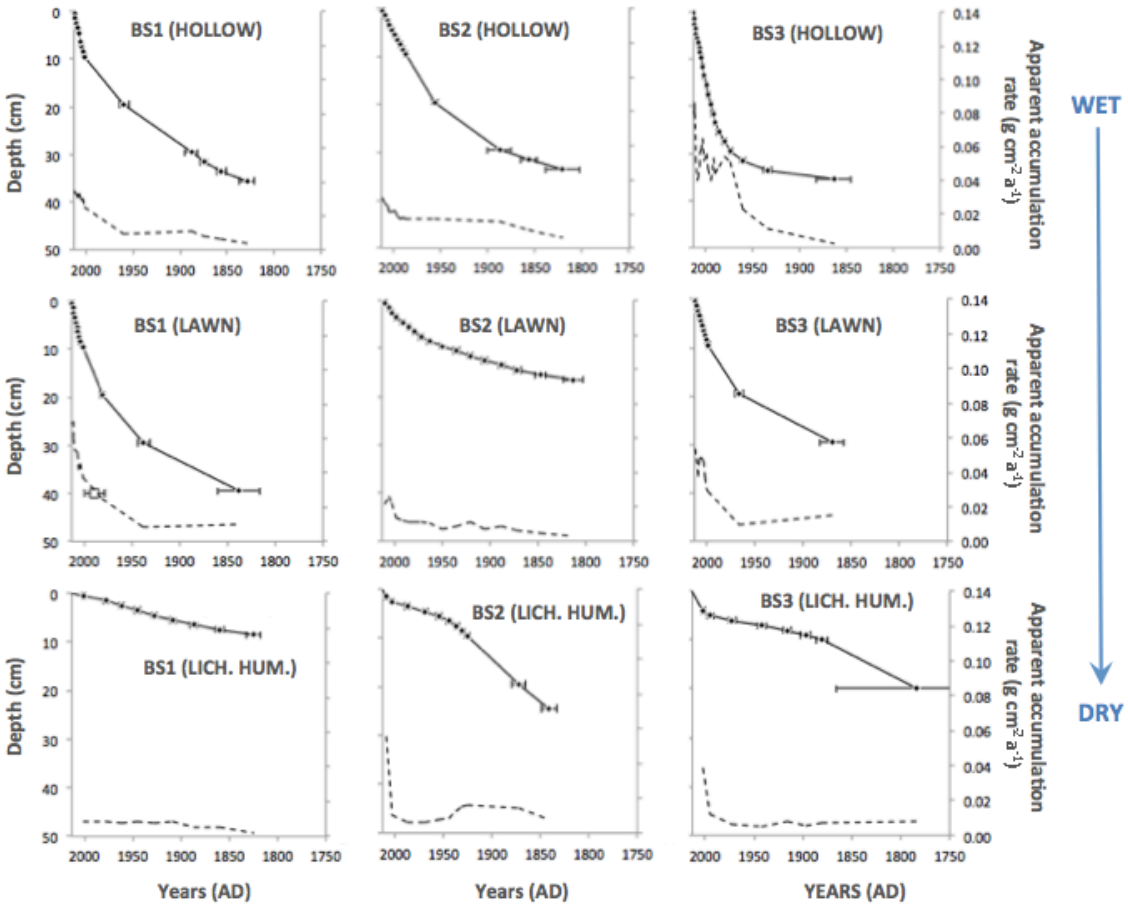

Figure 6.6. ^{210}Pb CRS age models (solid line) plotted against depth for all Blanc Sablon cores; each column is one peatland (from left to right, 1: Red Bay, 2: Trout Lake, 3: Valley) and each row is one replicate microform core, from wet (top) to dry (bottom). The dotted line is the CRS-derived apparent accumulation rate; open squares are available calibrated ^{14}C dates.

6.3.1.3 *^{210}Pb inventories and annual fallout rate*

Inventories are expected to vary between regions based on geography, precipitation patterns and available substrate. As cores within the same region and within the same sites are expected to receive similar atmospheric ^{210}Pb deposition, differences between the inventories and annual fallout rates could indicate post-depositional mobility or preferential deposition. The mean total inventory across all cores (n = 30) is 4614 Bq m^{-2} and total annual fallout is 144 Bq m^{-2} a^{-1}. These are broken down by region and by microform in Table 6.2 and Figure 6.7 (n = 3 for each value).

There is considerable variability in total inventories within the same regions, with standard deviations of up to ± 2000 Bq m^{-2} in some cases (Figure 6.7a). Mean inventory and fallout at Blanc Sablon is significantly higher than at Baie Comeau and Havre-St-Pierre (ANOVA, $p < 0.01$). There is no significant difference between the inventories and fallout for Baie Comeau and Havre-St-Pierre.

Table 6.2. Mean ^{210}Pb inventories and annual fallout rate for all regions and microforms ± S.E. (n = 3 for each data point)

	Total ^{210}Pb inventory (Bq/m^{-2})			**^{210}Pb fallout rate (Bq m^{-2} a^{-1})**		
	Baie Comeau	**Havre-St-Pierre**	**Blanc Sablon**	**Baie Comeau**	**Havre-St-Pierre**	**Blanc Sablon**
Hollow	2910 ± 585	2991 ± 411	5514 ± 493	91 ± 18	93 ± 13	172 ± 15
Lawn	3597 ± 653	3867 ± 869	5508 ± 618	112 ± 20	120 ± 27	172 ± 19
Sphagnum hummock	5027 ± 602	4225 ± 347	--	157 ± 19	132 ± 11	--
Lichen hummock	--	5748 ± 146	6758 ± 941	--	179 ± 5	210 ± 29

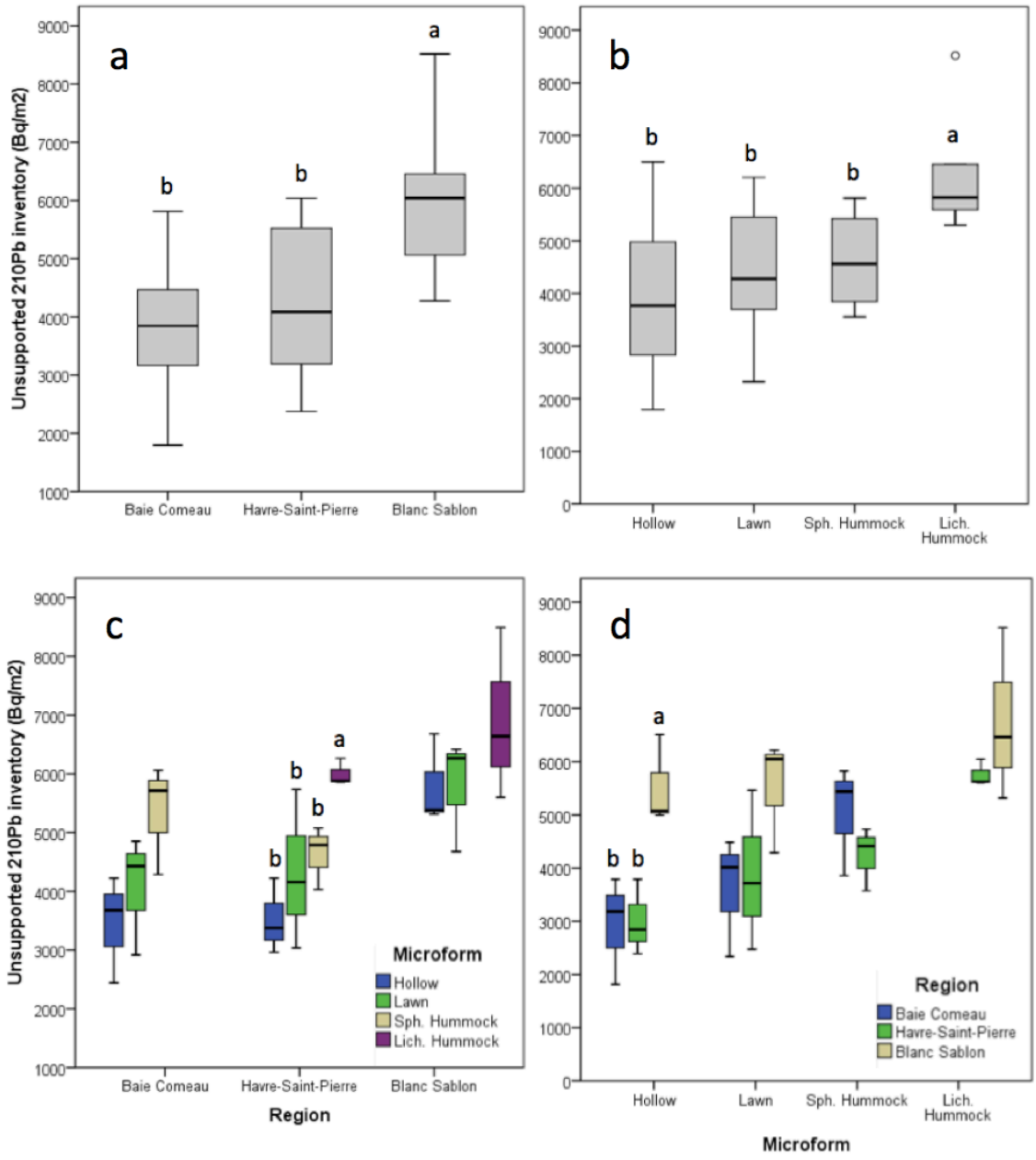

Figure 6.7 Total $^{210}Pb_{ex}$ inventory comparisons: a) between regions (n = 9 for Baie Comeau and Blanc Sablon, n = 12 for Havre-St-Pierre); b) between microform type (n = 9 for hollows and lawns, n = 6 for each hummock type); c) microform breakdown for each region (n = 3 for each bar); d) regional breakdown for each microform (n = 3 for each bar). Bars that share a letter are not significantly different; if no letters are present, analysis showed no significant difference.

Across all sites, the ^{210}Pb inventory increases with water table depth, as wetter microforms have lower total inventories than drier microforms (Figure 6.7b). This trend is not significant; however, the driest microforms (lichen hummocks) do have significantly larger total inventories than the intermediate and wet microforms (ANOVA, $p < 0.01$). Within each region, Baie Comeau microforms do not have significantly different inventories, however total inventory increases with microform dryness. The pattern is similar at Havre-St-Pierre, where lichen hummocks have significantly larger inventories than other microforms (Figure 6.7c; ANOVA, $p < 0.05$). Inventories recorded in Blanc Sablon microforms are larger than at the other 2 sites, significantly so for the hollows (Figure 6.7d; ANOVA, $p < 0.05$). While the hollows are the wettest microforms at Blanc Sablon, they are relatively dry (water table depth not recorded due to the persistence of ice) compared to hollows at the other 2 sites where the water table depth is within 5-10 cm of the surface.

6.3.2 Patterns of recent carbon accumulation

Recent apparent rates of carbon accumulation (RERCA) were calculated for the last *ca*. 150 years using ^{210}Pb dates for all cores (n = 30) ranging from wettest to driest microforms. The average recent apparent rates of carbon accumulation (RERCA) for all regions and microforms is 62.1 ± 4.4 g C m^{-2} a^{-1}, with values ranging from 26.5 g C m^{-2} a^{-1} (a lichen hummock at Havre-St-Pierre) to 105.2 g C m^{-2} a^{-1} (a *Sphagnum* hummock at Baie Comeau). Table 6.3 summarises mean RERCA across all microforms using 3 replicate cores for each region. Carbon accumulation values are ± standard error (SE) unless otherwise indicated.

Table 6.3 Mean RERCA (in g C m^{-2} a^{-1}) for all microforms and regions (± SE), and overall mean for the North Shore of the St Lawrence, covering the ^{210}Pb period for each core; n = 3 for each site/microform combination.

	Hollow	**Lawn**	***Sph.* hummock**	**Lichen hummock**
Baie Comeau	80.7 ± 7.7	74.4 ± 8.4	98.8 ± 2.7	--
Havre-Saint-Pierre	48.8 ± 8.6	40.5 ± 5.9	61.1 ± 5.6	39.7 ± 9.9
Blanc Sablon	80.1 ± 16.2	70.3 ± 15.0	--	45.7 ± 9.3
NORTH SHORE	69.9 ± 7.8	61.7 ± 7.8	79.9 ± 8.9	42.7 ± 6.2

6.3.2.1 *Regional patterns*

RERCA across all regions is significantly different between microforms (ANOVA: $F = 3.242$, $p = 0.038$). It is lowest for lichen hummocks and highest for *Sphagnum* hummocks. Recent carbon accumulation for the past 150 years is significantly lower for lichen hummocks than hollows and *Sphagnum* hummocks (LSD: $p < 0.05$) (Table 6.3; Figure 6.8). There is also a significant difference in RERCA between regions (ANOVA: $F = 0.863$, $p = 0.001$); RERCA is lowest at in the centre of the region at Havre-St-Pierre and highest at Baie Comeau in the South (LSD, $p < 0.05$).

6.3.2.2 *Within-site variability*

Within each region, RERCA is lowest for lichen hummocks and highest for *Sphagnum*-accumulating microforms, e.g. *Sphagnum* hummocks at Baie Comeau and Havre-St-Pierre, and hollows at Blanc Sablon. No significant differences in RERCA between microforms within sites were measured (ANOVA: $p > 0.1$) (Table 6.3; Figure 6.9).

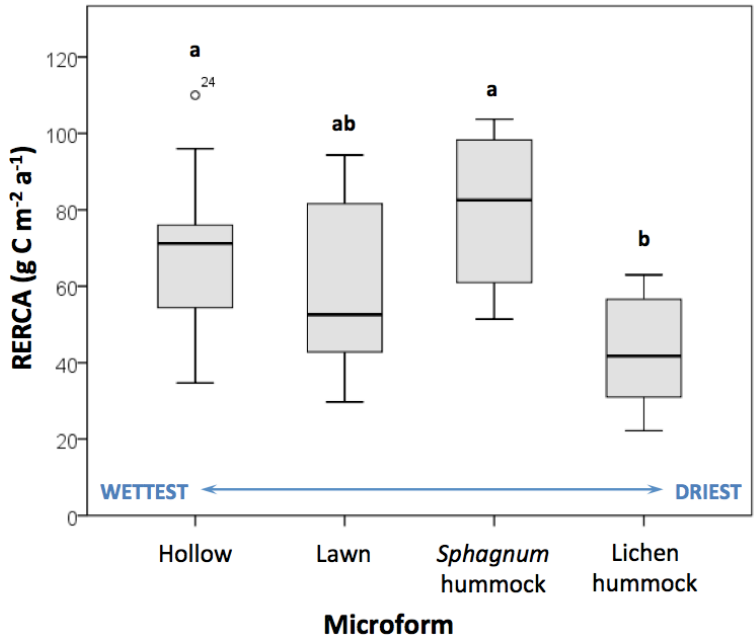

Figure 6.8. Recent apparent rate of carbon accumulation for microforms within three sites along the North Shore of the Gulf of St Lawrence. Microforms are ordered from wettest to driest within each site. The median (black line), interquartile range (grey boxes) and ranges (whiskers) are represented for each microform. Bars that share a letter are not significantly different.

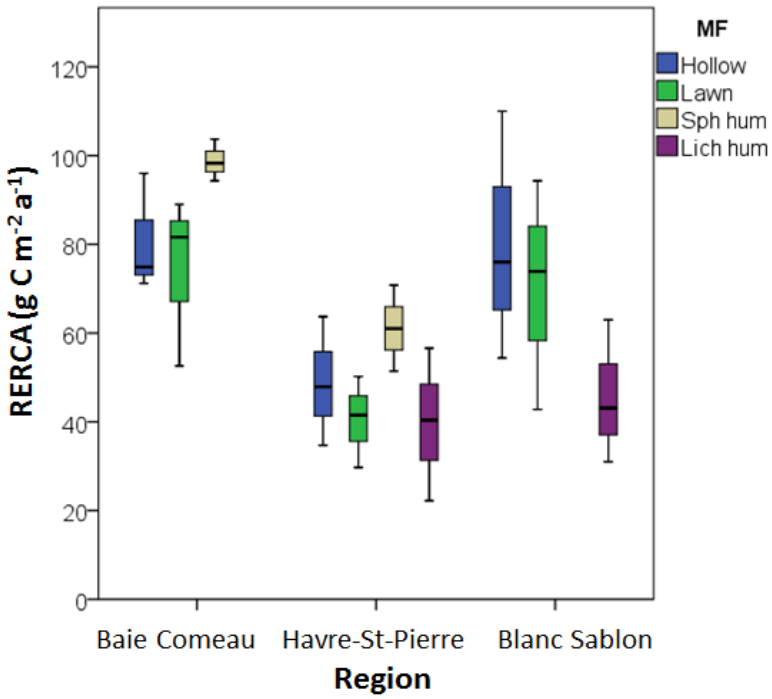

Figure 6.9. Within-site variability of recent apparent rates of carbon accumulation (RERCA). The median (black line), interquartile range (coloured boxes) and range (whiskers) are represented for each microform. There are no significant differences in RERCA between microforms within each region.

6.3.3 Temporal variations in recent carbon accumulation

Carbon accumulation rates (CAR) were calculated for each 1 cm section, and binned into 50- and 10-year time periods for analysis.

For the entire North Shore region, mean CAR was 59.1 ± 3.4 g C m^{-2} a^{-1} for the last 150 years and 79.0 ± 7.2 g C m^{-2} a^{-1} for the last 50 years (range: 18-300 g C m^{-2} a^{-1}). CAR is significantly higher with time for the entire North Shore region between each 50-year period (Repeated Measures ANOVA: $F = 19.442$, $p < 0.001$). Within each site, CAR increased significantly with time at Baie Comeau (LSD: $p < 0.01$). Differences in CAR over time were not significant at Havre-St-Pierre (LSD: $p > 0.5$). The sphericity assumption was violated at Blanc Sablon so the ANOVA test was not applied.

Regionally, there is a positive trend in CAR over time during the 150-year period for hollows, lawns and *Sphagnum* hummocks; the latter show the largest change in rate of accumulation. The error also increases with time, reflecting variability in microform accumulation between regions. CAR for lichen hummocks decreased slightly over time for the 150-year period (Figure 6.10). The relationship between CAR and microtopography (between-factor effect) over time (within-factor effect) was analysed for the whole region and within each site using a two-way mixed ANOVA. There is a statistically significant interaction between microforms and age on CAR ($F = 2.737$, $p = 0.044$); CAR for microforms was not significantly different from 50-100 and 100-150 years before coring. However, there is a statistically significant difference between microform CAR for the last 50 years (ANOVA: $F = 3.791$, $p = 0.022$); LSD post-hoc tests show that the accumulation rate for lichen hummocks is lower than that of lawns ($p = 0.054$), and significantly lower than that of hollows ($p = 0.017$) and *Sphagnum* hummocks ($p = 0.006$) (Figure 6.10).

Within sites, CAR at Baie Comeau and Havre-St-Pierre increase over time, with *Sphagnum* hummocks showing the highest rate of increase during the 150-year period.

Blanc Sablon hollows have the most variable CAR; however, values for 100-150 year mean CAR may be inflated and may not reflect apparent accumulation as *Sphagnum* forms a carpet over degraded permafrost collapse zones with high bulk density. Limited ^{210}Pb dates for deeper samples at these sites may also bias the ages and therefore CAR. Lichen hummocks at Havre-St-Pierre and Blanc Sablon have relatively constant CAR over time. Within both Baie Comeau and Havre-St-Pierre, there was no significant interaction between age and microtopography for CAR, and no effect of microform (two-way mixed ANOVA: $p > 0.5$ for both sites). The sphericity assumption (including Greenhouse-Geisser corrected) was violated for Blanc Sablon, so no significant results were recorded (Figure 6.11).

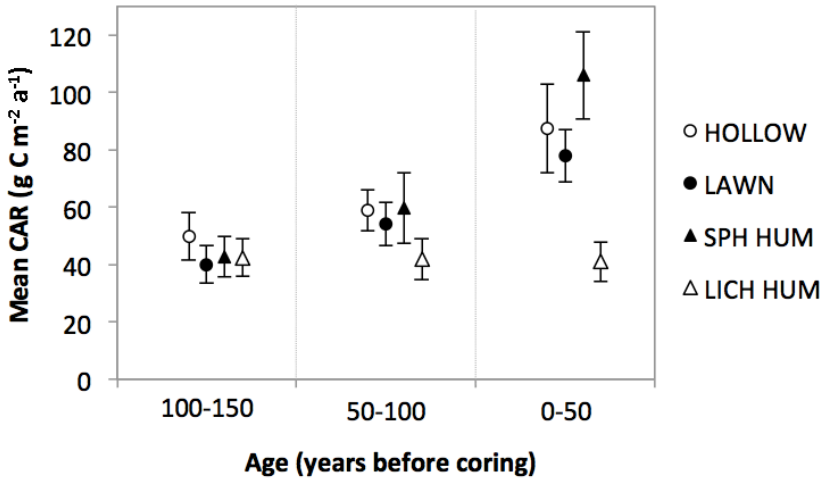

Figure 6.10. Mean carbon accumulation rate for all microforms from wettest to driest for all regions; mean CAR is calculated in 50-year bins (n = 3 for each point).

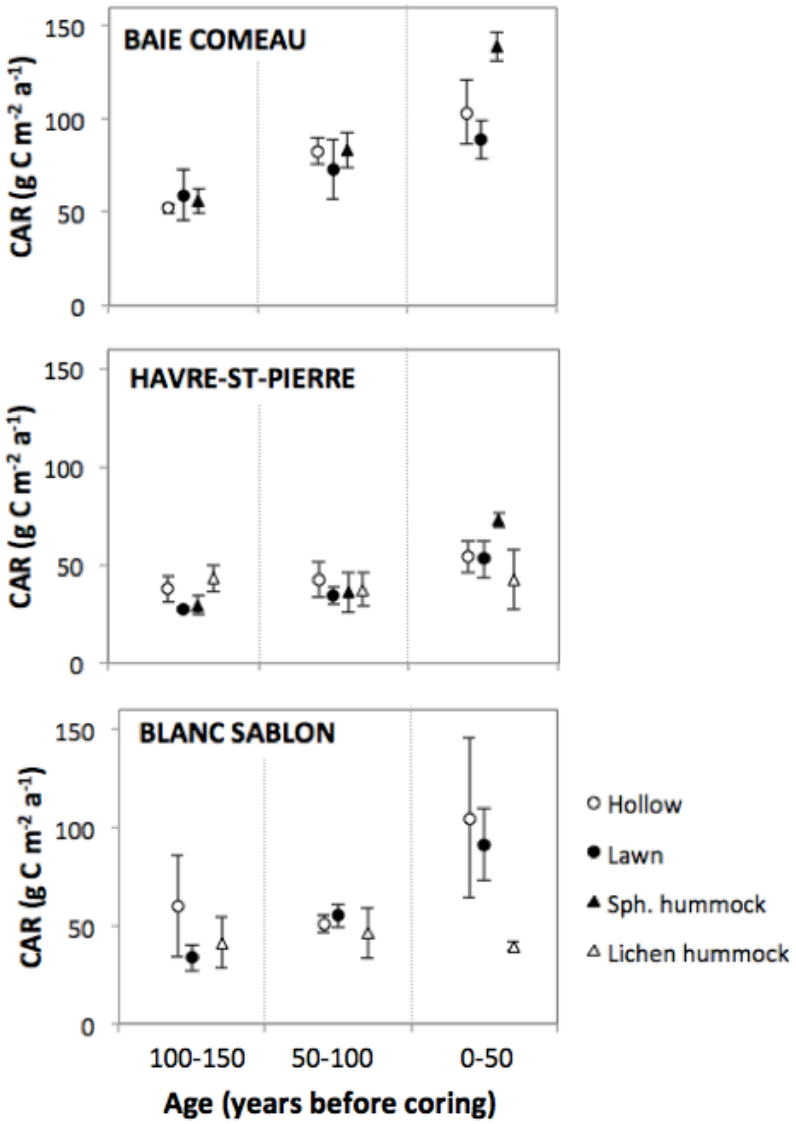

Figure 6.11. Within-site variability in carbon accumulation rates between microforms for each region of study over time: within each bin, the mean and standard errors are plotted for wettest to driest microforms, from left to right. CAR is averaged in 50-year bins, with n = 3 for each point.

Figure 6.12 shows the 10-year bins of CAR. While CAR differences were significant for all samples over time (Repeated Measures ANOVA: $F = 23.596$, $p < 0.001$), Mixed ANOVA analyses showed no significant interactions ($F = 1.965$, $p = 0.074$) or microform effect ($F = 2.370$, $p = 0.094$), likely due to small sample sizes and large error bars. There are large error bars within microform types representing the diversity.

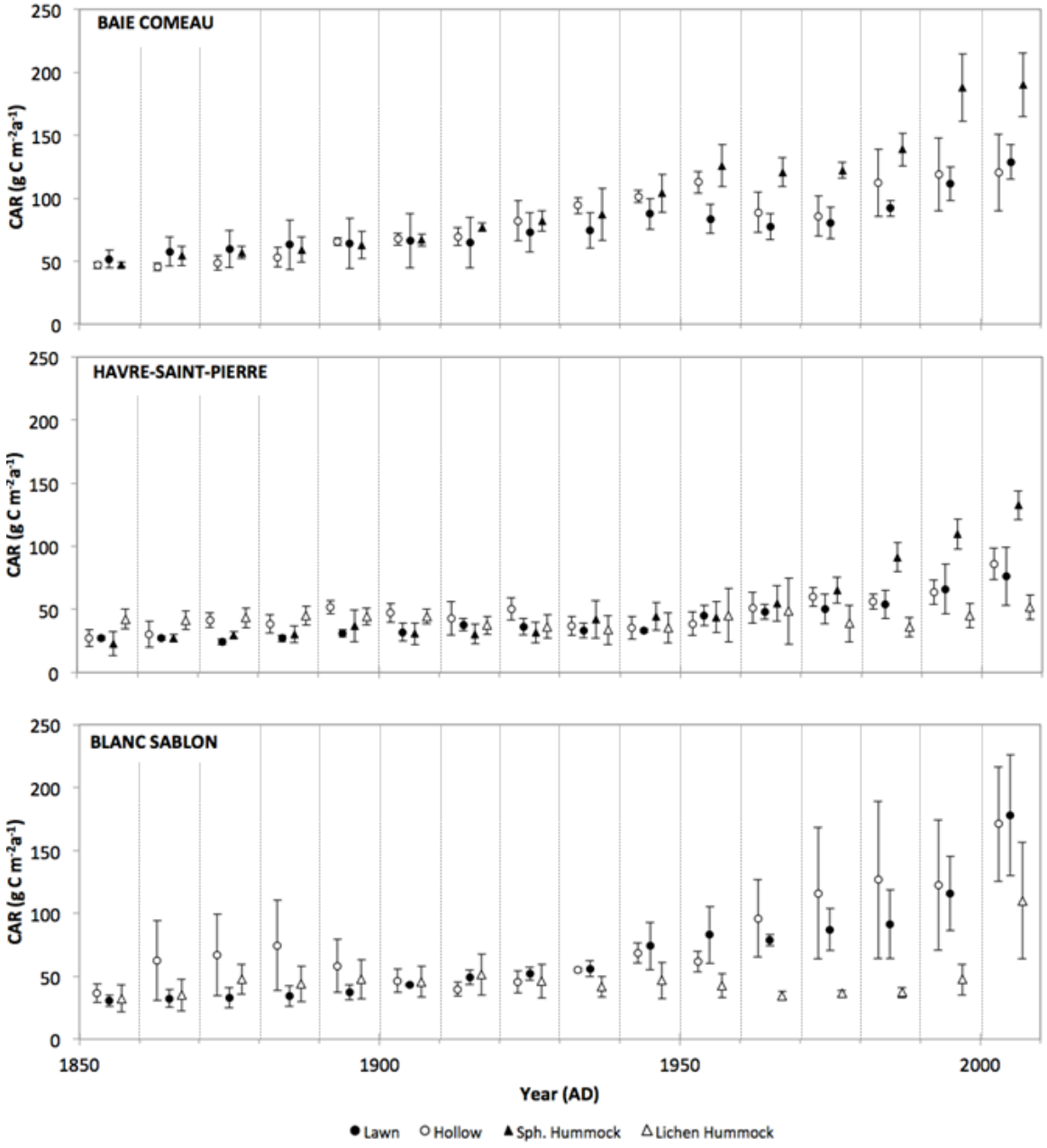

Figure 6.12 Within-site variability in carbon accumulation rates between microforms for each region of study over time: within each bin, the mean and standard errors are plotted for wettest to driest microforms, from left to right. CAR is averaged in 10-year bins, with n = 3 for each point. Error bars represent standard error.

6.4 Discussion

The role of microtopography and surface pattering in regulating changes in carbon accumulation rates over the past 150 years has been analysed using replicate cores. Depositional patterns of ^{210}Pb and activity profiles reflect peat accumulation during this period, and the calculation and subsequent statistical analysis of carbon accumulation rates allows us consider trends over time and to pick apart allogenic and autogenic drivers of change, which is often a challenge as not all change in water table depth is climate-driven (Swindles *et al.,* 2012; Losiel *et al.,* 2014).

6.4.1 ^{210}Pb deposition patterns

The use of ^{210}Pb dating allows for the measurement of continuous, absolute dates. The CRS model relies on key assumptions of a constant supply of ^{210}Pb from the atmosphere and post-depositional immobility (Appleby and Oldfield, 1978; Appleby, 2001). While we assume that the rate of supply has been constant over time, several studies indicate the possibility of mobility, reporting poor agreement with independent markers (Oldfield *et al.,* 1979) and losses around the zone of water table fluctuation, likely due to lateral dissolved organic matter transport (e.g. Urban *et al.,* 1990; Damman, 1991). Other studies found no mobility, due to the high cation exchange capacity (CEC) of *Sphagnum* and geochemical inertia of ^{210}Pb (Vile *et al.,* 1994) (Parry *et al.,* 2014; MacKenzie *et al.,* 1997). Studies from the same geographical area also found no indication of down-core mobility (e.g. Pratte *et al.,* 2013).

The wide variety in profile patterns and total inventories, even within the same sites and microform types (Figures 6.1-6.3), could question the validity of the method based on the assumptions. However, the use of replicate cores from the same sites and along a microform transect, with cores taken within a few metres of each other, has led to some of these questions being answered.

6.4.1.1 *Deposition patterns*

Regional deposition of ^{210}Pb is linked to geography and climate. Globally, deposition varies with distance from the coast as marine air influences precipitation patterns (Jia *et al.,* 2001; Du *et al.,* 2015). Wind direction and precipitation patterns, as well as the exposure of individual peatlands therefore play an important role in determining regional fallout rates. The mean fallout rate for the region has not been published, but the measured range 91-210 Bq m^{-2} a^{-1} is consistent with nearby recorded values from south-central Ontario (183 ± 9 Bq m^{-2} a^{-1} in Evans *et al.,* 1988).

We expect that regionally, closer to the sea would have lower inventories/fallout. The inventories and annual fallout rates at Blanc Sablon were significantly different from those at Baie Comeau and Havre-St-Pierre. This is not related to precipitation (HP has the highest), but this is likely due to the fact that the sites are further inland from the coast, that they are more sheltered from the influence of the Gulf, and have a larger source for ^{222}Rn and ^{210}Pb outgassing from the soil into the atmosphere. If we assume that deposition within a region is the same, differences are due to local factors. Within each region, the sites that have the lowest inventory are from peatlands nearest to the coast. At Baie Comeau, lowest inventories were recorded at the Baie peatland; for the Havre-St-Pierre region, the Plaine peatland, atop the peat plateau and furthest from the coast, had the highest total inventories, as did Vallée for Blanc Sablon (*cf.* Chapter 3 Site maps).

Within sites, it is assumed that deposition is the same. However, the driest microforms (lichen hummocks) have significantly higher inventories and therefore receive the most (or lose the least) amount of fallout. ^{210}Pb deposition was found to vary seasonally, with >30% of the total annual global fallout occurring in winter and the lowest rates in summer (Du *et al.,* 2015). More exposed microforms, such as high lichen hummocks, have less snow cover and therefore the peat surface may directly receive more annual

deposition, and more wintertime dry deposition, relative to adjacent snow-covered microforms. Drier microforms tend to be shrubbier with a greater surface area of vegetation to capture the deposition; lichen is an excellent scavenger of ^{210}Pb (Turetsky *et al.,* 2007).

6.4.1.2 *Post-depositional mobility*

Assuming that deposition onto each microform within a site is the same, differences can be explained by leaching (lateral) or post-depositional (vertical) mobility.

Lichen hummocks have significantly higher inventories than the other microforms, overall and within Havre-St-Pierre. As the lichen layers are underlain with thick ligneous layers, there is less likely to be infiltration or percolation to lower layers as opposed to more porous microforms. There is a trend of higher inventories in drier microforms (hollow < lawn < *Sphagnum* hummock). Other studies found a similar trend of depletion in wet hollows and near-pool sites compared to dry hummocks, as the former are affected by lateral water flow and lower accumulation rates (Urban *et al.,* 1990; Turunen *et al.,* 2004). There is a slight trend of lateral mobility of ^{210}Pb (presumably collecting in pools), but this trend is not statistically significant.

To consider down-core mobility, the profiles themselves need to be examined. Deviations from the 'ideal' undisturbed core, representing divergence from exponential decay, could indicate additional inputs (non-ombrotrophic peatland), post-depositional mobility of ^{210}Pb (e.g. percolation through surface layers), rapid changes in peat accumulation, or local disturbance such as cryoturbation from permafrost (Turetsky *et al.,* 2004). There is some deviation at the surface, which is common for ^{210}Pb activity profiles (e.g. Ali *et al.,* 2008; Pratte *et al.,* 2013; Parry *et al.,* 2013). It is suggested that this could be due to ^{210}Pb and its measured daughter product ^{210}Po not reaching secular equilibrium at the time of alpha-spectrometry analysis (Ali *et al.,* 2008); however, these cores were analysed more than 6 months after collection which is more

than 10 half-lives (Le Roux and Marshall, 2011). This 'dip' at the surface can also be found in cores analysed using gamma spectrometry (e.g. Parry *et al.,* 2013), and is likely due to some surface peat and vegetation types being poor scavengers (Belyea, 1996). It could also be that some of the inventory is missing from the record, as surface vegetation is not always included in the analysis (Olid *et al.,* 2008).

In general, $R^2 > 0.80$ for linear regressions of $\log(^{210}Pb_{ex})$ vs. cumulative peat mass (Le Roux and Marshall, 2011). Cores with the lowest R^2 values show marked stratigraphic and bulk density changes to 'fresh' rapidly accumulating *Sphagnum* peat (Chapter 4), indicating that the deviations from the 'ideal' core are likely due to high accumulation rates rather than ^{210}Pb mobility. These include the *Sphagnum* hummocks at Havre-St-Pierre (e.g. HP3C), and the intermediate microforms at Lac à la Truite and Vallée peatlands at Blanc Sablon, which are *Sphagnum* wedges growing in between high hummocks (BS2A, BS3A) or over permafrost collapse zones (BS2B and BS3B), similar to the 'internal lawns' described by Turetsky *et al. (*2002, 2007). However, these microforms are porous and it is reasonable to assume that there is some percolation of deposited ^{210}Pb through the surface layers. New models adapting the CRS model could account for surface percolation (e.g. IP-CRS model: Olid *et al.,* 2014). There is some evidence of peaks around the zone of water table fluctuation (Figures 6.1-6.3), which may indicate slight leaching from the layers around it (as in Damman *et al.,* 2014; Oldfield *et al.,* 1995; Pratte *et al.,* 2013). This was not found to affect calculated ages.

At Blanc Sablon, hollows (wettest microforms) were found to have significantly higher total inventories than for the other 2 regions. It is possible that the total inventory was overestimated for some cores as the sampling resolution was limited for some cores between 20-30 cm; however, the changes in stratigraphy and bulk density discussed previously suggest high peat accumulation rather than down-core mobility of ^{210}Pb. As these sites in general were drier (still frozen in some places), it is hypothesised that this

is due to the lack of lateral mobility of ^{210}Pb into pools. In addition, Oldfield *et al. (*1995) found that rapidly infilling hollows (such as BS2B and BS3B) are good scavengers of ^{210}Pb. Indeed, the higher ^{210}Pb inventories for the Blanc Sablon region are likely due to a combined influence higher deposition (sheltered sites further from the coast) and lower post-depositional mobility (drier sites and a higher density of ^{210}Pb scavenging microforms including lichen hummocks and rapidly accumulating intermediate microforms).

6.4.1.3 *Validity of age-depth models*

One of the main concerns of ^{210}Pb dating is that the assumptions of the CRS model are violated, those of constant deposition and of mobility. These questions are often addressed by using independent dating markers, such as Caesium-137 (^{137}Cs) or Americium-241 (^{241}Am), which may also be subject to post-depositional mobility (Parry *et al.,* 2013; Chapter 5). However, using replicate cores has allowed us to address these questions. If the supply rate changed over time, for instance due to mining or industrial processes (Mackenzie *et al.,* 2010), peaks were not observed for multiple cores from the same site. While there is some evidence of lateral transfer, this is not significant. There is no evidence of significant down-core mobility.

A major source of uncertainty for the CRS model is that it depends on choosing an equilibrium depth at which there is no more unsupported lead ($^{210}Pb_{ex}$), this can be a considerable source of error depending on sampling resolution (Appleby, 2001). Dates prior to 1900AD should be considered cautiously, especially those from Blanc Sablon, which has a lower sampling resolution around this depth. This work is contributing to a current project being undertaken to attempt to statistically model this equilibrium depth and supported value ($^{210}Pb_{sup}$) (Marco Aquino-Lopez, *pers. comm.).* Independent dating techniques such as other fallout radionuclides (^{137}Cs and ^{241}Am), while helpful in some ways, cover the post-1950 period where there is less age uncertainty. There is

good agreement between the CRS model dates and radiocarbon (^{14}C) dates (Figures 6.1-6.3), however not all dates fell within the ^{210}Pb period. Age-depth models including both CRS-derived and ^{14}C dates are calculated and discussed in Chapter 7.

6.4.2 Microtopography controls on recent carbon accumulation

This analysis of 30 ^{210}Pb-dated cores spanning a range of replicated microform cores in three peatland regions evaluates hypotheses related to the within-site variability in carbon accumulation for the past 150 years (Sections 2.5 and 6.1), in particular that CAR would be highest for *Sphagnum* hummocks and lowest for microforms at hydrological extremes, e.g. lichen hummocks and hollows. The hypothesis that there was permafrost at Havre-St-Pierre during the LIA was also in part tested by replication at this level.

6.4.2.1 *Recent carbon accumulation along the North Shore of the St Lawrence*

Overall mean RERCA for all cores from the North Shore region is 62.1 ± 4.4 g C m^{-2} a^{-1} and values range from 26.5-105.2 g C m^{-2} a^{-1}. This is within the range of other published values for RERCA from other eastern Canadian peatland regions (30-122 g C m^{-2} a^{-1}: Turunen *et al.,* 2002; 40-177 g C m^{-2} a^{-1}: Turunen *et al.,* 2004; 53-115 g C m^{-2} a^{-1}: Loisel and Garneau, 2010), from Western North America (31-93 g m^{-2} a^{-1}: Wieder *et al.,* 1994; Turetsky *et al.,* 2000) and from Finland (40-81 g C m^{-2} a^{-1}: Tolonen and Turunen, 1996). Holocene long-term apparent carbon accumulation rates (LORCA) for Baie Comeau and Havre-St-Pierre have been measured at 60.6 g C m^{-2} a^{-1} and 32.0 g C m^{-2} a^{-1}, respectively (Magnan and Garneau, 2014a). RERCA for lawn cores at these sites are 74.4 ± 8.4 g C m^{-2} a^{-1} and 40.5 ± 5.9 g C m^{-2} a^{-1}; these higher values compared to LORCA are expected as RERCA considers only peat added to the acrotelm, while LORCA has longer-term catotelm decomposition. RERCA values are higher than the global average LORCA for Northern peatlands of 23 g C m^{-2} a^{-1} (Loisel *et al.,* 2014).

6.4.2.2 *Within-site spatial patterns of carbon accumulation*

The hypothesis put forward by the Belyea and Clymo (2001) model of a humpbacked relationship between acrotelm thickness and increasing peat accumulation was tested using replicate cores. For 23 Eastern Canadian peatlands, Turunen *et al. (*2004) found that the difference in RERCA between hummocks (78 g C m^{-2} a^{-1}) and hollows (65 g C m^{-2} a^{-1}) was significant. In this study, no such significant differences between intermediate microforms were found in the region as a whole or within each site, and accumulation for hollows (shallower acrotelm, higher water table) was higher than that for lawns for all three sites.

The driest microforms (lichen hummocks: 42.7 ± 6.2 g C m^{-2} a^{-1}) had significantly lower RERCA than the intermediate and wettest microforms (79.9 ± 8.9 and 69.9 ± 7.8 g C m^{-2} a^{-1}), and are the only microform for which CAR remains constant or decreases over time, due to a combination of negative ecohydrological feedbacks including plant composition and water table depth. As distance from the water table increases, lichen growth is favoured over *Sphagnum* in drier microforms (Belyea and Clymo, 2001; Belyea and Malmer, 2004). Taller microforms are also more exposed to wind and frost, leading to persistence of ice lenses longer into the growing season or permafrost over time and further drying. Lichen growth at the surface also has a cooling effect on subsurface layers as albedo is reduced (van der Molen and Wijmstra, 1994). Fire may also have played a role; while charcoal was not observed in the stratigraphy, there were charred stumps at Red Bay, and charcoal layers were detected at a nearby core (Garneau, unpublished data). Fire was recorded at another Blanc Sablon peatland around 4400 cal. BP (Dionne and Richard, 2006). However, fire does not play as important a role in peatland accumulation feedbacks in Eastern Canada as it does in the West (Magnan *et al.,* 2012; van Bellen *et al.,* 2012)

At Baie Comeau and Havre-St-Pierre, the relationship between water table depth or acrotelm thickness and RERCA along within-site microtopography gradients is not linear. RERCA is highest for 'intermediate' microforms and lowest for the extreme driest microforms, as modelled by Belyea and Clymo (2001). It is highest for *Sphagnum* hummocks and lowest for lichen hummocks. However, the relationship is not simply 'humpbacked' based on acrotelm thickness, as lawn cores have lower RERCA than hollows at all three sites (Figure 6.9); hollows have higher water tables (shallower acrotelms) and therefore relatively less aerobic decomposition than lawns, and hollow/pool species tend to decompose more quickly than recalcitrant hummock species (Johnson & Damman, 1991). At Blanc Sablon, the within-site relationship between water table depth (or ice depth) and RERCA is linear and negative, with the highest RERCA is for the wettest microform along within-site gradients. At two of the three Blanc Sablon peatlands, these microforms are *Sphagnum* mats infilling a collapse zone, so they are relatively dry compared to hollows at the other two sites (water table depth > 20 cm).

Peatlands are 'complex adaptive systems' (Belyea and Baird, 2006) and the development and expansion of transitional microforms should be considered when studying relative changes in peat accumulation, at least in the most recent period.

6.4.2.3 *Within-site trends in recent carbon accumulation*

Carbon accumulation rates (CAR) increased overall over time. Between time periods, changes in CAR between time periods should be considered with caution, as increasing CAR with time is expected as a result of incomplete autogenic decay processes. Comparing the same time-periods for different microforms and sites is useful for studying the relative importance accumulation and decomposition processes in different microforms (e.g. Frolking *et al.,* 2014). Within each time period, variability for a given microform within each period reflects natural variability and different timings

for lawn-hummock or hollow-lawn margins in response to ecohydrological feedbacks. Trends or variations detected using replicate cores reflect large-scale effects of autogenic or allogenic change rather than localised ecohydrological drivers.

At Baie Comeau, CAR increases over time for the 150-year period for all microforms, with the driest, more aerated microform (*Sphagnum* hummock) increasing the fastest. Decomposition processes compensate for this high accumulation rate, as all three microforms have similar rates for the 100-150 year periods. There is a decrease 10-year mean CAR from 1940 AD for lawns and from 1950 AD for hollows and hummocks until 1980 AD. This decreasing CAR coincided with a colder period recorded for boreal Quebec (Naulier *et al.,* 2015).

Hummocks at Havre-St-Pierre are particularly interesting to consider. *Sphagnum* layers at the top of the *Sphagnum* hummocks (HP1C, 2C and 3C) accumulated over highly decomposed ligneous layers containing small amounts of lichen. This replicated study allowed the testing of the initiation of this re-accumulation, i.e. was this shift from dark/light sections driven by a change in climate (as in Barber, 1981) or in autogenic drivers such as hummock-hollow cycling (e.g. Belyea and Malmer, 2004)?

CRS-derived dates indicated that the transition happened at roughly the same time: 1967 ± 2 (HP1C), 1960 ± 2 (HP2C) and 1967 ± 3 (HP3C) years AD. HP2 (Morts) is more sheltered than the other two peatlands located on the peat plateau, so it is likely that the shift from ligneous to *Sphagnum* peat was driven by a regional climatically driven ecohydrological shift. Permafrost has not been found in the field at the studied Havre-St-Pierre peatlands; however, it was found to persist on one of the nearby islands (Ile Nue-de-Mingan) and was hypothesised to be relict permafrost from the LIA (Boivin, 2005). There was a cold period recorded for Northern Quebec from 1940-1960s (Naulier *et al.,* 2015), and temperatures for the region have been increasing since the 1960s (MDDELCC, 2015). It is therefore plausible that LIA permafrost was

present until the late 1960s in mainland Havre-St-Pierre peatlands and that *Sphagnum* growth between high lichen hummocks was driven by the degrading permafrost and subsequent hydrological and climatic changes. The addition of longer-term records studying changes in CAR since the start of the LIA (see Chapter 7), or climate/water table depth records from macrofossil or testate amoebae reconstructions would help with this interpretation, as there is no direct proxy for permafrost.

The timing of permafrost degradation at Blanc Sablon can also be considered. The expansion of *Sphagnum* carpets into the collapse scars/mud bottoms was dated at *ca*. 1900AD at Lac à la Truite (BS2B) and Vallée (BS3B) peatlands (the palsa at Red Bay was still intact). However, the change in stratigraphy associated with this regrowth (30-35 cm) is at the bottom end of the ^{210}Pb activity profile. In addition, the material dated below the stratigraphic change may have been subjected to mobility, mixing or erosion prior to and during the collapse process, meaning that there is greater uncertainty in the ages. Despite this, it is possible that the palsas in these two peatlands collapsed around 1900AD, earlier than reported by Payette (2004). Dionne and Richard (2006) reported variable palsa conditions at Blanc Sablon peatlands, and the warmer 1900-1950AD period could have degraded smaller LIA-relict palsas in the region while larger ones were maintained (e.g. at Red Bay). Additional ^{14}C dates just above this stratigraphic change could be useful to clarify the this timing. In the intermediate *Sphagnum*-dominated microforms ('lawns') at Blanc Sablon, i.e. similar sequences to the *Sphagnum* hummocks at Havre-St-Pierre, stratigraphic changes from darker to lighter surface layers were also dated to the 1960s (1963 ± 2 years AD at Red Bay; 1967 ± 4 years AD at Vallée; mid-1900s at Lac à la Truite as dating resolution was poor and the stratigraphic changes were more gradual). While the palsas likely collapsed in the early 1900s, permafrost persisted locally until the 1960s and still persists in palsas and lichen hummocks, some of which were still frozen at the time of coring (late August 2013).

Changes in vegetation were found to have little impact on Holocene LORCA for Baie Comeau and Havre-St-Pierre (Magnan and Garneau, 2014). As these changes affect recent CAR, such as the previously considered transitions from collapse zone to *Sphagnum* mat at Blanc Sablon or from slow-accumulating humified peat to *Sphagnum* hummock at Havre-St-Pierre, aerobic decay processes may account for these differences to stabilise apparent accumulation in the long-term. While these high measured accumulation rates for the last 150 years do not represent net carbon storage in the catotelm, and may be only short-term responses to ecohydrological feedbacks, variable within-site patterns at Blanc Sablon have important implications for future longer-term C sequestration. (Turetsky *et al.,* 2000) estimated increases of 60% of organic matter in internal lawns post-permafrost degradation in the last 100-200 years, offsetting methane (CH_4) emissions for an estimated 60 years post-degradation. Following a change in hydrology due to permafrost degradation, *Sphagnum* infilling into recently exposed mud bottoms in hollows (e.g. Foster, 1984) and rapid establishment in thermokarst ponds (e.g. Arlen-Pouliot and Bhiry, 2005), i.e. terrestrialisation of the collapse scars by *Sphagnum* mats, as observed in this study at Blanc Sablon, could represent future net C sinks (Payette, 2004; Christensen *et al.,* 2004).

The climatic context will be considered in more detail in the following chapter. This work highlights that there is an urgent need to understand interactions between surface structure, vegetation and microform developmental changes in order to predict the magnitude and direction of changes in accumulation (Belyea and Baird, 2006).

6.5 Conclusion

This chapter used replicated microform cores in order to evaluate within-site variability in carbon accumulation rates for the last 150 years (Section 2.5). In addition, the use of ^{210}Pb as a chronological tool and the assumptions behind the CRS model were also considered. Often-raised questions of limitations due to post-depositional mobility were

addressed; the method provides reliable dates, and there was no statistically significant mobility or leaching measured within the cores used in this study.

Within sites, carbon accumulation rates vary along microform gradients, with dry lichen hummocks < lawns < transitional (e.g. pool or mud-bottom infilling, regrowth wedges) or *Sphagnum*-dominated microforms (e.g. hummocks); the humpbacked relationship modelled by Belyea and Clymo (2001) is an oversimplification as it does not account for the high accumulation rates in transitional microforms with favourable conditions for rapid *Sphagnum* growth. Despite the wide variability in accumulation rates within sites, there were no statistically significant changes detected between microforms. Multiple cores should be the standard approach to account for dating uncertainty and natural variability (e.g. Watson *et al.,* 2015).

At this scale, a main driver of CAR changes in autogenic, where CAR increases with time due to autogenic factors, namely incomplete decomposition. Some allogenic changes were detected across microforms related to hypothesised permafrost-related topographical changes. In order to address these questions, the next chapter (Chapter 7) considers longer-term accumulation in lawn cores for all sites and in a range of cores at Havre-St-Pierre. Furthermore, the role of microtopography and permafrost on carbon accumulation could be better understood in this case by including plant macrofossil assemblages to look at vegetation (and microform) succession over time.

7 Long-term peat accumulation and the influence of climate

7.1 Overview

Northern peatlands are widespread in boreal and subarctic regions. During the Holocene, large amounts of carbon (C) were stored in peat owing to the imbalance between peat accumulation and decomposition rates. Under current warming conditions, permafrost has been degrading during the last 150-200 years in Western Canada (Turetsky *et al.,* 2007), and during the last 50 years in Eastern Canada (Payette, 2004). This degradation corresponds with the end of the Little Ice Age in different regions of North America.

During the last millennium, studies linking recent carbon accumulation rates (CAR) and Little Ice Age cooling have been limited by poor dating resolution, especially in the most recent 200 years. In part for this reason, the LIA impact on C accumulation in Quebec peatlands is not clear, although CAR is at its lowest between 800 and 200 cal a BP (Garneau *et al.,* 2014). Mean summer temperature (MST), growing degree days above 0^{o}C (GDD0) and photosynthetically active radiation (PAR) were found to be the main drivers of net carbon accumulation during the Holocene (Yu et al 2010; Loisel et al 2014) and within the last millennium (Charman *et al.,* 2013), rather than decomposition acting as the primary driver as previously hypothesised (Ise et al 2008; Dorepaal et al 2009). Decadal-scale changes and within-site variability were considered in the previous chapter. This chapter discusses changes in C accumulation for each of the three regions (boreal and subarctic) along a South-North climate, permafrost transect as well as statistical variability within regions.

Chapter aims and objectives:

Chapter 6 considered within site variability. The overall aim of this chapter was to evaluate the role of climate and permafrost history on regional carbon accumulation rates (CAR) (Section 1.2, Objectives 3 and 4). Chapter objectives were to (1) reconstruct centennial-scale regional and temporal changes in carbon accumulation between sites along a climate gradient, and (2) to evaluate potential climate-related drivers of CAR.

Hypotheses (Section 2.5) relating to spatial and temporal variability were addressed using the high degree of replication for each region, thus allowing the distinction between internal and overarching regional climatic effects. Hypothesis H3 suggested that regional (between-site) carbon accumulation would be influenced by climate along a latitudinal gradient, with the southernmost site, Baie Comeau, having the highest accumulation rates and the northernmost, Blanc Sablon, would have the lowest rates. LIA signals would be detectable in the carbon accumulation records, in part due to greater dating resolution (H4/5). In addition, the hypothesis put forward by Magnan and Garneau (2014a) regarding the past presence of LIA permafrost at Havre-St-Pierre and its impact on carbon accumulation rates for the last few centuries was considered by incorporating additional multi-centennial dating records for a range of microforms.

7.2 Methodology

7.2.1 Core collection

Lawn cores (n = 9) from all three regions were analysed in this chapter, representing 3 replicate cores for each region, Baie Comeau (BC: 49°06'N, 68°14'W), Havre-Saint-Pierre (HP: 50°16'N, 63°40'W) and Blanc Sablon (BS: 51°29'N, 57°11'W). Additional microform cores from Havre-St-Pierre (n = 9) were also included in this analysis. Coring locations were selected from the central dome, based on previous studies of

Holocene peat accumulation (Magnan and Garneau, 2014a,b). As in previous chapters, microforms were differentiated in the field by their surface vegetation and relative height compared to other microforms (*cf.* Chapter 3 for site descriptions and definitions).

7.2.2 Laboratory methods

For all cores, bulk density and carbon content using loss-on-ignition were measured at 0.5 cm increments using a volumetric sampler as in Chapter 3 (Equations 3.1-3.4). Lead-210 (^{210}Pb) dates for all cores were included in this chapter (Chapter 6).

Lawn cores were allocated a total of 35 radiocarbon (^{14}C) dates, or 2-5 dates per core. For this project, 14 dates were obtained from a Natural Environment Research Council (NERC) radiocarbon grant (NERC Radiocarbon Allocation Number 1737.1013). The remaining dates were analysed in conjunction with other projects: 19 dates from the Millipeat project (NERC Standard grant NE/I012915/1; Radiocarbon Allocation Number 1681.1012) and 2 dates from a parallel MSc project (Sauvé, 2016: dates from the Keck Radiocarbon Facility, University of California Irvine). The first round of dates was selected as basal dates for each core and as evenly distributed rangefinders, then subsequently allocated based on marked changes in stratigraphy. A further 18 dates were allocated under NERC code 1737.1013 at Havre-St-Pierre for hollow, *Sphagnum* hummock and lichen hummock cores in order to consider the spatial distribution of carbon accumulation history at the site; these were selected at 35 and 50 cm depth. Based on results from the lawn core dates, these depths were estimated to cover the Little Ice Age period. Samples were washed through a 125 µm sieve with DI water; *Sphagnum* stems were preferentially picked and sent to the NERC Radiocarbon Facility in East Kilbride. Resulting radiocarbon ages were calibrated using IntCal13 (Reimer et al 2013). Modern dates in pMC (% modern carbon) were converted to radiocarbon ages prior to analysis using NH1 postbomb curve.

7.2.3 Data analysis

7.2.3.1 *Combined age-depth models*

The age-depth models were constructed using ^{14}C dates and ^{210}Pb-inferred calendar dates from the date of coring at the surface (2011, 2012 and 2013). The open-source R package BACON v.2.2 (Blaauw and Christen, 2011; R Development Team, 2014) was used to calculate age-depth models. This model divides each core into sections for which sedimentation times are estimated, and uses Bayesian statistics based on prior information (e.g. stratigraphy and relative accumulation rates, known hiatus) to calculate the best fit for age vs. depth.

7.2.3.2 *Calculating carbon accumulation*

Carbon accumulation rates were calculated using the cumulative carbon mass for a set period of time (300, 500 and 1000 years). CAR (Carbon Accumulation Rate) is the rate of change in carbon accumulation, and was calculated by multiplying the C mass of each 1 cm peat horizon, or C density (in g C cm^{-2}), by the accretion rate (in yr cm^{-1}) for each depth (as in Garneau *et al.,* 2014) modelled using BACON weighted mean ages. Mean CAR was calculated and compared for 50-year bins in SPSS v.21.0 (IBM Corp., 2012) with a minimum of n = 3 replicates for the last 300 years. As the peat accretion rates were more elevated than initially hypothesised for some Baie Comeau and Blanc Sablon cores, n = 3 for longer time periods was not possible.

7.2.3.3 *Evaluating spatial and temporal patterns in carbon accumulation*

Regional patterns in carbon accumulation between sites and over time were evaluated for lawn cores at all three sites. Long-term temporal trends in CAR within Havre-St-Pierre microforms were also measured. All datasets were tested for normality and homogeneity of variances using Kolmogorov-Smirnov and Levene's tests, respectively. Differences over time were tested using one-way Repeated Measures ANOVA and the interactions between carbon accumulation and site over time were analysed using a

one-way Mixed ANOVA, using the Greenhouse-Geisser correction for sphericity if the assumption is violated. In the case of an overall significant ANOVA, pairwise comparisons were considered for each time period using Bonferroni confidence interval adjustments in order to reduce the likelihood of Type I (false positive) error (Maxwell and Delaney, 2004; Dytham, 2010; Laerd Statistics, 2015). Results are reported for $p < 0.1$; statistically significant results ($p < 0.05$) are reported in bold.

7.2.4 Analysis of environmental variables

Environmental variables, including mean summer temperature (MST), mean summer precipitation (MSP), mean annual precipitation (MAP), growing degree days (> 0^{o}C) (GDD0) and photosynthetically active radiation (PAR), were selected because of their important roles in regulating peatland water table and carbon accumulation and demonstrated links in other studies (Charman *et al.,* 2013, 2015; Garneau *et al.,* 2014). MST, MSP and MAP were calculated using Environment Canada's Climate Normals 1971-2000 (Environment Canada, 2015) for the nearest weather station (Baie Comeau, Rivière-au-Tonnerre and Blanc Sablon). PAR and GDD0 were calculated for Baie Comeau, Havre-St-Pierre, Blanc Sablon (Lac à la Truite and Vallée peatlands) and Red Bay, using PeatStash as in Charman *et al. (*2013) from the CLIMATE2.2 data (Kaplan *et al.,* 2003) (Table 7.1).

Relationships between environmental variables, Holocene LORCA, peat thickness and basal age (Magnan and Garneau, 2014 for Baie Comeau and Havre-St-Pierre; Dionne and Richard, 2006 for thickness and basal age for a nearby peatland at Blanc Sablon), RERCA (Chapter 6), microform type (coded 1-4), approximate water table depth, and mean CAR for different time periods (this chapter) were analysed using simple linear regressions and a stepwise multiple regression to evaluate the main explanatory variables. All carbon datasets were normally distributed.

Table 7.1. Environmental variables from Chapter 3. GDD and PAR were calculated using grid references; Red Bay is in a separate grid.

	LAT	MAT (°C)	MST (°C)	MAP (mm)	MSP (mm)	GDD0	PAR
Baie Comeau	49.04	1.5	14.2	1014	84.9	2364.01	6111.92
Havre-St-Pierre	50.09	1.1	13.1	1080	99.4	2101.56	5409.78
Blanc Sablon	51.43	0.2	10.8	1066	103.1	1720.13	5459.64
(Red Bay)	51.73	0.2	10.8	1066	103.1	1473.78*	5211.13*

7.3 Results

This section presents the results of the previous analyses. Age-depth models are presented along with the measured radiocarbon ages and calibrated dates, followed by the carbon accumulation results during the last few centuries.

7.3.1 Chronologies

Chronologies for the three regions were developed using ^{210}Pb dates (Chapter 6) and the radiocarbon dates listed in Tables 7.2 (lawn cores for all three regions) and Table 7.3 (Havre-St-Pierre microform cores). Age-depth models are shown in Figures 7.1-7.3 (lawn cores for all three regions) and Figures 7.4-7.6 (Havre-St-Pierre microforms).

7.3.1.1 *Lawn cores*

At Baie Comeau, there were no age reversals or outliers. Age-depth models (Figure 7.1) show consistent peat accumulation over time within cores; however, for the same depth, calibrated dates varied considerably between peatlands. At Lebel (BC1A) and Baie (BC2A), 1 m of peat accumulated since *ca.* 700 cal. BP, while 1 m of peat accumulated since 412 cal. BP at Manic (HP3A). The mean peat accumulation rate for the region is 1.82 ± 0.33 mm a^{-1}.

For the same depths at Havre-St-Pierre, there is considerable variability between the cores (Figure 7.2). Indeed, the age at the deepest part of the HP2A core (Morts) is

almost half as young as the other two peatlands in this region. A post-bomb spike ^{14}C date underestimates the age at 25 cm compared to the ^{210}Pb dates. There are no age reversals. The mean peat accumulation rate for the region at 70 cm depth is 0.52 ± 0.10 mm a^{-1} for lawn cores.

Blanc Sablon cores are in Figure 7.3. The mean peat accumulation rate at Blanc Sablon is 0.88 ± 0.42 mm a^{-1}. At BS1A, between the bottom of the ^{210}Pb profile and the first radiocarbon date measured (between 17-20 cm), the accretion rate is *ca*. 450 a cm^{-1} indicating a slow accumulation rate or erosion due to the presence of permafrost. As the core was taken next to a palsa, and the stratigraphy did not change, erosion was excluded. There was an age reversal at 40 cm in BS1A, likely due to cryoturbation as the core is adjacent to a palsa and the $\delta^{13}C$ is consistent with other samples so the date was likely not contaminated. This date was excluded from the model. However, the radiocarbon dates are all > 1000 years, so outside the timeframe of interest for this study. A similar 'kink' in the BACON model for BS3A is evident, also indicating the role of permafrost in slowing down peat accumulation (*ca.* 50 a cm^{-1} between 33-36 cm). Peat accumulation in BS2A and BS3A was much more rapid, with ages of 396 and 670 cal. BP at 50 cm. For BS2A, a post-bomb spike date at 40 cm underestimates the age compared to the ^{210}Pb CRS method.

Table 7.2 Summary of radiocarbon dates for lawn cores, the calibrated 2-sigma age range (clam) for each sample and weighted mean age from the age-depth models (BACON).

Region/ Site	Depth (cm)	SUERC code	^{14}C age (years BP)	δ^{13}C	2σ range (cal. BP)	BACON wmean
BAIE COMEAU:						
BC1A	59.5-60	50051	133 ± 37	-26.7	7-280	98.1
(Lebel)	79.5-80	50052	394 ± 37	-27.9	319-512	395.8
	99.5-100	49621	869 ± 37	-27.3	695-906	696.7
	100-101	123620[a]	765 ± 20	-27.8	672-725	706.9
	128-129	50053	1051 ± 37	-25.7	921-1055	1031.7
	140-141	123621[a]	1560 ± 20	-29.0	1402-1520	1322.1
BC2A	54.5-55	51647	164 ± 37	-24.5	(-3)-288	172.5
(Baie)	64.5-65	51650	182 ± 35	-26.1	(-4)-300	240.6
	84.5-85	51651	295 ± 37	-23.6	287-465	395.3
	99.5-100	49622	782 ± 37	-22.8	667-764	542.1
BC3A	54.5-55	51652	132 ± 37	-24.8	7-280	91.3
(Manic)	84.5-85	51653	241 ± 35	-28.0	(-4)-428	271.0
	99.5-100	50054	368 ± 37	-25.8	316-503	359.0
HAVRE-ST-PIERRE:						
HP1A	24.5-25	50055	113 ± 37	-28.0	11-271	241.5
(Plaine)	34.5-35	50056	357 ± 37	-25.4	316-498	405.2
	44.5-45	50059	1006 ± 37	-26.0	769-1045	802.8
	55.5-56	50060	1171 ± 37	-26.5	967-1238	1127.5
	69.5-70	49625	1993 ± 37	-27.0	1868-2009	1731.8
HP2A	24.5-25	51654	-1030 ± 37[b]	-26.9	(-45)-(-7)	39.4
(Morts)	39.5-40	51655	186 ± 37	-25.7	(-4)-302	223.1
	69.5-70	49626	1063 ± 37	-24.9	927-1055	936.0
	79.5-80	50061	1277 ± 37	-26.6	1092-1290	1171.1
HP3A	34.5-35	58265	454 ± 37	-26.2	341-543	386.3
(Romaine)	44.5-45	58266	562 ± 37	-26.6	519-648	530.6
	69.5-70	51656	1742 ± 35	-26.7	1551-1730	1514.5
	79.5-80	51657	1994 ± 37	-25.5	1869-2040	1913.4
BLANC SABLON:						
BS1A	19.5-20	53628	1290 ± 35	-25.2	1175-1295	1056.0
(Red Bay)	25.5-26	53629	1481 ± 37	-25.2	1301-1516	1338.5
	32.5-33	53630	1430 ± 35	-24.9	1290-1385	1474.6
	39.5-40	53631	3493 ± 35	-25.7	3646-3860	-
	49.5-50	50052	1987 ± 37	-23.2	1835-2037	1920.9
BS2A (Lac	39.5-40	58269	-1157 ± 35[c]	-26.6	(-43)-(-8)	84.9
à la Truite)	49.5-50	50053	339 ± 37	-23.2	309-485	247.6
BS3A	34.5-35	58270	343 ± 35	-25.9	310-485	273.1
(Vallée)	49.5-50	51660	725 ± 37	-25.8	568-728	643.5

[a]UCI-AMS lab code (University of California Irvine)

[b]F14 = 113.68 ± 0.52 (^{14}C enrichment: % abs. modern ± 1σ); postbomb curve: NH1

[c]F14 = 115.49 ± 0.51 (^{14}C enrichment: % abs. modern ± 1σ); postbomb curve: NH1

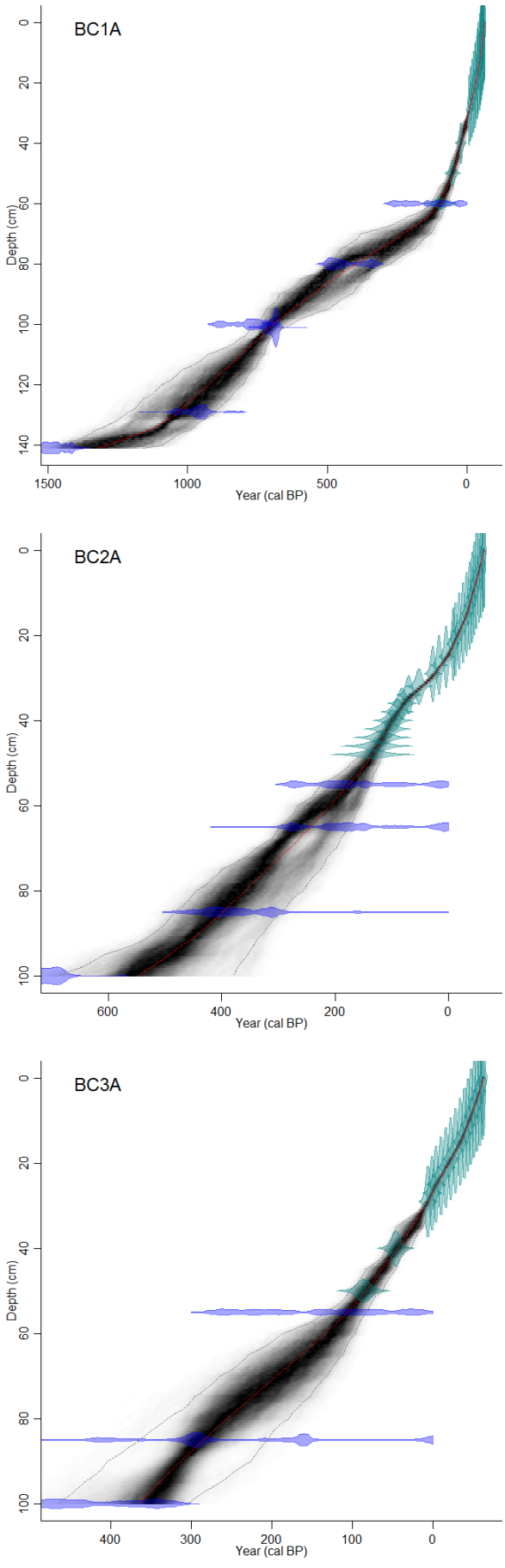

Figure 7.1 Age-depth models for Baie Comeau (BC) **lawn** cores (A), modelled using BACON package (Blaauw and Christen, 2011). ^{210}Pb dates calculated using the CRS model (Chapter 6) are in green; calibrated ^{14}C dates in blue; darker greys indicate more likely ages; grey lines show 95% CI; red curve shows single 'best' model based on the weighted mean age.
Panels from top to bottom – BC1A: Lebel, BC2A: Baie, BC3A: Manic.

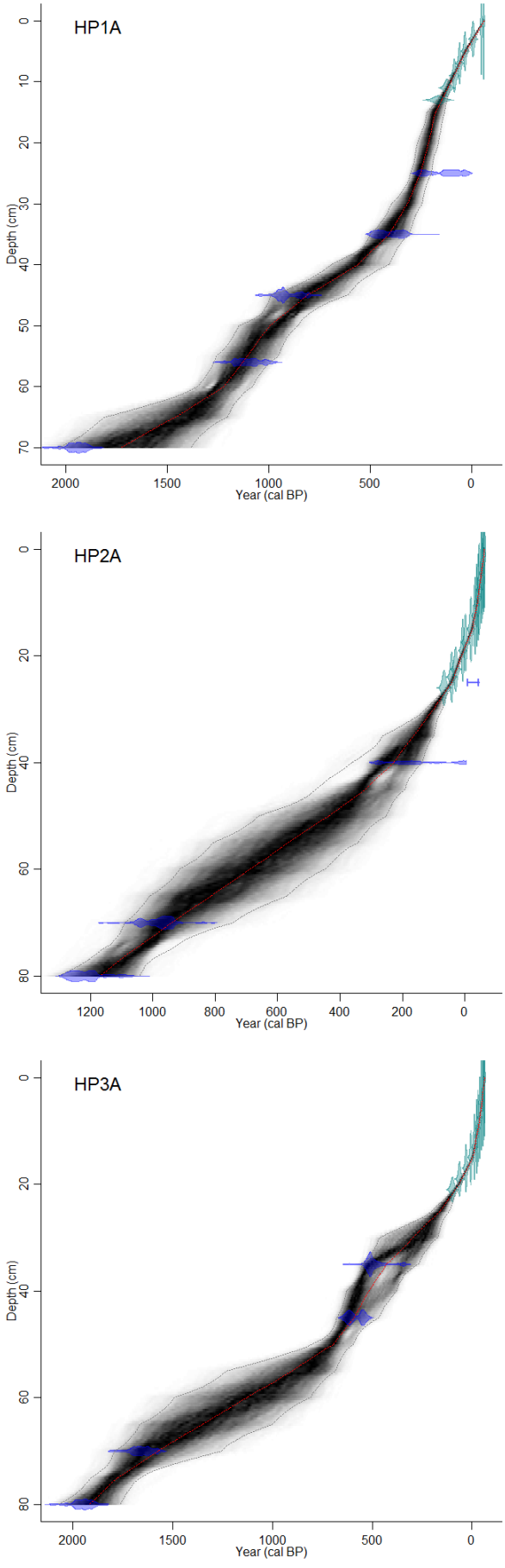

Figure 7.2 Age-depth models for Havre-St-Pierre (HP) **lawn** cores (A), modelled using BACON package (Blaauw and Christen, 2011). ^{210}Pb dates calculated using the CRS model (Chapter 6) are in green; calibrated ^{14}C dates in blue; darker greys indicate more likely ages; grey lines show 95% CI; red curve shows single 'best' model based on the weighted mean age.
Panels from top to bottom – HP1A: Plaine, HP2A: Morts, HP3A: Romaine.

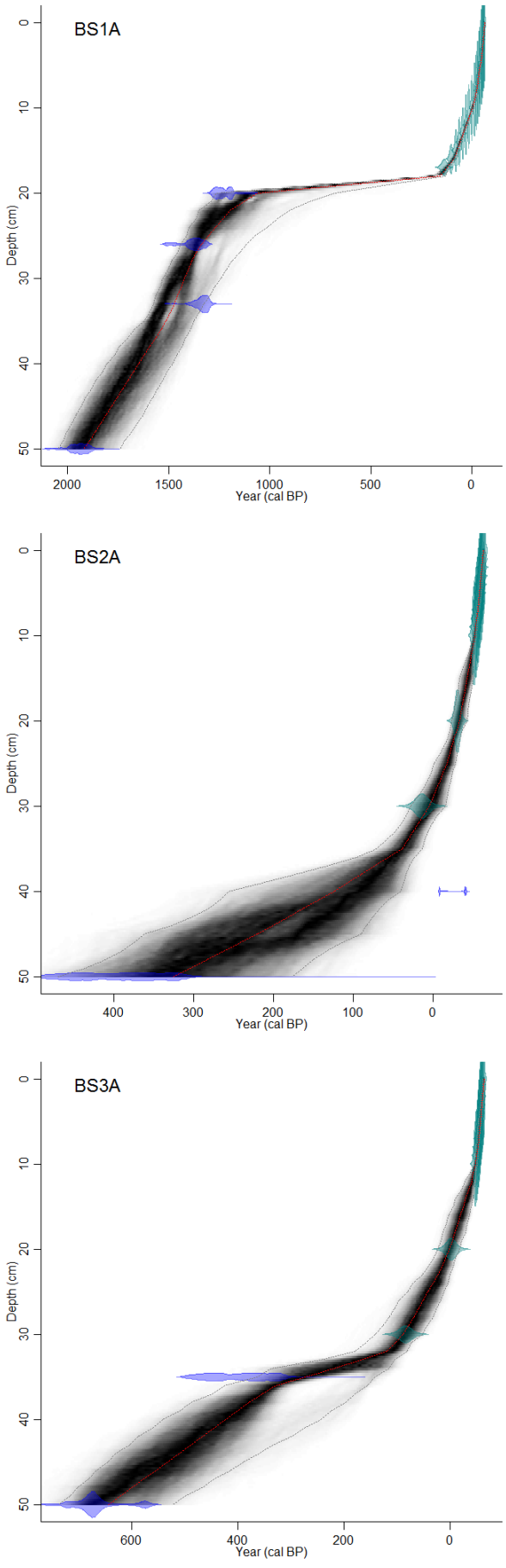

Figure 7.3 Age-depth models for Blanc Sablon (BS) **lawn** cores (A), modelled using BACON package (Blaauw and Christen, 2011). ^{210}Pb dates calculated using the CRS model (Chapter 6) are in green; calibrated ^{14}C dates in blue; darker greys indicate more likely ages; grey lines show 95% CI; red curve shows single 'best' model based on the weighted mean age.
Panels from top to bottom – BS1A: Red Bay, BS2A: Lac à la Truite, BS3A: Vallée.

7.3.1.2 *Havre-St-Pierre microform cores*

Radiocarbon results for Havre-St-Pierre micfororms are presented in Table 7.3 and Figures 7.4-7.6. For non-lawn microforms (at 50 cm), the mean peat accumulation rates are, from wettest to driest: 1.18 ± 0.62 mm a^{-1} (hollows), 1.80 ± 0.63 mm a^{-1} (*Sphagnum* hummocks) and 0.86 ± 0.06 mm a^{-1} (lichen hummocks). Figures 7.3-7.5 show the age-depth models for the microform cores. Peat ages at 50 cm are variable between and within sites, ranging from 136-929 cal. BP. In some cores, slow-downs in peat accumulation are detected in the age-depth models, including *ca*. 200-600 cal. BP (HP2B), 100-800 cal. BP (HP3B), 0-100 cal. BP (HP1C), and 50-600 cal. BP (HP3C).

Table 7.3 Summary of radiocarbon dates for Havre-St-Pierre microform cores, the calibrated 2-sigma age range (clam, CI 95.4%) for each sample and weighted mean age from the age-depth models (BACON).

Region/ Site	Depth (cm)	SUERC code	^{14}C age (years BP)	δ^{13}C	2σ range (cal. BP)	BACON wmean
HOLLOWS:						
HP1B	34.5-35	58271	58 ± 37	-27.1	25-261	56.9
	49.5-50	58272	200 ± 35	-26.0	(-4)-307	156.0
HP2B	34.5-35	58902	639 ± 35	-26.5	552-668	518.9
	49.5-50	58903	765 ± 35	-27.7	662-741	767.5
HP3B	34.5-35	58910	99 ± 37	-26.8	11-270	166.3
	49.5-50	58911	1367 ± 35	-26.9	1187-1347	928.7
***SPHAGNUM* HUMMOCKS:**						
HP1C	34.5-35	58273	95 ± 35	-28.3	13-270	119.6
	49.5-50	63952	240 ± 37	-28.1	333-536	182.4
HP2C	34.5-35	58904	48 ± 35	-27.2	29-259	38.9
	49.5-50	58905	369 ± 35	-26.0	315-504	136.9
HP3C	34.5-35	58912	585 ± 37	-28.0	533-653	368.9
	49.5-50	58913	958 ± 37	-28.0	788-934	825.2
LICHEN HUMMOCKS:						
HP1D	34.5-35	58274	292 ± 35	-26.6	286-465	284.9
	49.5-50	58275	437 ± 37	-27.0	334-535	473.9
HP2D	34.5-35	58908	516 ± 37	-28.9	504-631	498.6
	49.5-50	58909	528 ± 35	-28.6	507-634	625.4
HP3D	34.5-35	58915	197 ± 37	-28.2	(-4)-306	167.1
	49.5-50	58918	575 ± 35	-26.2	527-653	519.9

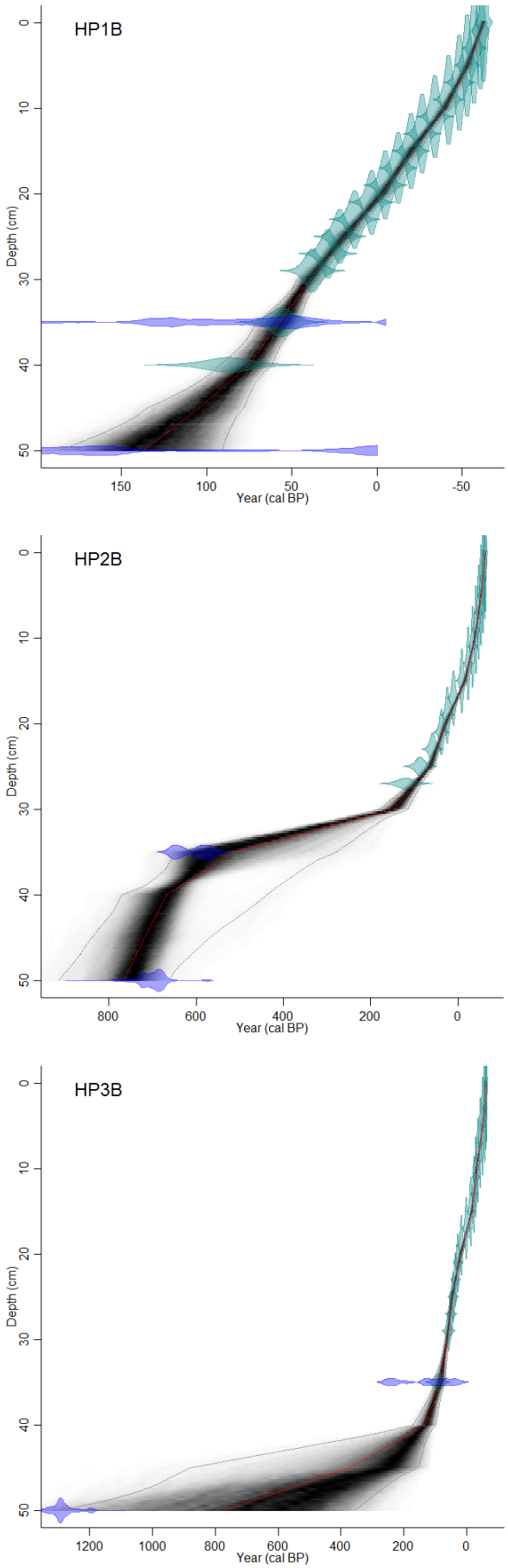

Figure 7.4 Age-depth models for Havre-St-Pierre (HP) **hollow** cores (B), modelled using BACON package (Blaauw and Christen, 2011). ^{210}Pb dates calculated using the CRS model (Chapter 6) are in green; calibrated ^{14}C dates in blue; darker greys indicate more likely ages; grey lines show 95% CI; red curve shows single 'best' model based on the weighted mean age.
Panels from top to bottom – HP1B: Plaine, HP2B: Morts, HP3B: Romaine.

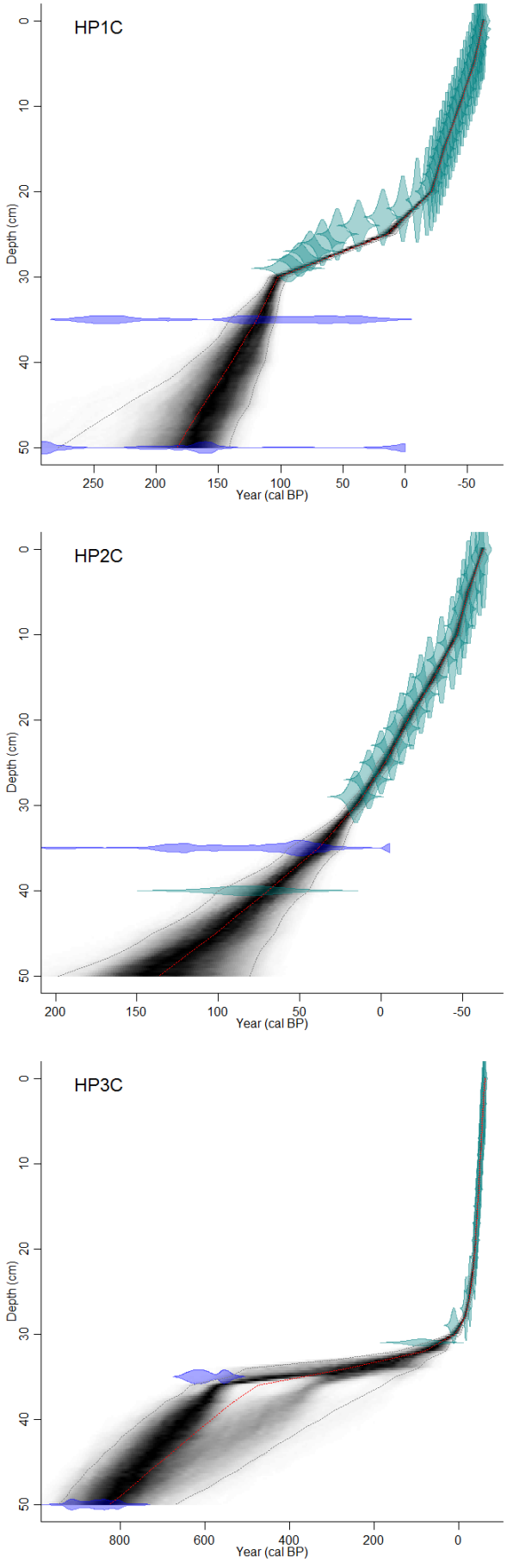

Figure 7.5 Age-depth models for Havre-St-Pierre (HP) ***Sphagnum* hummock** cores (C), modelled using BACON package (Blaauw and Christen, 2011). ^{210}Pb dates calculated using the CRS model (Chapter 6) are in green; calibrated ^{14}C dates in blue; darker greys indicate more likely ages; grey lines show 95% CI; red curve shows single 'best' model based on the weighted mean age. Panels from top to bottom – HP1C: Plaine, HP2C: Morts, HP3C: Romaine.

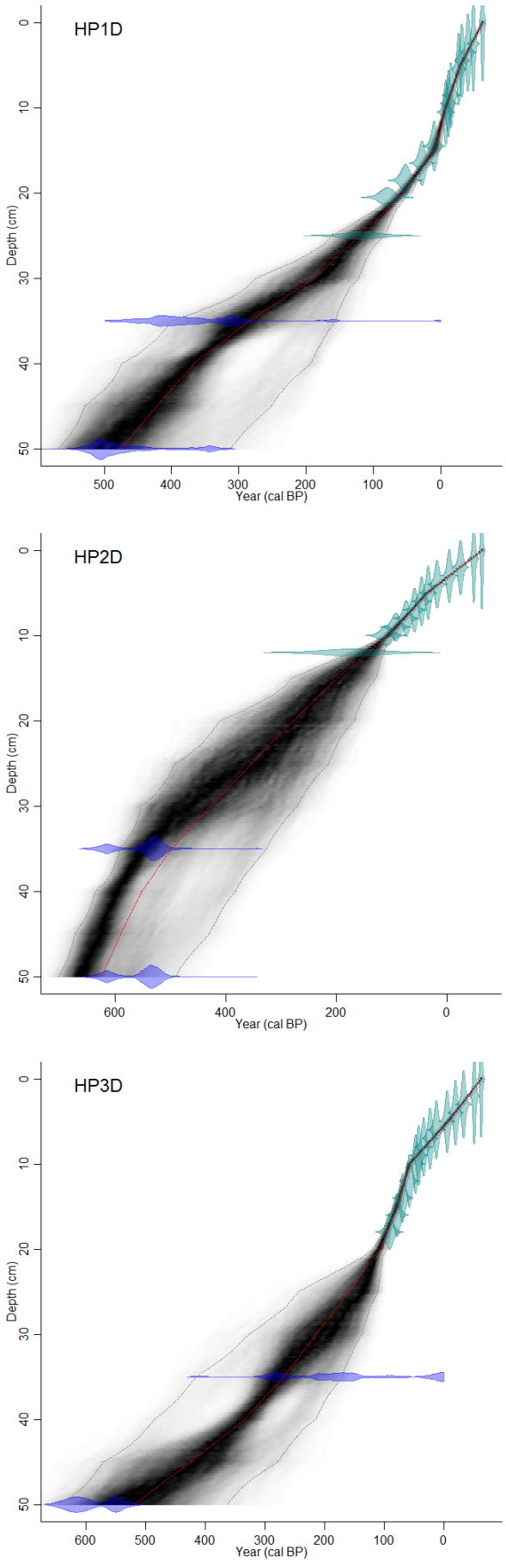

Figure 7.6 Age-depth models for Havre-St-Pierre (HP) **lichen hummock** cores (D), modelled using BACON package (Blaauw and Christen, 2011). ^{210}Pb dates calculated using the CRS model (Chapter 6) are in green; calibrated ^{14}C dates in blue; darker greys indicate more likely ages; grey lines show 95% CI; red curve shows single 'best' model based on the weighted mean age.

Panels from top to bottom – HP1D: Plaine, HP2D: Morts, HP3D: Romaine.

7.3.2 Carbon results

Figures 7.7 to 7.9 show carbon data for lawn cores, incorporating dating-related uncertainties. Figures 7.10-7.12 show the same for other Havre-St-Pierre microforms. Error is lowest for carbon data around the ^{14}C dated depths, and for the ^{210}Pb-dated sections, as indicated by darker grey and narrower distribution in the figures.

7.3.2.1 *Lawn cores*

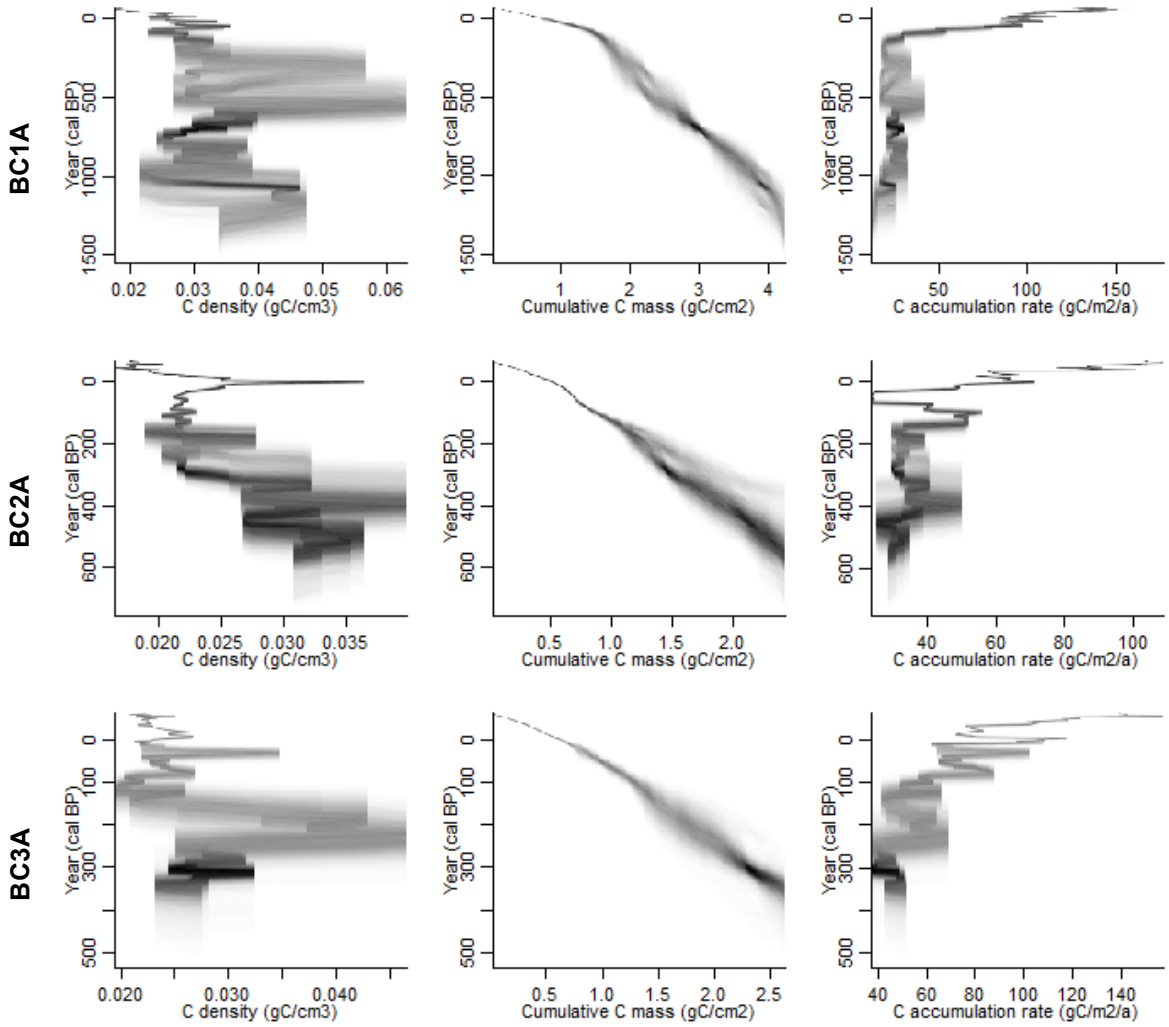

Figure 7.7. Carbon results for Baie Comeau **lawn** cores (BC1A: Lebel, BC2A: Baie, BC3A: Manic). For each core, C density, cumulative C and CAR (from left to right) were modelled using the BACON package for R (Blaauw and Christen, 2011; R Development Team, 2014), with darker grey indicating more likely calendar ages for each carbon value.

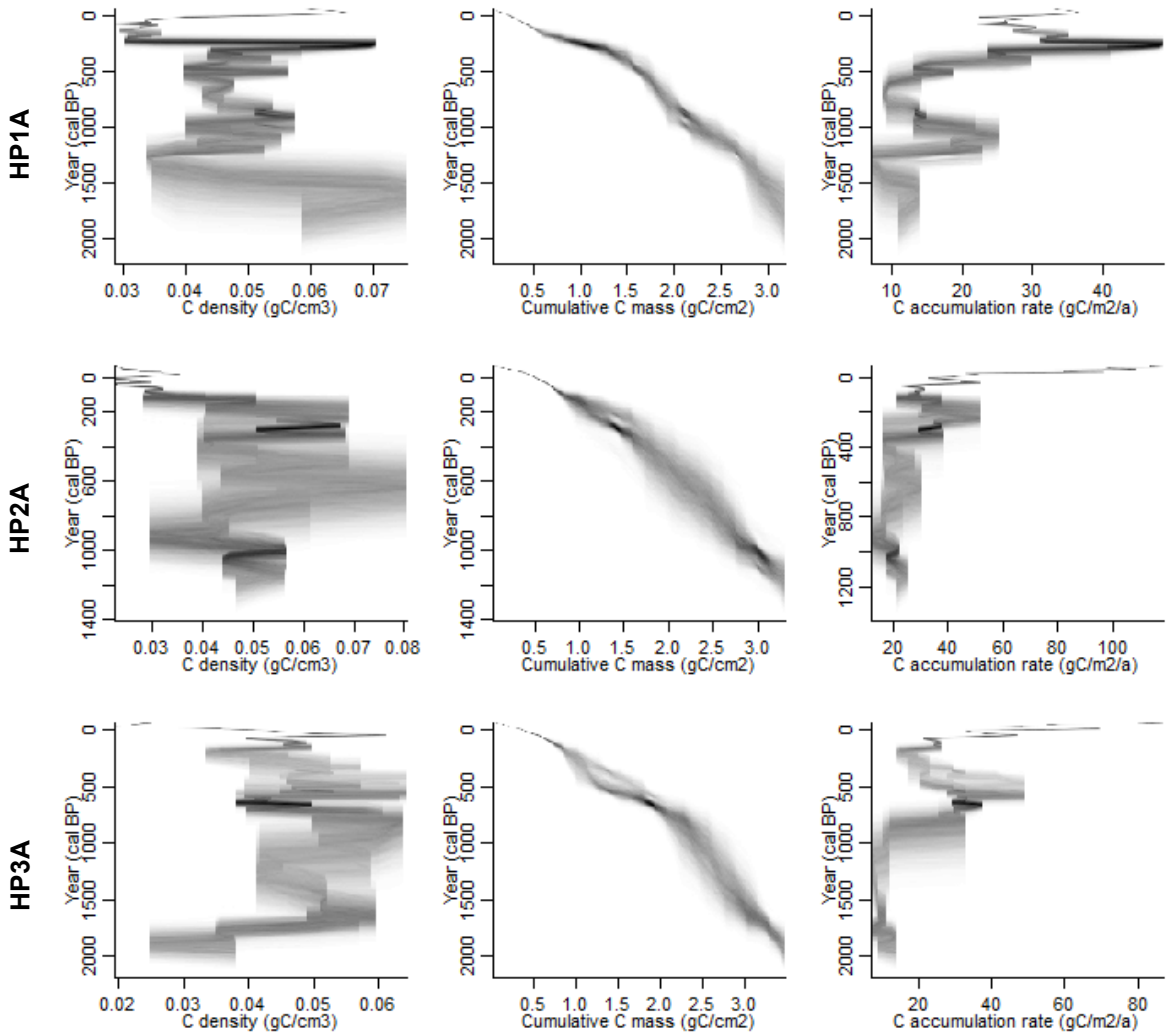

Figure 7.8 Carbon results for Havre-St-Pierre **lawn** cores (HP1A: Plaine, HP2A: Morts, HP3A: Romaine). For each core, C density, cumulative C and CAR (from left to right) were modelled using the BACON package for R (Blaauw and Christen, 2011; R Development Team, 2014), with darker grey indicating more likely calendar ages for each carbon value.

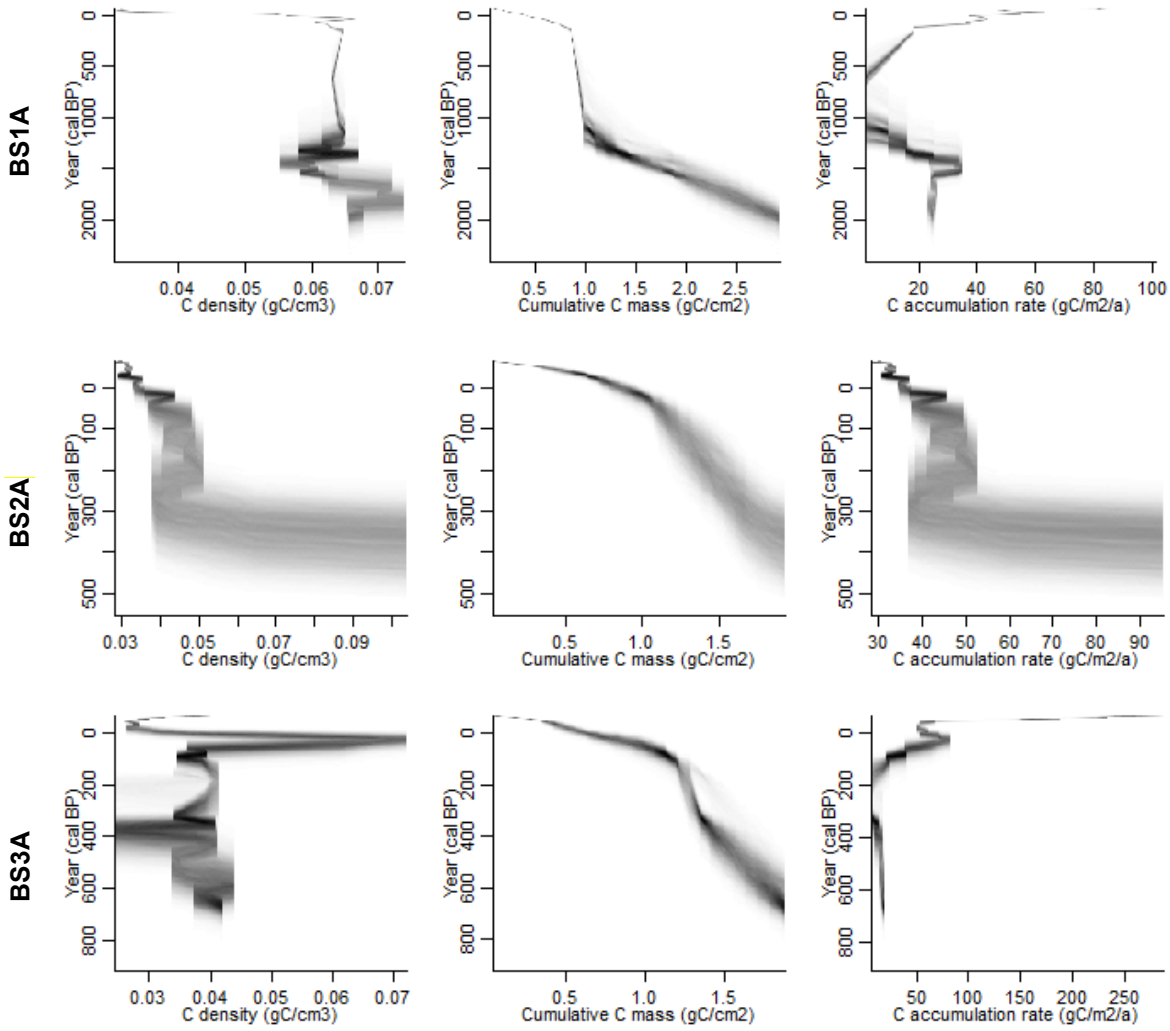

Figure 7.9 Carbon results for Blanc Sablon **lawn** cores (BS1A: Red Bay, BS2A: Lac à la Truite, BS3A: Vallée). For each core, C density, cumulative C and CAR (from left to right) were modelled using the BACON package for R (Blaauw and Christen, 2011; R Development Team, 2014), with darker grey indicating more likely calendar ages for each carbon value.

7.3.2.2 *Havre-St-Pierre microform cores*

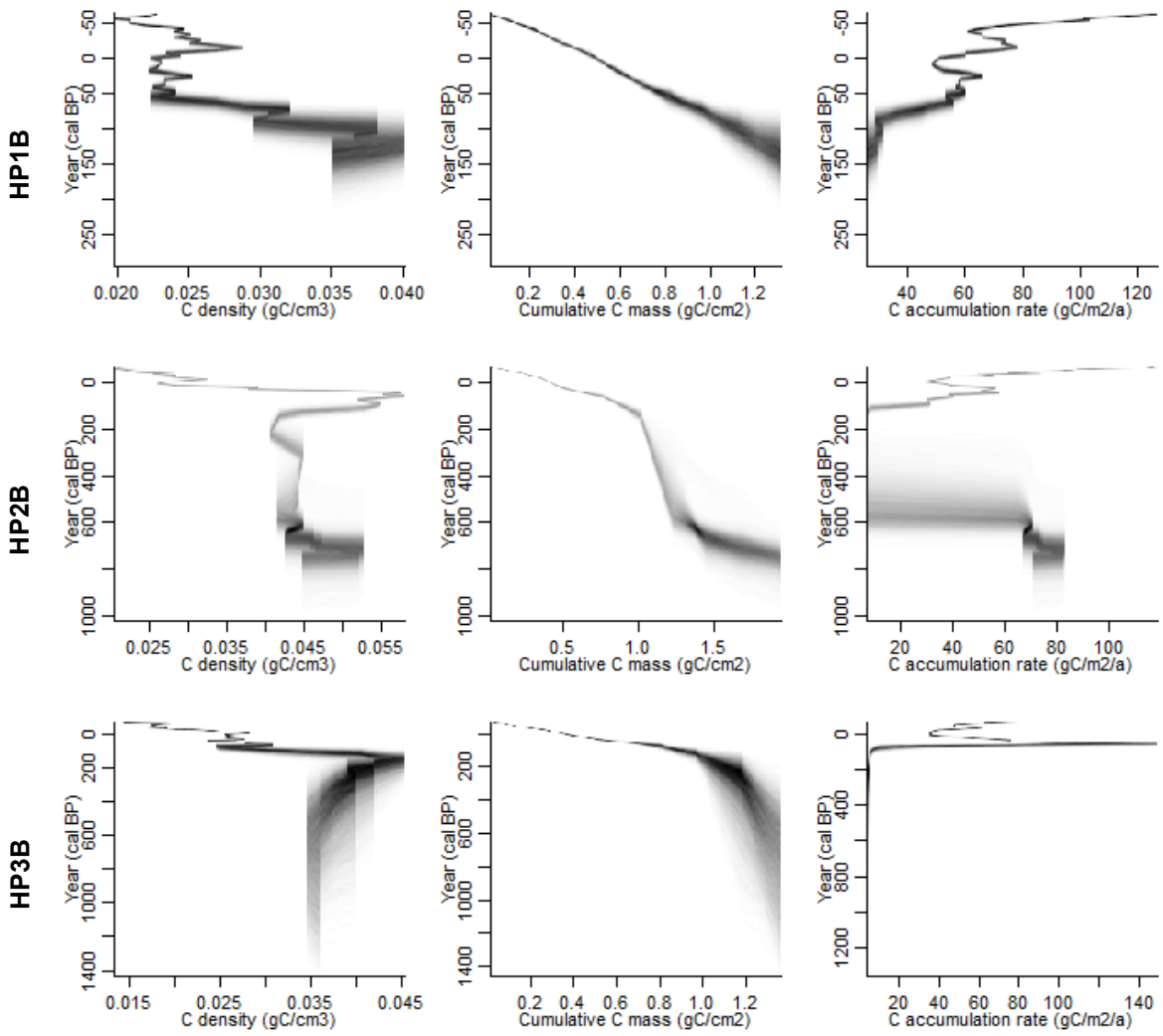

Figure 7.10 Carbon results for Havre-St-Pierre **hollow** cores (HP1B: Plaine, HP2B: Morts, HP3B: Romaine). For each core, C density, cumulative C and CAR (from left to right) were modelled using the BACON package for R (Blaauw and Christen, 2011; R Development Team, 2014), with darker grey indicating more likely calendar ages for each carbon value.

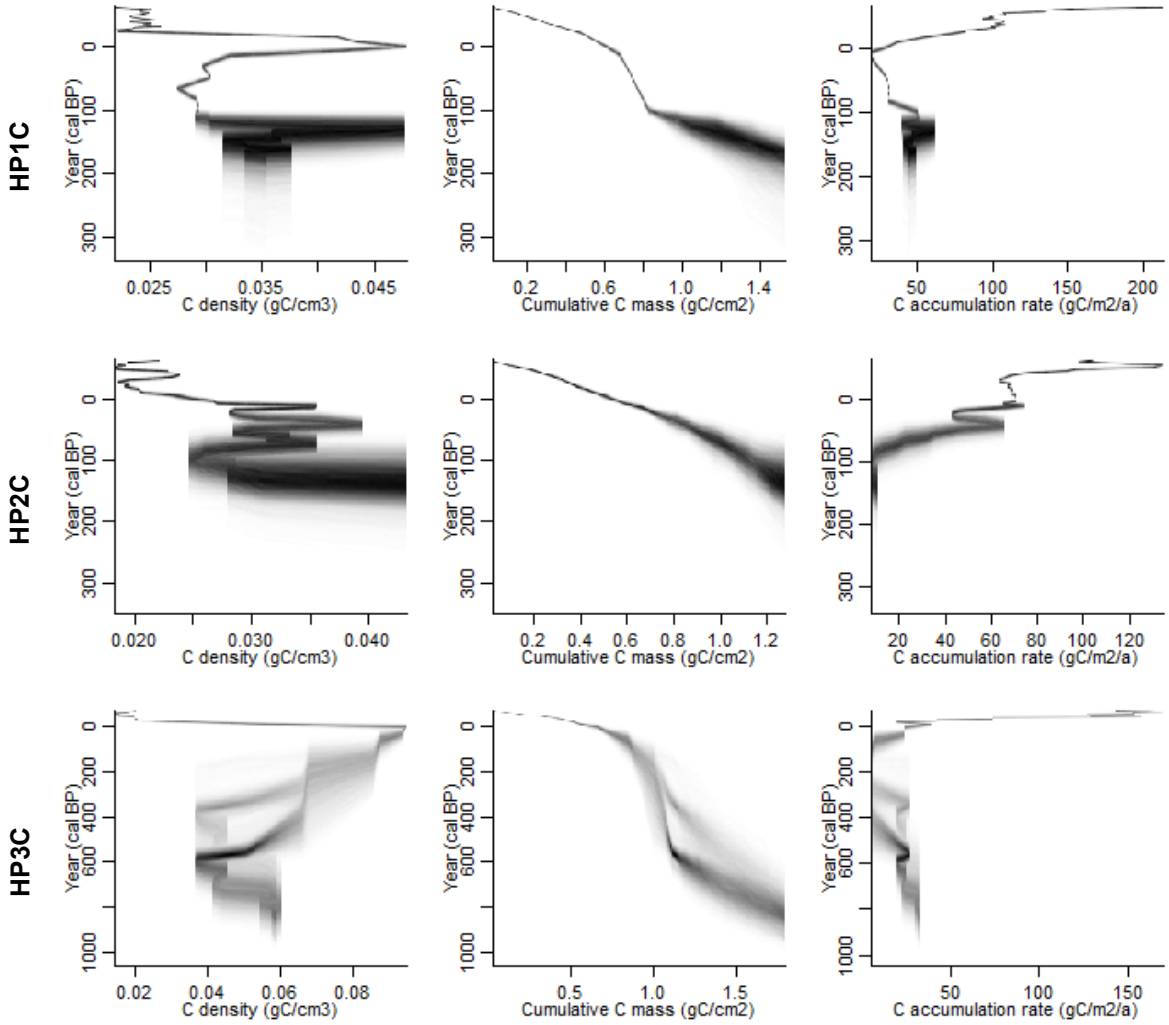

Figure 7.11 Carbon results for Havre-St-Pierre ***Sphagnum*** **hummock** cores (HP1C: Plaine, HP2C: Morts, HP3C: Romaine). For each core, C density, cumulative C and CAR (from left to right) were modelled using the BACON package for R (Blaauw and Christen, 2011; R Development Team, 2014), with darker grey indicating more likely calendar ages for each carbon value.

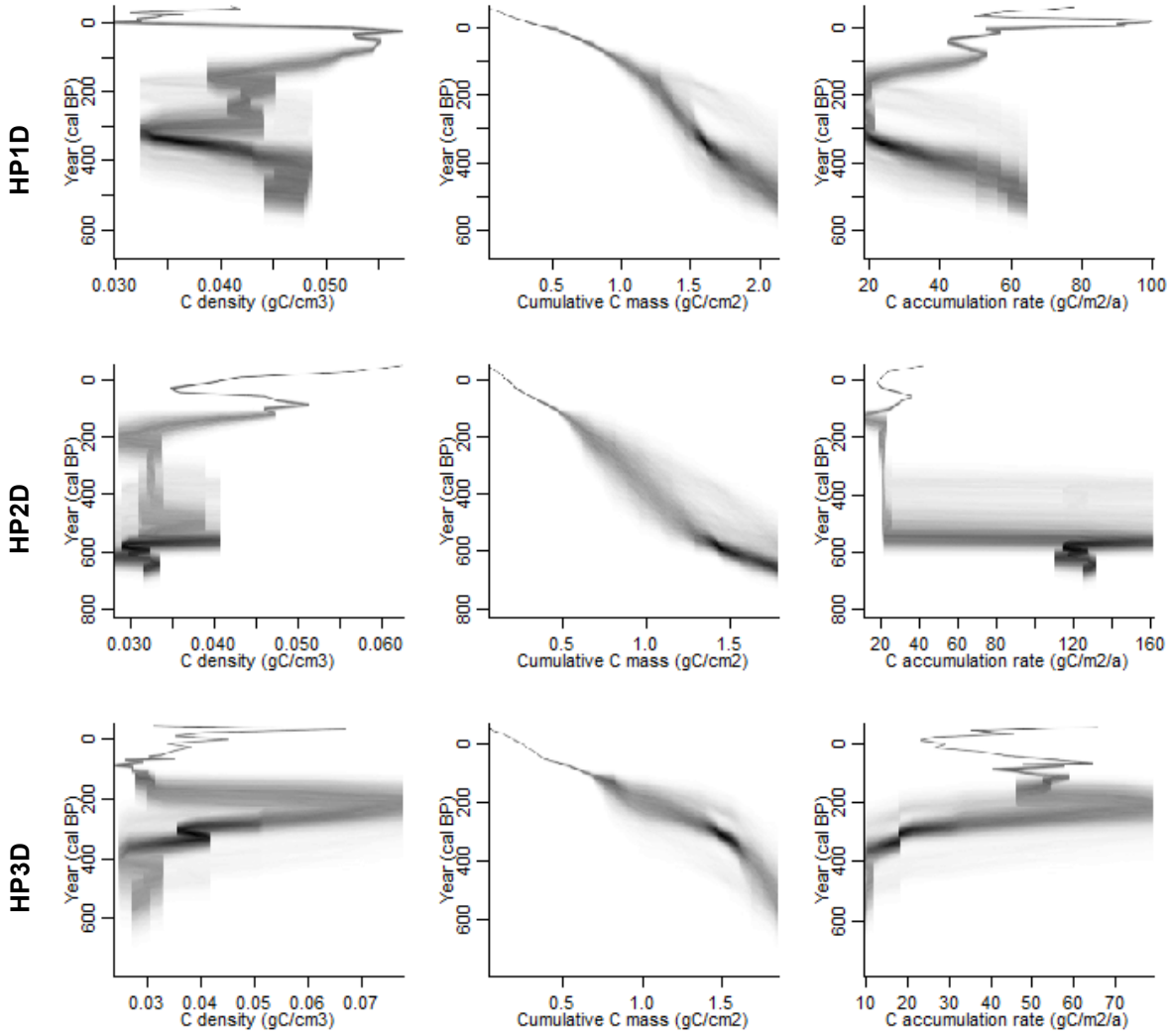

Figure 7.12 Carbon results for Havre-St-Pierre **lichen hummock** cores (HP1D: Plaine, HP2D: Morts, HP3D: Romaine). For each core, C density, cumulative C and CAR (from left to right) were modelled using the BACON package for R (Blaauw and Christen, 2011; R Development Team, 2015), with darker grey indicating more likely calendar ages for each carbon value.

7.3.3 Patterns and trends in carbon accumulation

7.3.3.1 *Regional patterns*

Carbon accumulation is highly variable on a centennial scale, both within and between the three regions. Table 7.4 presents the regional cumulative C mass (± SE) for ages represented by three replicates. For the last 200 and 300 years, Havre-St-Pierre was the lowest peat accumulator, and Baie Comeau the highest. During the last 100 years, Blanc Sablon peatlands accumulated the most peat.

Table 7.4 Cumulative C mass (g C cm^{-2}) ± SE accumulated over time (n = 3 in each case).

	Baie Comeau	**Havre-Saint-Pierre**	**Blanc Sablon**
Last 100 years	0.97 ± 0.15	0.53 ± 0.10	0.99 ± 0.19
Last 200 years	1.48 ± 0.19	0.81 ± 0.10	1.30 ± 0.20
Last 300 years	1.81 ± 0.22	1.12 ± 0.13	1.45 ± 0.27

Statistical analysis of variance was only possible with a minimum of n = 3 replicates so spatial analysis was constrained from 250 cal. BP (1700AD) to the present day. Results indicate that while the mean cumulative C mass accumulated during the last 100 years at Havre-St-Pierre was less than the C accumulated at the other two regions, this difference was not significant (Kruskall-Wallis for non-normal data: $p < 0.1$). No significant differences were detected overall.

Mean CAR for the last millennium is related to the regional climatic gradient: the southernmost warmest and most continental site, Baie Comeau, without a history of permafrost, had the highest CAR. Havre-St-Pierre, the intermediate site with a hypothesised history of permafrost, had the intermediate CAR. Blanc Sablon, the coolest and northernmost, most oceanic site had the lowest 1000-year mean CAR. The same geographic trend is calculated for the 500-year mean CAR. From 300 years, the Blanc Sablon sites CAR is higher for Blanc Sablon than for Havre-St-Pierre indicating either higher accumulation, or relatively lower decomposition. However, the 500- and

1000-year values for Blanc Sablon were calculated using only one core for the region (BS1A: Red Bay); it is therefore possible that there is bias towards lower values (Figure 7.13).

7.3.3.2 *Regional trends in CAR over time*

Figure 7.13 shows that for all three regions, CAR increases with time, which is expected for accumulating peatlands. Figure 7.14 shows the changes in mean 100-year CAR for the last millennium for the three regions. The overall mean CAR was 42.2 ± 5.1 g C m^{-2} a^{-1} at Baie Comeau, 24.3 ± 2.1 g C m^{-2} a^{-1} at Havre-St-Pierre, and 14.0 ± 5.7 g C m^{-2} a^{-1} at Blanc Sablon; however, the 1000-year CAR values were not all calculated with 3 replicates. For all three sites, CAR increases over time, with highest rate of increase during the last 200 years at Baie Comeau and Blanc Sablon and last 100 years at Havre-St-Pierre. CAR was lower at Blanc Sablon compared to the other two regions until the last 200 years (Figure 7.14).

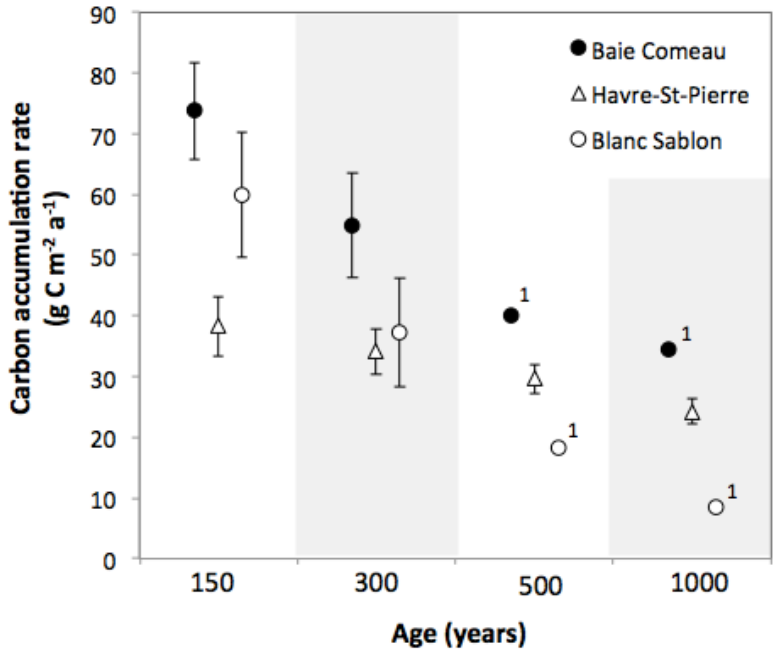

Figure 7.13 Spatial distribution of mean 50-year carbon accumulation rate for each time period (from left to right, last 150 to 1000 years). N = 3 was only possible for all three regions within the last 300 years; n = 1 is indicated for Baie Comeau and Blanc Sablon cores for the mean CAR for the last 500 and 1000 years. Mean 50-year CAR for the last 150 years is from Chapter 6.

At all three sites, there was a decrease in 100-year mean CAR between the 450-550 cal. BP and 350-450 cal. BP periods, coinciding with the Spörer Minimum. This drop in CAR persisted through the 250-350 cal. BP period, while CAR increased at Baie Comeau and Havre-St-Pierre. There was also a decrease in CAR at Baie Comeau between the 250-350 cal. BP and 150-250 cal. BP periods, coinciding with the Maunder Minimum. Level CAR for the 250-350 cal. BP and 150-250 cal. BP periods, and a drop in CAR to the 50-150 cal. BP period coincided with the Maunder and Dalton Minima.

Figure 7.15 presents mean CAR calculated in 50-year bins for all three regions from 250 cal. BP, as this was the oldest period with n = 3 replicates for all regions, and in high-resolution 10-year bins from 100 cal. BP. CAR decreased for all sites from 250-150 cal. BP and continued to decrease at Havre-St-Pierre until 50 cal. BP. Considering the most recent period, there were decreasing trends in 10-year mean CAR in the mid-1900s (AD) at all three sites, i.e. between 1950-1970AD at Baie Comeau, 1920-1950AD at Havre-St-Pierre and 1960-1970AD at Bland Sablon (see also Chapter 6). From 1950AD, Blanc Sablon CAR increased faster than at Baie Comeau. Statistical analyses using Repeated Measures ANOVA for both the 50- and 10-year time series did not reveal any statistically significant interactions or differences between regions over time ($p > 0.1$).

7.3.3.3 *Within-site variability on a millennial scale*

This section builds on the previous chapter's results, by looking at multi-centennial CAR at Havre-St-Pierre. CAR results in 50-year bins are presented in Figure 7.16 for three replicates of each microform (hollows, lawns, *Sphagnum* hummocks and lichen hummocks). For all four microforms, CAR generally increased over time, with the highest rates of increase for hollows, lawns and *Sphagnum* hummocks for the last 150-

300 years; mean CAR for lichen hummocks plateaued for the last 150 years, however error was large for this period, likely reflecting natural variability between peatlands.

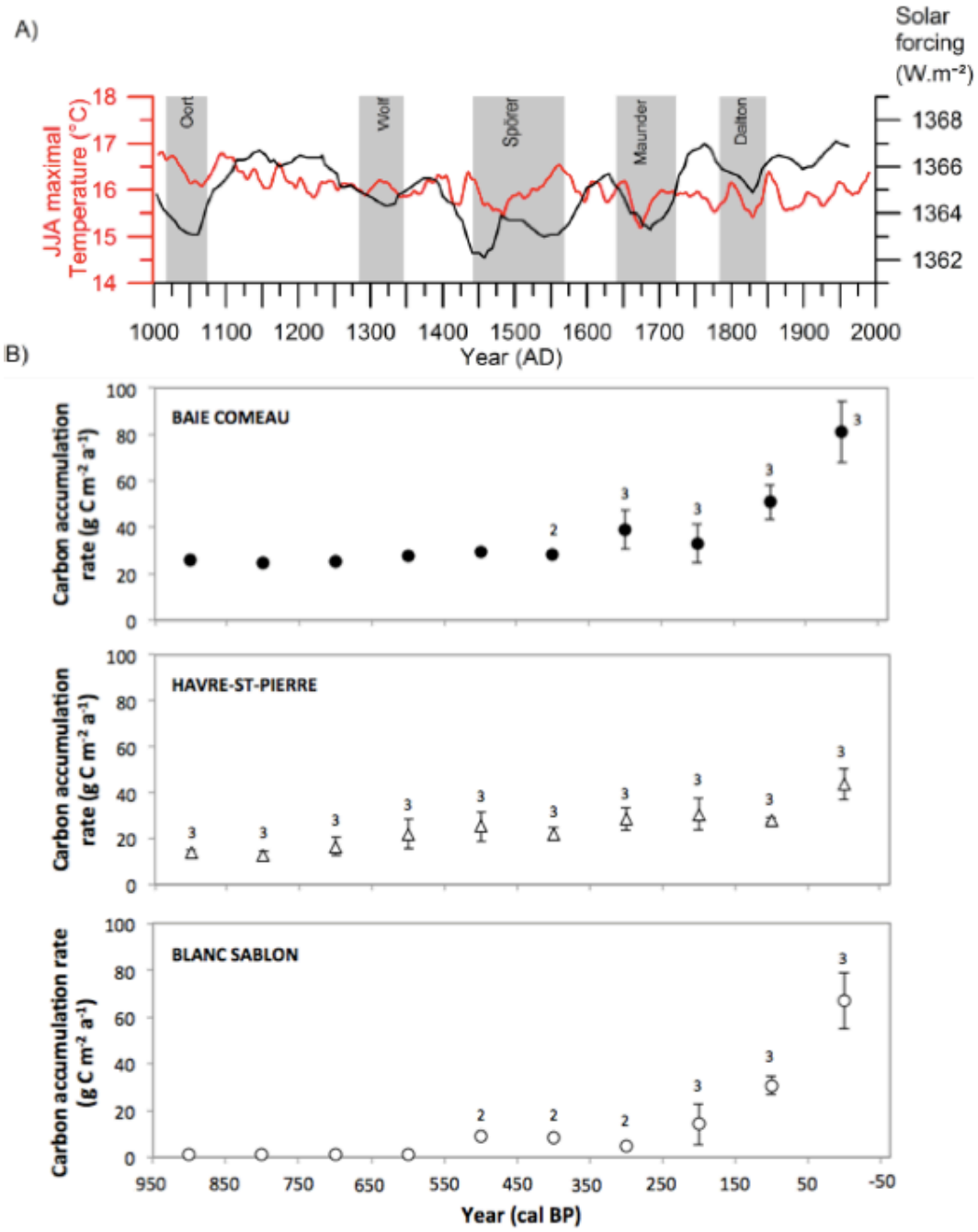

Figure 7.14 Relationships between mean 100-year carbon accumulation rates and climate; A) I-STREC reconstructed summer temperature for Eastern Canada (red line; 21-year smoothed), solar forcing (black line; Bard *et al.,* 2000) and solar minima (grey bands) (reproduced from Naulier *et al.,* 2015). B) Mean carbon accumulation rates for the three regions during the last millennium (1000-2000AD); data points represent mean CAR ± SE for 100-year bins, numbers are the number of replicates for each point (if no number, then n = 1; standard error was only calculated if n = 3).

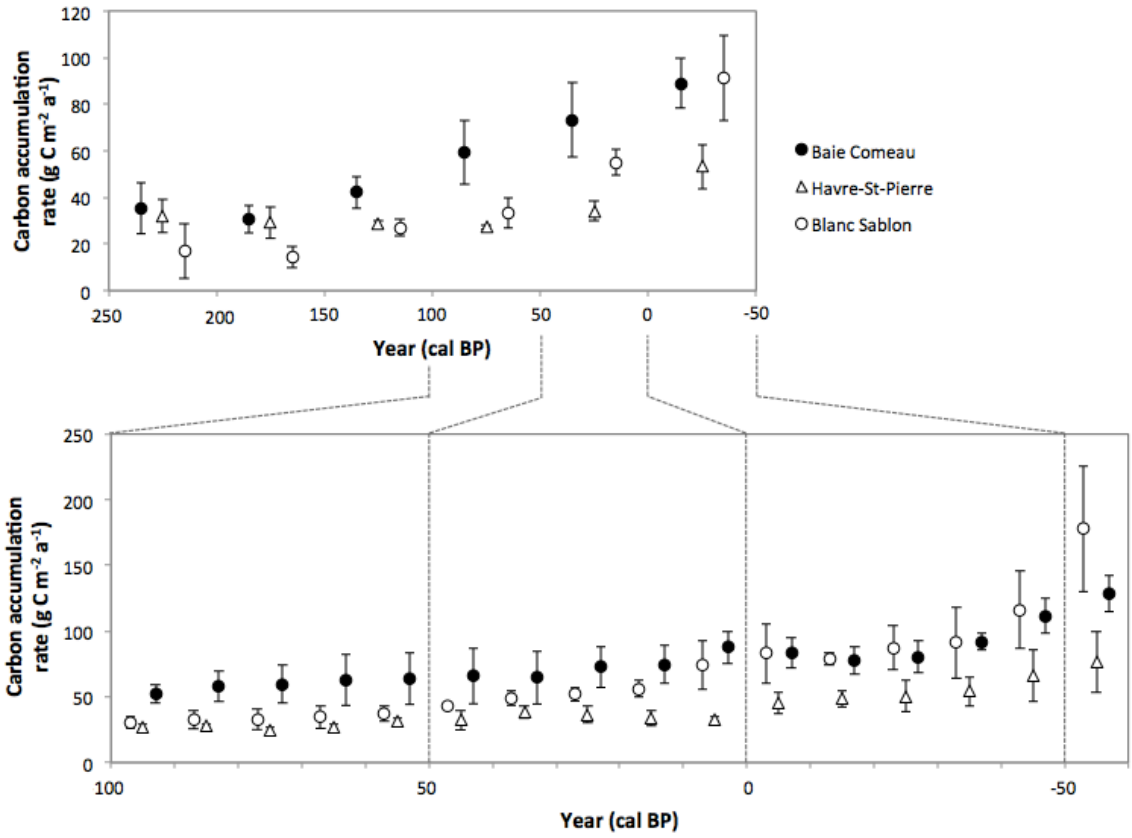

Figure 7.15 Mean carbon accumulation rates for the three regions; data points represent the mean CAR ± SE for 50-year bins from 1700-2000AD (top) and 10-year bins from 1850-2010AD (bottom) (based on n = 3 cores). Note that the y-axis scales are different for the two graphs.

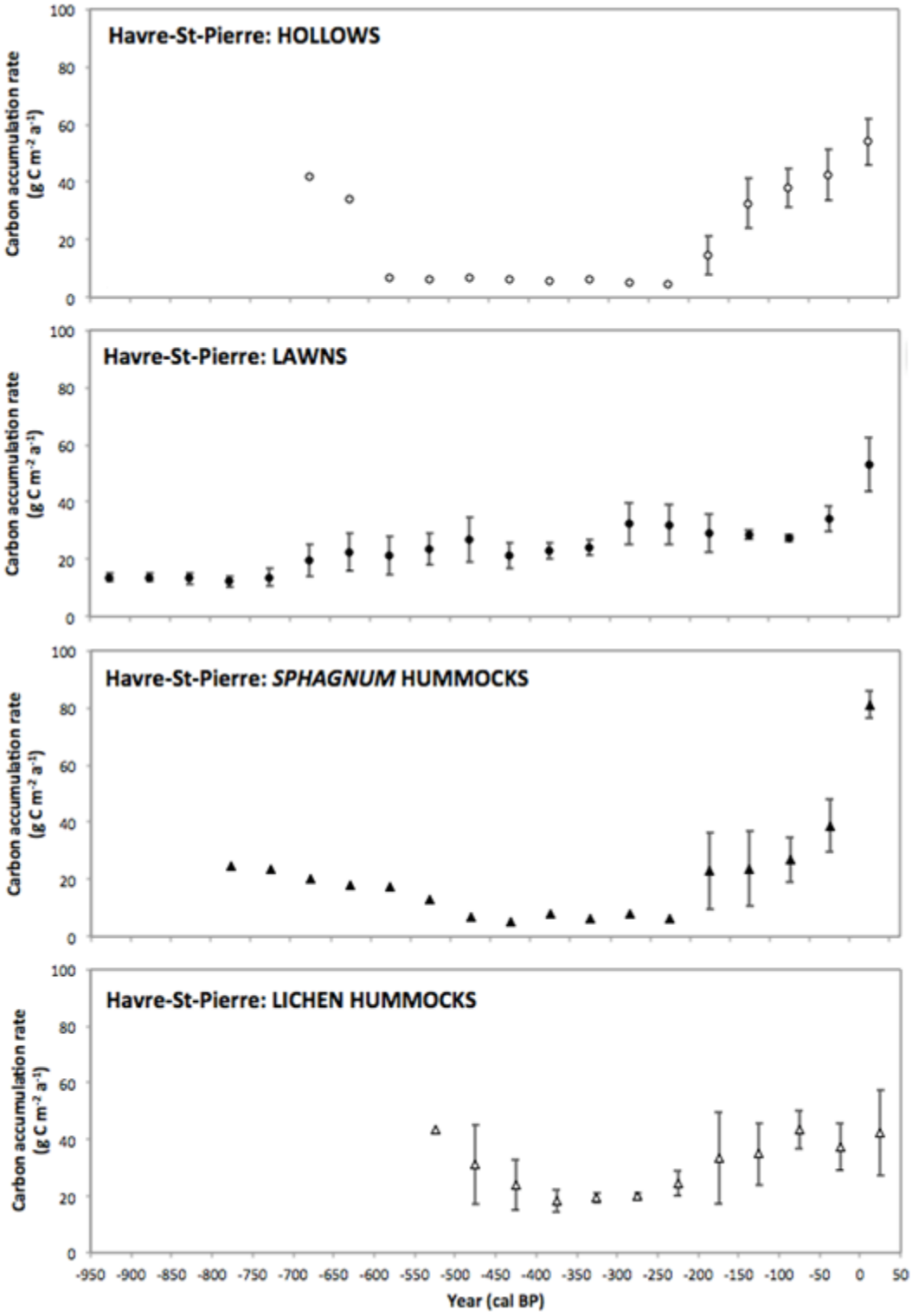

Figure 7.16 Microforms trends, 50-year bins (n = 3 for all points with error bars, representing the standard error). Exclude the two outlier points from the hollow = changes from n = 1 to n = 2.

For lawn cores, n = 3 replicates were included for the whole CAR record. Rates were relatively high and with small variability compared to other microforms. Decreasing CAR are associated with the Spörer, Maunder and Dalton LIA Minima. Hollows had higher CAR than lawns and *Sphagnum* hummocks, decreasing from 650-700 cal. BP period (Wolf Minimum) to the 550-600 cal. BP period (n = 2 cores) before levelling out to low and steady CAR until 150-200 cal. BP, then increasing rapidly. The two hummock types also have broadly similar CAR trends over time, until the 100-150 cal. BP period. CAR for present-day lichen hummocks was higher than for *Sphagnum* hummocks during that period. CAR decreased until 450-500 cal. BP for *Sphagnum* hummocks, and 350-400 cal. BP for lichen hummocks (Spörer Minumim) and remained more or less steady until the 200-250 cal. BP period, coinciding with the end of the Maunder Minimum, after which CAR increased for both microforms. A drop in CAR was measured around 100-150 cal. BP for *Sphagnum* hummocks (Dalton Minimum), and from the 50-100 cal. BP period to the present for lichen hummocks.

Statistical analyses using Repeated Measures ANOVA for the 50-year bin time series did not reveal any statistically significant interactions or differences between regions over time for the last 250 years where n = 3 for all microforms ($p > 0.23$), likely due to the large error bars.

7.3.4 Influence of environmental variables

7.3.4.1 *Selection of variables*

The results from correlation and simple regression analyses are summarised in Table 7.5 and 7.6, respectively. These results were used in order to select the variables for the multiple regression analyses. Several environmental variables are correlated with each other, for instance temperature data, PAR and GDD0. As they explain mainly the same component of the relationships, PAR was selected to represent the influence of climate changes (Charman *et al.,* 2013; Garneau *et al.,* 2014). Simple linear regression

results showed that PAR was also significantly related to RERCA and CAR for the last 300 and 500 years ($p < 0.001$ for all three); GDD0 was used to look at climate and CAR1000 ($R^2 = 0.92$; $p < 0.01$). Basal age (AGE) was included as a measure of autogenic influences. While peat depth showed significant relationships with C data for < 500 years, DEPTH and LORCA were significantly correlated with PAR and GDD0 ($R > 0.7$, $p < 0.001$). Snow cover (SNOW) was also included in the first instance, as the role of exposure has been discussed as a factor influencing local ecohydrology and carbon accumulation; it is not auto-correlated with any of the other variables included here. Neither of the microform-related variables (water table depth and coded microform) were significantly related to C data (linear regression: $R^2 < 0.07$; $p > 0.3$ in all cases) and so were not included in the analysis.

7.3.4.2 *Multiple regression results*

For RERCA, i.e. carbon accumulated for the last 150 years, PAR and snow cover were the significant explanatory variables, see equation 7.1 below ($R^2 = 0.61$, $F = 21.123$, $p < 0.001$). For the other measures of carbon accumulation for the last 300, 500 and 1000 years, the strongest relationships were with a single variable. CAR300 and CAR500 were found to be significantly influenced by PAR (CAR300: $R^2 = 0.41$, $F = 11.269$, $p = 0.004$; CAR500: $R^2 = 0.53$, $F = 13.526$, $p = 0.003$). See equations 7.2 and 7.3. PAR was not included in the CAR1000 model; however, results also indicated a climatic influence, with GDD0 as the significant variable (CAR1000: $R^2 = 0.99$, $F = 34.657$, $p = 0.01$). Simple regressions also showed a stronger relationship with GDD0.

$$RERCA = -204.14 + 0.10 \times \mathrm{SNOW} + 0.04 \times \mathrm{PAR} \quad (7.1)$$

$$CAR300 = -115.72 + 0.03 \times \mathrm{PAR} \quad (7.2)$$

$$CAR500 = -98.19 + 0.02 \times \mathrm{PAR} \quad (7.3)$$

$$CAR1000 = -29.70 + 0.03 \times \mathrm{GDD0} \quad (7.4)$$

	Site	MAT	MST	MWT	MAP	MSP	Snow	GDD0	PAR	WTD	MF	LORCA	B Age	Depth
Site	--													
MAT	**-0.951 (0.000)**	--												
MST	**-0.954 (0.000)**	**1.000 (0.000)**	--											
MWT	**0.960 (0.000)**	**-0.997 (0.000)**	**-0.998 (0.000)**	--										
MAP	0.628 (0.000)	-0.534 (0.002)	-0.550 (0.002)	0.601 (0.000)	--									
MSP	**0.872 (0.000)**	**0.835 (0.000)**	**-0.845 (0.000)**	**0.877 (0.000)**	**0.911 (0.000)**	--								
Snow	0.356 (0.054)	-0.503 (0.005)	-0.487 (0.006)	0.431 (0.017)	-0.462 (0.010)	-0.056 (0.769)	--							
GDD0	**-0.995 (0.000)**	**0.974 (0.000)**	**0.975 (0.000)**	**-0.976 (0.000)**	-0.574 (0.001)	**-0.848 (0.000)**	-0.435 (0.016)	--						
PAR	**-0.825 (0.000)**	**0.711 (0.000)**	**0.723 (0.000)**	**-0.764 (0.000)**	**-0.952 (0.000)**	**-0.966 (0.000)**	0.227 (0.227)	**0.777 (0.000)**	--					
WTD	0.443 (0.014)	-0.537 (0.002)	-0.358 (0.002)	-0.541 (0.002)	0.346 (0.061)	0.487 (0.006)	0.209 (0.267)	-0.466 (0.009)	-0.375 (0.041)	--				
MF	0.100 (0.601)	-0.079 (0.678)	-0.082 (0.666)	0.093 (0.321)	0.188 (0.321)	0.161 (0.329)	-0.109 (0.567)	-0.088 (0.644)	-0.173 (0.362)	0.510 (0.000)	--			
LORCA	**-0.874 (0.000)**	**0.862 (0.000)**	**0.869 (0.000)**	**-0.889 (0.000)**	**-0.768 (0.000)**	**-0.920 (0.000)**	-0.120 (0.528)	**0.865 (0.000)**	**0.860 (0.000)**	-0.554 (0.001)	-0.131 (0.000)	--		
B Age	0.699 (0.000)	-0.627 (0.000)	-0.626 (0.000)	-0.620 (0.000)	0.289 (0.121)	0.494 (0.006)	0.362 (0.050)	-0.695 (0.000)	-0.486 (0.006)	0.362 (0.050)	0.040 (0.833)	**-0.728 (0.000)**	--	
Depth	**-0.729 (0.000)**	**-0.733 (0.000)**	**-0.744 (0.000)**	**-0.777 (0.000)**	**-0.869 (0.000)**	**-0.923 (0.000)**	0.120 (0.529)	**0.711 (0.000)**	**0.869 (0.000)**	-0.440 (0.015)	-0.155 (0.413)	**0.779 (0.000)**	-0.203 (0.282)	--

Table 7.5 Correlations table including correlation coefficients (R values) for environmental variables; p-values are indicated in brackets, and significant correlations for R > 0.7 are highlighted in bold.

Table 7.6. Summary of results from simple regression analyses for carbon accumulation for the last 150 (RERCA, n = 3), 300 (CAR300, n = 3), 500 (CAR500, n = x) and 1000 (CAR1000, n = x) years; Pearson correlation coefficients (R) are listed, along with F statistics (F) p-values (p) and slope (B); significant relationships ($p < 0.05$) are in highlighted in grey (relationships for $p < 0.1$ are also highlighted in light grey).

Variable	RERCA				CAR300				CAR500				CAR1000			
	R^2	F	p	B	R^2	F	p	B	R^2	F	p	B	R^2	F	p	B
Site	0.183	0.6254	0.019	-9.695	0.155	2.938	0.106	-6.534	0.383	7.449	0.018	-7.070	0.931	40.167	0.008	-12.295
MAT[1]	0.074	2.241	0.146	11.246	0.058	0.982	0.336	7.149	0.284	4.766	0.050	11.730	0.926	37.459	0.009	18.083
MST[1]	0.082	2.485	0.126	4.529	0.065	1.105	0.309	2.910	0.296	5.068	0.044	4.618	0.932	41.037	0.008	6.981
MWT[1]	0.108	3.388	0.076	-22.418	0.089	1.571	0.228	-14.834	0.338	6.138	0.029	-21.395	0.945	51.644	0.006	-30.413
MAP[1]	0.543	33.333	0.000	-0.562	0.396	10.503	0.005	-0.306	0.407	8.246	0.014	-0.225	0.272	1.118	0.368	-0.164
MSP[1]	0.375	16.833	0.000	-1.723	0.324	7.680	0.014	-1.131	0.521	13.057	0.004	-1.058	0.689	6.636	0.082	-1.047
SNOW[1]	0.219	7.852	0.009	0.145	0.145	2.707	0.119	0.068	0.022	0.271	0.612	0.019	0.127	0.435	0.557	-0.042
GDD0[2]	0.133	4.284	0.048	0.027	0.108	1.947	0.182	0.018	0.335	6.057	0.030	0.021	0.920	34.657	0.010	0.026
PAR[2]	0.512	29.352	0.000	0.046	0.413	11.269	0.004	0.028	0.530	13.526	0.003	0.023	0.693	6.785	0.080	0.022
WTD	0.000	0.000	0.987	0.004	0.030	0.487	0.495	0.136	0.015	0.187	0.673	0.074	0.034	0.106	0.766	-0.262
MF[3]	0.032	0.932	0.343	-3.492	0.061	1.045	0.322	-2.506	0.027	0.336	0.573	-1.085	--	--	--	--
LORCA[4]	0.232	8.443	0.007	0.526	0.096	1.692	0.212	0.226	0.207	3.126	0.102	0.260	0.861	18.650	0.023	0.526
B_AGE[4]	0.025	0.731	0.400	-0.002	0.016	0.256	0.620	0.001	0.001	0.014	0.987	0.014	0.592	4.358	0.128	-0.003
DEPTH[4]	0.410	19.428	0.000	0.102	0.487	15.174	0.001	0.075	0.517	12.870	0.004	0.059	0.294	1.252	0.345	0.037

[1] Environment Canada (2015): Climate Normals 1971-2001
[2] Calculated as in Charman et al (2013) from the gridded CLIMATE2.2 data (Kaplan *et al.,* 2003)
[3] Coded 1-4 (wettest to driest) from this study
[4] Measured in Magnan and Garneau, 2014 for Baie Comeau and Havre-St-Pierre. Peat depth and basal age for Blanc Sablon were from the Dionne and Richard (2006) values; LORCA was estimated based on the accretion rate (0.32 mm/year)

7.4 Discussion

The relationship between changes in climate and carbon accumulation is important when understanding past changes for the Holocene and projecting into the future. While it was initially suggested that warming would drive increases in decomposition (Ise *et al.,* 2008; Dorrepaal *et al.,* 2009), recent studies suggest that it is accumulation on a millennial scale (Charman *et al.,* 2013), particularly PAR, with higher net primary productivity (NPP) compensating for decomposition. This study, using replicate cores, allowed testing of the hypotheses (Section 2.5) related to between-site variability of carbon accumulation rates and trends over time; Carbon accumulation is related to a latitudinal gradient due to climate, and cold periods during the LIA will have lower carbon accumulation rates. Replicate cores mean that autogenic signals related to site-specific variability are accounted for. In addition, the dating resolution means that changes within the last 200 years are evident (LIA trends).

7.4.1 Between-site variability carbon accumulation

General N-S trends in carbon accumulation patterns are found in the literature (e.g. Central Canada: Vardy *et al.,* 2000; Siberia: Beilman *et al.,* 2009; Global northern peatlands: Charman *et al.,* 2013; Eastern North America: Charman *et al.,* 2015), with carbon accumulation rates decreasing with latitude.

The regional spatial patterns along the North Shore of the St Lawrence suggest that the latitudinal hypothesis is not supported, with the addition of the Blanc Sablon region. In Magnan and Garneau (2014a), Baie Comeau LORCA (32 g C m^{-2} a^{-1}) was higher than Havre-St-Pierre LORCA (60.6 g C m^{-2} a^{-1}). In this study, apparent carbon accumulation was also highest at Baie Comeau and lowest at Havre-St-Pierre. However, Havre-St-Pierre was the ‘intermediate’ site, with Blanc Sablon peatlands showing higher accumulation rates further north. Other important factors, such as exposure, which affects snow cover, winter frost penetration (Magnan and Garneau,

2014a), and the thermal insulation of certain sites and microforms (van der Molen and Wijmstra, 1994). Coastal systems are vulnerable to changes in sea ice cover along the Gulf (Halfar *et al.,* 2013). The Minganie islands off the coast of Havre-St-Pierre in the Gulf of St. Lawrence have widely variable peat accumulation rates, depending on exposure. Ile Nue-de-Mingan was deforested by fires, and relict permafrost from the Little Ice Age was found to persist under the surface (Boivin, 2005). Conversely, a new 2016 study by Pratte *et al.,* at Ile du Havre (IDH) found peat accumulation rates for the catotelm nearing those of Baie Comeau (Baie: 0.4-1.0 mm a^{-1}; IDH: 0.8 mm a^{-1}); the acrotelm depth was 36 cm at the Baie site and 70 cm at IDH. Mean peat accumulation rate in this study at Blanc Sablon peatlands for the last millennium was 0.88 mm a^{-1}, almost three times higher than the rate measured since initiation for another nearby palsa peatland (0.3 mm a^{-1}: Dionne and Richard, 2006).

For the Holocene, LORCA was found to vary depending on initiation substrate and basal peat age, with average LORCA for Baie Comeau and Havre-St-Pierre peatlands calculated as 55.2 g C m^{-2} a^{-1} over marine deposits (younger peatlands) and 30.8 g C m^{-2} a^{-1} over deltaic deposits (older peatlands) (Magnan and Garneau, 2014b), with younger peatlands having had less time to undergo long-term catotelm decomposition (e.g. Clymo, 1984). No such relationships were established for the last millennium with basal age as a measure for long-term autogenic influence. However, results from the regression analyses (Table 7.6) showed significant relationships with peat depth for the last 500 years ($0.41 < R^2 < 0.52$, $p < 0.01$), but not with basal age. LORCA was significant a significant predictor of CAR for the last millennium (linear regression: $R^2 = 0.86$; $p = 0.023$). For the last millennium, water table depth was found to decrease at Baie Comeau and increase at Havre-St-Pierre, although the rates in the latter site were more variable (Magnan and Garneau, 2014b; Pratte *et al.,* 2016), however no significant relationships were found between carbon accumulation for any time period in this study and water table depth or microform type in this study (Table 7.6; multiple

regression results). Modelled microtopography studies showed that with increasing water table depth, peat accumulation also increases until a threshold is passed and the acrotelm becomes too thick for surface peat-forming plants to reach the water table (humpbacked relationship: Belyea and Clymo, 2001). Between sites, the water table depth varied for the different microforms, and the water table depth measured in the field was highest for Blanc Sablon, as there was still ice present at the time of coring.

Multiple regression analyses different timescales for the last millennium showed that carbon accumulation rates were significantly predicted by PAR (< 500 years) and GDD0 (1000 years), as in Charman *et al. (*2013) and Garneau *et al. (*2014). The recent accumulation rates (last 150 years) were also significantly explained by snow cover (SNOW), which reflects exposure. PAR and GDD0 were significantly correlated with other environmental variables, including a combination of most of the temperature and precipitation variables. Including MAP (mean annual precipitation) and GDD0 for all time periods instead of PAR meant that MAP explained most of the carbon accumulation relationships within the last 500 years. However, the simple linear regression analyses showed weak relationships with GDD0 ($R^2 < 0.3$), although these were significant ($p < 0.01$) for all time periods. Relationships with PAR were the strongest. The slopes for the relationships between environmental variables and carbon accumulation were often weak (< 1) due to the dominant role of exposure in regulating relative peat and carbon accumulation between sites. For instance, while temperature increases with latitude (highest at Baie Comeau, lowest at Blanc Sablon), Havre-St-Pierre had the lowest CAR at all scales; as the relationship is not linear for these three sites, regression analyses may not be appropriate for this dataset. Incorporating site-specific meteorological data for each coring location, as opposed to instrumental data from regional weather stations, or incorporating more sites with different exposure from additional climate grids along the Estuary and Gulf St Lawrence, would increase the spread of the data. Adding a variable representing

exposure, such as wind speed, would also be beneficial to interpreting the drivers of variability in CAR along the climatic transect.

7.4.2 Climatic context over time

The carbon accumulation patterns changed over time. In the recent period, and as seen in Chapter 6, CAR for Blanc Sablon were higher than for Baie Comeau, indicating a response of relative accumulation and decomposition processes to microtopography changes and ecohydrological feedbacks, in particular *Sphagnum* expansion into collapse scars and inter-hummocks due to recent warming and permafrost degradation. In northeastern Québec, major climate deteriorations after 600 cal. BP were documented by permafrost development in the bogs of the Lower North Shore (Dionne and Richard, 2006), coinciding with a cooling of the sea-surface temperatures in the Gulf of St. Lawrence (Dharhi, 2010), increasing sea ice cover off Labrador (Halfar *et al.,* 2013) and an opening of the forest cover in the Labrador plateau (Payette, 2004). This chapter has sought to evaluate the effects of such recent climate changes on the C accumulation dynamics in the bogs of the North Shore region.

The chronologies show peat accumulation over time: 'kinks' in the age-depth models represent periods of low accumulation rates. For instance for HP3A, 2B, 3B and 3C, kinks likely relate to the presence of permafrost between *ca.* 50-600 cal. BP, covering the Little Ice Age (Payette, 2004). Interpretations of changes in carbon accumulation rates during the LIA relating to relative cooling and warming in previous studies have been limited by poor ^{14}C resolution (e.g. Lamarre *et al.,* 2012; Magnan and Garneau, 2014a; Garneau *et al.,* 2014; Gao and Couwenberg, 2015). Except for Havre-St-Pierre, dating records for all cores did not cover the entire millennium, and full replication (n = 3 cores) was only possible for all sites and cores for the last 300 years. As seen in Chapter 6, the last 150 years is dominated overall by autogenic influences, where acrotelm peat has not yet undergone full decomposition processes. This is reflected in

the use of 'apparent' calculations of carbon accumulation rates (e.g. Yu, 2011; Frolking *et al.,* 2014). Lawn cores at all three sites, decreasing and increasing trends in the 100-year means for carbon accumulation rates were likely driven by the onset and end of cold periods within the LIA; accumulation slowdowns during the Spörer, Maunder and Dalton Minima associated with lower temperatures were recorded. Havre-St-Pierre and Blanc Sablon lawn cores saw the most variability in carbon accumulation rates coinciding with these minima and permafrost was likely established at both sites during this time and persisted until the last 50 years.

7.4.3 Drivers of multi-centennial within-site variability in CAR

A more in-depth look at longer term carbon accumulation rates for Havre-St-Pierre microforms expanded on the results from Chapter 6. As for lawn cores, C accumulation rate responses corresponding to LIA cold periods, including the Wolf, Spörer, Maunder and Dalton Minima, were detectable in all cores. However, the variability between lawn cores was smaller than for the other microforms, reflecting the natural variability in the hollow-lawn and lawn-hummock borders from the expansion and contraction of microforms. Changes in CAR for hollows and hummocks could indicate changes in ecohydrological feedbacks in response to changing microtopography and hydrological regime relating to the formation and degradation of permafrost; however, some of the variability may be explained by incomplete replication, where n = 3 cores was not possible for all microforms until the last 250 years. For instance, the change from low to high CAR around 200 cal. BP for hollows could represent infilling of mud-bottom microforms resulting from previous permafrost collapse or from the expansion and retreat of *Sphagnum* mats along hollow-lawn margins. For hummocks, the low CAR can be explained by the establishment and persistence of permafrost during the Spörer and Maunder periods in more exposed microforms (Chapter 6). For lichen hummocks, the main driver of the slowdown in CAR for the last 100 years is uncertain, as a combination of autogenic and allogenic drivers interact, including possible permafrost

or longer winter frost persistence under lichen (vs. under *Sphagnum*) surfaces restricting plant growth due to albedo and relative microform height and exposure (e.g. van der Molen and Wijmstra, 1994).

Plant macrofossil and bog surface wetness reconstructions would be invaluable to include as a complement to the carbon accumulation data, as the persistence of microforms and their responses to ecohydrological change could further inform adaptive bog development models (e.g. Morris *et al.,* 2011; Belyea and Baird, 2006).

7.5 Conclusions

This chapter considered drivers of changes in carbon accumulation on a regional scale, between sites. Three main hypotheses were tested. In the first instance, carbon accumulation rates did not vary according to a latitudinal climatic and permafrost gradient. For the last millennium overall, they were highest at Baie Comeau (no history of permafrost), and lowest at Havre-St-Pierre (history of permafrost), indicating the importance of exposure in regulating carbon accumulation rates; however, this trend was variable over time. For the last 500-1000 years, Blanc Sablon had the lowest CAR, and from 500 years until the present, Havre-St-Pierre had the lowest CAR. Blanc Sablon had the highest CAR for the last 150 years, indicating a response to conditions favouring high carbon accumulation rates including higher temperatures and the expansion of rapidly accumulating *Sphagnum* mats into degraded permafrost formations.

Age-depth models using a combination of lead-210 and radiocarbon dates allowed for decal-scale high resolution reconstructions of carbon accumulation rates over time. Finally, using these reconstructions, signals relating to short-term climate variability were detected, with carbon accumulation rates reflecting changes in temperature and permafrost formation/degradation relating to the Little Ice Age periods of solar minima,

and to more recent cooling in boreal Quebec in the late-1900s (Figure 3.7). It is likely that there was permafrost at Havre-St-Pierre during the Little Ice Age, and may be an analogue for future peatland accumulation patterns along the North Shore of the Gulf of St Lawrence, as the southern limit of permafrost moves northward with climate change.

8 Discussion

The aim of this thesis was to study recent changes in spatial and temporal patterns in carbon accumulation in peatlands from three ecoclimatic regions with differing permafrost histories along the North Shore of the St Lawrence. Using replicate cores for each region, research questions related to the role of allogenic vs. autogenic changes in a range of microforms were considered. Four main objectives were outlined and addressed throughout the thesis. First, methodological practices were addressed to evaluate the validity of ^{210}Pb dating in this study (Chapter 5); the use of geochemical inventories from replicate cores also statistically examined of often-raised questions ^{210}Pb depositional and mobility patterns (Chapters 5 and 6). Second, ^{210}Pb dating records from replicate cores were used to compare within-site spatial variability in carbon accumulation for the last 150 years along a microtopography gradient (Chapter 6). Third, changes in between-site carbon accumulation rates were considered on a multi-centennial scale along a climatic gradient, as well as within one site (Havre-St-Pierre) in order to assess the long-term relative roles of climatic and autogenic controls (Chapter 7). Finally, temporal changes in carbon accumulation and overall peatland sensitivity to autogenic vs. allogenic drivers were assessed during transitions to and from the LIA (Chapters 7 and 8).

This chapter will discuss the overall results of the thesis in three parts. Section 8.1 will summarise and discuss the controls on peatland carbon accumulation in the context of continuing climate change and permafrost degradation. Section 8.2 will expand on the methodological considerations related to this thesis, including the use of ^{210}Pb to date recent peat, and limitations related to the statistical approach and methods for calculating carbon sequestration. Section 8.3 will outlines some avenues for further research. The hypotheses generated from the Literature Review (Section 2.5) will be addressed throughout sections 8.1 and 8.2.

8.1 Controls on carbon accumulation

Replication of records allowed for large-scale allogenic (climatic) controls on carbon accumulation to be distinguished from local autogenic (microtopographical) controls. This section summarises the main findings from the results chapters, and addresses hypotheses on between- and within-site patterns and trends of carbon accumulation on decadal and multi-centennial scales (Section 2.5); these are re-stated where appropriate in this section.

8.1.1 Autogenic controls on carbon accumulation

The unique level of replicated carbon accumulation records used in this thesis addressed hypotheses related to within site variability of carbon accumulation rates along a microtopography/hydrology gradient. As peatlands are complex adaptive systems, dynamic peatland accumulation models should be informed by studies considering ecohydrological feedback variability (Belyea and Baird, 2006). Peat accumulation along microform gradients has been modelled to show a humpbacked relationship with acrotelm thickness, whereby as intermediate (non-waterlogged) microforms have increasing peat (and carbon) accumulation rates with increasing water table depth, until the distance between vegetation at the peat surface and the water table becomes unfavourable to peat accumulating plants such as *Sphagnum* mosses (Belyea and Clymo, 2001). In order to test this relationship statistically, this thesis addressed the hypothesis that within sites, recent CAR would be variable along a microtopography gradient and that *Sphagnum* hummocks would have the highest CAR and 'extreme' microforms such as dry lichen hummocks and wet hollows the lowest.

Results from Chapter 6 for the last 150 years showed that this modelled relationship is simplistic. At the drier end of the hydrology gradient, *Sphagnum* hummocks had the highest accumulation rates, and lichen hummocks had the lowest rates overall.

However, for the intermediate microforms, *Sphagnum* hummocks, hollows and lawns did not have significantly different carbon accumulation rates. This is in contrast to RERCA comparisons for Mer Bleue, Canada, where the differences in microforms were statistically significant (Turunen *et al.,* 2004). The wider range of hollow-type microforms, from cores collected near pools to *Sphagnum* 'wedges' in permafrost collapse scars, included in this thesis increased the variability between replicate cores. Divergences from the theorised humpbacked relationship, and within-site variability, were greatest for Blanc Sablon peatlands where recent changes in microtopography and local ecohydrology have been driven by permafrost degradation.

While using RERCA and CAR for the acrotelm does not account for decomposition processes and is an overestimate of carbon sequestration, comparing carbon accumulation between microforms at this level can provide insights into relative accumulation processes and ecohydrological drivers. For the most recent ages (0-50-year bins), autogenic and ecohydrological differences between microforms within the sites are dominant, and the wide range of natural variability is evident in the large error bars. For the 100-150 year period, there was no significant difference between CAR for all microforms within all the sites, suggesting that differing decomposition processes dominate for different microforms; for instance, higher levels of aerobic decomposition occur in well-aerated *Sphagnum* hummocks to compensate for the high productivity rates (e.g. Belyea and Malmer, 2004). While single-core analyses may not always lead to representative interpretations, especially in peatlands with 'hot' or 'cold' spots (Morris *et al.,* 2011) or in peatlands with recent changes in microtopography and ecohydrological balance due to disturbance, increasing replication accounts for some of this natural variability.

CAR results for all microforms on a multi-centennial timescale, as was done for Havre-St-Pierre cores in this thesis (Chapter 7), are useful when considering changes in

microtopography over time. All microforms did not have the same accumulation rates prior to the last 150 years. Multiple and simple regression analyses showed no significant relationships between (coded) microform and RERCA or longer term CAR for the last 300, 500 and 1000 years (Chapter 7). However, rather than using coded microforms from wet-dry within each site, perhaps a more accurate measure would be absolute values for acrotelm thickness or water table depth, which could be measured in the field. For instance, Blanc Sablon peatlands are much drier than the other two regions (ice was still present at the time of coring), and 'hollows' at Blanc Sablon may have thicker acrotelm peat than some lawns or hummocks at other sites. Lawn cores were the least spatially variable microforms for the three peatlands (n = 3 replicates with ages covering the last millennium) and did not exhibit major shifts in CAR over time, for instance low carbon accumulation rates due to persistent permafrost and ice lenses that may occur in hummocks (Turetsky, 2004; Turetsky *et al.,* 2002a). Indeed, lawn cores are usually selected for palaeoclimate analyses as they are less sensitive to inter-annual variability in water balance and hollow-lawn and lawn-hummock borders shift over time (Barber, 1981; van der Molen and Hoekstra, 1988). However, palaeoclimate analyses on alternate microform cores could also be informative, e.g. related to the persistence of permafrost, or timing of aggradation or degradation.

While changes in permafrost regimes are a direct consequence of allogenic (climate) drivers, within-site peatland microtopography and ecohydrology are also affected by autogenic change, and may lead to additional feedbacks from changes in water table depth and fire (e.g. Robinson and Moore, 2000; Turetsky *et al.,* 2007).

8.1.2 Climate controls on carbon accumulation

In this thesis, replicate cores were used to compare regional patterns and multi-centennial trends in carbon accumulation rates along a SW-NE transect along the North Shore of the Gulf of St Lawrence. Sites were located in three distinct

ecohydrological zones with differing permafrost regimes, along climate and oceanicity gradients. In Section 2.5, two main hypotheses were generated relating to allogenic drivers: (1) carbon accumulation rates would be highest for Baie Comeau in the south and lowest at Blanc Sablon where there are still palsas and localised permafrost; and (2) a regional LIA signal would be detectable, and carbon accumulation over time would be reduced during cold periods and by permafrost formation.

Carbon accumulation rates were not only lowest at Havre-St-Pierre during the last millennium but also had the lowest rate of increase for the last 150 years. At Baie Comeau and Blanc Sablon, the last 150 years were characterised by higher rates of increase in CAR due to partial decomposition of material in the acrotelm and warming since the end of the LIA. The lowest temperatures for boreal Quebec were recorded around 1850AD, likely linked to a period of successive volcanic eruptions (Gennaretti *et al.,* 2014). Site exposure plays an important role in these areas in regulating peat accumulation as more exposed sites have less snow cover and deeper frost penetration in winter (Magnan and Garneau, 2014a). Within Havre-St-Pierre, the Morts bog (more sheltered) had higher CAR compared to the Plaine and Romaine bogs (open, at the top of a peat plateau). Relict LIA permafrost was recorded on an island off the coast of Havre-St-Pierre where fire has removed all the forest cover (Ile-Nue-de-Mingan: *cf.* Boivin, 2005). Conversely, a sheltered peatland surrounded by forest on a neighbouring island (Ile du Havre) was found to have peat accumulation rates comparable to those recorded in the Baie Comeau area (Pratte *et al.,* 2016).

In addition, it was hypothesised from field observations and in Magnan and Garneau (2014b) that permafrost was present at Havre-St-Pierre during the LIA and that carbon accumulation changes for the last few centuries was driven by changing permafrost regimes. In particular, the stark change from dark ligneous peat to ‘fresh’ *Sphagnum* peat in the *Sphagnum* hummock cores was hypothesised to have been driven by

warming climate since the end of the LIA. This change was dated at *ca*. 1960s in all three cores, suggesting that *Sphagnum* re-accumulation was likely driven by a regional allogenic event such as the end of a cold period recorded for *ca.* 1940-1960AD in Boreal Eastern Canada. Due to the role of exposure on peat accumulation at Havre-St-Pierre compared to the sheltered Blanc Sablon sites discussed previously, it is possible that LIA permafrost persisted locally into the mid-late 1990s (Payette, 2004).

Blanc Sablon peatlands were located further from the coast and in valleys and therefore are less exposed than Havre-St-Pierre peatlands. CAR for the last 50 years at Blanc Sablon were the highest of all the three sites. In this region, large-scale ecohydrological changes driven by permafrost degradation favoured the small-scale rapid expansion of *Sphagnum* mats into collapse scars or 'internal lawns' (Vitt *et al.,* 1994; Turetsky *et al.,* 2002a,b; Beilman and Robinson, 2003), and into wetter inter-hummock spaces (Foster, 1984).

Climate for the North Shore of the St Lawrence has been warming for the past 150 years, and warming at a faster rate at Blanc Sablon than in the other two regions (Hutchinson *et al.,* 2009; Figure 3.7 in Section 3.2.2). Multiple and simple regression analyses (Chapter 7) showed that CAR is affected by different drivers at different timescales. For all sites and microforms, RERCA (150 years) was primarily explained by a combination of PAR and snow cover/exposure, while 300-, 500- and 1000-year CAR were explained by PAR and GDD0. There was no significant relationship between carbon accumulation data, Holocene LORCA and basal age/substrate. Similarly to findings for the last millennium from Charman *et al. (*2013), Garneau *et al. (*2014) and Loisel *et al. (*2014), the relatively rapid accumulation at Blanc Sablon is likely due to an increase in accumulation rates rather than a reduction in decomposition.

8.2 Methodological considerations

8.2.1 Using ^{210}Pb for high resolution chronologies

This thesis has included ^{210}Pb profiles for replicate cores along microtopography gradients within three peatland regions. The method was reliably tested prior to analysis, and questions of mobility and deposition patterns were addressed (Hypothesis 1, Section 2.5). Such questions have often been raised in the literature throughout the last few decades (e.g. Urban *et al.,* 1990; MacKenzie *et al.,* 1997; Vile *et al.,* 1999; Ali *et al.,* 2008; Parry *et al.,* 2013), and this study is the first to statistically evaluate the spatial variability in ^{210}Pb inventories (*cf.* Chapter 6). Within sites, total inventories were significantly higher for the driest microforms (lichen hummocks) and there was a small trend in decreasing inventories with increasing water levels indicating some leaching in wetter microforms. Regionally, total inventories were highest at Blanc Sablon, which is not only more sheltered than the other two sites from the influence of the Gulf, but is also drier due to the presence of permafrost and composed of a greater proportion of lichen hummocks.

The Constant Rate of Supply (CRS) model (Appleby and Oldfield, 1978; Appleby, 2001, 2008) has some limitations, the most reported of which concerns percolation or downward movement of ^{210}Pb through the upper, less consolidated, surface peat. New models adapting the CRS model are being developed and tested for peat (e.g. the Initial Penetration, or IP-CRS: (Olid *et al.,* 2013, 2015). Cores with a thicker or more porous acrotelm would be more affected by potential 'flushing' through the upper layers. However, without independent dating markers covering the last few decades on the cores included in this project, it was not possible to evaluate both models.

Estimating the equilibrium depth, i.e. the depth at which all the excess or unsupported ^{210}Pb deposited from the atmosphere has decayed to undetectable levels, was a challenge in some cases and has been reported as a potentially large source of error

(Appleby, 2001), in particular for dates older than 1900AD as indicated by this study. Carbon accumulation rates for Blanc Sablon between 1850-1900AD are inflated likely due to younger modelled ^{210}Pb dates from poor resolution and incorrect estimation of the equilibrium depth based on exponential decay models. There is most often an insufficient amount of data points for samples deeper than the equilibrium depth to statistically fit an asymptote. When using this dating method, larger errors for deeper ages should be taken into consideration, and if possible, additional independent dates for this period should be included in the age-depth models (e.g. wiggle-matching AMS dates, pollen markers, SCPs). While the artificial radionuclides ^{137}Cs and ^{241}Am have been shown to be useful age markers (e.g. Parry *et al.,* 2013), they only help to constrain the model around the mid- to late 1900s and do not contribute to reducing dating uncertainty for older ages.

Yu (2012) highlighted the need to incorporate dating methods focusing on recent peat (^{210}Pb or post-bomb AMS ^{14}C dates) when considering changes in carbon accumulation for the last millennium. Previous studies from Northeastern Quebec did not consider carbon accumulation for the last *ca.* 200 years (e.g. van Bellen *et al.,* 2011a,b; Lamarre *et al.,* 2012; Magnan and Garneau, 2014a) as this period generally covered the acrotelm in which much of the peat is still undergoing decomposition. Garneau *et al. (*2014) hypothesised that the lack of LIA signals for Quebec peatland carbon accumulation was likely due to the poor dating resolution in recent peat layers. Similarly, a study from a permafrost/ice wedge polygon peatland in Eastern Siberia showed no significant difference between CAR for the last millennium in microforms ranging from wet depressions to high hummock ridges, and found that CAR increased during the LIA (Gao and Couwenberg, 2015). The probability distributions for the calibrated ages were large, and age-depth models included pollen density data from extra-regional pollen (e.g. *Artemisia*) to constrain and interpolate between ages, meaning that the recent period was also not directly dated. It is possible that an LIA

signal was not detected (e.g. of re-accumulation in the permafrost collapse site) due to the dating resolution. A 2009 study in Western Canada, using four ^{210}Pb- and ^{14}C-dated fen, bog and forest margin cores, measured ^{210}Pb dates as younger than ^{14}C dates (Bauer *et al.,* 2009). It is uncertain whether errors are the result of underestimating ^{210}Pb ages due to mobility in non-*Sphagnum* deposits, or overestimating ^{14}C dates due to possible sample contamination (as in Kilian *et al.,* 1995) or post-1950AD local calibration errors (Garnett and Stevenson, 2004; Reimer *et al.,* 2004)

Data from this thesis have been contributed to on-going work attempting to generate models and software packages (in the style of clam or BACON for R) to calculate ^{210}Pb dates using the CRS model and potentially to modify BACON to incorporate 'raw' ^{210}Pb data rather than calendar dates from the CRS modelling (M. Aquino Lopez, *pers. comm.*). The first DANTE (Dating the ANThropocene in Environmental Archives) workshop focussing on 'bridging the gap between ^{210}Pb and ^{14}C' and other dating markers (e.g. tephra, pollen) will take place in Toulouse, France in October 2016 and will address some of these age-depth modelling issues.

This study used a total of 30 cores, all of which were dated with ^{210}Pb and 18 allocated ^{14}C dates. This provided an opportunity to consider age-depth models used to calculate recent carbon accumulation rates with and without including ^{210}Pb and contribute to 'bridging the gaps' between the methods. Figure 8.1 presents BACON age-depth models for one core per region with and without ^{210}Pb dates. Without ^{210}Pb dates, the model effectively linearly interpolates between the youngest ^{14}C date and the surface. Figure 8.2 shows the age-depth models with and without ^{210}Pb dates for the two cores in the study that included post-bomb ^{14}C dates. Figure 8.3 shows the carbon accumulation rates calculated using both types of age-depth models for all lawn cores, and Figure 8.4 plots the millennial 100-year CAR from Chapter 7 along with 100-year CAR calculated without using ^{210}Pb dates.

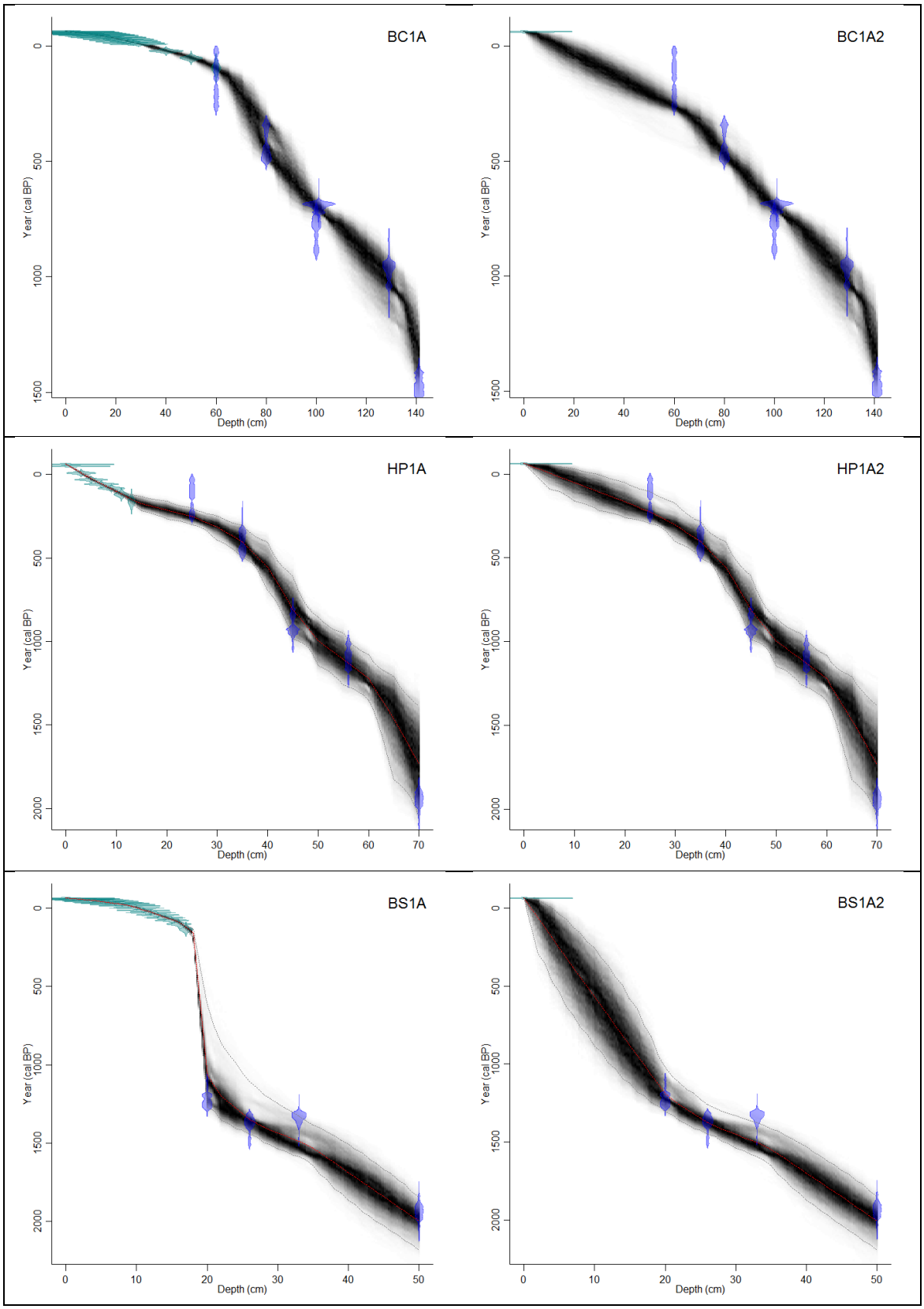

Figure 8.1. Examples of age-depth relationships used to calculate recent CAR, modelled with (left, from Chapter 7) and without (right) ^{210}Pb dates. From top to bottom: Baie Comeau (BC1A), Havre-St-Pierre (HP1A) and Blanc Sablon (BS1A). Calibrated ^{14}C dates in blue; darker greys indicate more likely ages; grey lines show 95% CI; red curve shows single 'best' model based on the weighted mean age (Blaauw and Christen, 2011).

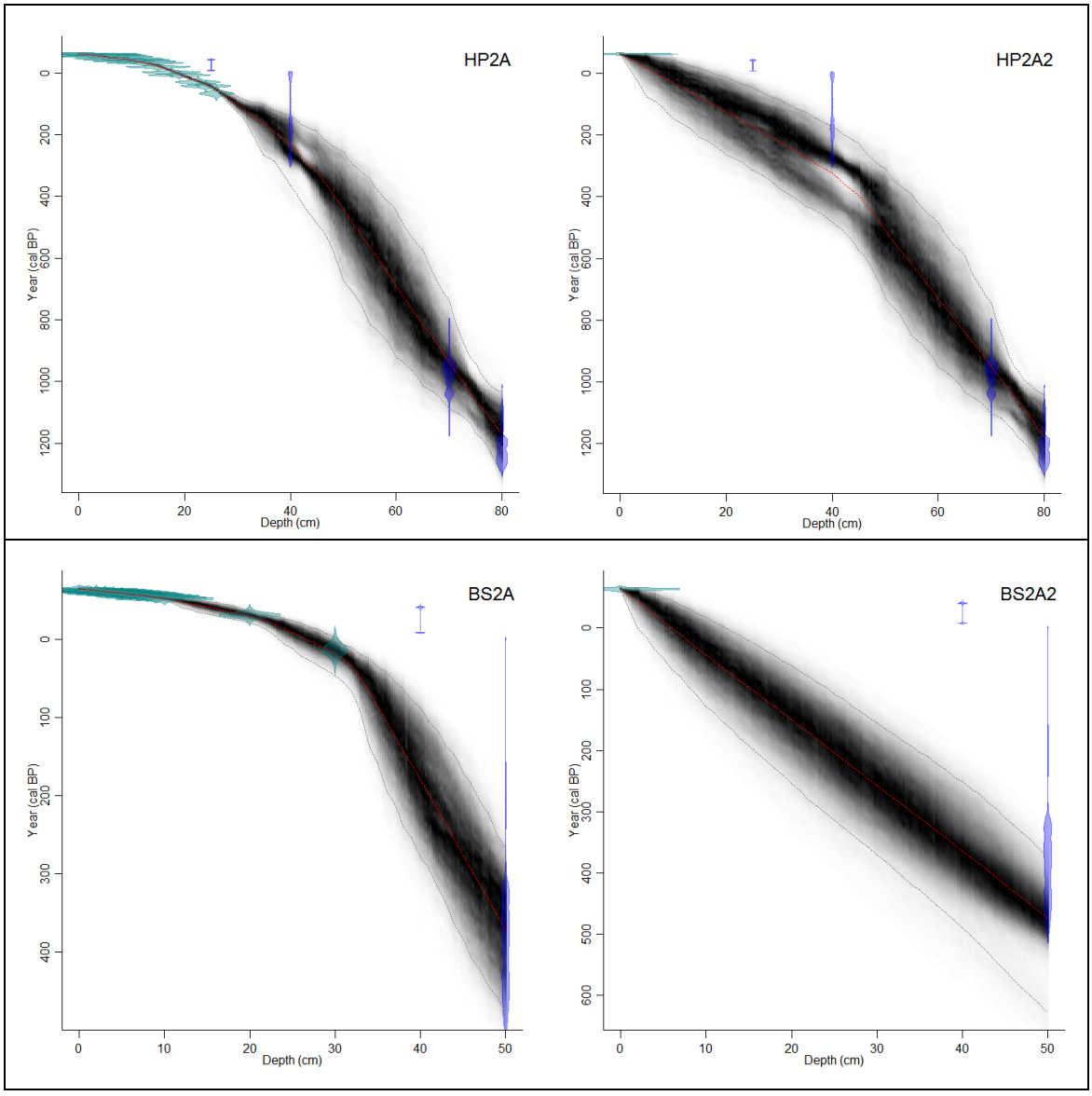

Figure 8.2. Age-depth models affecting carbon accumulation rate calculations for the last millennium for the 2 cores with a post-bomb ^{14}C date (Havre-St-Pierre, Morts: HP2A and Blanc Sablon, Lac à la Truite: BS2A). Left: Chapter 7 age-depth models; right: age-depth model using only ^{14}C dates. Calibrated ^{14}C dates in blue; darker greys indicate more likely ages; grey lines show 95% CI; red curve shows single 'best' model based on the weighted mean age (Blaauw and Christen, 2011).

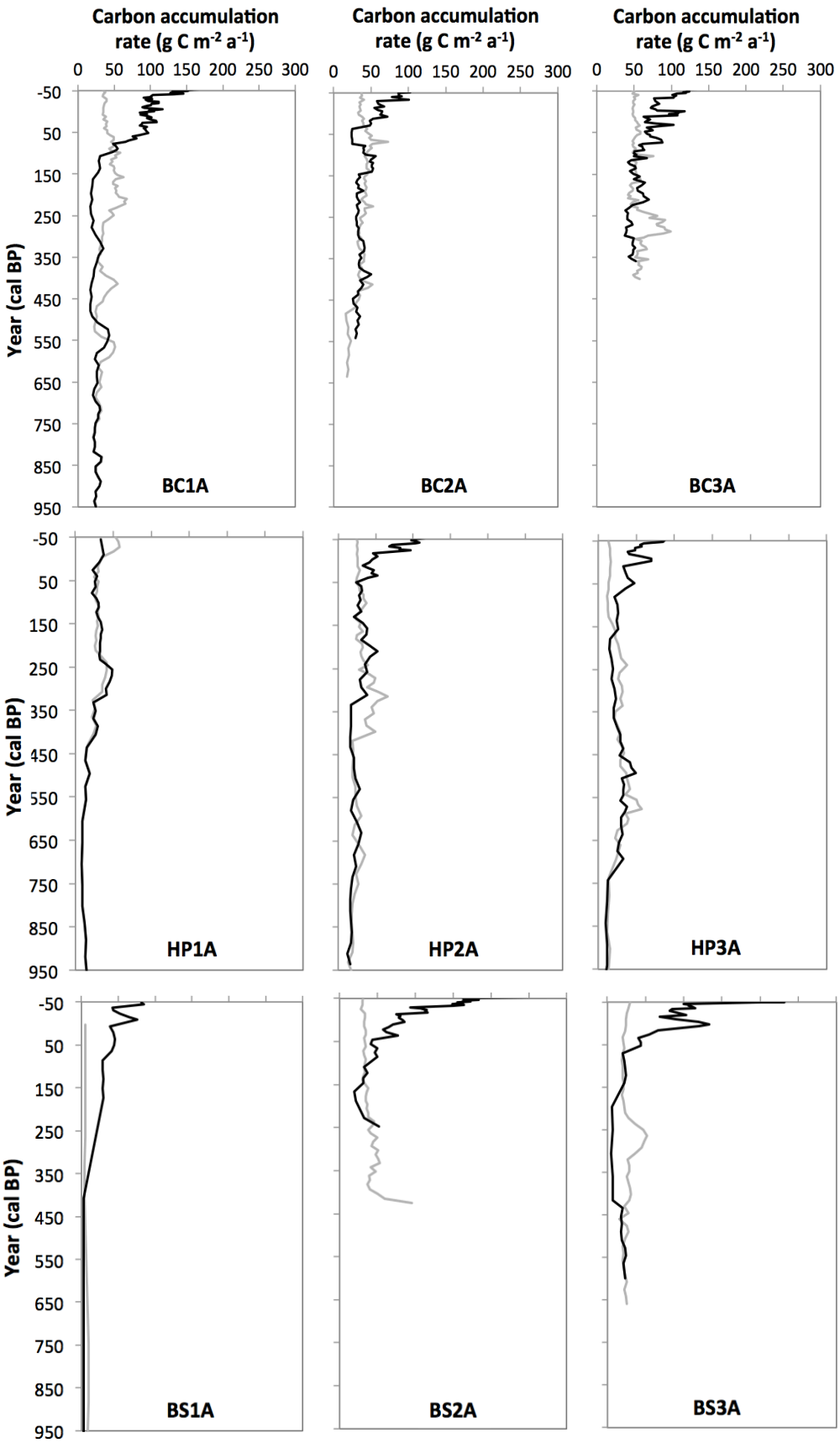

Figure 8.3. Carbon accumulation rates for lawn cores for all three sites calculated for each 1 cm depth interval (Chapter 7) from age-depth models using a combination of ^{14}C and ^{210}Pb dates (black line) and age-depth models using ^{14}C dates only (grey line) (see models in Figure 8.1)

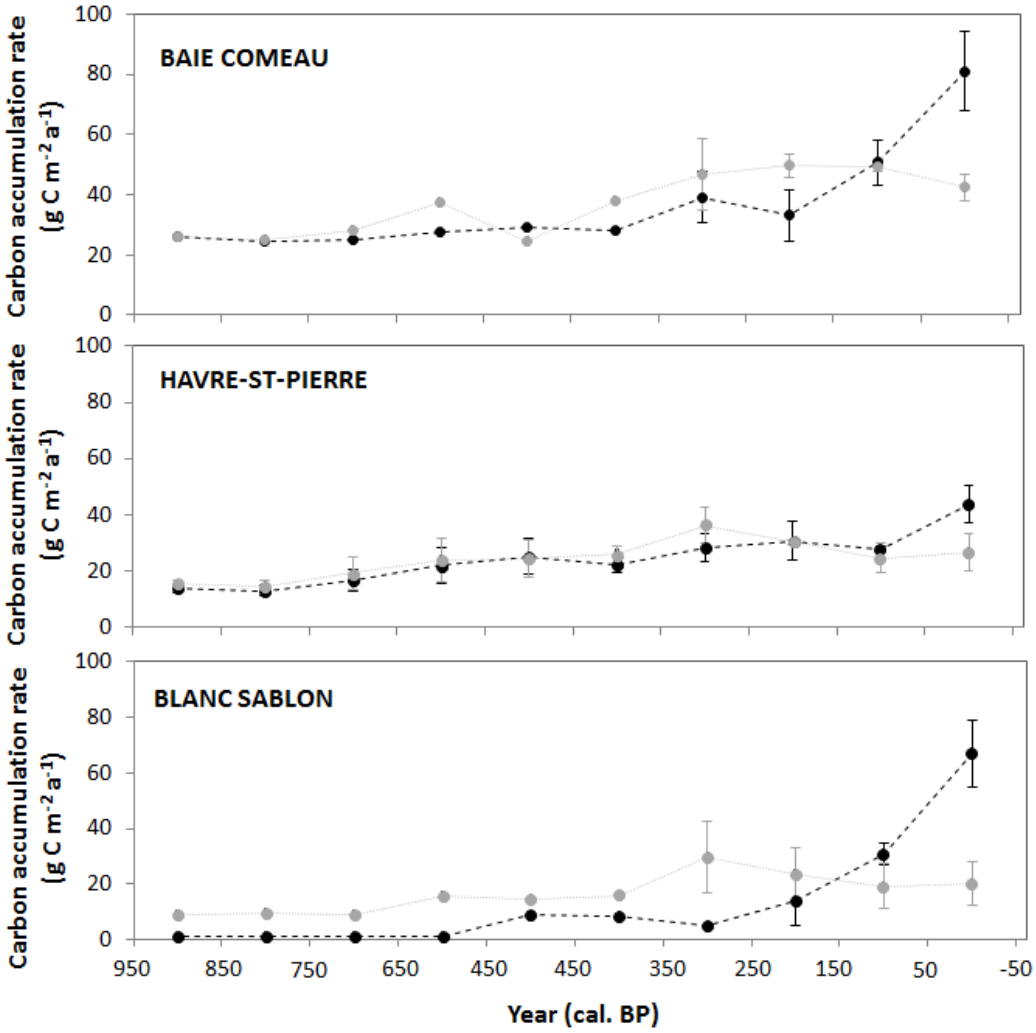

Figure 8.4. Comparison between carbon accumulation rates for Baie Comeau, Havre-St-Pierre and Blanc Sablon regions calculated from age-depth models incorporating ^{210}Pb dates (black, data from Chapter 7) and from age-depth models using only ^{14}C dates (light grey). CAR is in 100-year bins; dotted lines between points are to indicate trends and do not represent the measured values (see Figures 8.1 and 8.3 for models and continuous CAR data for each lawn core). Note that the number of replicates is not indicated; if error bars are present, n = 3.

In most cases, CAR was higher at the surface (last 100-200 years) when ages were modelled including ^{210}Pb dates. Profiles showed different trends up to *ca.* the last 800 years, which could affect the conclusions drawn. For instance, increases and decreases in CAR for the two age-depth model types at BC1A between *ca.* 550 cal a BP and the present are inverse (Figure 8.3), and the timings of low CAR do not correspond with the know colder LIA periods (e.g. the Spörer and Maunder minima) when using the ^{14}C-only model. The ^{14}C-only model also shows very little accumulation

at BS1A; however, field observation showed that there has been recent *Sphagnum* growth at the site. The comparison between regions is also affected by the choice of age-depth model (Figure 8.4). At all three sites, when using the ^{14}C-only model, CAR decreases for the last 400 years. Profiles diverge more for Baie Comeau and Blanc Sablon than for Havre-St-Pierre.

For millennial timescales, including ^{210}Pb dates may not be necessary; however it can have important effects on age-depth models and carbon accumulation rates for the last millennium on centennial and decadal scales, in particular for sites with high accumulation or affected by recent disturbance and microtopography changes such as permafrost thaw.

8.2.2 Calculating carbon accumulation

As well as dating limitations, the carbon accumulation rate calculations are debated. Apparent rates of accumulation (RERCA, LORCA and CAR) are directly measured by core observations, and as they do not account for future decomposition losses of acrotelm and upper catotelm peat, these metrics tend to overestimate accumulation and the C sequestration values, in particular in the recent layers (Turunen *et al.,* 2004; Yu, 2011).

The Net Carbon Balance (NCB) has been suggested as an alternative measure to account for carbon uptake as well as decomposition when modelled over time (Yu, 2011, 2012; Yu *et al.,* 2011). An advantage of the NCB approach is that values can be compared between the contemporary, recent, and older peat ages without including a caveat to consider incomplete decomposition nearer the surface. Under baseline conditions in modelled peatlands, CAR was found to behave as a running mean for NCB on a millennial scale (Frolking *et al.,* 2014), and LORCA should be the same as NCB (Yu, 2011). However, in early peat initiation stages and in the last 500 years, CAR was shown to be respectively lower and higher than NCB due to decomposition

processes (Frolking *et al.,* 2014). Under disturbance scenarios, CAR and NCB diverged. As CAR is calculated from core measurements, it cannot be negative; therefore CAR measured for time periods on either side of the disturbance event could be affected (Frolking *et al.,* 2014). For instance, the modelled case based on simulated disturbance, i.e. the draining and drying of peat in the last 150 years, had reduced CAR compared to baseline levels for 2000 years (Frolking *et al.,* 2014). Similar divergences between CAR and NCB could be expected for permafrost degradation and therefore may provide different insights for peatlands in regions such as Blanc Sablon.

In order to generate comparable results with other C accumulation studies from global averages, from Eastern Canada, and from the North Shore of the St. Lawrence (e.g. Magnan and Garneau, 2014a; Garneau *et al.,* 2014), apparent carbon accumulation rate calculations over various timescales (RERCA, LORCA and CAR) were used in this thesis. While using an NCB-based approach (reviewed in Section 2.2) could provide alternate perspectives on within-site variability of C dynamics, a number of uncertainties still remain, including accurately estimating decay constants which may vary down-core over time with peat type as well as spatially, and back-calculating the net carbon release from palaeo-observations (e.g. the Yu, 2011 decay model).

Some estimates for decay coefficients have been cited based on Net Primary Productivity (NPP) and the Clymo peat model (1984) (e.g. 0.05 a^{-1} in (Frolking *et al.,* 2001; Wieder, 2001). Similarly, Belyea and Malmer (2004) indicate variable decay coefficients, ranging from 0.18-1.1 10^{-4} a^{-1}, across three hummock vegetation stages (*Sphagnum magellanicum, Spagnum rubellum-Sphagnum fuscum*, and *Sphagnum fuscum*) in two Swedish peatlands. However, even a rough estimate of NCB could not be included in this thesis given the data available, both from a top-down approach using NPP (NCB = NPP – carbon losses from CO_2/CH_4/DOC: Frolking *et al.,* 2014) or from the bottom-up (as in Yu, 2011). For the former method, some CO_2 Net Ecosystem

Exchange (NEE-CO_2) data have been collected at one Baie Comeau and one Havre-St-Pierre peatland for two summers (Pelletier, 2014). In order to calculate NCB, data on emissions are also required but not available at this time, and a model such as the Holocene Peat Model (HPM: Frolking *et al.,* 2014) would need to be applied to the core sections. In the latter case, it was possible to calculate initial estimates for the Net Carbon Pool (NCP) and Net Carbon Uptake for each region and time period (150 and 1000 years); however, there is insufficient data to estimate the Net Carbon Release (NCR) without a decay model (as in Yu, 2011, where NCB = NCU – NCR), as it includes decomposition since peat initiation.

8.2.3 Replication and statistical approach

Palaeoclimate studies often use single core records to consider the impacts of climate or hydrology on peat and carbon accumulation, or to upscale to regional scales. Studies considering lateral expansion of peatlands have shown that such estimates are not always representative and could affect global peat carbon pool calculations (e.g. van Bellen *et al.,* 2011a). Similarly, a study using replicated tephra records demonstrated that tephra deposition and the resulting carbon accumulation rate calculations can vary by orders of magnitude within the same peatland (Watson *et al.,* 2015). Climatic drivers are often favoured over interpretations of changes in carbon accumulation rates based on local ecohydrology (Swindles *et al.,* 2012; Loisel *et al.,* 2014). This thesis has demonstrated that using a greater number of replicates accounts for natural variability and can more reliably associate changes in CAR with climate signals occurring in multiple cores. In the context of large global peat databases (e.g. Yu *et al.,* 2011; Charman *et al.,* 2013; Loisel *et al.,* 2014), these results are useful as they provide high-resolution, well-dated replicates across diverse ecoclimatic regions, peatland types and microforms for a region that has not previously well-represented (Roulet *et al.,* 2007; Yu, 2011, 2012)

8.3 Further research

This section suggests research directions for publications and future projects to improve the overall understanding of peatland carbon dynamics and sensitivity to climatic changes on decadal and centennial scales.

- **Plant macrofossils and bog surface wetness proxies**

An interesting outcome of this thesis was using the replication to evaluate deposition patterns and post-depositional mobility of ^{210}Pb between and within sites. Incorporating proxy records, such as plant macrofossil analyses and testate amoebae, are key to taking this research further, not only by providing climatic and environmental contexts to the carbon accumulation data, but also by studying the replicability of proxy records between and within sites. Plant macrofossil assemblages are representative of microform type and past ecohydrological changes, and testate amoeba assemblages are related to water table depth (e.g. Barber *et al.,* 2003*;* Hendon and Charman*,* 2004*;* Charman *et al.,* 2006). Peat humification has also been used as a proxy, with the consideration that it can be affected by vegetation composition and does not only reflect changes in climate-driven decomposition (e.g. Charman *et al.,* 2006; Yeloff and Mauquoy, 2008). More recently, C isotopes have been investigated as proxies for climate change and bog surface wetness in peatlands (e.g. Loisel *et al.,* 2009; Markel and Booth, 2010; Amesbury *et al.,* 2015). Changes in proxy records can occur independently from climate variations and may be misinterpreted in a single core (Swindles *et al.,* 2012). However, applying these methods to the replicate cores from this thesis would allow the distinction between allogenic and autogenic drivers of change, as variations in wetness across multiple cores at the same time is likely due to regional-scale climatic drivers as opposed to within-site local ecohydrology.

Adding these proxy measures would help to assess the persistence of microforms over time and the sensitivity of carbon accumulation to water table depth changes and

ecohydrological feedbacks, e.g. the timing of permafrost formation or its persistence in different microforms. Magnan and Garneau (2014a) found that the water table depth at Baie Comeau was relatively stable in lawn cores during the last millennium, while it was highly variable at Havre-St-Pierre. No such analyses have been performed at Blanc Sablon. While there has been recorded evidence of relict permafrost just off the coast of Havre-St-Pierre at Ile Nue de Mingan (Boivin, 2005) and likely also North of the coring sites (Michelle Garneau, *pers. comm.*), its presence has not been confirmed, and at present there is no proxy for past permafrost; therefore, adding water table depth and plant macrofossil data would help to interpret drivers of increased carbon accumulation in the *Sphagnum* hummocks post-1960s and whether this was due to persistent LIA permafrost or seasonal ice.

In addition, studying microform succession would provide valuable information to predict future carbon emissions relating to permafrost degradation in vulnerable peatlands along the southern limit of the Discontinuous Permafrost Zone (DPZ); methane emissions (C source) or subsequent *Sphagnum* re-accumulation (C sink) could be dominant depending on the hydrology and dominance of microforms and this balance has been an important recent focus (e.g. Schuur *et al.,* 2015; Swindles *et al.,* 2015; Treat *et al.,* 2016).

- **Additional coring and replication**

With a greater number of replicates, the statistical power is greater and significant differences are more likely to be detected. Further studies considering replicate cores should focus on within-site variability within each individual peatland as well as within regions. This additional level of replication would be beneficial for accounting for variability in peat and carbon accumulation rates due to lateral expansion of peatlands. As seasonal water table depth variability increases with distance from the peatland central dome, short-term ecohydrological feedbacks, such as a rapid *Sphagnum*

expansion after permafrost degradation (as in Lac à la Truite and Vallée peatlands, Blanc Sablon), increasing the number of microform replicates within individual peatlands would be beneficial to account for natural variability when considering upscaling carbon sequestration values to larger regions.

In this thesis, regions located in three ecoclimatic zones with differing permafrost histories were sampled. In order to consider the role of permafrost and the relationship between peatland carbon accumulation and environmental variables along the North Shore of the St Lawrence, a greater number of sites could be sampled along the transect. Indeed, there is a stark change in peatland topography and vegetation cover between Baie Comeau and Havre-St-Pierre. With a greater number of sites within distinct geographical grids, statistically stronger relationships could be explored. Additional transects could also be considered from the coast-inland (e.g. Pratte *et al.,* 2016) along continentality gradients to build up a realistic picture of peat carbon for Northeastern Canada.

At Baie Comeau and Blanc Sablon, the peat accumulation rates were higher than anticipated based on existing studies for the regions. Therefore, statistical analyses of trends over time were limited to the last 300 years for n = 3. Deeper cores would be required in order to consider trends and patterns in CAR during the last millennium using this statistical approach. This period would encompass climatic shifts from the warmer Medieval Climate Anomaly (MCA) to the cool Little Ice Age (LIA) and to the recent warming period.

- **Further dating**

As discussed in 8.2.1, the incorporation of ^{210}Pb activity into age-depth modelling packages such as BACON, rather than re-model CRS-modelled dates, is currently of interest. The relationship between ^{14}C post-bomb dates and ^{210}Pb should also be further investigated. To this effect, incorporating lead isotope analyses would be

essential in order to better constrain lead profiles and to investigate the integrity of profiles, i.e. to verify inventory deficits due to mobility (Farmer *et al.,* 2006). The sites studied in this thesis would be ideal for this as anthropogenic influence was minimal until the mid- to late 19th century. For instance, industrial development including the construction of an aluminium smelter, a maritime harbour construction, and a pulp and paper mill, and a titanium mine took place from 1940-1970AD in the vicinities of Baie Comeau and Havre-St-Pierre (Frenette, 1996; Pratte *et al.,* 2013).

- **Temporal context: Carbon cycling over time**

These high-resolution data on recent carbon accumulation rates provide the trends for the last few centuries, and have been analysed in this thesis alongside published Holocene carbon accumulation for Baie Comeau and Havre-St-Pierre (from Magnan and Garneau, 2014a). Similar Holocene analyses for Blanc Sablon would be of interest to contextualise the longer-term peatland development and expansion. To this effect, peat profiles were extracted during the 2013 field campaign from the centre of palsas at Red Bay and at Lac à la Truite peatlands using a CRREL (Cold Regions Research and Engineering Laboratory) mechanical ice corer and will be analysed as part of on-going research at UQAM.

Carbon flux data (including CO_2, CH_4, NEE) for peatlands and pools have been measured using eddy covariance towers and vegetation chamber measurements over three summers at Baie Comeau and Havre-St-Pierre (Pelletier, 2014). Combined with C/N analyses and the recent carbon accumulation rates measured in this thesis, these data could provide insight into the relative roles of accumulation and decomposition from the surface through the acrotelm-catotelm transition. Surface analyses including quadrats and vegetation surveys along the microtopography gradients and long-term measurements of seasonal water table depth at the sites would be useful additional data to consider for assessing the spatial patterns of carbon accumulation between

microforms and the role of ecohydrological feedbacks. For instance, Belyea and Baird's (2006) humpbacked relationship between peat accumulation and microform type, or thickness of the acrotelm (i.e. water table depth), could be evaluated with absolute values for acrotelm thickness across all sites rather than relative wet to dry microform codes as in this thesis.

- **Spatial context: Upscaling**

Upscaling carbon values from a single or few cores to a peatland- or regional-scale is often the goal of such studies. If the approximate distribution of microforms is known, the carbon accumulation estimates calculated for replicate cores would allow for more reliable estimates of regional values. For this thesis, QuickBird high-resolution satellite images were downloaded from the Digital Globe Foundation for each region in an attempt to classify and estimate the relative areas of microform groups in ArcGIS (e.g. lichen vs. Black spruce vs. ericaceous hummocks, lawns and pools) and to roughly calculate regional carbon accumulation based on microform distribution. The spatial distribution of pools is important to include in carbon balance studies as they represent important sources of CO_2 as well as CH_4 (Pelletier *et al.,* 2014). Such site maps could also be used to statistically compare within-site variability in surface vegetation assemblages (as in Graham *et al.,* 2015) and carbon accumulation rates. As changes in permafrost regimes have been found to impact the sink-source balance of peatlands, mapping the spatial heterogeneity and distribution of features such as collapse scars and palsas is important for regional upscaling, as these features respond differently over time to temperature increases and hydrology or vegetation changes (Euskirchen *et al.,* 2014).

The image resolution (max. 50 cm) did not provide sufficient differentiation between microform groups at the time of writing this thesis. However, further trials will be undertaken before publication of this work with a model developed by DigitalGlobe for

pan-sharpening raster data files in ArcGIS, specifically adapted for the QuickBird images (Holly East, *pers.comm.*). Aerial photographs could be more useful for such a project and the expanding role of UAVs (Unmanned Aerial Vehicles) in collecting such landscape information (e.g. vegetation cover) is extremely relevant in this context (Anderson and Gaston, 2013). This has been successful at Mer Bleue (Ottawa, Canada) in a study focusing on the distribution of *Eriophorum vaginatum* as a contributor to methane emissions, and scale up the locally measured seasonal CH_4 exchange to peatland-scale (Kalacska *et al.,* 2013). Such images combined with carbon data from replicate microform cores or C fluxes would provide realistic estimates for peatland carbon sequestration or fluxes depending on their permafrost status, exposure and microtopography and address the representativity of a single core in palaeoenvironmental studies.

- **Policy implications**

As 56% of Canada's soil carbon is stored in peatlands (Tarnocai, 2006), studies such as this one can be used to inform broader environmental policy, such as areas to focus on for recovery from tar sands, or conservation practices, e.g. protection from peat extraction or fossil fuel excavation (Rooney *et al.,* 2012), and environmental management (e.g. wildfire control). For instance, while large amounts of methane are emitted during initial stages of permafrost melt (Christensen *et al.,* 2004), the balance of C emissions and accumulation varies in peatlands depending on the permafrost status (e.g. Alaskan peatland fluxes: Euskirchen *et al.,* 2014). Therefore, the protection of areas which are likely to have rapid carbon accumulation rates, e.g. with internal lawns along the southern limit of the DPZ, or further south where sporadic permafrost and palsas can persist in peatlands (e.g. Turetsky, 2004) may be favourable from a carbon credit perspective in a global carbon market. In Western Canada, post-wildfire succession was found to increase the hummock abundance due to surface drying and

Sphagnum expansion into hollows (Benscoter *et al.,* 2015). Suppressing natural fire cycles, or increasing wildfire frequency in these areas has implications for the relative peatland C storage vs. emissions balance. While fire has not had much of an impact in Eastern Canada (van Bellen *et al.,* 2012), more research is needed on the large scale role of fire on regional peatland carbon balances due to climate change and its effect on microtopography.

As northern latitudes continue to warm more rapidly than the global average (Collins *et al.,* 2013), permafrost degradation is projected to continue *(*Schuur *et al.,* 2015; Treat *et al.,* 2016) and arctic and sub-arctic regions of Canada are projected to be severely affected by climate change (Kettles and Tarnocai, 1999; Tarnocai *et al.,* 2009). It is therefore important to establish the geographical limits of potentially vulnerable peatlands and to adapt management strategies depending on the region, permafrost status and peatland response to climate changes.

9 Conclusion

The aim of this thesis was to study recent changes in spatial and temporal patterns of in carbon accumulation. Using replicate cores between and within regions allowed us to consider the role of allogenic vs. autogenic changes in a range of microforms, as well as considering the effectiveness of dating techniques. Four main objectives were outlined and addressed throughout the thesis.

The use of lead-210 (^{210}Pb) was evaluated as a method for dating recent peat deposits in Chapter 5 (**Objective 1**). The choice of method depends on resources and sample material available, as results from a range of preparation treatments and spectrometry measurement techniques were not found to differ significantly. This is the first time that alpha- and gamma-spectrometry were evaluated for peat samples. Several limitations were highlighted concerning the current CRS method for modelling dates, including the estimation of the equilibrium depth; improving modelling techniques of ^{210}Pb could reduce this uncertainty. Using replicate cores, ^{210}Pb deposition patterns and post-depositional mobility were also evaluated for the first time on this scale in Chapter 6. The driest site and microform were found to have significantly larger ^{210}Pb inventories and supply rates; however, while a slight positive trend was detected between inventory and water table depth, this was not significant. The use of replicated records is therefore recommended to reduce dating uncertainty. ^{210}Pb dates should also be incorporated into radiocarbon age-depth models when considering recent changes on a multi-centennial scale in order to assess feedbacks from rapid shifts in climate or in microtopography.

Carbon accumulation rates along the North Shore of the Gulf of St Lawrence were affected in the short term (**Objective 2**) and in the long-term (**Objective 3**) by a combination of allogenic and autogenic drivers. Models of microform development were

assessed in Chapter 6 using replicate cores within sites along a microtopography gradient. Peat and carbon accumulation in response to acrotelm thickness is confounded by natural variability in microforms of intermediate wetness, and a larger range of microform types should be considered, such as 'internal lawns', where *Sphagnum* rapidly re-establishes in thermokarst ponds and collapse scars after permafrost degradation. However, the driest microforms had the lowest overall accumulation rates, as modelled by Belyea and Clymo (2001). At this scale, ecohydrological feedbacks dominate, in particular vegetation and water table feedbacks, as well as incomplete acrotelm decomposition. On a multi-centennial scale, within-site variability is also affected by climate change, including permafrost advance and retreat, and regional change driven by Little Ice Age temperature variations (Chapter 7).

On a regional scale (**Objective 4**), the role of exposure was highlighted as a key factor influencing differences in carbon accumulation between sites. While the southernmost site had the highest accumulation rates for the last millennium, it was the intermediate site, the most exposed, which had the lowest accumulation rates. Exposure was also important on a microform scale. Responses to Little Ice Age temperature variations driven by solar and volcanic forcing and to mid- late 1900s temperature changes were recorded in the carbon accumulation records. These were found to be mainly influenced by temperature-driven variables, including photosynthetically active radiation and growing degree days (Chapter 7). Future research directions should help to understand peatland sensitivity in the short term and in the long term and future responses to climatic changes. The North Shore region is projected to continue warming, which will have influence on water table depth, permafrost status, and carbon sequestration.

References

Aalto, R. and Nittrouer, C. A. (2012). ^{210}Pb geochronology of flood events in large tropical river systems. *Philosophical Transactions of the Royal Society A: Mathematical, Physical and Engineering Sciences* 370: 2040–2074.

Ali, A. A., Ghaleb, B., Garneau, M., Asnong, H. and Loisel, J. (2008). Recent peat accumulation rates in minerotrophic peatlands of the Bay James region, Eastern Canada, inferred by ^{210}Pb and ^{137}Cs radiometric techniques. *Applied Radiation and Isotopes* 66: 1350–1358.

Alm, J., Talanov, A., Saarnio, S., Silvola, J., Ikkonen, E., Aaltonen, H., Nykänen, H. and Martikainen, P. J. (1997). Reconstruction of the carbon balance for microsites in a boreal oligotrophic pine fen. *Oecologia* 110: 423–431.

Alm, J., Schulman, L., Walden, J., Nykänen, H., Martikainen, P. J. and Silvola, J. (1999). Carbon balance of a boreal bog during a year with an exceptionally dry summer. *Ecology* 80: 161–174.

Amesbury, M. J., Mallon, G., Charman, D. J., Hughes, P. D. M., Booth, R. K., Daley, T. J. and Garneau, M. (2013). Statistical testing of a new testate amoeba-based transfer function for water-table depth reconstruction on ombrotrophic peatlands in north-eastern Canada and Maine, United States. *Journal of Quaternary Science* 28: 27–39.

Amesbury, M. J., Charman, D. J., Newnham, R. M., Loader, N. J., Goodrich, J. P., Royles, J., Campbell, D. R., Roland, T. P. and Gallego-Sala, A. (2015). Carbon stable isotopes as a palaeoclimate proxy in vascular plant-dominated species. *Geochimica et Cosmochimica Acta* 164: 161–174.

Anderson, K. and Gaston, K. J. (2013). Lightweight unmanned aerial vehicles will revolutionize spatial ecology. *Frontiers in Ecology and the Environment* 11: 138–146.

Appleby, P. G. (2001). Chronostratigraphic techniques in recent sediments. In W. M. Last and J. P. Smol (Eds.), *Tracking Environmental Change Using Lake Sediments Volume 1: Basin Analysis, Coring and Chronological Techniques* (pp. 171–203). Dordrecht: Klower Academic Publishers.

Appleby, P. G. (2008). Three decades of dating recent sediments by fallout radionuclides: A review. *The Holocene* 18: 83–93.

Appleby, P. G. and Oldfield, F. (1978). The calculation of lead-210 dates assuming a constant rate of supply of unsupported ^{210}Pb to the sediment. *Catena* 5: 1–8.

Arlen-Pouliot, Y. and Bhiry, N. (2005). Palaeoecology of a palsa and a filled thermokarts pond in a permafrost peatland, subarctic Québec, Canada. *The*

Holocene 15: 408–419.

Balshi, M. S., McGuire, A. D., Duffy, P., Flannigan, M., Kicklighter, D. W. and Melillo, J. (2009). Vulnerability of carbon storage in North American boreal forests to wildfires during the 21st century. *Global Change Biology* 15: 1491–1510.

Bao, K., Yu, X., Jia, L. and Wang, G. (2010). Recent carbon accumulation in Changbai Mountain peatlands, northeast China. *Mountain Research and Development* 30: 33–41.

Barber, K. (1981). *Peat Stratigraphy and Climatic Change: A Palaeoecological Test of the Theory of Cyclic Peat Bog Regeneration*. Rotterdam: Balkema.

Barber, K. E., Chambers, F. M. and Maddy, D. (2003). Holocene palaeoclimates from peat stratigraphy: macrofossil proxy climate records from three oceanic raised bogs in England and Ireland. *Quaternary Science Reviews* 22: 521–539.

Bard, E., Raisbeck, G., Yiou, F. and Jouzel, J. (2000). Solar irradiance during the last 1200 years based on cosmogenic nuclides. *Tellus B* 52: 985–992.

Bauer, I. E., Bhatti, J. S., Swanston, C., Wieder, R. K. and Preston, C. M. (2009). Organic matter accumulation and community change at the peatland-upland interface: Inferences from ^{14}C and ^{210}Pb dated profiles. *Ecosystems* 12: 636–653.

Beilman, D. W. and Robinson, S. D. (2003). Peatland permafrost thaw and landform type along a climatic gradient. In S. and A. Phillips (Ed.), *Permafrost* (pp. 61–65). Lisse: Swets & Zeitlinger.

Beilman, D. W., Vitt, D. H. and Halsey, L. A. (2001). Localized permafrost peatlands in western Canada: definition, distributions, and degradation. *Arctic, Antarctic, and Alpine Research* 33: 70–77.

Beilman, D, W., MacDonald, G. M., Smith, L. C. and Reimer, P. J. (2009). Carbon accumulation in peatlands of West Siberia over the last 2000 years. *Global Biogeochemical Cycles* 23: GB1012, doi:10.1029/2007GB003112

Belyea, L. R. (1996). Separating the effects of litter quality and microenvironment on decomposition. *Oikos* 77: 529–539.

Belyea, L. R. and Baird, A. J. (2006). Beyond “the limits to peat bog growth”: cross-scale feedback in peatland development. *Ecological Monographs* 76: 299–322.

Belyea, L. R. and Clymo, R. S. (2001). Feedback control of the rate of peat formation. *Proceedings of the Royal Society London B: Biological Sciences* 268: 1315–1321.

Belyea, L. R. and Malmer, N. (2004). Carbon sequestration in peatlands: patterns and mechanisms of response to climate change. *Global Change Biology* 10: 1043–1052.

Bennett, K. D. (1994). Confidence intervals for age estimates and deposition times in

late-Quaternary sediment sequences. *The Holocene* 4: 421–429.

Benscoter, B. W. and Vitt, D. H. (2008). Spatial patterns and temporal trajectories of the bog ground layer along a post-fire chronosequence. *Ecosystems* 11: 1054–1064.

Benscoter, B. W., Kelman, W. R. and Vitt, D. H. (2005). Linking microtopography with post-fire succession in bogs. *Journal of Vegetation Science* 16: 453–460.

Benscoter, B. W., Greenacre, D. and Turetsky, M. R. (2015). Wildfire as a key determinant of peatland microtopography. *Canadian Journal of Forest Research* 45: 1133–1137.

Bernatchez, P. and Dubois, J.-M. M. (2004). Bilan des connaissances de la dynamique de l'érosion des côtes du Québec maritime laurentien. *Géographie Physique et Quaternaire* 58: 45–71.

Blaauw, M. (2010). Methods and code for "classical" age-depth modelling of radiocarbon sequences. *Quaternary Geochronology* 5: 512–518.

Blaauw, M. and Christen, J. A. (2011). Flexible paleoclimate age-depth models using an autoregressive gamma process. *Bayesian Analysis* 6: 457–474.

Blaauw, M. and Heegaard, E. (2012). Estimation of age-depth relationships. In H.J.B. Birks, A.F. Lotter, S. Juggins and J. P. Smol (Eds.), *Tracking Environmental Change Using Lake Sediments Volume 5: Data Handling and Numerical Techniques* (pp. 379-414). Dordrecht, Heidelberg, New York, London: Springer.

Blaauw, M., Heuvelink, G. B. M., Mauquoy, D., van der Plicht, J. and van Geel, B. (2003). A numerical approach to ^{14}C wiggle-match dating of organic peat deposits: best fits and confidence intervals. *Quaternary Science Reviews* 22: 1485–1500.

Blaauw, M., Van Geel, B., Mauquoy, D. and van der Plicht, J. (2004a). Carbon-14 wiggle-match dating of peat deposits: advantages and limitations. *Journal of Quaternary Science* 19: 177–181.

Blaauw, M., van der Plicht, J. and van Geel, B. (2004b). Radiocarbon dating of bulk peat samples from raised bogs: non-existence of a previously reported 'reservoir effect'? *Quaternary Science Reviews* 23: 1537–1542.

Boivin, A. (2005). *Relations entre l'évolution des îlots de pergélisol côtiers et les conditions climatiques. Cas de l'île Nue de Mingan, nord du golfe du Saint-Laurent, Québec, Canada*. MSc Thesis, Université de Sherbrooke.

Bollhöffer, A. and Rosman, K. J. R. (2001). Isotopic source signatures for atmospheric lead: The Northern Hemisphere. *Geochimica et Cosmochimica Acta* 65: 1727–1740.

Bonk, A., Tylmann, W., Goslar, T., Wacnik, A. and Grosjean, M. (2015). Comparing varve counting and ^{14}C-AMS chronologies in the sediments of Lake Żabińskie,

Northeastern Poland: implications for accurate ^{14}C dating of lake sediments. *Geochronometria* 42: 159–171.

Braconnot, P., Harrison, S. P., Kageyama, M., Bartlein, P. J., Masson-Delmotte, V., Abe-Ouchi, A., Otto-Bliesner, B. and Zhao, Y. (2012). Evaluation of climate models using palaeoclimatic data. *Nature Climate Change* 2: 417–424.

Bragazza, L., Buttler, A., Robroek, B. J. M., Albrecht, R., Zaccone, C., Jassey, V. E. J. and Signarbieux, C. (2016). Persistent high temperature and low precipitation reduce peat carbon accumulation. *Global Change Biology* doi:10.111/gcb.13319.

Bronk Ramsey, C. (2009). Bayesian analysis of radiocarbon dates. *Radiocarbon* 51: 337–360.

Brugham, R. B. (1978).Pollen indicators of land-use change in southern Connecticut. *Quaternary Research* 9: 349–362.

Bubier, J. L., Moore, T. R., Bellisario, L., Comer, N. T. and Crill, P. M. (1995). Ecological controls on methane emissions from a northern peatland complex in the zone of discontinuous permafrost, Manitoba, Canada. *Global Biogeochemical Cycles* 9: 455–470.

Bunzl, K., Schmidt, W. and Sansoni, B. (1976). Kinetics of ion exchange in soil organic matter. IV. Adsorption and desorption of Pb^{2+}, Cu^{2+}, Cd^{2+}, Zn^{2+} and Ca^{2+} by peat. *Journal of Soil Science* 27: 32–41.

Cambray, R. S., Playford, K., Lewis, G. N. J. and Carpenter, R. C. (1989). *Radioactive fallout in air and rain: results to the end of 1987.* AERE-R 13226: Harwell.

Campbell, I. D. and Campbell, C. (2000). Late Holocene vegetation and fire history at the southern boreal forest margin in Alberta, Canada. *Palaeogeography, Palaeoclimatology, Palaeoecology* 164: 263–280.

Charman, D. (2002). *Peatlands and Environmental Change*. Chichester, England: John Wiley & Sons Ltd.

Charman, D. J., Blundell, A., Chiverrell, R. C., Hendon, D. and Langdon, P. G. (2006). Compilation of non-annually resolved Holocene proxy climate records: stacked Holocene peatland palaeo-water table reconstructions from northern Britain. *Quaternary Science Reviews* 25: 336–350.

Charman, D. J., Barber, K. E., Blaauw, M., Langdon, P. G., Mauquoy, D., Daley, T. J., Hughes, P. D. M., Karofeld, E. (2009). Climate drivers for peatland palaeoclimate records. *Quaternary Science Reviews* 28: 1811–1819.

Charman, D. J., Beilman, D. W., Blaauw, M., Booth, R. K., Brewer, S., Chambers, F. M., Christen, J. A., Gallego-Sala, A., Harrison, S. P., Hughes, P. D. M., Jackson, S. T., Korhola, A., Mauquoy, D., Mitchell, F. J. G., Prentice, I. C., van der Linden, M., De Vleeschouwer, F., Yu, Z. C., Alm, J., Bauer, I. E., Corish, Y. M. C.,

Garneau, M. Hohl, V., Karofeld, E., Le Roux, G., Loisel, J., Moschen, R., Nichols, J. E., Nieminen, T. M., MacDonald, G. M., Phadtare, N. R., Rausch, N., Sillassoo, Ü., Swindles, G. T., Tuittila, E.-S., Ukonmaanaho, L., Väliranta, M., van Bellen, S., van Geel, B., Vitt, D. H. and Zhao, Y. (2013). Climate-related changes in peatland carbon accumulation during the last millennium. *Biogeosciences* 10: 929–944.

Charman, D. J., Amesbury, M. J., Hinchcliffe, W., Hughes, P. D. M., Mallon, G., Blake, W. H., Daley, T. J., Gallego-Sala, A., Mauquoy, D. (2015). Drivers of Holocene peatland carbon accumulation across a climate gradient in northeastern North America. *Quaternary Science Reviews* 121: 110–119.

Christensen, T. R., Johansson, T., Åkerman, H. J., Mastepanov, M., Malmer, N., Friborg, T., Crill, P. and Svensson, B. H. (2004). Thawing sub-arctic permafrost: Effects on vegetation and methane emissions. *Geophysical Research Letters* 31: L04501, doi:10.1029/2003GL018680.

Church, T., Rigaud, S., Baskaran, M., Kumar, A., Friedrich, J., Masque, P., Puigcorbé, V., Kim, G., Radakovitch, O., Hong, G., Choi, H. and Stewart, G. (2012). Intercalibration studies of ^{210}Po and ^{210}Pb in dissolved and particulate seawater samples. *Limnology and Oceanography: Methods* 10: 776–789.

Ciais, P., Sabine, C., Bala, G., Bopp, L., Brovkin, V., Canadell, J., Chhabra, A., DeFries, R., Galloway, J., Heimann, M., Jones, C., Le Quéré, C., Myneni, R. B., Piao, S. and Thornton, P. (2013). Carbon and Other Biogeochemical Cycles. In T. Stocker, D. Qin, G.-K. Plattner, M. Tignor, S. K. Allen, J. Boschung, Nauels, A., Xia, Y., Bex, V. and P. M. Midgley (Eds.), *Climate Change 2013: The Physical Science Basis* (pp. 465–570). Cambridge, UK and New York, NY, USA: Cambridge University Press.

Cleary, J., Roulet, N. T. and Moore, T. R. (2005). Greenhouse gas emissions from Canadian peat extraction, 1990-2000: A life-cycle analysis. *Ambio* 34: 456–461.

Cliche-Trudeau, N., Garneau, M. and Pelletier, L. (2013). Methane fluxes from a patterned fen of the northeastern part of the La Grande river watershed, James Bay, Canada. *Biogeochemistry* 113: 409–422.

Cliche-Trudeau, N., Garneau, M. and Pelletier, L. (2014). Interannual variability in the CO_2 balance of a boreal patterned fen, James Bay, Canada. *Biogeochemistry* 118: 371–387.

Clymo, R. S. (1984). The limits to peat bog growth. *Philosophical Transactions of the Royal Society of London. Series B, Biological Sciences* 303: 605–654.

Clymo, R. S. (1992). Models of peat growth. *Suo* 43: 127–136.

Clymo, R. S., Oldfield, F., Appleby, P. G., Pearson, G. W., Ratnesar, P. and Richardson, N. (1990). The record of atmospheric deposition on a rainwater-dependent peatland. *Philosophical Transactions of the Royal Society B: Biological Sciences* 327: 331–338.

Clymo, R. S., Turunen, J. and Tolonen, K. (1998). Carbon accumulation in peatland. *Oikos* 81: 368–388.

Cole, K. L., Engstrom, D. R., Futyma, R. P. and Stottlemyer, R. (1990). Past atmospheric deposition of metald in Northern Indiana measured in a peaet core from Cowles Bog. *Environmental Science and Technology* 24: 543–549.

Collins, M., Knutti, R., Arblaster, J., Dufresne, J.-L., Fichefet, T., Friedlingstein, P., Gao, X., Gutowski, W. J., Johns, T., Krinner, G., Shongwe, M., Tebaldi, C., Weaver, A. J. and Wehner, M. (2013). Long-term climate change: projections, committments and irreversibility. In T. F. Stocker, D. Qin, G.-K. Plattner, M. Tignor, S. K. Allen, J. Boschung, Nauels, A., Xia, Y., Bex, V. and P. M. Midgley (Eds.), *Climate Change 2013: The Physical Science Basis. Contribution of Working Group I to the Fifth Assessment Report of the Intergovernmental Panel on Climate Change* (pp. 1030–1136). Cambridge, UK and New York, NY, USA: Cambridge University Press.

Couwenbert, J. and Joosten, H. (2005). Self-organization in raised bog patterning: the origin of microtope zonation and mesotope diversity. *Journal of Ecology* 93: 1238–1248.

Cox, P. and Jones, C. (2008). Climate change. Illuminating the modern dance of climate and CO_2. *Science* 321: 1642–1644.

Crill, P., Hargreaves, K. and Korhola, A. (2000). *The Role of Peat in Finnish Greenhouse Gas Balances*. Ministry of Trade and Industry, Helsinki.

Damman, W. H. (1978). Distribution and movement of elements in ombrotrophic peat bogs. *Oikos* 30: 480–495.

Davies, G. M., Gray, A., Rein, G. and Legg, C. (2013). Peat consumption and carbon loss due to smouldering wildfire in a temperate peatland. *Forest Ecology and Management* 308: 169–177.

Dawson, J. J. C., Billett, M. F. and Hope, D. (2004). Sources and sinks of aquatic carbon in a peatland stream continuum. *Biogeochemistry* 70: 71–92.

De Vleeschouwer, F., Sikorski, J. and Fagel, N. (2010). Development of lead-210 measurement in peat using polonium extraction. A procedural comparison. *Geochronometria* 36: 1–8.

de Groot, W. J., Flannigan, M. D. and Cantin, A. S. (2013). Climate change impacts on future boreal fire regimes. *Forest Ecology and Management* 294: 35–44.

Dean, W. E. J. (1974). Determination of carbonate and organic mater in calcareous sediments and sedimentary rocks by loss on ignition: comparison with other methods. *Journal of Sedimentary Petrology* 44: 242–248.

Denman, K. L., Brasseur, G., Chidthaisong, A., Ciais, P., Cox, P. M., Dickinson, R. E.,

Hauglustaine, D., Heinze, C., Holland, E., Jacob, D., Lohmann, U., Ramachandran, S., da Silva Dias, P. L., Wofsy, S. C. and Zhang, X. (2007). Couplings between changes in the climate system and biogeochemistry. In S. Solomon, D. Qin, M. Manning, Z. Chen, M. Marquis, K. B. Averyt, M. Tignor and H. L. Miller (Eds.), *Climate Change 2007: The Physical Science Basis. Contribution of Working Group I to the Fourth Assessment Report of the Intergovernmental Panel on Climate Change* (pp. 507–587). Cambridge, UK and New York, NY, USA: Cambridge University Press.

Dionne, J.-C. and Richard, P. J. H. (2006). Origine, âge et taux d'accrétion verticale de la tourbiè à palses de Blanc Sablon, basse Côte Nord, Golfe du Saint-Laurent, Québec. *Géographie Physique et Quaternaire* 60: 199–205.

Dorrepaal, E., Toet, S., van Logtestijn, R. S. P., Swart, E., van de Weg, M. J., Callaghan, T. V. and Aerts, R. (2009). Carbon respiration from subsurface peat accelerated by climate warming in the subarctic. *Nature* 460: 616–619.

Du, J., Du, J., Baskaran, M., Bi, Q., Huang, D. and Jiang, Y. (2015). Temporal variations of atmospheric depositional fluxes of ^{7}Be and ^{210}Pb over 8 years (2006-2013) at Shanghai, China, and synthesis of global fallout data. *Journal of Geophysical Research: Atmospheres* 120: 4323–4339.

Dugmore, A. J., Larsen, G., Newton, A. J. and Sugden, D. E. (1992). Geochemical stability of fine-grained silicic Holocene tephras in Iceland and Scotland. *Journal of Quaternary Science* 7: 173–183.

Dyke, A. S. (2004). An outline of North American deglaciation with emphasis on central and northern Canada. *Developments in Quaternary Science* 2: 373–424.

Dytham, C. (2010). *Choosing and Using Statistics: A Biologist's Guide* (3rd Editio). West Sussex, UK: Wiley-Blackwell.

Eakins, J. D. and Morrison, R. T. (1978). A new procedure for the determination of lead-210 in lake and marine sediments. *The International Journal of Applied Radiation and Isotopes* 29: 531–536.

Ebaid, Y. Y. and Khater, A. E. M. (2006). Determination of ^{210}Pb in environmental samples. *Journal of Radioanalytical and Nuclear Chemistry* 270: 609–619.

El-Daoushy, F., Olsson, K. and Garcia-Tenorio, R. (1991). Accuracies in Po-210 determination for lead-210 dating. *Hydrobiologia* 214: 43–52.

Environment Canada. (2015). 1981-2010, 1961-1990 and 1971-2000 Climate Normals and Averages. Retrieved February 24, 2015, from: http://climate.weather.gc.ca/climate_normals/

EPA. (2011). Radionuclides in drinking water, Module 4: detection techniques. United States Environmental Protection Agency. Retrieved August 25, 2013, from:

http://www.epa.gov/ogwdw000/radionuclides/training/module4/index.html

Eppinga, M. B., Rietkerk, M., Wassen, M. J. and De Ruiter, P. C. (2007). Linking habitat modification to catastrophic shifts and vegetation patterns in bogs. *Plant Ecology* 200: 53–68.

Eppinga, M. B., de Ruiter, P. C., Wassen, M. J. and Rietkerk, M. (2009). Nutrients and hydrology indicate the driving mechanisms of peatland surface patterning. *The American Naturalist* 173: 803–18.

Euskirchen, E. S., Edgar, C. W., Turetsky, M. R., Waldrop, M. P. and Harden, J. W. (2014). Differential response of carbon fluxes to climate in three peatland ecosystems that vary in the presence and stability of permafrost. *Journal of Geophysical Research: Biogeosciences* 119: 1576–1595.

Evans, H. E., Dikkon, P. J., Scholer, P. J. and Evans, R. D. (1986). The use of Pb/^{210}Pb ratios in lake sediments for estimating atmospheric fallout of stable lead in south-central Ontario, Canada. *Science of the Total Environment* 54: 77–93.

Farmer, J. G. Graham, M. C., Yafa, C., Cloy, J. M., Freeman, A. J. and MacKenzie, A. B. (2006). Use of ^{206}Pb/^{207}Pb ratios to investigate the surface integrity of peat corse to study the recent depositional history and geochemical behaviour of inorganic elements in peat bogs. *Global and Planetary Change* 53: 240–248.

Fillion, M.È., Bhiry, N. and Touzi, M. (2014). Differential development of two palsa fields in a peatland located near Whapmagoostui-Kuujuarapik, Northern Québec, Canada. *Arctic, Antarctic and Alpine Research* 46: 40–54.

Flannigan, M., Logan, K., Amiro, B., Skinner, W. and Stocks, B., (2005). Future area burned in Canada. *Climate Change* 71: 1–16.

Flannigan, M. D., Krawchuck, M. A., de Groot, W. J., Wotton, B. M. and Gowman, L. M. (2009). Implications of chancing climate for global wildfire. *International Journal of Wildland Fire* 18: 483–507.

Flynn, W. W. (1968). The determination of low levels of polonium-210 in environmental materials. *Analytica Chimica Acta* 43: 221–227.

Foster, D. R. (1984). The dynamics of *Sphagnum* in forest and peatland communities in Southeastern Labrador, Canada. *Arctic* 37: 133–140.

Foster, D. R. and Wright, H. E. J. (1990). Role of ecosystem development and climate change in bog formation in Central Sweden. *Ecology* 71: 450–463.

Frank, D. C., Esper, J., Raible, C. C., Büntgen, U., Trouet, V., Stocker, B. and Joos, F. (2010). Ensemble reconstruction constraints on the global carbon cycle sensitivity to climate. *Nature* 463: 527–30.

Frenette, P. (1996). Histoire de la Côte-Nord. *Les Régions du Québec.* Québec*:* Les Presses de l'Université Laval, 672 pp.

Friedlingstein, P., Cox, P. and Betts, R. (2006). Climate-carbon cycle feedback analysis: Results from the C4MIP model intercomparison. *Journal of Climate* 19: 3337–3353.

Frolking, S. and Roulet, N. T. (2007). Holocene radiative forcing impact of northern peatland carbon accumulation and methane emissions. *Global Change Biology* 13: 1079–1088.

Frolking, S., Roulet, N. T., Moore, T. R., Richard, P. J. H., Lacoie, M. and Muller, S. (2001). Modeling northern peatland decomposition and peat accumulation. *Ecosystems* 4: 479–498.

Frolking, S., Roulet, N. T., Tuittila, E., Bubier, J. L., Quillet, A., Talbot, J. and Richard, P. J. H. (2010). A new model of Holocene peatland net primary production, decomposition, water balance, and peat accumulation. *Earth System Dynamics* 1: 115–167.

Frolking, S., Talbot, J. and Subin, Z. M. (2014). Exploring the relationship between peatland net carbon balance and apparent accumulation rate at century to millennial time scales. *The Holocene* 24: 1167–1173.

Gallon, C., Tessier, A., Gobeil, C. and Beaudin, L. (2005). Sources and chronology of atmospheric lead deposition to a Canadian Shield lake: inference from Pb isotopes and PAH profiles. *Geochimica et Cosmochimica Acta* 69: 3199–3210.

Gao, Y. and Couwenberg, J. (2015). Carbon accumulation in a permafrost polygon peatland: steady long-term rates in spite of shifts between dry and wet conditions. *Global Change Biology* 21: 803–815.

Garneau, M., van Bellen, S., Magnan, G., Beaulieu-Audy, V., Lamarre, A. and Asnong, H. (2014). Holocene carbon dynamics of boreal and subarctic peatlands from Quebec, Canada. *The Holocene* 24: 1043–1053.

Garnett, M. H. and Stevenson, A. C. (2004). Testing the use of bomb radiocarbon to date the surface layers of blanket peat. *Radiocarbon* 46: 841–851.

Gatis, N., Luscombe, D. J., Grand-Clement, E., Hartley, I. P., Anderson, K., Smith, D. and Brazier, R. E. (2015). The effect of drainage ditches on vegetation diversity and CO_2 fluxes in a *Molina caerulea*-dominated peatland. *Ecohydrology* doi:10.1002/eco.1643.

Gavin, D. G., Hu, F. S., Lertzman, K. and Corbett, P. (2006). Weak climatic control of stand-scale fire history during the late Holocene. *Ecology* 87: 1722–1732.

Gehrels, M. J., Newnham, R. M., Lowe, D. J., Wynne, S., Hazell, Z. and Castledine, C. (2008). Towards rapid assay of cryptotephra in peat cores: review and evaluation of various methods. *Quaternary International* 178: 68–184.

Gennaretti, F., Arsenault, D. and Bégin, Y. (2014). Millennial disturbance-driven forest

stand dynamics in the Eastern Canadian taiga reconstructed from subfossil logs. *Journal of Ecology* 102: 1612–1622.

Glaser, P. H. and Janssen, J. A. (1986). Raised bogs in eastern North America: transitions in landformd and gross stratigraphy. *Canadian Journal of Botany* 64: 395–415.

Goldberg, E. D. (1963). Geochronology with ^{210}Pb. In *Radioactive Dating* (pp. 121–130). Vienna: International Atomic Energy Agency.

Gorham, E. (1991). Northern peatlands: role in the carbon cycle and probable responses to climatic warming. *Ecological Applications* 1: 182–195.

Gorham, E., Lehman, C., Dyke, A., Janssens, J. and Dyke, L. (2007). Temporal and spatial aspects of peatland initiation following deglaciation in North America. *Quaternary Science Reviews* 26: 300–311.

Graham, J. A., Hartsock, J. A., Vitt, D. H., Wieder, R. K. and Gibson, J. J. (2015). Linkages between spatio-temporal patterns of environmental factors and distribution of plant assemblages across a boreal peatland complex. *Boreas* doi:10.111/bor.12151.

Grand-Clement, E., Anderson, K., Smith, D. M., Luscombe, D., Gatis, N., Ross, M. and Brazier, R. E. (2013). Evaluating ecosystem goods and services after restoration of marginal Upland peatlands in south-west England. *Journal of Applied Ecology* 50: 324–334.

Graney, J. R., Halliday, A. N., Keeler, G. J., Nriagu, J. O., Robbins, J. A. and Norton, S. A. (1995). Isotopic record of lead pollution in lake sediments from the northeastern United States. *Geochimica et Cosmochimica Acta* 59: 1715–1728.

Grant, M. J., Hughes, P. D. M. and Barber, K. E. (2014). Climatic influence upon early to mid-Holocene fire regimes within temperate woodlands: a multi-proxy reconstruction from the New Forest, southern England. *Journal of Quaternary Science* 29: 175–188.

Greenhouse, S. W. and Geisser, S. (1959). On the methods in the analysis of profile data. *Psychometrika* 24: 95–112.

Gunnarsson, U., Granberg, G. and Nilsson, M. (2005). Growth, production and interspecific competition in *Sphagnum*: effects of temperature, nitrogen and sulphur treatments on a boreal mire. *New Phytologist* 163: 349–359.

Gurney, S. D. (2001). Aspects of the genesis, geomorphology and terminology of palsas: perennial cryogenic mounts. *Progress in Physical Geography* 25: 249–260.

Halfar, J., Adey, W. H., Kronz, A., Hertzinger, S., Edinger, E. and Fitzhugh, W. W. (2013). Annual sea-ice decline archived by multicentury annual-resolution record

from crustose coralline algal proxy. *Proceedings of the National Academy of Sciences of the United States of America* 110: 19737–19741.

Halsey, L. A., Vitt, D. H. and Zoltai, S. C. (1995). Disequilibrium response of permafrost in boreal continental western Canada to climate change. *Climatic Change* 30: 57–73.

Heiri, O., Lotter, A. F. and Lemcke, G. (2001). Loss on ignition as a method for estimating organic and carbonate content in sediments: reproducibility and comparability of results. *Journal of Paleolimnology* 25: 101–110.

Hellberg, E., Niklasson, M. and Granström, A. (2004). Influence of the landscape structure on patterns of forest fires in boreal forest landscapes in Sweden. *Canadian Journal of Forest Research* 34: 332–338.

Hendon, D. and Charman, D. J. (2004). High-resolution peatland water-table changes for the past 200 years: the influence of climate and implications for management. *The Holocene* 14: 125–134.

Holden, J., Evans, M. G., Burt, T. P. and Horton, M., (2006). Impact of land drainage on peatland hydrology. *Journal of Environmental Quality* 35: 1764–1778.

Hooijer, A., Page, S., Canadel, J. G., Silvius, M., Kwadijk, J. and Jauhiainen, J. (2010). Current and future CO_2 emissions from drained peatlands in Southeast Asia. *Biogeosciences* 7: 1505–1514.

Howie, S. A. and van Meerveld, H. J. (2012). Temporal variation in depth to water table and hydrochemistry. *Hydrology and Earth System Sciences Discussions* 9: 14065–14107.

Hutchinson, M. F., McKenney, D. W., Lawrence, K. M., Pedlar, J. H., Hopkinson, R. F., Milewska, E. and Papadopol, P. (2009). Development and testing of Canada-wide interpolated spatial models of daily minimum-maximum temperature and precipitation for 1961-2003. *American Meteorological Society* 48: 725–741.

IBM. (2012). IBM SPSS for Windows. Armonk, NY, United States: IBM Corp.

Indermühle, A., Stocker, T. F., Joos, F. and Fischer, H. (1999). Holocene carbon-cycle dynamics based on CO_2 trapped in ice at Taylor Dome, Antarctica. *Nature* 398: 121–126.

Ingram, H. A. P. (1978). Soil layers in mires: function and terminology. *Journal of Soil Science* 29: 224–227.

Innes, J. B. and Simmons, I. G. (2000). Mid-Holocene charcoal stratigraphy, fire history and palaeoecology at North Gill, North York Moors, UK. *Palaeogeography, Palaeoclimatology, Palaeoecology* 164: 155–164.

Ise, T., Dunn, A. L., Wofsy, S. C. and Moorcroft, P. R. (2008). High sensitivity of peat decomposition to climate change through water-table feedback. *Nature*

Geosciences 1: 763–766.

Ivanov, K. E. (1981). *Water movement in Mirelands*. Academic Press, London.

Jansen, E., Overpeck, J., Brigga, K. R., Duplessy, J.-C., Joos, F., Masson-Delmotte, V., Olago, D., Otto-Bliesner, B., Peltier, W. R., Rahmstorf, S., Ramesh, R., Raynaud, D., Rind, D., Solomina, O., Villalba, R. and Zhang, D. (2007). Palaeoclimate. In S. Solomon, D. Quin, M. Manning, Z. Chen, M. Marquis, K. B. Averyt, M. Tignor and H. L. Miller (Eds.), *Climate Change 2007: The Physical Science Basis. Contribution of Working Group I to the Fourth Assessment Report of the Intergovernmental Panel on Climate Change* (pp. 435–484). United Kingdom and New York, NY, USA: Cambridge University Press.

Jeglum, J. K., Rothwell, R. L., Berry, G. J. and Smith, G. K. M. (1991). *New volumetric sampler increases speed and accuracy of peat surveys*. Frontline Forestry Research Applications, Technical Note No. 9. Forestry Canada: Ontario Region.

Jia, G., Belli, M., Blasi, M., Marchetti, A., Rosamilla, S. and Sansone, U. (2001). Determination of 210Pb and 210Po in mineral and biological environmental samples. *Journal of Radioanalytical and Nuclear Chemistry* 247: 491–499.

Johnson, L. C. and Damman, W. H. (1991). Species-controlled *Sphagnum* decay on a South Swedish raised bog. *Oikos* 61: 234–241.

Jungclaus, J. H., Lorenz, S. J., Timmreck, C., Reick, C. H., Brovkin, V., Six, K., Segschneider, J., Giorgetta, M. A., Crowley, T. J., Pongratz, J., Krivova, N. A., Solanki, S. K., Klocke, D., Botzet, M., Esch, M., Gayler, V., Haak, H., Raddatz, T. J., Roeckner, E., Schnur, R., Widmann, H., Claussen, M., Stevens, B. and Marotzke, J. (2010). Climate and carbon-cycle variability over the last millennium. *Climate of the Past* 6: 723–737.

Kalacska, M., Arroyo-More, J. P., de Gea, J., Snirer, E., Herzog, C. and Moore, T. R. (2013). Videographic analysis of *Eriophorum vaginatum* spatial coverage in an ombrotrophic bog. *Remote Sensing* 5: 6501–6512.

Karofeld, E. (2004). Mud-bottom hollows: exceptional features in carbon accumulating bogs? *The Holocene* 14: 119–124.

Kasin, I., Blank, Y.-I., Storaunet, K. O., Rolstad, J. and Ohlson, M. (2013). The charcoal record in peat and mineral soil across a boreal landscape and possible linkages to climate change and recent fire history. *The Holocene* 23: 1052–1065.

Kaufman, D. S., Schneider, D. P., McKay, N. P., Ammann, C. M., Bradley, R. S., Briffa, K. R., Miller, G. D., Otto-Bleisner, B. L., Overpeck, J. T., Vinther, B. M., Arctic Lakes 2k Project Members. (2009). Recent warming reverses long-term arctic cooling. *Science* 325: 1236–1239.

Kelly, T. J., Lawson, I. T., Roucoux, K. H., Baker, T. R., Jones, T. D. and Sanderson, N. K. (*submitted*). The historica; development, stability, and climate sensitivity of

an Amazonian domed peatland. Submitted to *Palaeogeography, Palaeoclimatology, Palaeoecology* in March 2016.

Kershaw, A. (1997). A modification of the Troëls-Smith system of sediment description and portrayal. *Quaternary Australasia* 15: 63–68.

Kettles, I. M. and Tarnocai, C. (1999). Development of a model for estimating the sensitivity of Canadian peatlands to climate warning. *Géographie Physique et Quaternaire* 53: 323–338.

Kilian, M. R., van der Plicht, J. and van Geel, B. (1995). Dating raised bogs: new aspects of AMS ^{14}C wiggle matching, a reservoir effect and climate change. *Quaternary Science Reviews* 14: 959–966.

Kilian, M. R., van Geel, B. and van der Plicht, J. (2000). ^{14}C AMS wiggle matching of raised bog deposits and models of peat accumulation. *Quaternary Science Reviews* 19: 1011–1033.

Klacska, M., Arroyo-Mora, J. P., de Gea, J., Snirer, E., Herzog, C., Moore, T. R. (2013). Videographic analysis of *Eriophorum vaginatum* spatial coverage in an ombrotrophic bog. *Remote Sensing* 5: 6501–6512.

Koehler, A.-K., Sottocornola, M. and Kiely, G. (2011). How strong is the current carbon sequestration of an Atlantic blanket bog? *Global Change Biology* 17: 309–319.

Komárek, M., Ettler, V., Chrastný, V. and Mihaljevič, M. (2008). Lead isotopes in environmental sciences: a review. *Environment International* 34: 562–577.

Korhola, A., Ruppel, M., Seppä, H., Väliranta, M., Virtanen, T. and Weckström, J. (2010). The importance of northern peatland expansion to the late-Holocene rise of atmospheric methane. *Quaternary Science Reviews* 29: 611–617.

Kuhry, P. (1994). The role of fire in the development of *Sphagnum*-dominated peatlands in western boreal Canada. *Journal of Ecology* 82: 899–910.

Kurkjian, R., Dunlap, C. and Flegal, A. R. (2002). Lead isotope tracking of atmospheric response to post-industrial conditions in Yerevan, Armenia. *Atmospheric Environment* 36: 1421–1429.

Kylander, M. E., Klaminder, J., Blinder, R. and Weiss, D. J. (2010). Natural lead isotope variations in the atmosphere. *Earth and Planetary Science Letters* 290: 44–53.

Lamarre, A., Garneau, M. and Asnong, H. (2012). Holocene paleohydrological reconstruction and carbon accumulation of a permafrost peatland using testate amoeba and macrofossil analyses, Kuujjuarapik, subarctic Québec, Canada. *Review of Palaeobotany and Palynology* 186: 131–141.

Le Quéré, C., Moriarty, R., Andrew, R. M., Peters, G. P., Ciais, P., Friedlingstein, P., Jones, S. D., Sitch, S., Tans, P., Arneth, A., Boden, T. A., Bopp, L., Bozec, Y., Canadell, J. G., Chini, L. P., Chevalier, F., Cosca, C. E., Harris, I., Hoppema, M.,

Houghton, R. A., House, J. I., Jain, A. K., Johannessen, T., Kato, E., Keeling, R. F., Kitidis, V., Klein Goldewijk, K., Koven, C., Landa, C. S., Landschützer, P., Lenton, A., Lima, I. D., Marland, G., Mathis, J. T., Metzl, N., Nojiri, Y., Olsen, A., Ono, T., Peng, S., Peters, W., Pfeil, B., Poulter, B., Raupach, M. R., Regnier, P., Rödenbeck, C., Saito, S., Salisbury, J. E., Schuster, U., Schwinger, J., Séférian, R., Segschneider, J., Steinhoff, T., Stocker, B. D., Sutton, A. J., Takahashi, T., Tilbrook, B., van der Werf, G. R., Viovy, N., Wang, Y.-P., Wanninkhof, R., wiltshire, A. and Zeng, N. (2015). Global carbon budget 2014. *Earth System Science Data* 7: 47–85.

Le Roux, G. and Marshall, W. A. (2011). Constructing recent peat accumulation chronologies using atmospheric fall-out radionuclides. *Mires and Peat* 7: 1–14.

Le Roux, G., Weiss, D., Grattan, J., Givelet, N., Krachler, M. Cheburkin, A., Rausch, N., Kober, B. and Shotyk, W. (2004). Identifying the sources and timing of ancient and medieval atmospheric lead pollution in England using a peat profile from Lindow bog, Manchester. *Journal of Environmental Monitoring* 6: 502–510.

Lee, H. M., Hong, G. H., Baskaran, M., Kim, S. H. and Kim, Y. I. L. L. (2014). Evaluation of plating conditions for the recovery of ^{210}Po on a Ag planchet. *Applied Radiation and Isotopes* 90: 170–176.

Libby, W. F., Anderson, E. C. and Arnold, J. R. (1949). Age determination by radiocarbon content: World-wide assay of natural radiocarbon. *Science* 109: 227–228.

Loisel, J. and Garneau, M. (2010). Late Holocene paleoecohydrology and carbon accumulation estimates from two boreal peat bogs in eastern Canada: Potential and limits of multi-proxy archives. *Palaeogeography, Palaeoclimatology, Palaeoecology* 291: 493–533.

Loisel, J., Garneau, M. and Hélie, J. F. (2009). Modern *Sphagnum* δ^{13}C signatures follow a surface moisture gradient in two boreal peat bogs, James Bay lowlands, Québec. *Journal of Quaternary Science* 24: 209–214.

Loisel, J. and Yu, Z. (2013). Surface vegetation patterning controls carbon accumulation in peatlands. *Geophysical Research Letters* 40: 5508–5513.

Loisel, J., Yu, Z., Beilman, D. W., Camill, P., Alm, J., Amesbury, M. J., Anderson, D., Andersson, S., Bochicchio, C., Barber, K., Belyea, L. R., Bunbury, J., Chambers, F. M., Charman, D. J., De Vleeschouwer, F., Bialkiewicz-Koziel, B., Finkelstein, S. A., Galka, M., Garneau, M., Hammarlund, D., Hinchcliffe, W., Holmquist, J., Hughes, P., Jones, M. C., Klein, E. S., Kokfelt, U., Korhola, A., Kuhry, P., Lamarre, A., Lamentowicz, M., Large, D., Lavoie, M., MacDonald, G., Magnan, G., Mäkilä, M., Mallon, G., Mathijsen, P., Mauquoy, D., McCarroll, J., Moore, T. R., Nichols, J., O'Reilley, B., Oksanen, P., Packalen, M., Peteet, D., Richard, P. J. H., Robinson, S., Ronkainen, T., Rundgren, M., Sannell, A. B. K., Tarnocai, C., Thom, T., Tuittila, E.-S., Turetsky, M., Väliranta, M., van der Linden, M., van Geel, B., van Bellen, S., Vitt, D., Zhao, Y. and Zhou, W. (2014). A database and synthesis of

northern peatland soil properties and Holocene carbon and nitrogen accumulation. *The Holocene* 24: 1028–1042.

Lowe, D. J. (2011). Tephrochronology and its application: a review. *Quaternary Geochronology* 6: 107–153.

MacDonald, G. M., Beilman, D. W., Kremenetski, K. V., Sheng, Y., Smith, L. C. and Velichko, A. A. (2006). Rapid early development of circumarctic peatlands and atmospheric CH_4 and CO_2 variations. *Science* 314: 285–8.

Mackay, H., Hughes, P. D. M., Jensen, B. J. L., Langdon, P. G., Pyne-O'Donnell, S. D. F., Plunkett, G., Froese, D. G., Coulter, S. and Gardner, J. E. (2016). A mid to late Holocene cryptotephra framework from eastern North America. *Quaternary Science Reviews* 132: 101–113.

MacKenzie, A. B., Farmer, J. G. and Sugden, C. L. (1997). Isotopic evidence of the relative retention and mobility of lead and radiocaesium in Scottish ombrotrophic peats. *Science of the Total Environment* 203: 115–127.

MacKenzie, A. B., Hardie, S. M. L., Farmer, J. G., Eades, L. J. and Pulford, I. D. (2011). Analytical and sampling constraints in ^{210}Pb dating. *Science of the Total Environment* 409: 1298–1304.

Magnan, G. and Garneau, M. (2014a). Climatic and autogenic control on Holocene carbon sequestration in ombrotrophic peatlands of maritime Quebec, eastern Canada. *The Holocene* 24: 1054–1062.

Magnan, G. and Garneau, M. (2014b). Evaluating long-term regional climate variability in the maritime region of the St. Lawrence North Shore (eastern Canada) using a multi-site comparison of peat-based paleohydrological records. *Journal of Quaternary Science* 29: 209–220.

Magnan, G., Lavoie, M. and Payette, S. (2012). Impact of fire on long-term vegetation dynamics of ombrotrophic peatlands in northwestern Québec, Canada. *Quaternary Research* 77: 110–121.

Malmer, N. (1986). Vegetation graidnets in relation to environmental conditions in northwestern European mires. *Canadian Journal of Botany* 96: 375–383.

Mann, M. E., Zhang, Z., Hughes, M. K., Bradley, R. S., Miller, S. K., Rutherford, S. and Ni, F. (2008). Proxy-based reconstructions of hemispheric and global surface temperature variations over the past two millennia. *Proceedings of the National Academy of Sciences of the United States of America* 105: 13252–13257.

Mann, M. E., Zhang, Z., Rutherford, S., Bradley, R. S., Hughes, M. K., Shindell, D., Ammann, C., Faluvegi, G. and Ni, F. (2009). Global signatures and dynamical origins of the Little Ice Age and Medieval Climate Anomaly. *Science* 326: 1256–1260.

Markel, E. R. and Booth, R. K. (2010). Testate amoebae and δ ^{13}C of *Sphagnum* as surface-moisture proxies in Alaskan peatlands. *The Holocene* 20: 463–475.

Martin, A. and Blanchard, R. L. (1969). The thermal volatilisation of caesium-137, polonium-210 and lead-210 from in vivo labelled samples. *Analyst* 44: 441–446.

Matthews, K. M., Kim, C.-K. and Martin, P. (2007). Determination of ^{210}Po in environmental materials: a review of analytical methodology. *Applied Radiation and Isotopes* 65: 267–79.

Mauquoy, D., Engelkes, T., Groot, M. H. M., Markesteijn, F., Oudejans, M. G., van der Plicht, J. and van Geel, B. (2002a). High-resolution records of late-Holocene climate change and carbon accumulation in two north-west European ombrotrophic peat bogs. *Palaeogeography, Palaeoclimatology, Palaeoecology* 186: 275–310.

Mauquoy, D., van Geel, B., Blaauw, M., & van der Plicht, J. (2002b). Evidence from northwest European bogs shows “Little Ice Age” climatic changes driven by variations in solar activity. *The Holocene* 1: 1–6.

Mauquoy, D., van Geel, B., & Blaauw, M. (2004). Changes in solar activity and Holocene climatic shifts derived from ^{14}C wiggle-match dated peat deposits. *The Holocene* 1: 45–52.

Maxwell, S. E., & Delaney, H. D. (2004). *Designing Experiments and Analysing Data: A Model Comparison Perspective* (Second Edition). New York, NY, United States: Psychology Press.

MDDELCC. (2015). Tendances des températures. Ministère du Dévelopement Durable, Environement et Lutte Contre les Changements Climatiques. Retrieved February 23, 2015 from: http://www.mddelcc.gouv.qc.ca/climat/tendances/

Ménot, G. and Burns, S. J. (2001). Carbon isotopes in ombrogenic peat bog plants as climatic indicators: calibration from an altitudinal transect in Switzerland. *Organic Geochemistry* 32: 233–245.

Mikaloff Fletcher, S. E., Tans, P. P., Bruhwiler, L. M., Miller, J. B. and Heimann, M. (2004). CH_4 sources estimated from atmospheric observations of CH_4 and its $^{13}C/^{12}C$ isotopic ratios: 1. Inverse modeling of source processes. *Global Biogeochemical Cycles* 18: GB4004, doi:10.1029/2004GB002224.

Miller, K. M. (1987). Self-absorption corrections for gamma ray spectral measurements of ^{210}Pb in environmental samples. *Nuclear Instruments and Methods in Physics Research Section A: Accelerators, Spectrometers, Detectors and Associated Equipment* 258: 281–285.

Moore, T. R., Roulet, N. T. and Waddington, J. M. (1998). Uncertainty in predicting the effect of climatic change on the carbon cycling of Canadian peatlands. *Climatic Change* 40: 229–245.

Morris, P. J., Waddington, J. M., Benscoter, B. W. and Turetsky, M. R. (2011). Conceptual frameworks in peatland ecohydrology: looking beyond the two-layered (acrotelm-catotelm) model. *Ecohydrology* 4: 1–11.

Naulier, M., Savard, M. M., Bégin, C., Gennaretti, F., Arseneault, D., Marion, J., Nicault, A. and Bégin, Y. (2015). A millennial summer temperature reconstruction for northeastern Canada using oxygen isotopes in subfossil trees. *Climate of the Past* 11: 1153–1164.

Nilsson, K. and Nilsson, M. (2004). *The climate impact of energy peat utilisation in Sweden – the effect of former land-use and after-treatment*. IVL Report B1606, IVL Swedish Environmental Research Institute.

Nilsson, M., Klarqvist, M., Bohlin, E. and Possnert, G. (2001). Variation in ^{14}C age of macrofossils and different fractions of minute peat samples dated by AMS. *The Holocene* 11: 579–586.

Nilsson, M., Sagerfors, J., Buffam, I., Laudon, H., Eriksson, T., Grelle, A., Klemedtsson, L., Weslien, P. and Lindroth, A. (2008). Contemporary carbon accumulation in a boreal oligotrophic minerogenic mire - a significant sink after accounting for all C-fluxes. *Global Change Biology* 14: 2317–2332.

NWWG. (1997). *The Canadian wetland classification system* (Second Edition), B. G. Warner & C. D. A. Rubec, (Eds.). Waterloo, ON: Wetlands Research Centre, University of Waterloo.

Ohlson, M. and Tryterud, E. (2000). Interpretation of the charcoal record in forest soils: Forest fires and their production and deposition of macroscopic charcoal. *The Holocene* 10: 519–525.

Oldfield, F., Appleby, P. G., Cambray, R. S., Eakins, J. D., Barber, K. E., Battarbee, R. W., Pearson, G. W. and Williams, J. M. (1979). ^{210}Pb, ^{137}Cs and ^{239}Pu profiles in ombrotrophic peat. *Oikos* 33: 40–45.

Oldfield, F., Richardson, N. and Appleby, P. G. (1995). Radiometric dating (^{210}Pb, ^{137}Cs, ^{241}Am) of recent ombrotrophic peat accumulation and evidence for changes in mass balance. *The Holocene* 5: 141–148.

Olid, C., Garcia-Orellana, J., Martínez-Cortizas, A., Masqué, P., Peiteado, E. and Sanchez-Cabeza, J.-A. (2008). Role of surface vegetation in 210Pb-dating of peat cores. *Environmental Science & Technology* 42: 8858–8864.

Olid, C., Garcia-Orellana, J., Masqué, P., Cortizas, A. M., Sanchez-Cabeza, J. A. and Bindler, R. (2013). Improving the ^{210}Pb-chronology of Pb deposition in peat cores from Chao de Lamoso (NW Spain). *Science of the Total Environment* 443: 597–607.

Olid, C., Diego, D., Garcia-Orellana, J., Cortizas, A. M. and Klaminder, J. (2015). Modeling the downward transport of ^{210}Pb in peatlands: Initial Penetration-

Constant Rate of Supply (IP-CRS) model. *Science of the Total Environment* 541: 1222–1231.

Osvald, H. (1923). Die vegetation des Hochmoores Kmosse, Sven. *Växttsociologiska Sallskäpets Handl.* 1: 1–436.

Page, S. E., Siegert, F., Rieley, J. O., Boehm, H.-D., V., Jaya, A. and Limin, S. (2002). The amount of carbon released from peat and forest fires in Indonesia during 1997. *Nature* 420: 61–65.

PAGES 2k Consortium (2013). Continental-scale temperature variability during the past two millennia. *Nature Geoscience* 6: 339–346.

Parnell, A. C., Buck, C. E., and Doan, T. K. (2011). A review of statistical chronology models for high-resolution, proxy-based Holocene palaeoenvironmental reconstruction. *Quaternary Science Reviews* 30: 2948–2960.

Parry, L. E., Charman, D. J. and Blake, W. H. (2013). Comparative dating of recent peat deposits using natural and anthropogenic fallout radionuclides and Spheroidal Carbonaceous Particles (SCPs) at a local and landscape scale. *Quaternary Geochronology* 15: 11–19.

Patterson, W. A., Edwards, K. J. and Maguire, D. J. (1987). Microscopic charcoal as a fossil indicator of fire. *Quaternary Science Reviews* 6: 3–23.

Payette, S. (2004). Accelerated thawing of subarctic peatland permafrost over the last 50 years. *Geophysical Research Letters* 31: L18208, doi:10.1029/2004GL020358.

Payette, S. and Rochefort, L. (2001). *Écologie des tourbières du Québec-Labrador*. Québec: Les presses de l'Université Laval.

Pelletier, L. (2014). *Surface to atmosphere carbon exchange in peatlands with permanent open water pools*. PhD Thesis, McGill University.

Pelletier, L., Garneau, M. and Moore, T. R. (2011). Variation in CO_2 exchange over three summers at microform scale in a boreal bog, Eastmain region, Québec, Canada. *Journal of Geophysical Research* 116: G03019, doi:10.1029/2011JG001657.

Pelletier, L., Strachan, I. B., Garneau, M. and Roulet, N. T. (2014). Carbon release from boreal peatland open water pools: Implication for the contemporary C exchange. *Journal of Geophysical Research: Biogeosciences* 119: 207–222.

Pitkänen, A., Huttunen, P., Junger, H., Meriläinen, J. and Tolonen, K. (2003). Holocene fire history of middle boreal ping forest sites in eastern Finland. *Annales Botanici Fennici* 40: 15–33.

Pratte, S., Mucci, A. and Garneau, M. (2013). Historical records of atmospheric metal deposition along the St. Lawrence Valley (eastern Canada) based on peat bog cores. *Atmospheric Environment* 79: 831–840.

Pratte, S., Garneau, M. and De Vleeschouwer, F. (2016). Late-Holocene atmospheric dust deposition in eastern Canada (St. Lawrence North Shore). *The Holocene* doi:10.1177/0959683616646185.

Pyne-O'Donnell, S. D. F., Hughes, P. D. M., Froese, D. G., Jensen, B. J. L., Kuehn, S. C., Mallon, G., Amesbury, M. J., Charman, D. J., Daley, T. J., Loader, N. J., Mauquoy, D., Street-Perrott, F. A. and Woodman-Ralph, J. (2012). High-precision ultra-distal Holocene tephrochronology in North America. *Quaternary Science Reviews* 52: 6–11.

Quillet, A., Peng, C. and Garneau, M. (2010). Toward dynamic global vegetation models for simulating vegetation–climate interactions and feedbacks: recent developments, limitations, and future challenges. *Environmental Reviews* 18: 333–353.

R Development Team. 2014. *R: A Language and Environment for Statistical Computing*. Vienna, Austria.: R Foundation for Statistical Computing. Retrieved from http://www.r-project.org/.

Reimer, P. J., Brown, T. A. and Reimer, R. W. (2004). Discussion: Reporting and calibration of post-bomb 14C data. *Radiocarbon* 46: 1299–1304.

Reimer, P. J., Baillie, M. G. L., Bard, E., Bayliss, A., Beck, J. W., Blackwell, P. G., Bonk Ramsey, C., Buck, C. E., Burr, G. S., and Edwards, R. L. (2009). IntCal09 and Marine 09 radiocarbon age calibration curves, 0-50,000 years cal. BP. *Radiocarbon* 51: 1111–1150.

Reimer, P. J., Bard, E., Bayliss, A., Beck, J. W., Blackwell, P. G., Bronk Ramsey, C., Grootes, P. M., Guilderson, T. P., Haflidason, H., Hajdas, I., Hattz, C., Heaton, T. L., Hoffmann, D. L., Hohh, A. G., Hughen, K. A., Kaiser, K. F., Kromer, B., Manning, S. W., Niu, M., Reimer, R. W., Richard, D. A., Scott, E. M., Southon, J. R., Staff, R. A., Turney, C. S. M and van der Plicht, J. (2013). IntCal13 and Marine13 radiocarbon age calibration curves 0-50,000 years cal. BP. *Radiocarbon* 55: 1869–1887.

Rein, G., Cleaver, N., Ashton, C., Pironi, P. and Torero, J. L. (2008). The severity of smouldering peat fires and damage to the forest soil. *Catena* 74: 304–309.

Rezanezhad, F., Price, J. S., Quinton, W. L., Lennartz, B., Milojevic, T. and van Cappellen, P. (2016). Structure of peat soils and implications for water storage, flow and solute transport: a review update for geochemists. *Chemical Geology* 429: 75–84.

Robinson, S. D. and Moore, T. R. (2000). The influence of permafrost and fire upon carbon accumulation in high boreal peatlands, Northwest Territories, Canada. *Arctic, Antarctic, and Alpine Research* 32: 155–166.

Rooney, R. C., Bayley, S. E. and Schindler, D. W. (2012). Oil sands mining and reclamation cause massive loss of peatland and stored carbon. *Proceedings of*

the National Academy of Sciences of the United States of America 109: 4933–4937.

Roulet, N. T. (2000). Peatlands, carbon storage, greenhouse gases, and the Kyoto Protocol: Prospects and significance for Canada. *Wetlands* 20: 605–615.

Roulet, N. T., Lafleur, P. M., Richard, P. J. H., Moore, T. R., Humpfreys, E. R. and Bubier, J. (2007). Contemporary carbon balance and late Holocene carbon accumulation in a northern peatland. *Global Change Biology* 13: 397–411.

Rydin, H., & Jeglum, J. (2006). *The Biology of Peatlands*. Oxford, UK: Oxford University Press.

Sanchez-Cabeza, J. A., Masque, P., & Ani-Ragolta, I. (1998). ^{210}Pb and ^{210}Po analysis in sediments and soils by microwave acid digestion. *Journal of Radioanalytical and Nuclear Chemistry* 227: 19–22.

Sauvé, A. (2016). *Reconstitution holocène de la végétation et du climat pour les régions de Baie-Comeau et Havre-Saint-Pierre, QC*. MSc Thesis, Université du Québec à Montréal.

Schell, W. R., Tobin, M. J. and Massey, C. (1989). Evaluation of trace metal deposition history and potential element mobility in selected cores from peat and wetland ecosystems. *Science of the Total Environment* 88/89: 19–42.

Shore, J. S., Bartley, D. D. and Harkness, D. D. (1995). Problems encountered with the ^{14}C dating of peat. *Quaternary Science Reviews* 14: 373–383.

Schulze, E. D., Prokuschkin, A., Arneth, A., Knorre, N. and Vaganov, E. A. (2002). Net ecosystem productivity and peat accumulation in a Siberian Aapa mire. *Tellus B* 54: 531–536.

Schuur, E. A. G., Bockheim, J., Canadell, J. G., Euskirchen, E., Christopher, B., Goryachkin, S. V., Hagemann, S., Kuhry, P., Lafleur, M. M., Lee, H., Mazhitova, G., Nelson, F. E., Rinke, A., Romanovsky, V. E., Shiklomanoc, N., Tarnocai, C., Venevsky, S., Vogel, J. G. and Zimov, S. A. (2008). Vulnerability of Permafrost Carbon to Climate Change : Implications for the Global Carbon Cycle. *BioScience* 58: 701–714.

Seppälä, M. (1994). Snow depth controls on palsa growth. *Permafrost and Periglacial Processes* 5: 283–288.

Schurer, A. P., Tell, S. F. B. and Hergel, G. C. (2014). Small influence of solar variability on climate over the past millennium. *Nature Geoscience* 7: 104–108.

Schuur, E. A. G., McGuire, A. D., Schädel, C., Gross, G., Harden, J. W., Hayes, D. J., Hugelius, G., Koven, C. D., Kuhry, P., Lawrence, D. M., Natali, S. M., Olefeldt, D., Romanovsky, V. E., Schaefer, K., Turetsky, M. R., Treat, C. C. and Volk, J. E. (2015). Climate change and the permafrost feedback. *Nature* 520: 171–179.

Shindell, D. T., Schmidt, G. A., Mann, M. E., Rind, D. and Waple, A. (2001). Solar forcing of regional climate change during the Maunder Minimum. *Science* 294: 2149–2152.

Shotyk, W., Weiss, D., Appleby, P. G., Cheburkin, A. K., Frei, R., Floor, M., Kramers, J. D., Reese, S. and Van Der Knapp, W. O. (1998). History of atmospheric lead deposition since 12,370 ^{14}C yr BP from a peat bog, Jura Mountains, Switzerland. *Science* 281: 1635–1640.

Shotyk, W., Blaser, P., Grünig, A. and Cheburkin, A. K. (2000). A new approach for quantifying cumulative, anthropogenic, atmospheric lead deposition using peat cores from bogs: Pb in eight Swiss peat bog profiles. *Science of the Total Environment* 249: 281–295.

Sigl, M., Winstrup, M., McConnell, J. R., Welten, K. C., Plunkett, G., Ludlow, F., Büntgen, U., Caffee, M., Cellman, N., Dahl-Jensen, D., Fischer, H., Kipfstuhl, S., Kostick, C., Maselli, O. J., Mekhaldi, F., Mulvaney, R., Muscheler, R., Pasteris, D. R., Pilcher, J. R., Salzer, M., Schüpbach, S., Steffensen, J. P., Vinther, B. M., Woodruff, T. W. (2015). Timing and climate forcing of volcanic eruptions for the pst 2,500 years. *Nature* 532: 543-549.

Sikorski, J. and Bluszcz, A. (2008). Application of α and γ Spectrometry in the ^{210}Pb Method to Model Sedimentation in Artificial Retention Reservoir. *Geochronometria* 31: 65–75.

Sillasoo, Ü., Mauquoy, D., Blundell, A., Charman, D. J., Blaauw, M., Daniell, J. R. G., Toms, P., Newberry, J., Chamber, F. M. and Karofeld, E. (2007). Peat multi-proxy data for Männikjärve bog as indicators of late Holocene climate changes in Estonia. *Boreas* 36: 1–18.

Smith, L. C., Sheng, Y. and MacDonald, G. M. (2007). A first pan-Arctic assessment of the influence of glaciation, permafrost, topography and peatlands on northern hemisphere lake distribution. *Permafrost and Periglacial Processes* 208: 201–208.

Sottocornola, M. and Kiely, G. (2005). An Atlantic blanket bog is a modest CO_2 sink. *Geophysical Research Letters* 32: L23804, doi:10.1029/2005GL024731.

Statistics, L. (2015). *One-way repeated measures ANOVA using SPSS Statistics*. Last retrieved May 25, 2016 from: https://statistics.laerd.com/

Swindles, G. T., De Vleeschouwer, F., and Plunkett, G. (2011). Dating peat profiles using tephra: stratigraphy, geochemistry and chronology. *Mires and Peat* 7: 1–9.

Swindles, G. T., Morris, P. J., Baird, A. J., Blaauw, M. and Plunkett, G. (2012). Ecohydrological feedbacks confound peat-based climate reconstructions. *Geophysical Research Letters* 39: L11401, doi: 10.1029/2012GL051500.

Swindles, G. T., Galloway, J., Outram, Z., Turner, K., Schofield, J. E., Newton, A. J., Dugmore, A. J., Church, M. J., Watson, E. J., Batt, C., Bond, J., Edwards, K. J.,

Turner, V. and Bashford, D. (2013). Re-deposited cryptotrephra layers in Holocene peats linked to anthropogenic activity. *The Holocene* 23: 1493–1501.

Swindles, G. T., Morris, P. J., Mullan, D., Watson, E. J., Turner, T. E., Roland, T. P., Amesbury, M. J., Kokfelt, U., Schoning, K., Pratte, S., Gallego-Sala, A., Charman, D. J., Sanderson, N., Garneau, M., Carrivick, J., Woulds, C., Holden, J., Parry, L. and Galloway, J. M. (2015). The long-term fate of permafrost peatlands under rapid climate warming. *Nature Scientific Reports* 5: 17951–17955.

Tanner, P. A., Pan, S. M., Mao, S. Y. and Yu, K. N. (2000). γ-Ray spectrometric and α-counting method comparison for the determination of Pb-210 in estuarine sediments. *Applied Spectroscopy* 54: 1443–1446.

Tarnocai, C. (2006). The effect of climate change on carbon in Canadian peatlands. *Global and Planetary Change* 53: 222–232.

Tarnocai, C., Canadell, J. G., Schuur, E. A. G., Kuhry, P., Mazhitova, G. and Zimov, S. A. (2009). Soil organic carbon pools in the northern circumpolar permafrost region. *Global Biogeochemical Cycles* 23: GB2023, doi:10.1029/2008GB003327.

Tarnocai, C., Kettles, I. M. and Lacelle, B. (2011). *Peatlands of Canada*. Geological Survey of Canada, Open File 6561. Ottawa: Natural Resources Canada. doi:10.495/288786.

Telford, R. J., Heegaard, E. and Birks, H. J. B. (2004). All age-depth models are wrong: but how badly? *Quarternary Science Reviews* 23: 1–5.

Tolonen, K. and Turunen, J. (1996). Accumulation rates of carbon in mires in Finland and implications for climate change. *The Holocene* 6: 171–178.

Touflan, P. and Talon, B. (2009). Spatial reliability of soil charcoal analysis: the case of subalpine forest soils. *Ecoscience* 16: 23–27.

Treat, C. C., Jones, M. C., Camill, P., Gallego-Sala, A., Garneau, M., Harden, J. W., Hugelius, G., Klein, E. S., Kokfelt, U., Kuhry, P., Loisel, J., Mathijssen, P. J. H., O'Donnell, J. A., Oksanen, P. O., Ronkainen, T. M., Sannel, A. B. K., Talmot, J., Tarnocai, C. and Väliranta, M. (2016). Effects of permafrost aggradation on peat properties as determined from a pan-Arctic synthesis of plant macrofossils. *Journal of Geophysical Research: Biogeosciences* 121: 78–94.

Truman, H. V. (1937). Fossil evidence of two prairie invasions of Wisconsin. *Transactions of the Wisconsin Academy of Sciences, Arts and Letters* 30: 35-42.

Turetsky, M. R. (2004). Decomposition and organic matter quality in continental peatlands: the ghost of permafrost past. *Ecosystems* 7: 740–750.

Turetsky, M. R., Wieder, R. K., Williams, C. J. and Vitt, D. H. (2000). Organic matter accumulation, peat chemistry, and permafrost melting in peatlands of boreal Alberta. *Ecoscience* 7: 379–392.

Turetsky, M. R., Wieder, R. K., Halsey, L. and Vitt, D. H. (2002a). Current disturbance and the diminishing peatland carbon sink. *Geophysical Research Letters* 29: 7–10.

Turetsky, M. R., Wieder, R. K. and Vitt, D. H. (2002b). Boreal peatland C fluxes under varying permafrost regimes. *Soil Biology and Biochemistry* 34: 907–912.

Turetsky, M. R., Manning, S. W. and Wieder, R. K. (2004). Dating recent peat deposits. *Wetlands* 24: 324–356.

Turetsky, M. R., Wieder, R. K., Vitt, D. H., Evans, R. J. and Scott, K. D. (2007). The disappearance of relict permafrost in boreal north America: Effects on peatland carbon storage and fluxes. *Global Change Biology* 13: 1922–1934.

Turetsky, M. R., Crow, S. E., Evans, R. J., Vitt, D. H. and Wieder, R. K. (2008). Trade-offs in resource allocation among moss species control decomposition in boreal peatlands. *Journal of Ecology* 96: 1297–1305.

Turetsky, M. R., Benscoter, B., Page, S. Rein, G. van der Werf, G. R. and Watts, A. (2015). Global vulnerability of paetlands to fire and carbon loss. *Nature Geoscience* 8: 11-14.

Turner, T. E., Swindles, G. T. and Roucoux, K. H. (2014). Late Holocene ecohydrological and carbon dynamics of a UK raised bog: impact of human activity and climate change. *Quaternary Science Reviews* 84: 65–85.

Turunen, J., Tomppo, E., Tolonen, K. and Reinikainen, A. (2002). Estimating carbon accumulation rates of undrained mires in Finland – application to boreal and subarctic regions. *The Holocene* 12: 69–80.

Turunen, J., Roulet, N. T., Moore, T. R. and Richard, P. J. H. (2004). Nitrogen deposition and increased carbon accumulation in ombrotrophic peatlands in eastern Canada. *Global Biogeochemical Cycles* 18: GB3002, doi:10.1029/2003GB002154.

Urban, N. R., Eisenreich, S. J., Grigal, D. F. and Schurr, K. T. (1990). Mobility and diagenesis of ^{210}Pb in peat. *Geochimica et Cosmochimica Acta* 54: 3329–3346.

van Bellen, S., Dallaire, P.-L., Garneau, M. and Bergeron, Y. (2011a). Quantifying spatial and temporal Holocene carbon accumulation in ombrotrophic peatlands of the Eastmain region, Quebec, Canada. *Global Biogeochemical Cycles* 25: GB2016, doi: 10.1029/2010GB003877.

van Bellen, S., Garneau, M. and Booth, R. K. (2011b). Holocene carbon accumulation rates from three ombrotrophic peatlands in boreal Quebec, Canada: Impact of climate-driven ecohydrological change. *The Holocene* 21: 1217–1231.

van Bellen, S., Garneau, M., Ali, A. A. and Bergeron, Y. (2012). Did fires drive Holocene carbon sequestration in boreal ombrotrophic peatlands of eastern

Canada? *Quaternary Research* 78: 50–59.

van Breemen, N. (1995). How *Sphagnum* bogs down other plants. *Trends in Ecology and Evolution* 10: 270–275.

van der Molen, P. C. and Hoekstra, S. P. (1988). A palaeoecological study of a hummock-hollow complex from Engbertsdijksveen, in the Netherlands. *Review of Palaeobotany and Palynology* 56: 213–274.

van der Molen, P. C. and Wijmstra, T. A. (1994). The thermal regime of hummock-hollow complexes on Clara Bog, Co. Offaly. *Biology and Environment: Proceedings of the Royal Irish Academy B* 94: 209–221.

Vardy, S. R., Warner, B. G., Turunen, J. and Aravena, R. (2000). Carbon accumulation in permafrost peatlands in the Northwest Territories and Nunavut, Canada. *The Holocene* 10: 273–280.

Viau, A. E. and Gajewski, K. (2009). Reconstructing Millennial-Scale, Regional Paleoclimates of Boreal Canada during the Holocene. *Journal of Climate* 22: 316–330.

Viau, A. E. and Gajewski, K. (2012). The climate of North America during the past 2000 years reconstructed from pollen data. *Global and Planetary Change* 84/85: 75–83.

Vile, M. A., Wieder, R. K. and Novák, M. (1999). Mobility of Pb in *Sphagnum*-derived peat. *Biogeochemistry* 45: 35–52.

Vile, M. A., Wieder, R. K. and Novák, M. (2000). 200 Years of Pb Deposition throughout the Czech Republic: Patterns and Sources. *Environmental Science and Technology* 34: 12–21.

Vitt, D. H., Halsey, L. A. and Zoltai, S. C. (1994). The bog landforms of continental western Canada in relation to climate and permafrost patterns. *Arctic and Alpine Research* 26: 1–13.

Vitt, D. H., Halsey, L. A. and Zoltai, S. C. (2000). The changing landscape of Canada's western boreal forest: the current dynamics of permafrost. *Canadian Journal of Forest Research* 30: 283–287.

Vitt, D. H., Wieder, R. K., Scott, K. D. and Faller, S. (2009). Decomposition and peat accumulation in rich fens of boreal Alberta, Canada. *Ecosystems* 12: 360–373.

Wang, Y., Field, R. D. and Roswintiarti, O. (2004). Trends in atmospheric haze induced by peat fires in Sumatra Island, Indonesia and El Niño phenomenon from 1973 to 2003. *Geophysical Research Letters* 31: L04103, doi:10.1029/2003GL018853.

Wanner, H., Mercolli, L., Grosjean, M. and Ritz, S. P. (2014). Holocene climate variability and change; a data-based review. *Journal of the Geological Society* 172: 254–263.

Watson, E. J., Swindles, G. T., Lawson, I. T. and Savov, I. P. (2015). Spatial variability of tephra and carbon accumulation in a Holocene peatland. *Quaternary Science Reviews* 124: 248–264.

Weiss, D., Shotyk, W., Kramers, J. D. and Gloor, M. (1999). *Sphagnum* mosses as archives of recent and past atmospheric lead deposition in Switzerland. *Atmospheric Environment* 33: 3751–3763.

Wieder, R. K. (1990). Metal cation binding to *Sphagnum* peat and sawdust: relation to wetland treatment of metal-polluted waters. *Water, Air, and Soil Pollution* 53: 391–400.

Wieder, R. K. (2001). Past, present, and future peatland carbon balance: an empirical model based on ^{210}Pb-dated cores. *Ecological Applications* 11: 327–342.

Wieder, R. K., Novák, M., Schell, W. R. and Rhodes, T. (1994). Rates of peat accumulation over the past 200 years in five *Sphagnum*-dominated peatlands in the United States. *Journal of Paleolimnology* 1: 35–47.

Wieder, R. K., Scott, K. D., Kamminga, K., Vile, M. A., Vitt, D. H., Bone, T. Xu, B., Benscoter, B. W. and Bhatti, J. S. (2009). Postfire carbon balance in boreal bogs of Alberta, Canada. *Global Change Biology* 15: 63–81.

Yafa, C. and Farmer, J. G. (2006). A comparative study of acid-extractable and total digestion methods for the determination of inorganic elements in peat material by inductively coupled plasma-optical emission spectrometry. *Analytica Chimica Acta* 557: 296–303.

Yeloff, D. and Mauquoy, D. (2008). The influence of vegetation composition on peat humification: implications for palaeoclimatic studies. *Boreas* 35: 662–673.

Yeloff, D. E., Labadz, J. C. and Hunt, C. O. (2006a) Causes of degradation and erosion of a blanket mire in the southern Pennines, UK. *Mires and Peat* 1: 1–18.

Yeloff, D., Bennett, K. D., Blaauw, M., Mauquoy, D., Sillasoo, U., van der Plicht, J. and van Geel, B. (2006b). High precision ^{14}C dating of Holocene peat deposits: a comparison of Bayesian calibration and wiggle-matching approaches. *Quaternary Geochronology* 1: 222–235.

Yu, Z. (2011). Holocene carbon flux histories of the world's peatlands: Global carbon-cycle implications. *The Holocene* 21: 761–774.

Yu, Z. C. (2012). Northern peatland carbon stocks and dynamics: a review. *Biogeosciences* 9: 4071–4085.

Yu, Z., Vitt, D. H., Campbell, I. D., & Apps, M. J. (2003). Understanding Holocene peat accumulation pattern of continental fens in western Canada. *Canadian Journal of Botany* 81: 267–282.

Yu, Z., Beilman, D. W. and Jones, M. C. (2009). Sensitivity of northern peatland carbon

dynamics to Holocene climate change. In A. J. Baird, L. R. Belyea, X. Comas, A. S. Reeve, & L. D. Slater (Eds.), *Carbon Cycling in Northern Peatlands* (pp. 55–69). Washington, DC: American Geophysical Union.

Yu, Z., Beilman, D. W., Frolking, S., MacDonald, G. M., Roulet, N. T., Camill, P. and Charman, D. J. (2011). Peatlands and their role in the global carbon cycle. *Eos* 92: 97–108.

Yu, Z., Loisel, J., Brosseau, D. P., Beilman, D. W. and Hunt, S. J. (2010). Global peatland dynamics since the Last Glacial Maximum. *Geophysical Research Letters* 37: L13402, doi:10.1029/2010GL043584.

Zaborska, A., Carroll, J., Papucci, C. and Pempkowiak, J. (2007). Intercomparison of alpha and gamma spectrometry techniques used in ^{210}Pb geochronology. *Journal of Environmental Radioactivity* 93: 38–50.

Zoltai, S. C. (1972). Palsas an dpeat plateaus in central Manitoba and Saskatchewan. *Canadian Journal of Forest Research* 2: 291–301.

Zoltai, S. C. and Tarnocai, C. (1972). Perennially frozen peatlands in the Western Arctic and Subarctic of Canada. *Canadian Journal of Earth Sciences* 12: 28–43.

APPENDIX

Appendix A ^{210}Pb-dating methodology

A.1 Laboratory method for the preparation of peat samples for lead-210 determination by alpha spectrometry

Before starting:
- Freeze-dry and grind samples;
- Wash silver planchets in acetone and spray-paint convex side with protective paint

Day 1:
1. In acid-washed beakers, add: 0.5 g dry weight sample + 1 ml ^{209}Po spike
2. Add 10 ml conc. nitric acid (HNO_3);
   Bring to dryness at 80-90 ^{o}C (approx. 4.2 on the hotplate dial);
   Remove from hotplate and cool.
3. Add 10 ml 30% hydrogen peroxide (H_2O_2);
   Heat for 1 hour on low heat (monitor reaction);
   Let sit overnight, no heat.

Day 2:
4. Bring to dryness;
   Remove from hotplate and cool.
5. Add 5 ml 6M hydrochloric acid (HCl) and bring to dryness;
   Repeat step 5.
6. Dissolve residue into 5 ml 6M HCl solution;
7. Rinse solution into centrifuge tubes with 0.5M HCl;
   Centrifuge for 10 min at 2500 rpm;
   Pour off supernatant into acid-washed 120 ml plating jars;
   Repeat step 7 if residue in beakers.
8. Top up plating jars with 0.5M HCl
   Place on magnetic stirring table, set at 850 rpm.
9. Add 1 small scoop (0.2 g) ascorbic acid.
10. Suspend silver planchets for 24 hrs.

Day 3:
11. Rinse planchets with DI water;
    Wash up glassware.
12. Bring planchets to radiometry lab (queue).

Counting:
- See Appendix A.2 for details;
- Using Ortec Octête Plus Integrated Alpha-Spectrometry System;
- Software: Maestro-32;
- Count for a minimum of 24 hours; if possible, count until N > 400 (< 5% counting error)

A.2 Alpha Spectrometer

Lead-210 (^{210}Pb) activity is determined using alpha spectrometry by indirectly measuring radiation during alpha decay of its daughter nuclide, polonium-210 (^{210}Po) into stable lead-206 (^{206}Pb). At the University of Exeter (UK) Radiometry Lab, this is done using the Ortec Octête Plus Integrated Alpha-Spectrometry System (Figure A.1).

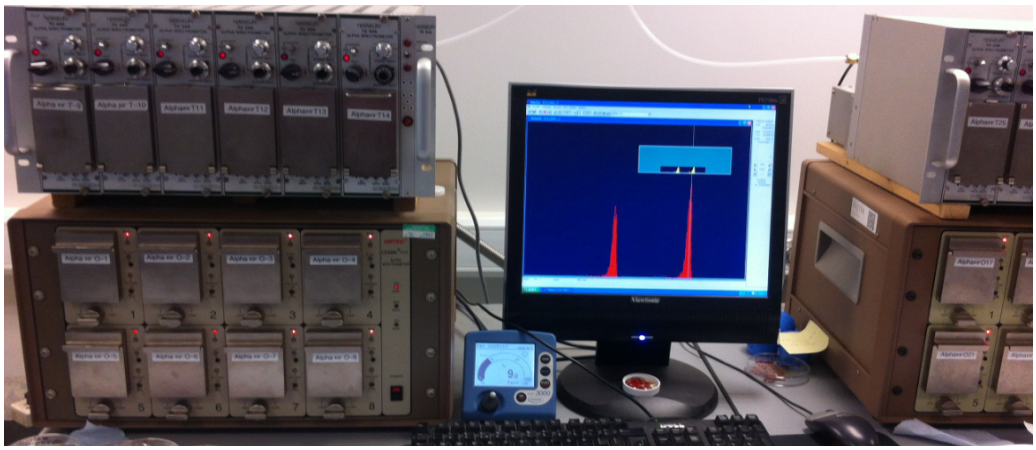

Figure A.1 Set-up of alpha-spectrometry chambers at the University of Exeter Lab.

Each sample is spiked with a chemical yield tracer (here, ^{209}Po) digested and electroplated in a weak acidic solution onto a silver planchet with a painted convex side (as in Appendix A.1). Each silver planchet is placed concave (unpainted) side up into a counting chamber, on a tray directly below the detector (Figure A.2).

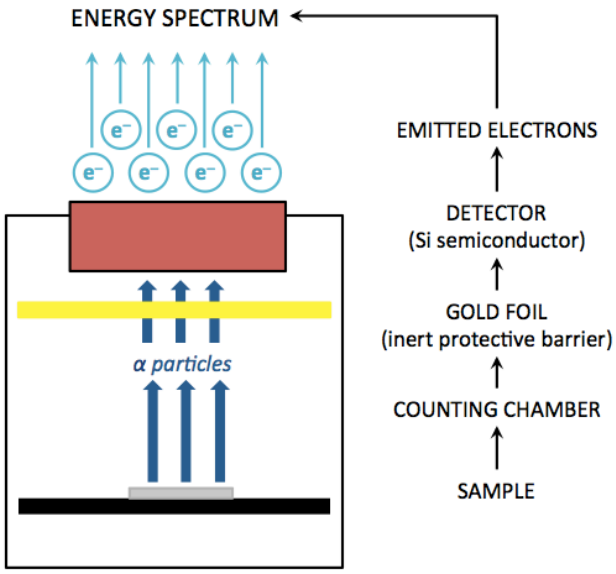

Figure A.2 Schematic diagram of an alpha detector counting chamber, modified from (EPA, 2011). Alpha particles are emitted from the sample and registered by the detector.

A vacuum is created in each chamber to eliminate interference from other atoms (EPA, 2011). ^{210}Po decays into ^{206}Pb and emits alpha particles; these have two protons and two electrons, as helium:

$$^{210}\mathrm{Po} \rightarrow {}^{206}\mathrm{Pb} + 4\ \mathrm{He} \qquad \text{Equation 1}$$

In the chamber, alpha particles pass through a silicon surface barrier into the detector. The silicon surface barrier is a protection for the detector and also functions as an electrical contact for the detection system; it is very thin (< 1 µm) and does not affect the momentum of the alpha particles (EPA, 2011). Within the detector, electrons are counted and a computer program (Alpha Vision®) plots energy (in keV) per number of alpha particles emitted over time (Figure A.6) (EPA, 2011). As each radionuclide emits alpha particles with a characteristic energy (3-10 MeV), the programme is set up to highlight and count only the alpha decay from ^{210}Po (5.304 MeV) and for the chemical yield tracer (in this case, ^{209}Po: 4.883 MeV) (Matthews *et al.,* 2007). As the background noise for each alpha counter is very low and the two Po peaks are very distinct (i.e. no overlap), the subsequent activity calculations are reliable (Figure A.3).

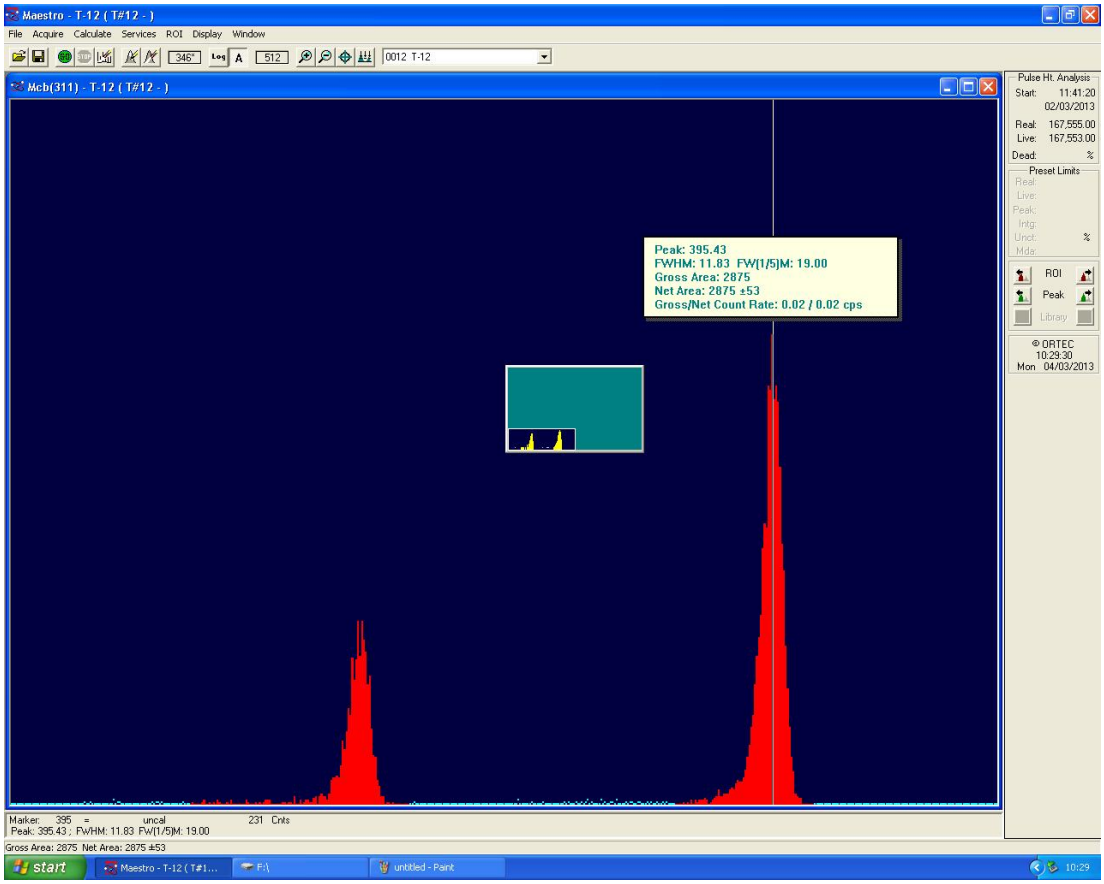

Figure A.3 Screenshot of ^{209}Po tracer (left) and ^{210}Po (right) peaks.

A.3 Calculating lead-210 activity from polonium counts

This was adapted from EPA, 2011; Le Roux and Marshall, 2011; Turetsky *et al.,* 2004.

The **^{210}Pb-specific activity** (A) for each sample is:

$$A = \frac{A_T \, m_T \, N_{210Po} \, e^{\lambda_1 \, t_1}}{m_s \, N_{209Po} \, e^{\lambda_2 \, t_2}} \qquad \text{Equation 2}$$

Where: A_T is the spike- (or tracer-) specific activity (1 mBq g^{-1} = 1 Bq kg^{-1});

m_T and m_S represent the mass of the tracer/spike added and of the dried sample, respectively (g);

N_{209Po} and N_{210Po} are the number of counts measured from the ^{209}Po and ^{210}Po spectra, respectively;

λ_1 and λ_2 are decay constants for ^{209}Po and ^{210}Po, respectively; these are calculated based on the half-life for each radionuclide (EPA, 2011);

t_1 is the time from spike preparation (dilution) to the middle of counting;

t_2 is the time from sample preparation (plating) to the middle of counting.

The **counting error** (ε) is as follows:

$$\varepsilon = \frac{\sqrt{N}}{N} = \frac{1}{\sqrt{N}} \qquad \text{Equation 3}$$

Where N is the number of alpha decay counts for ^{209}Po or ^{210}Po.

Therefore, the **^{210}Pb activity error** (σ_A) is:

$$\sigma_A = A \, (\varepsilon_{209Po}^2 + \varepsilon_{210Po}^2 + \sigma_T^2 + \sigma_S^2) \qquad \text{Equation 4}$$

Where: σ_T is the standard error specific to the ^{209}Po spike activity (1%);

σ_S is the standard errors for sampling error (e.g. pipette, balance); assumed to be approximately 1%;

ε_{209Po} and ε_{210Po} are the counting errors for ^{209}Po (spike) and ^{210}Po (sample), respectively.

A.4 CRS model calculations

The equations for calculating the Constant Rate of Supply (CRS) model dates are adapted from (Appleby, 2001; Turetsky *et al.,* 2004).

Table A.1 Symbols, units and terminology for following equations

D	Unit	Description
x_n	cm	Depth of sample n
x_{eq}	cm	Equilibrium depth, corresponding to supported ^{210}Pb activity level
ρ_n	g cm^{-3}	Dry bulk density of sample n
m_n	g cm^{-2}	Cumulative dry mass
C_n	Bq kg^{-1}	Unsupported mass-specific concentrations/^{210}Pb activity level
$\hat{A}_n$	Bq m^{-2}	Cumulative unsupported ^{210}Pb inventory
A_n	Bq m^{-2}	Residual unsupported ^{210}Pb, inventory below sample n
A_0	Bq m^{-2}	Total unsupported ^{210}Pb inventory, or Cumulative unsupported ^{210}Pb inventory where total activity reaches radioactive equilibrium with ^{226}Ra (based on x_{eq} selection)
t_n	a	Date of n, or number of years from coring date until n
λ	a^{-1}	^{210}Pb decay constant (λ = 0.03114)
r_n	kg m^{-2} a^{-1}	Sedimentation rate
P	Bq m^{-2} a^{-1}	^{210}Pb supply rate

Step 1: Calculating cumulative dry mass (m_n)

If sections are consecutive:

$$m_n = m_{n-1} + \rho_n(x_n - x_{n-1}) \quad \text{Equation 5}$$

If sections are non-consecutive (trapezium rule):

$$m_n = m_{n-1} + 1/2(\rho_n + \rho_{n-1})(x_n - x_{n-1}) \quad \text{Equation 6}$$

Step 2: Calculating the unsupported ^{210}Pb activity, or $^{210}Pb_{ex}$ (C_n)

$$C_n = (activity\ at\ x_n) - (activity\ at\ x_{eq}) \quad \text{Equation 7}$$

Step 3: Calculating the cumulative unsupported inventory ($^{210}Pb_{ex}$)

$$\hat{A}_n = \hat{A}_{n-1} + 10\ \frac{C_n + C_{n-1}}{2}(m_n - m_{n-1}) \quad \text{Equation 8}$$

Note that the results are multiplied by 10 in order to obtain values in Bq m^{-2}.

The previous equation can be modified to include exponential decay between points, as in the following:

$$\hat{A}_n = \hat{A}_{n-1} + 10\ \frac{C_{n-1} - C_n}{\ln(C_{n-1}/C_n)}(m_n - m_{n-1}) \quad \text{Equation 9}$$

Step 4: Calculating the total unsupported ^{210}Pb inventory (A_0)

The total unsupported inventory is the value of the cumulative inventory (A_n) where the total activity is estimated to reach radioactive equilibrium with the supporting ^{226}Ra; defining the equilibrium depth is crucial at this stage.

Step 5: Calculating the residual unsupported ^{210}Pb inventory (A_n)

$$A_n = A_0 - \hat{A}_n \quad \text{Equation 10}$$

Step 6: Calculating ages using the CRS dating equation

$$t_n = \frac{1}{\lambda} \ln \left(1 + \frac{\hat{A}_n}{A_n}\right) \quad \text{Equation 11}$$

Which can also be written as:

$$t_n = \frac{1}{\lambda} \ln \left(\frac{A_0}{A_n}\right) \quad \text{Equation 12}$$

Additional calculations

Sedimentation rate:

$$r_n = \lambda \frac{A_n}{C_n} \quad \text{Equation 13}$$

Supply rate:

$$P = \lambda A_0 \quad \text{Equation 14}$$

Standard error calculations (σ):

Below are the basic calculations for standard errors. Combined with propagation of error, we can calculate standard errors for each term. We assume that $\hat{A}$ and A are independent for the purpose of error calculation. We also assume a constant percentage error p of 7% in the dry mass increments.

$$\sigma_{\hat{A}_n} = \left[\sigma^2_{\hat{A}_{n-1}} + 100\,(\sigma^2_{C_n} + (p^2 C_n^2)(m_n - m_{n-1})^2 \right]^{1/2} \quad \text{Equation 15}$$

$$\sigma_t = \frac{1}{\lambda} \left[\left(\frac{\sigma_{A_0}}{A_0}\right)^2 + \left(1 - \frac{2A_n}{A_0}\right) \left(\frac{\sigma_{A_n}}{A_n}\right)^2 \right]^{1/2} \quad \text{Equation 16}$$

$$\frac{\sigma_r}{r} = \left[\left(\frac{\sigma_{A_n}}{A_n}\right)^2 + \left(1 - \frac{A_n - A_{n+1}}{A_n}\right) \left(\frac{\sigma_{C_n}}{C_n}\right)^2 \right]^{1/2} \quad \text{Equation 17}$$

A.5 Individual core results for alpha/gamma spectrometry comparisons

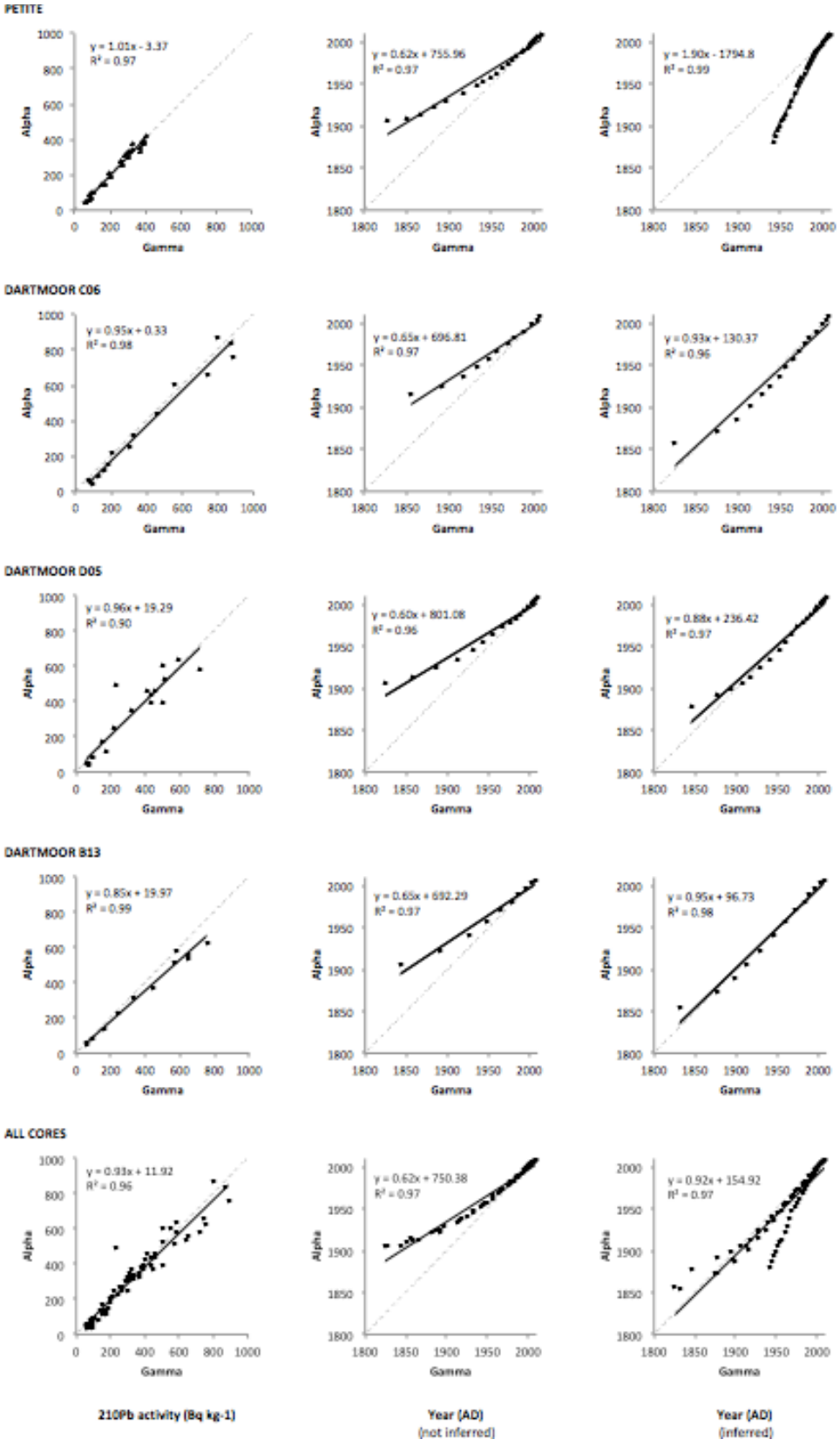

Figure A.4 Alpha and gamma comparisons for activities and ages. Dotted line is 1:1; solid black is trendline (equation indicated). Left-hand graphs are activity, right-hand are age